Publishing House ASV

begell house, inc. publishers

Scientific coordination is carried out by the Russian Academy of Architecture and Construction Sciences (RAACS)

Volume 15 • Issue 1 • 2019

ISSN 2588-0195 (Online)
ISSN 2587-9618 (Print) Continues ISSN 1524-5845

International Journal for

Computational Civil and Structural Engineering

Международный журнал по расчету гражданских и строительных конструкций

http://raasn.ru/public.php
http://ijccse.iasv.ru

DOI: 10.22337/2587-9618
GICID: 71.0000.1500.2830

EXECUTIVE EDITOR

Vladimir I. Travush,
Full Member of RAACS, Professor, Dr.Sc.,
Vice-President of the Russian Academy
of Architecture and Construction Sciences;
Urban Planning Institute
of Residential and Public Buildings;
24, Ulitsa Bolshaya Dmitrovka, 107031, Moscow, Russia

EDITOR-IN-CHIEF

Vladimir N. Sidorov,
Corresponding Member of RAACS, Professor, Dr.Sc.,
Russian University of Transport (RUT – MIIT);
Russian University of Friendship of Peoples;
Moscow Institute of Architecture (State Academy);
Perm National Research Polytechnic University;
Kielce University of Technology (Poland);
9b9, Obrazcova Street, Moscow, 127994, Russia

EDITORIAL DIRECTOR

Valery I. Telichenko,
Full Member of RAACS, Professor, Dr.Sc.,
The First Vice-President of the Russian Academy
of Architecture and Construction Sciences;
National Research Moscow State University
of Civil Engineering;
24, Ulitsa Bolshaya Dmitrovka, 107031, Moscow, Russia

MANAGING EDITOR

Nadezhda S. Nikitina,
Professor, Ph.D.,
Director of ASV Publishing House;
National Research Moscow State University
of Civil Engineering;
26, Yaroslavskoe Shosse, 129337, Moscow, Russia

ASSOCIATE EDITORS

Pavel A. Akimov,
Full Member of RAACS, Professor, Dr.Sc.,
Executive Scientific Secretary of the Russian Academy
of Architecture and Construction Sciences;
Scientific Research Center "STADYO";
Tomsk State University of Architecture and Building;
Russian University of Friendship of Peoples;
24, Ul. Bolshaya Dmitrovka, 107031, Moscow, Russia

Alexander M. Belostotsky,
Corresponding Member of RAACS, Professor, Dr.Sc.,
Research & Development Center "STADYO";
Russian University of Transport (RUT – MIIT);
Russian University of Friendship of Peoples;
Perm National Research Polytechnic University;
Tomsk State University of Architecture and Building;
8th Floor, 18, ul. Tretya Yamskogo Polya,
125040, Moscow, Russia

Vladimir Belsky, Ph.D.,
Dassault Systèmes Simulia;
1301 Atwood Ave Suite 101W
02919 Johnston, RI, United States

Mikhail Belyi, Professor, Dr.Sc.,
Dassault Systèmes Simulia;
1301 Atwood Ave Suite 101W
02919 Johnston, RI, United States

Vitaly Bulgakov, Professor, Dr.Sc.,
SemanticPro;
Boston, USA

Nikolai P. Osmolovskii, Professor, Dr.Sc.,
Systems Research Institute, Polish Academy of
Sciences; Kazimierz Pulaski University
of Technology and Humanities in Radom;
29, ul. Malczewskiego, 26-600, Radom, Poland

Gregory P. Panasenko, Professor, Dr.Sc.,
Equipe d'Analise Numerique; NMR CNRS 5585
University Gean Mehnet;
23 rue. P.Michelon 42023, St.Etienne, France

Leonid A. Rozin, Professor, Dr.Sc.,
Peter the Great Saint-Petersburg
Polytechnic University;
29, Ul. Politechnicheskaya,
195251 Saint-Petersburg, Russia

Scientific coordination is carried out by the Russian Academy of Architecture and Construction Sciences (RAACS)

PUBLISHER

ASV Publishing House
(ООО «Издательство АСВ»)
19/1,12, Yaroslavskoe Shosse, 120338, Moscow, Russia
Tel. +7(925)084-74-24; E-mail: iasv@iasv.ru; Интернет-сайт: http://iasv.ru/

ADVISORY EDITORIAL BOARD

Robert M. Aloyan,
Corresponding Member
of RAACS, Professor, Dr.Sc.,
Ivanovo State Polytechnic
University; 20, Ulitsa 8 Marta,
Ivanovo, 153037, Russia

Vladimir I. Andreev,
Full Member of RAACS,
Professor, Dr.Sc.,
National Research Moscow State
University of Civil Engineering;
Yaroslavskoe Shosse 26,
Moscow, 129337, Russia

Mojtaba Aslami, Ph.D,
Fasa University; Daneshjou blvd,
Fasa, Fars Province, Iran

Klaus-Jurgen Bathe, Professor
Massachusetts Institute
of Technology;
Cambridge, MA 02139, USA

Yuri M. Bazhenov,
Full Member of RAACS,
Professor, Dr.Sc.,
National Research Moscow State
University of Civil Engineering;
Yaroslavskoe Shosse 26,
Moscow, 129337, Russia

Alexander T. Bekker,
Corresponding Member
of RAACS, Professor, Dr.Sc.,
Far Eastern Federal University;
Russian Academy of Architecture
and Construction Sciences;
8, Sukhanova Street, Vladivostok,
690950, Russia

Tomas Bock, Professor, Dr.-Ing.,
Technical University of Munich,
Arcisstrasse 21, D-80333
Munich, Germany

Jan Buynak, Professor, Ph.D.,
University of Žilina;
1, Univerzitná, Žilina, 010 26,
Slovakia

Evgeniy M. Chernishov,
Full Member of RAACS,
Professor, Dr.Sc.,
Voronezh State Technical
University; 14, Moscow Avenue,
Voronezh, 394026, Russia

Vladimir T. Erofeev,
Full Member of RAACS,
Professor, Dr.Sc.,
Ogarev Mordovia State
University; 68, Bolshevistskaya
Str., Saransk 430005, Republic of
Mordovia, Russia

Victor S. Fedorov,
Full Member of RAACS,
Professor, Dr.Sc.,
Russian University of Transport
(RUT – MIIT);
9b9 Obrazcova Street, Moscow,
127994, Russia

Sergey V. Fedosov,
Full Member of RAACS,
Professor, Dr.Sc.,
Ivanovo State Polytechnic
University;
20, Ulitsa 8 Marta, Ivanovo,
153037, Russia

Sergiy Yu. Fialko,
Professor, Dr.Sc.,
Cracow University of
Technology;
24, Warszawska Street, Kraków,
31-155, Poland

Vladimir G. Gagarin,
Corresponding Member
of RAACS, Professor, Dr.Sc.,
Research Institute of Building
Physics of Russian Academy
of Architecture and Construction
Sciences;
21, Lokomotivny Proezd,
Moscow, 127238, Russia

Alexander S. Gorodetsky,
Foreign Member of RAACS,
Professor, Dr.Sc.,
LIRA SAPR Ltd.;
7a Kiyanovsky Side Street
(Pereulok), Kiev, 04053, Ukraine

Vyatcheslav A. Ilyichev,
Full Member of RAACS,
Professor, Dr.Sc.,
Russian Academy of Architecture
and Construction Sciences;
Podzemproekt Ltd.;
24, Ulitsa Bolshaya Dmitrovka,
Moscow, 107031, Russia

Marek Iwański,
Professor, Dr.Sc.,
Kielce University of Technology;
7, al. Tysiąclecia Państwa
Polskiego Kielce, 25 – 314,
Poland

Sergey Yu. Kalashnikov,
Advisor of RAACS,
Professor, Dr.Sc.,
Volgograd State Technical
University; 28, Lenin avenue,
Volgograd, 400005, Russia

Semen S. Kaprielov,
Corresponding Member
of RAACS, Professor, Dr.Sc.,
Research Center of Construction;
6, 2nd Institutskaya St., Moscow,
109428, Russia

Nikolay I. Karpenko,
Full Member of RAACS,
Professor, Dr.Sc.,
Research Institute of Building
Physics of Russian Academy
of Architecture and Construction
Sciences; Russian Academy of
Architecture and Construction
Sciences; 21, Lokomotivny
Proezd, Moscow, 127238, Russia

Vladimir V. Karpov,
Professor, Dr.Sc.,
Saint Petersburg State University
of Architecture and Civil
Engineering;
4, 2-nd Krasnoarmeiskaya Steet,
Saint Petersburg, 190005, Russia

Galina G. Kashevarova,
Corresponding Member
of RAACS, Professor, Dr.Sc.,
Perm National Research
Polytechnic University;
29 Komsomolsky pros., Perm,
Perm Krai, 614990, Russia

John T. Katsikadelis,
Professor, Dr.Eng, PhD, Dr.h.c.,
National Technical University of
Athens; Zografou Campus
9, Iroon Polytechniou str
15780 Zografou, Greece

Vitaly I. Kolchunov,
Full Member of RAACS,
Professor, Dr.Sc.,
Southwest State University;
Russian Academy of Architecture
and Construction Sciences;
94, 50 let Oktyabrya, Kursk,
305040, Russia

Markus König, Professor
Ruhr-Universität Bochum;
150, Universitätsstraße, Bochum,
44801, Germany

Sergey B. Kositsin,
Professor, Dr.Sc.,
Russian University of Transport
(RUT – MIIT); 9b9 Obrazcova
Street, Moscow, 127994, Russia

Sergey B. Krylov,
Corresponding Member
of RAACS, Professor, Dr.Sc.,
Research Center of Construction;
6, 2nd Institutskaya St., Moscow,
109428, Russia

Sergey V. Kuznetsov,
Professor, Dr.Sc.,
Ishlinsky Institute for Problems
in Mechanics of the Russian
Academy of Sciences;
101-1, Prosp. Vernadskogo,
Moscow, 119526, Russia

Vladimir V. Lalin,
Professor, Dr.Sc.,
Peter the Great Saint-Petersburg
Polytechnic University;
29, Ul. Politechnicheskaya,
Saint-Petersburg, 195251, Russia

Leonid S. Lyakhovich,
Full Member of RAACS,
Professor, Dr.Sc.,
Tomsk State University
of Architecture and Building;
2, Solyanaya Sq., Tomsk,
634003, Russia

Rashid A. Mangushev,
Corresponding Member
of RAACS, Professor, Dr.Sc.,
Saint Petersburg State University
of Architecture and Civil
Engineering;
4, 2-nd Krasnoarmeiskaya Steet,
Saint Petersburg, 190005, Russia

Ilizar T. Mirsayapov,
Advisor of RAACS,
Professor, Dr.Sc., Kazan State
University of Architecture and
Engineering; 1, Zelenaya Street,
Kazan, 420043, Republic
of Tatarstan, Russia

Vladimir L. Mondrus,
Corresponding Member
of RAACS, Professor, Dr.Sc.,
National Research Moscow State
University of Civil Engineering;
Yaroslavskoe Shosse 26,
Moscow, 129337, Russia

Valery I. Morozov,
Corresponding Member
of RAACS, Professor, Dr.Sc.,
Saint Petersburg State University
of Architecture and Civil
Engineering;
4, 2-nd Krasnoarmeiskaya Steet,
Saint Petersburg, 190005, Russia

Anatoly V. Perelmuter,
Foreign Member of RAACS,
Professor, Dr.Sc., SCAD Soft;
Office 1,2, 3a Osvity street,
Kiev, 03037, Ukraine

Alexey N. Petrov,
Advisor of RAACS, Professor,
Dr.Sc., Petrozavodsk State
University; 33, Lenina Prospect,
Petrozavodsk, 185910,
Republic of Karelia, Russia

Vladilen V. Petrov,
Full Member of RAACS,
Professor, Dr.Sc.,
Yuri Gagarin State Technical
University of Saratov;
77 Politechnicheskaya Street,
Saratov, 410054, Russia

Jerzy Z. Piotrowski,
Professor, Dr.Sc.,
Kielce University of Technology;
al. Tysiąclecia Państwa Polskiego
7, Kielce, 25 – 314, Poland

Chengzhi Qi, Professor, Dr.Sc.,
Beijing University of Civil
Engineering and Architecture;
1, Zhanlanlu, Xicheng District,
Beijing, China

Vladimir P. Selyaev,
Full Member of RAACS,
Professor, Dr.Sc., Ogarev
Mordovia State University;
68, Bolshevistskaya Str., Saransk
430005, Republic of Mordovia,
Russia

Eun Chul Shin,
Professor, Ph.D.,
Incheon National University;
(Songdo-dong)119 Academy-ro,
Yeonsu-gu, Incheon, Korea

D.V. Singh,
Professor, Ph.D,
University of Roorkee;
Roorkee, India, 247667

Wacław Szcześniak,
Foreign Member of RAACS,
Professor, Dr.Sc.,
Lublin University of Technology;
Ul. Nadbystrzycka 40,
20-618 Lublin, Poland

Tadatsugu Tanaka,
Professor, Dr.Sc.,
Tokyo University; 7-3-1 Hongo,
Bunkyo, Tokyo, 113-8654, Japan

Josef Vican,
Professor, Ph.D,
University of Žilina;
1, Univerzitná, Žilina, 010 26,
Slovakia

Zbigniew Wojcicki,
Professor, Dr.Sc.,
Wroclaw University
of Technology;
11 Grunwaldzki Sq., 50-377,
Wrocław, Poland

Artur Zbiciak, Ph.D.,
Warsaw University of
Technology;
Pl. Politechniki 1, 00-661
Warsaw, Poland

Segrey I. Zhavoronok, Ph.D.,
Institute of Applied Mechanics of
Russian Academy of Sciences;
Moscow Aviation Institute
(National Research University);
7, Leningradsky Prt.,
Moscow, 125040, Russia

Askar Zhussupbekov,
Professor, Dr.Sc.,
Eurasian National University;
5, Munaitpassov street, Astana,
010000, Kazakhstan

TECHNICAL EDITOR

Taymuraz B. Kaytukov,
Advisor of RAACS,
Associate Professor, Ph.D.,
Deputy Executive Scientific
Secretary of the Russian
Academy of Architecture and
Construction Sciences;
24, Ul. Bolshaya Dmitrovka,
107031, Moscow, Russia

EDITORIAL TEAM

Alexander V. Kuzmin,
Full Member of RAACS,
President of the Russian Academy of Architecture and Construction Sciences;
Research Center of Construction;
24, Ulitsa Bolshaya Dmitrovka,
107031, Moscow, Russia

Vadim K. Akhmetov, Professor, Dr.Sc., National Research Moscow State University of Civil Engineering; 26, Yaroslavskoe Shosse, 129337 Moscow, Russia

Pavel A. Akimov,
Full Member of RAACS,
Professor, Dr.Sc., Executive Scientific Secretary of the Russian Academy of Architecture and Construction Sciences;
Scientific Research Center "STADYO"; Tomsk State University of Architecture and Building; Russian University of Friendship of Peoples;
24, Ul. Bolshaya Dmitrovka,
107031, Moscow, Russia

Alexander M. Belostotsky,
Corresponding Member of RAACS, Professor, Dr.Sc.,
Research & Development Center "STADYO"; Russian University of Transport (RUT – MIIT); Russian University of Friendship of Peoples; Perm National Research Polytechnic University; Tomsk State University of Architecture and Building;
8th Floor, 18, ul. Tretya Yamskogo Polya,
125040, Moscow, Russia

Vladimir Belsky, Ph.D.,
Dassault Systèmes Simulia;
1301 Atwood Ave Suite 101W
02919 Johnston, RI, United States

Mikhail Belyi, Professor, Dr.Sc.,
Dassault Systèmes Simulia;
1301 Atwood Ave Suite 101W
02919 Johnston, RI, United States

Vitaly Bulgakov, Professor,
Dr.Sc., SemanticPro; Boston, USA

Charles El Nouty, Professor,
Dr.Sc., LAGA Paris-13 Sorbonne Paris Cite; 99 avenue J.B. Clément,
93430 Villetaneuse, France

Natalya N. Fedorova, Professor,
Dr.Sc., Novosibirsk State University of Architecture and Civil Engineering (SIBSTRIN);
113 Leningradskaya Street,
Novosibirsk, 630008, Russia

Darya Filatova, Professor,
Dr.Sc., Kielce University of Tecnology; 7, al. Tysiąclecia Państwa Polskiego, Kielce, 25-314, Poland

Vladimir Ya. Gecha, Professor,
Dr.Sc., Research and Production Enterprise All-Russia Scientific-Research Institute of Electromechanics with Plant Named after A.G. Iosiphyan;
30, Volnaya Street, Moscow,
105187, Russia

Taymuraz B. Kaytukov,
Advisor of RAACS, Ph.D,
Deputy Executive Scientific Secretary of the Russian Academy of Architecture and Construction Sciences;
24, Ul. Bolshaya Dmitrovka,
107031, Moscow, Russia

Amirlan A. Kusainov,
Foreign Member of RAACS,
Professor, Dr.Sc.,
Kazakh-American University,
9, Toraighyrov Str., Almaty,
050043, Republic of Kazakhstan

Marina L. Mozgaleva,
Professor, Dr.Sc., National Research Moscow State University of Civil Engineering;
26, Yaroslavskoe Shosse, 129337 Moscow, Russia

Nadezhda S. Nikitina,
Professor, Ph.D., Director of ASV Publishing House;
National Research Moscow State University of Civil Engineering;
26, Yaroslavskoe Shosse, 129337 Moscow, Russia

Nikolai P. Osmolovskii,
Professor, Dr.Sc.,
Systems Research Institute Polish Academy of Sciences;
Kazimierz Pulaski University of Technology and Humanities in Radom; 29, ul. Malczewskiego,
26-600, Radom, Poland

Gregory P. Panasenko, Professor,
Dr.Sc., Equipe d'Analise Numerique NMR CNRS 5585 University Gean Mehnet;
23 rue. P.Michelon 42023,
St.Etienne, France

Leonid A. Rozin, Professor,
Dr.Sc., Peter the Great Saint-Petersburg Polytechnic University;
29, Ul. Politechnicheskaya,
195251 Saint-Petersburg, Russia

Marina V. Shitikova, Professor,
Dr.Sc., Voronezh State Technical University; 14, Moscow Avenue,
Voronezh, 394026, Russia

Igor L. Shubin,
Corresponding Member of RAACS, Professor, Dr.Sc.,
Research Institute of Building Physics of Russian Academy of Architecture and Construction Sciences; 21, Lokomotivny Proezd, Moscow, 127238, Russia

Vladimir N. Sidorov,
Corresponding Member of RAACS, Professor, Dr.Sc.,
Russian University of Transport (RUT – MIIT); Russian University of Friendship of Peoples; Moscow Institute of Architecture (State Academy); Perm National Research Polytechnic University;
Kielce University of Technology (Poland); 9b9 Obrazcova Street,
Moscow, 127994, Russia

Valery I. Telichenko,
Full Member of RAACS,
Professor, Dr.Sc.,
The First Vice-President of the Russian Academy of Architecture and Construction Sciences;
National Research Moscow State University of Civil Engineering;
24, Ulitsa Bolshaya Dmitrovka,
107031, Moscow, Russia

Vladimir I. Travush,
Full Member of RAACS,
Professor, Dr.Sc., Vice-President of the Russian Academy of Architecture and Construction Sciences; Urban Planning Institute of Residential and Public Buildings; 24, Ulitsa Bolshaya Dmitrovka, 107031, Moscow, Russia

INVITED REVIEWERS

Akimbek A. Abdikalikov, Professor, Dr.Sc.,
Kyrgyz State University of Construction, Transport and Architecture n.a. N. Isanov;
34 Maldybayeva Str., Bishkek, 720020, Biskek, Kyrgyzstan

Irina N. Afanasyeva, Ph.D.,
University of Florida; Gainesville, FL 32611, USA

Ján Čelko, Professor, PhD, Ing.,
University of Žilina; Univerzitná 1, 010 26, Žilina, Slovakia

Tatyana L. Dmitrieva, Professor, Dr.Sc.,
Irkutsk National Research Technical University; 83, Lermontov street, Irkutsk, 664074, Russia

Petr P. Gaidzhurov, Professor, Dr.Sc.,
Don State Technical University; 1, Gagarina Square, Rostov-on-Don, 344000, Russia

Jacek Grosel, Associate Professor, Dr inz.
Wroclaw University of Technology; 11 Grunwaldzki Sq., 50-377, Wrocław, Poland

Stanislaw Jemioło, Professor, Dr.Sc.,
Warsaw University of Technology; 1, Pl. Politechniki, 00-661, Warsaw, Poland

Konstantin I. Khenokh, M.Ing., M.Sc.,
General Dynamics C4 Systems; 8201 E McDowell Rd, Scottsdale, AZ 85257, USA

Christian Koch, Dr.-Ing.,
Ruhr-Universität Bochum;
Lehrstuhl für Informatik im Bauwesen, Gebäude IA, 44780, Bochum, Germany

Gaik A. Manuylov, Professor, Ph.D.,
Moscow State University of Railway Engineering; 9, Obraztsova Street, Moscow, 127994, Russia

Alexander S. Noskov, Professor, Dr.Sc.,
Ural Federal University named after the first President of Russia B.N. Yeltsin;
19 Mira Street, Ekaterinburg, 620002, Russia

Nelli N. Rogacheva, Professor, Dr.Sc.,
National Research Moscow State University of Civil Engineering;
26, Yaroslavskoe Shosse, Moscow, 129337, Russia

Grzegorz Świt, Professor, Dr.hab. Inż.,
Kielce University of Technology; 7, al. Tysiąclecia Państwa Polskiego, Kielce, 25 – 314, Poland

AIMS AND SCOPE

The aim of the Journal is to advance the research and practice in structural engineering through the application of computational methods. The Journal will publish original papers and educational articles of general value to the field that will bridge the gap between high-performance construction materials, large-scale engineering systems and advanced methods of analysis.

The scope of the Journal includes papers on computer methods in the areas of structural engineering, civil engineering materials and problems concerned with multiple physical processes interacting at multiple spatial and temporal scales. The Journal is intended to be of interest and use to researches and practitioners in academic, governmental and industrial communities.

ОБЩАЯ ИНФОРМАЦИЯ О ЖУРНАЛЕ

International Journal for Computational Civil and Structural Engineering

(Международный журнал по расчету гражданских и строительных конструкций)

Международный научный журнал "International Journal for Computational Civil and Structural Engineering (Международный журнал по расчету гражданских и строительных конструкций)" (IJCCSE) является ведущим научным периодическим изданием по направлению «Инженерные и технические науки», издаваемым, начиная с 1999 года (ISSN 2588-0195 (Online); ISSN 2587-9618 (Print) Continues ISSN 1524-5845). В журнале на высоком научно-техническом уровне рассматриваются проблемы численного и компьютерного моделирования в строительстве, актуальные вопросы разработки, исследования, развития, верификации, апробации и приложений численных, численно-аналитических методов, программно-алгоритмического обеспечения и выполнения автоматизированного проектирования, мониторинга и комплексного наукоемкого расчетно-теоретического и экспериментального обоснования напряженно-деформированного (и иного) состояния, прочности, устойчивости, надежности и безопасности ответственных объектов гражданского и промышленного строительства, энергетики, машиностроения, транспорта, биотехнологий и других высокотехнологичных отраслей.

В редакционный совет журнала входят известные российские и зарубежные деятели науки и техники (в том числе академики, члены-корреспонденты, иностранные члены, почетные члены и советники Российской академии архитектуры и строительных наук). Основной критерий отбора статей для публикации в журнале − их высокий научный уровень, соответствие которому определяется в ходе высококвалифицированного рецензирования и объективной экспертизы, поступающих в редакцию материалов.

Журнал входит в Перечень ВАК РФ ведущих рецензируемых научных изданий, в которых должны быть опубликованы основные научные результаты диссертаций на соискание ученой степени кандидата наук, на соискание ученой степени доктора наук по научным специальностям и соответствующим им отраслям науки:

- 01.02.04 – Механика деформируемого твердого тела (технические науки),
- 05.13.18 – Математическое моделирование численные методы и комплексы программ (технические науки),
- 05.23.01 – Строительные конструкции, здания и сооружения (технические науки),
- 05.23.02 – Основания и фундаменты, подземные сооружения (технические науки),
- 05.23.05 – Строительные материалы и изделия (технические науки),
- 05.23.07 – Гидротехническое строительство (технические науки),
- 05.23.17 – Строительная механика (технические науки).

В Российской Федерации журнал индексируется Российским индексом научного цитирования (РИНЦ).

Журнал входит в базу данных Russian Science Citation Index (RSCI), полностью интегрированную с платформой Web of Science. Журнал имеет международный статус и высылается в ведущие библиотеки и научные организации мира.

Издатели журнала – *Издательство Ассоциации строительных высших учебных заведений /АСВ/* (Россия, г. Москва) и до 2017 года *Издательский дом Begell House Inc.* (США, г. Нью-Йорк). Официальными партнерами издания является *Российская академия архитектуры и строительных наук* (*РААСН*), осуществляющая научное курирование издания, и *Научно-исследовательский центр СтаДиО* (ЗАО НИЦ СтаДиО).

Цели журнала – демонстрировать в публикациях российскому и международному профессиональному сообществу новейшие достижения науки в области вычислительных ме-

тодов решения фундаментальных и прикладных технических задач, прежде всего в области строительства.

Задачи журнала:

- предоставление российским и зарубежным ученым и специалистам возможности публиковать результаты своих исследований;
- привлечение внимания к наиболее актуальным, перспективным, прорывным и интересным направлениям развития и приложений численных и численно-аналитических методов решения фундаментальных и прикладных технических задач, совершенствования технологий математического, компьютерного моделирования, разработки и верификации реализующего программно-алгоритмического обеспечения;
- обеспечение обмена мнениями между исследователями из разных регионов и государств.

Тематика журнала. К рассмотрению и публикации в журнале принимаются аналитические материалы, научные статьи, обзоры, рецензии и отзывы на научные публикации по фундаментальным и прикладным вопросам технических наук, прежде всего в области строительства. В журнале также публикуются информационные материалы, освещающие научные мероприятия и передовые достижения Российской академии архитектуры и строительных наук, научно-образовательных и проектно-конструкторских организаций.

Тематика статей, принимаемых к публикации в журнале, соответствует его названию и охватывает направления научных исследований в области разработки, исследования и приложений численных и численно-аналитических методов, программного обеспечения, технологий компьютерного моделирования в решении прикладных задач в области строительства, а также соответствующие профильные специальности, представленные в диссертационных советах профильных образовательных организациях высшего образования.

Редакционная политика. Политика редакционной коллегии журнала базируется на современных юридических требованиях в отношении авторского права, законности, плагиата и клеветы, изложенных в законодательстве Российской Федерации, и этических принципах, поддерживаемых сообществом ведущих издателей научной периодики.

За публикацию статей плата с авторов не взымается. Публикация статей в журнале бесплатная. На платной основе в журнале могут быть опубликованы материалы рекламного характера, имеющие прямое отношение к тематике журнала.

Журнал предоставляет непосредственный открытый доступ к своему контенту, исходя из следующего принципа: свободный открытый доступ к результатам исследований способствует увеличению глобального обмена знаниями.

Индексирование. Публикации в журнале входят в системы расчетов индексов цитирования авторов и журналов. «Индекс цитирования» — числовой показатель, характеризующий значимость данной статьи и вычисляющийся на основе последующих публикаций, ссылающихся на данную работу.

Авторам. Прежде чем направить статью в редакцию журнала, авторам следует ознакомиться со всеми материалами, размещенными в разделах сайта журнала (интернет-сайт Российской академии архитектуры и строительных наук (http://raasn.ru); подраздел «Издания РААСН» или интернет-сайт Издательства АСВ (http://iasv.ru); подраздел «Журнал IJCCSE»): с основной информацией о журнале, его целями и задачами, составом редакционной коллегии и редакционного совета, редакционной политикой, порядком рецензирования направляемых в журнал статей, сведениями о соблюдении редакционной этики, о политике авторского права и лицензирования, о представлении журнала в информационных системах (индексировании), информацией о подписке на журнал, контактными данными и пр. Журнал рабо-

тает по лицензии Creative Commons типа cc by-nc-sa (Attribution Non-Commercial Share Alike) – Лицензия «С указанием авторства – Некоммерческая – Копилефт».

Рецензирование. Все научные статьи, поступившие в редакцию журнала, проходят обязательное двойное слепое рецензирование (рецензент не знает авторов рукописи, авторы рукописи не знаю рецензентов).

Заимствования и плагиат. Редакционная коллегия журнала при рассмотрении статьи проводит проверку материала с помощью системы «Антиплагиат». В случае обнаружения многочисленных заимствований редакция действует в соответствии с правилами COPE.

Подписка. Журнал зарегистрирован в Федеральном агентстве по средствам массовой информации и охраны культурного наследия Российской Федерации. Индекс в общероссийском каталоге РОСПЕЧАТЬ − 18076.

По вопросам подписки на международный научный журнал “International Journal for Computational Civil and Structural Engineering (Международный журнал по расчету гражданских и строительных конструкций)” обращайтесь в Агентство «Роспечать» (Официальный сайт в сети Интернет: http://www.rosp.ru/) или в издательство Ассоциации строительных вузов (АСВ) в соответствии со следующими контактными данными:

ООО «Издательство АСВ»

Юридический адрес: 129337, Россия, г. Москва, Ярославское ш., д. 26, офис 705;

Фактический адрес: 129337, Россия, г. Москва, Ярославское ш., д. 19, корп. 1, 5 этаж, офис 12 (ТЦ Мебель России);

Телефоны: +7 (925) 084-74-24, +7 (926) 010-91-33

Интернет-сайт: www.iasv.ru. Адрес электронной почты: iasv@iasv.ru.

Контактная информация. По всем вопросам работы редакции, рецензирования, согласования правки текстов и публикации статей следует обращаться к главному редактору журнала члену-корреспонденту РААСН *Сидорову Владимиру Николаевичу* (адреса электронной почты: sidorov.vladimir@gmail.com, sidorov@iasv.ru, iasv@iasv.ru, sidorov@raasn.ru) или к техническому редактору журнала советнику РААСН *Кайтукову Таймуразу Батразовичу* (адреса электронной почты: tkaytukov@gmail.com; Kaytukov@raasn.ru). Кроме того, по указанным вопросам, а также по вопросам размещения в журнале рекламных материалов можно обращаться к генеральному директору ООО «Издательство АСВ» *Никитиной Надежде Сергеевне* (адреса электронной почты: iasv@iasv.ru, nsnikitina@mail.ru, ijccse@iasv.ru).

Журнал становится технологичнее. Издательство АСВ с сентября 2016 года является членом Международной ассоциации издателей научной литературы (Publishers International Linking Association (PILA)), осуществляющей свою деятельность на платформе CrossRef. Оригинальным статьям, публикуемым в журнале, будут присваиваться уникальные номера (индексы DOI – Digital Object Identifier), что значительно облегчит поиск метаданных и местонахождение полнотекстового произведения. DOI – это система определения научного контента в сети Интернет.

С октября 2016 года стал возможен прием статей на рассмотрение и рецензирование через онлайн систему приема статей Open Journal Systems на сайте журнала (электронная редакция): http://ijccse.iasv.ru/index.php/IJCCSE.

Автор имеет возможность следить за продвижением статьи в редакции журнала в личном кабинете Open Journal Systems и получать соответствующие уведомления по электронной почте.

В феврале 2018 года журнал был зарегистрирован в Directory of open access journals (DOAJ) (это один из самых известных поисковых сервисов в мире, который предоставляет открытый доступ к материалам и индексирует не только заголовки журналов, но и научные статьи), в сентябре 2018 года включен в продукты EBSCO Publishing.

International Journal for
Computational Civil and Structural Engineering
(Международный журнал по расчету гражданских и строительных конструкций)
Volume 15, Issue 1 ***2019***

Scientific coordination is carried out by the Russian Academy of Architecture and Construction Sciences (RAACS)

CONTENTS

Selection of the Computational Model of Wind Flow in the Problems of Computational Architectural and Civil Engineering Aerodynamics in Accordance with Regulatory and Technical Documents 14
Andrei V. Deineko, Aleksey I. Shamshurin, Narek A. Kazaryan

To the Question of the Determination of Geometric Characteristics of the Section of Corrugated Beams with Trapezoidal Webs Based on the Simulation Results 29
Tatiana L. Dmitrieva, Khukhuudei Ulambayar

The Method of Local Automatic Control of Thermophysical Parameters of External Walls of Buildings at the Locations of Condensate Loss 41
Sergej V. Fedosov, Pavel N. Mureev, Vitalij G. Kotlov, Aleksandr N. Makarov, Andrej V. Ivanov

Inelastic Analysis of Reinforced Concrete Structures in SCAD 54
Sergiy Yu. Fialko, Anatolii V. Perelmuter

The New Physically Nonlinear Finite Elements in Software Package LIRA 10.8 61
Yuriy D. Geraymovich, Isaak D. Yevzerov, Dmitriy V. Marchenko

Investigation of Heat-Humidity Transfer in High-Porous Gas-Filled Polymers to Calculate Its Heat Conductivity 67
Vladimir V. Gur'ev, Vadim I. Nikitin, Valeriy A. Kofanov

Using the Criterion of the Minimum Material Capacity of Rods Under Stability Restrictions for the Case of Multiple Critical Load 78
Leonid S. Lyakhovich, Pavel A. Akimov, Anatoly P. Malinowski

Bearing Capacity of Deep Pile Foundation for High-Rise Facility on Weak Soils: Comparing of Analysis Results and Experimental Data 90
Rashid A. Mangushev, Nadezhda S. Nikitina

Restabilization of the Postcritical Equilibrium of Elastic Systems 98
Gaik A. Manuylov, Sergey B. Kosytsyn, Maxim M. Begichev

Fire Design of Steel Structures 110
Anatolii V. Perelmuter

Simulation of Defectless Lifecycle of Unique Underground Structures of the Sewage System at the Stage of Their Construction in Difficult Soil Conditions 119
Nickolai A. Perminov

To the Assessment of Vertical Crane Load 131
Sergii F. Pichugin, Yulia E. Patenko

The Study of Complex Stress States of Elements Filling the Cells Between the Ribs of Wooden Large-Span Domes 140
Konstantin P. Pyatikrestovsky, Boris S. Sokolov

Searching Shear Forces Flows for an Arbitrary Cross-Section of a Thin-Walled Bar: Development of Numerical Algorithm Based on the Graph Theory 153
Vitalina V. Yurchenko

Control and Quality of Piles by Non-Destructive Express Methods: Low Strain Method and Cross-Hole Sonic Logging 170
Askar Zhussupbekov, Yoshinori Iwasaki, Eun Chul Shin, Nurgul Shakirova

International Journal for
Computational Civil and Structural Engineering
(Международный журнал по расчету гражданских и строительных конструкций)
Volume 15, Issue 1 ***2019***

Scientific coordination is carried out by the Russian Academy of Architecture and Construction Sciences (RAACS)

СОДЕРЖАНИЕ

Выбор расчетной модели ветрового потока в задачах вычислительной архитектурно-строительной аэродинамики в свете нормативно-технической базы 14
А.В. Дейнеко, А.И. Шамшурин, Н.А. Казарян

К вопросу определения геометрических характеристик сечения гофробалок с трапецеидальными стенками на основе компьютерного моделирования 29
Т.Л. Дмитриева, Х.Уламбаяр

Способ локального автоматического управления теплофизическими параметрами наружных стен зданий в местах выпадения конденсата 41
С.В. Федосов, П.Н. Муреев, В.Г. Котлов, А.Н. Макаров, А.В. Иванов

Реализация неупругого расчета железобетонных конструкций в программном комплексе SCAD 54
С.Ю. Фиалко, А.В. Перельмутер

Новые физически нелинейные конечные элементы в программном комплексе ЛИРА 10.8 61
Ю.Д. Гераймович, И.Д. Евзеров, Д.В. Марченко

Исследование тепловлагообмена в высокопористых газонаполненных полимерах применительно к расчету их теплопроводности 67
В.В. Гурьев, В.И. Никитин, В.А. Кофанов

Использование критерия минимальной материалоемкости стержней при ограничениях по устойчивости для случая кратной критической нагрузки 78
Л.С. Ляхович, П.А. Акимов, А.П. Малиновский

Несущая способность свайного фундамента глубокого заложения для высотных объектов на слабых грунтах: сопоставление результатов расчета и экспериментальных данных 90
Р.А. Мангушев, Н.С. Никитина

О возможности рестабилизации закритического равновесия некоторых упругих систем 98
Г.А. Мануйлов, С.Б. Косицын, М.М. Бегичев

Расчет огнестойкости стальных конструкций 110
А.В. Перельмутер

Моделирование бездефектного жизненного цикла уникальных подземных сооружений системы водоотведения на стадии их возведения в сложных грунтовых условиях 119
Н.А. Перминов

К оценке вертикальной крановой нагрузки 131
С.Ф. Пичугин, Ю.Э. Патенко

Исследование сложных напряженных состояний элементов заполнения ячеек между ребрами большепролетных куполов из древесины 140
К.П. Пятикрестовский, Б.С. Соколов

Поиск потоков касательных усилий для произвольного сечения токостенного стержня: разработка численного алгоритма на основе теории графов 153
В.В. Юрченко

Контроль качества свай неразрушающими экспресс-методами: методы отраженной волны при низкой нагрузке и межскважинной дефектоскопии 170
А. Жусупбеков, Й. Ивасаки, Юн Чул Шин, Н. Шакирова

SELECTION OF THE COMPUTATIONAL MODEL OF WIND FLOW IN THE PROBLEMS OF COMPUTATIONAL ARCHITECTURAL AND CIVIL ENGINEERING AERODYNAMICS IN ACCORDANSE WITH REGULATORY AND TECHNICAL DOCUMENTS

Andrei V. Deineko, Aleksey I. Shamshurin, Narek A. Kazaryan
Spectrum Group of Companies, Moscow, RUSSIA

Abstract: An overview of the main directions of numerical simulation of problems of architectural and civil engineering aerodynamics based on Computational Fluid Dynamics (CFD) is presented. The main advantages of numerical simulation in comparison with traditional methods of aero-physical modeling in wind tunnels are highlighted. The basic principles of numerical simulation of wind loads and actions on buildings and structures are outlined. In modern practice, numerical modeling by finite volume method is used with the decomposition of the velocity of the turbulent wind flow into the average and pulsation component within the averaged by Reynolds solution of Navier-Stokes equations using the semi-empirical turbulence model k-ω SST. In practice, the problem of the legitimate (in accordance with the requirements of building codes) selection of a computational model of wind flow is very important. This is equivalent to the assignment of boundary conditions within numerical simulation. The computational model of the wind, presented in the Russian building codes, requires additions to solve the problems of numerical simulation of architectural and civil engineering aerodynamics. A detailed comparison of the computational models of wind flow in Russian and foreign building codes is carried out. The following wind flow parameters are analyzed: the profile of the average wind speed, the profile of the intensity of turbulence, the profile of the scale of turbulence. A table of correspondence of terrain types according to the classification of Russian and foreign codes is proposed. The possibility of determining the parameters of the computational wind flow model based on the joint use of building codes in force in Russia and Belarus is shown. A set of measures is proposed with the goal of creating a regulatory and technical environment for the practical application of computational architectural and civil engineering aerodynamics in real design.

Keywords: numerical simulation, computational architectural and civil engineering aerodynamics, computational fluid dynamics (CFD), wind loads, pedestrian comfort

ВЫБОР РАСЧЁТНОЙ МОДЕЛИ ВЕТРОВОГО ПОТОКА В ЗАДАЧАХ ВЫЧИСЛИТЕЛЬНОЙ АРХИТЕКТУРНО-СТРОИТЕЛЬНОЙ АЭРОДИНАМИКИ В СВЕТЕ НОРМАТИВНО-ТЕХНИЧЕСКОЙ БАЗЫ

А.В. Дейнеко, А.И. Шамшурин, Н.А. Казарян
Группа компаний «Спектрум», г. Москва, РОССИЯ

Аннотация: Представлен обзор основных направлений численного моделирования задач архитектурно-строительной аэродинамики на основе вычислительной механики жидкости и газа (CFD-технологий). Отмечены основные преимущества численного моделирования по сравнению с традиционными способами аэрофизического моделирования в аэродинамических трубах. Изложены базовые принципы численного моделирования ветровых нагрузок и воздействий на здания и сооружения. В современной практике применяется численное моделирование методом конечных объёмов с разложением скорости турбулентного ветрового потока на среднюю и пульсационную составляющую в рамках решения осреднённых по Рейнольдсу уравнений Навье-Стокса с использованием полуэмпирической модели турбулентности k-ω SST. На практике большое значение имеет проблема легитимного (в соответствии с требованиями строительных норм) выбора расчётной модели ветрового потока, что эквивалентно назначению гранич-

ных условий в рамках численного моделирования. Расчётная модель ветра, представленная в российских строительных нормах, требует дополнения для решения задач численного моделирования архитектурно-строительной аэродинамики. Проведено детальное сопоставление расчётных моделей ветрового потока в российских и зарубежных строительных нормах. Проанализированы следующие параметры ветрового потока: профиль средней скорости ветра, профиль интенсивности турбулентности, профиль масштаба турбулентности. Предложена таблица соответствия типов местности по классификации российских и зарубежных норм. Показана возможность определения параметров расчётной модели ветрового потока на основе совместного использования строительных норм, действующих в России и Белоруссии. Предложен комплекс мер с целью создания нормативно-технический условий для практического применения вычислительной архитектурно-строительной аэродинамики в реальном проектировании.

Ключевые слова: численное моделирование,
вычислительная архитектурно-строительная аэродинамика,
вычислительная механика жидкости и газа (CFD-технологии), ветровые нагрузки,
пешеходная комфортность

1. INTRODUCTION IN COMPUTATIONAL ARCHITECTURAL-CONSTRUCTIONAL AERODYNAMIC

A major achievement of the theory and practice of design justification for buildings and structures in the 21st century becomes the development of a new direction of calculation - numerical modeling of architectural-constructional aerodynamics using computational fluid dynamics, CFD technology. The following areas of practical application of computational architectural-construction aerodynamics, as well as the environmental and wind energy aerodynamics that are close to one in the methodological sense, were formed [1–7]:

- external aerodynamics (environmental aerodynamics), i.e. modeling of wind flows in the surface boundary layer, taking into account the influence of the surrounding buildings and terrain:
  - determination of wind loads and impacts on buildings and structures;
  - determination of snow loads on buildings and structures;
  - evaluation of wind pedestrian comfort and justification of wind-protective measures;
  - modeling the spread of air pollution, evaluating the effectiveness of sanitary protection zones (SPZ), modeling accident scenarios;
  - assessment of environmental comfort and justification of measures for environmental protection;
  - modeling of the wind energy potential of the area, optimization of the arrangement of wind generators within wind power plants;
- internal aerodynamics, i.e. simulation of air movement in the premises, taking into account the operation of the heating system, ventilation and air conditioning (HVAC):
  - room microclimate modeling to optimize the HVAC system in order to achieve optimal (and not only acceptable) microclimate parameters in 100% of the working area, as well as to increase energy efficiency due to rationalization of air distribution;
  - modeling of the distribution and disposal of industrial air pollution and scenic smoke;
  - modeling of smoke removal and gas fire extinguishing.

Let us note the “flagship” role of numerical modeling of wind loads, the methodology of which summarizes the main scientific and practical issues of architectural-constructional aerodynamics, and the requirements for wind loads, methodological and reference data are regulated by regulatory and technical documents [8–12]. Let us reveal the advantages and new possibilities of numerical modeling of wind loads in

comparison with traditional methods of aerophysical research in wind tunnels:

- practical one, related to the expansion of the possibilities of computational justification:
  - consideration without any decrease in the accuracy of arbitrary area of the territory, arbitrary configuration of the building, arbitrary surrounding building, any terrain;
  - detailing the distribution of wind load during 100% of the facade area;
  - the ability to analyze the results at any point in the problem area of the numerical model, including the one that is not originally planned;
- calculational-theoretical advantages related to the refinement of the modeling statement:
  - modeling in natural scale of space and speed, that solves the problem of similarity;
  - transfer to the setting of the external flow (from the setting of the internal flow), that reduces the influence of the borders of the simulation region;
  - the absence of flow distortions from measuring instruments, which allows to obtain any necessary discretization of the results.

2. CFD-TECHNOLOGIES IN XXI CENTURY

The formation of continuous flow mechanics in the meaning, that is close to the modern, began in the XVIII century, that is associated with the names of academicians of the Russian Academy of Sciences Leonard Eyler and Daniel Bernoulli. In the 19th century, Navier, Poisson, Saint-Venant and Stokes formulated a general law of flow motion in the form of a system of differential partial differential equations (Navier-Stokes equations), which are the basis of modern numerical simulation.

The development of computational mechanics of liquids and gases (CFD-technologies) [13–14] dates back to the 1980s, when the first industrial software systems were developed, the new versions of which are used to this day: PHOENICS (Great Britain 1981); FIDAP (USA, 1982), Fluent (USA, 1983), TASCflow (Canada, 1985), Flow3D / CFX (United Kingdom, 1980s), the last four soft wares have been merged into ANSYS CFD now; Flow-3D (USA, 1985); Star CD (UK / USA, 1989); FlowVision (USSR / Russia, 1991).

Currently, CFD-technologies are widely implemented in practical engineering work in many industries, with deep integration into the design and design processes.

The technologies of high-performance computing are being improved, in particular, parallel computing on the graphic processors of the CUDA technology [15].

Multi-physical (interdisciplinary, connected) calculations are being actively implemented, based on the modeling of various physical aspects of the design scheme (such as stress-strain state, heat transfer, aerohydrodynamics) in interaction. In particular, this allows calculations of buildings and structures in an aeroelastic arrangement.

3. AN APPROACH TO NUMERICAL MODELING OF WIND FLOWS

Numerical modeling of aerodynamic problems is performed, as a rule, by the finite volume method (FVM). For this, a grid approximation of the calculated area of the airspace is carried out, and boundary and initial conditions are assigned. Analogously to the strength finite-element calculations, the construction of an effective finite-volume grid requires rational discretization of the characteristic regions of the aerodynamic design scheme taking into account the factor of grid convergence.

It is convenient to accept a cylindrical form of the calculated area of the airspace, in order that the conditions of numerical simulation are similar for any wind direction. The lower surface of the model reproduces the investigated building,

the surrounding building and the terrain. The height of the model equals to approximately 10 characteristic height of the highest object in the design scheme, but not less than the height of the prism boundary layer
0.5 km, within which the boundary conditions vary significantly throughout the height. The model's radius is assigned taking into account the specific features of the investigated building, surrounding constructions and terrain, and reaches 1–2 km.

Due to frictional forces, viscous air near the surface (ground or wind front of the building) is braked, as a result of which the air velocity at the surface tends to zero. In the wall laminar sublayer air velocity is small. As the distance from the surface increases, the speed increases according to the logarithmic law until the speed of the main flow is reached.

The thickness of the near-wall layer and the nature of the distribution of velocity in it depend on the roughness of the surface. It is formed, for example, by niches of window openings in the facade of a building or by trees on the surface of the earth. There are two approaches to the modeling of roughness: explicit or using near-wall functions. For the wind front of the building, the first method is suitable, which assumes accurate reproduction of the geometry of the wind front of the building (parapets, window openings, etc.). For large areas of the earth's surface, the second method is suitable, when the roughness (formed by vegetation and the construction of settlements) is assigned as a parameter of the wall function based on reference data. Approximate parameters of roughness for various types of terrain are given, for example, in foreign standards, discussed below.

Wind flows are assumed to be incompressible (since the wind speed is substantially lower than the speed of sound) and isothermal [1–5].

The simulation of turbulent air movement is based on the decomposition of velocity into the average and pulsating component. Reynolds-averaged Navier-Stokes equations (Reynolds-Averaged Navier-Stokes, RANS) proposed by Reynolds in 1895 are solved. In this case, turbulent stresses, or Reynolds stresses, are introduced that takes into account the losses and redistribution of energy in the turbulent flow (as compared to the laminar flow), which are random in nature. For its definition, semi-empirical models of turbulence are used.

For solving a wide range of practical engineering problems when modeling incompressible flows, the model of the type k-ε is used most often. For near-wall flows, models of the k-ω type are widely used, in particular, the shear stress transfer model k-ω SST (Shear Stress Transport) [16].

Since the interaction of flow with surfaces plays a large role in wind aerodynamic problems, it is advisable to use k-ω SST as the main model of turbulence.

According to the Euler method, the results of aerodynamic calculations are presented as flow parameters at a particular point in the non-moving space at certain points in time, i.e. the fields of flow parameters and the change of fields in time are considered. The trajectories of the movement of elementary volumes of air can be restrictedly represented as current lines.

The main engineering results of numerical simulation are:

- distribution of the main and peak wind load on the wind front of the building;
- spectrum of the main wind load;
- total aerodynamic force on the building and torque relative to the selected point;
- distribution of wind speeds at the height of pedestrians, assumed to be 1.5 m from the ground [12].

The wind load is understood to be the wind pressure (active pressure or wind suction, the sum of the average and pulsation component) determined in design conditions according to building codes.

The main wind load is the wind load at a specific wind direction.

Peak wind load is the largest wind loadб that is possible on the considered fragment of the wind front.

The main wind load is taken into account in constructive calculations of the bearing system

of the building as a set of loads of different size and direction, acting simultaneously on the entire area of the wind front (on the windward, leeward and lateral sides, on the envelop). Accordingly, the main wind load is determined for those wind directions for which constructive calculations of the bearing system are necessary (usually at four directions along the main axes).
Peak wind load is taken into account in constructive calculations of facade, large window, advertising and other structures, located at the wind front of the building and working locally, regardless of the load on the other parts of the wind front. Peak wind load corresponds to the lower and upper envelope (min / max imposition) of wind pressures obtained from calculations for various wind directions. Accordingly, it is necessary to take into account the representative number of directions of the wind. In practice, from 16 to 32 directions are taken into account, usually 24 directions (an angular step of 15 °) [1, 3].
The results of numerical simulation can be compared with the results of aero-physical tests in a wind tunnel:

- main and peak wind load, as well as the wind load spectrum - with the results of drainage tests, when the wind pressure is measured on the scale model at the points of drainage (holes connected to a pressure gauge);
- total aerodynamic force and torque — with the results of weight tests, when the force and torque are measured on a scale model using aerodynamic weights;
- wind speeds in the pedestrian zone - with the results of airflow visualization using the method of mulberry or a digital tracer visualization method.

4. SELECTION OF THE DESIGN MODEL OF A WIND FLOW

The legitimate choice of the design model of the wind flow, which corresponds to the purpose of the boundary conditions at numerical simulation, is one of the key issues that has been addressed by experts in the field of computer and experimental aerodynamics.
Let us emphasize that in wind aerodynamics, the design scheme of the airspace corresponds to the conditions of strong wind. The purpose of the calculations is to determine the wind load on the buildings, to study the interaction of the building and the wind flow in the aero elastic formulation, and also to estimate the wind pedestrian comfort. Consequently, the wind flow model should cover the range of average speeds starting from the level of wind discomfort of about 6 m/s and up to 45 m/s (which corresponds to the VII wind region according to Table 1 below). Other speed modes do not require regulation in documents on wind loads on buildings and structures.
The ability of the wind to exert wind pressure is due to the kinetic energy of the moving air and is characterized by the velocity head *W*:

$$W = \rho V^2/2 \qquad (1)$$

where V is velocity of air moving; ρ is air density.
The atmosphere is turbulent. The velocity of the air (and hence the velocity head) undergoes random fluctuations or pulsations, which are subject to statistical laws. In accordance with the above RANS-approach, the velocity is described by the average component of the velocity V_m, equal to its expectation, and the standard deviation σ_V. The degree of turbulence is conveniently characterized by the intensity of turbulence I, expressed in relative units or percentages:

$$I = \sigma_V/V_m \qquad (2)$$

In a gust, the wind speed deviates from V_m more than σ_V. Deviations of more than the pulsation velocity component $V_p = \gamma_V \sigma_V$ rarely occur, where γ_V is usually called the coefficient of security, which usually takes values from 3 to 4. Similarly, the velocity head W_m, its standard deviation σ_W, the velocity pulsation component

can be considered head W_p and coefficient of security γ_W.

It is fundamentally important to take into account the duration of the wind as the implementation of a random process, which determines the probability of deviation of the wind flow parameters from the expected values during the considered period of time.

Changes in wind speed occur in a wide range [17–20], and the spectrum is divided into two parts, as shown in figure 1 [17]. The left part is macro meteorological, in which changes in wind force are associated with changes in weather and have periods from several hours to a month. The right side is micrometeorological, where changes in speed are associated with turbulence and have periods from 3 seconds to 10 minutes.

From this it follows that it is rational to conduct statistical processing of wind measurements on two time scales - macro meteorological and micrometeorological, which is customary in world wind engineering.

For definiteness, let us denote the speed and wind pressure, given by specific recurrence, in lower case letters *v* and *w*.

The average wind speed v_m is usually understood as a speed averaged over a 10-minute period, exceeding on average 1 time in 5 years (the annual probability of exceeding 0.2 or 1 case for 262,980 10-minute observation cycles), or 1 time in 50 years (annual probability of exceeding 0.02 or 1 case per 2,629,800 observation cycles).

The pulsation component of the wind speed v_p means the maximum value of the speed averaged over a time interval significantly less than 10 minutes. As a rule, a 3-second period is considered. Accordingly, the standard deviation σ_v characterizes the distribution of the velocity deviation with a 3-second averaging of the corresponding speed with a 10-minute averaging under strong wind conditions. The probability of exceeding v_p in the regulatory documents is not specified. Moreover, the characteristic period for estimating the probability of exceeding v_p is 10 minutes, i.e. 200 cycles of 3 seconds.

Thus, the computational model is a wind flow with an average speed v_m with gusts up to the speed v_m+v_p. To describe the wind flow with engineering accuracy must be considered:

- average speed and its change in height $v_m(z)$;
- turbulence intensity and its change in height $I(z)$;
- the periodicity of the velocity pulsation, which can be represented by the scale of turbulence and its variation in the height $L(z)$.

The scale of turbulence is the length of the largest eddies. In the atmosphere, large eddies break up into smaller ones (turbulent cascade), which is taken into account in numerical simulation using the turbulence model. The passage of different-scale vortices carrying different kinetic energy forms the spectrum of wind impact.

The Russian regulatory documents [8–12] are based on regionalization by wind pressure; wind speed is not considered. The standard wind pressure w_0 is the velocity head of the wind flow in an open area at a height of 10 m, averaged over a 10-minute period, exceeding on average 1 time in 5 years.

The wind load is considered as the sum of the average w_m and the pulsation w_p component with a wind load coefficient γ_f of 1.4:

$$\gamma_f w(z_e) = \gamma_f \left(\mathrm{w}_m(z_e) + \mathrm{w}_p(z_e)\right) \quad (3)$$

The wind load reliability coefficient γ_f plays the role of a probabilistic transition coefficient from 5-year to 50-year repeatability [20].

The change in wind pressure in height and the influence of the type of terrain are taken into account separately for the average and pulsating component:

$$\gamma_f \mathrm{w}_m(z_e) = \gamma_f \mathrm{w}_0 k(z_e) c \quad (4)$$

$$\gamma_f \mathrm{w}_p(z_e) = \gamma_f \mathrm{w}_m \xi \zeta(z_e) \nu \quad (5)$$

where $k(z_e)$ is coefficient depending on the type of terrain, taking into account the change in

the average component for the equivalent height z_e;
$\zeta(z_e)$ is wind pressure ripple factor, depending on the type of terrain, taking into account the change in the pulsation component for the equivalent height z_e;
c is aerodynamic pressure coefficient depending on the shape of the wind front;
ν is the coefficient of spatial correlation of the wind pressure fluctuations, depending on the size and aspect ratio of the building surface under consideration;
ξ is the dynamic factor, depending on the height and first frequency of the building's natural oscillations, not taken into account for the majority of buildings of ordinary height.
Let us clarify, that to describe the wind flow in the framework of numerical modeling, instead of wind pressure, we consider a velocity head equivalent to wind pressure without taking into account coefficients depending on the building, i.e. with unit values of the coefficients c, ν, ξ, as well as with an equivalent height z_e equal to the ordinary height z. The wind load is formed taking into account the geometry of the building and the mode of wind flow around it as a result of aerodynamic calculation.
The relationship between velocity head and wind speed, taking into account the frequency of occurrence, is determined by the formulas [8–10]:

$$\mathrm{w}_0 = 0{,}43v_{50}^2 \quad (6)$$
$$\mathrm{w}_0 = 0{,}61v_0^2 \quad (7)$$

where v_0 and v_{50} are, respectively, wind speed exceeded on average once every 5 and 50 years.
Let us note that the coefficient of 0.61 is equal to ρ/2 at an air density of 1.22 kg/m^3, which corresponds to the conditions of the international standard atmosphere.
The coefficient 0.43 has a similar physical meaning and additionally includes a probabilistic coefficient of transition from 5-year to 50-year repeatability.
Therefore, we have:

$$v_{50}/v_0 = 1.19 \quad (8)$$
$$w_{50}/w_0 = 1.42 \approx \gamma_f = 1.4 \quad (9)$$

The estimated average wind speed, determined taking into account the coefficient γ_f, has a 50-year repeatability:

$$v_m(z) = \left(\gamma_f w_0 k(z)/0.61\right)^{0.5} \quad (10)$$

The maximum wind speed in the gust is determined in the formula

$$v_{max}(z) = \left(\gamma_f w_0 k(z)\left(1+\zeta(z)\right)/0.61\right)^{0.5} \quad (11)$$

Russian norms [8–12] do not provide information on the definition of the standard of speed $\sigma_v(z)$, standard of velocity head $\sigma_w(z)$, intensity of turbulence $I(z)$, scale of turbulence $L(z)$.
To estimate these values, additional data are needed that are not included in the materials [8–12]. Consider 2 variants for determining $I(z)$.
Variant 1. According to data [19–20], the coefficient of provision of the pulsation component of the wind load is 3.0, i.e.

$$\sigma_w(z) = \mathrm{w_p}(z_e)/3,$$

whence we have:

$$I(z) = (1+\zeta(z)/3)^{0.5} - 1 \quad (12)$$

Variant 2. According to the data of [2], the coefficient of security of the pulsation component of the wind speed is 3.5, i.e.

$$\sigma_v(z) = \mathrm{v_p}(z_e)/3.5,$$

whence we have:

$$I(z) = \left(\left(1+\zeta(z)\right)^{0.5} - 1\right)/3.5 \quad (13)$$

Thus, the assessment of the intensity of turbulence $I(z)$ is contradictory and requires additional data that are not fixed in the normative literature.

It is not possible to estimate the profile of the scale of turbulence $L(z)$ using normative data.

In general, the determination of turbulence parameters, in our opinion, is beyond the limits of the applicability of the method [8–10], therefore, formulas (12) and (13) cannot be used for practical calculations.

Thus, the computational model of wind flow, which forms the basis of Russian norms, is not enough for numerical simulation. This necessitates the recourse to foreign norms. The most detailed design model of wind flow, according to our assessment, is presented by Eurocode [21] and in the Italian CNR-DT standards [22]. These documents allow to explicitly define the desired parameters $v_m(z)$, $I(z)$, $L(z)$. Let us note that the Russian translation of the Eurocode [21] was officially introduced in Belarus as a technical code of established practice [23].

Foreign standards [21–23] use zoning by wind speed, which is taken as the speed in an open area at a height of 10 m, averaged over a 10-minute period, exceeded on average once every 50 years. This speed is equivalent to v_{50} according to the notation adopted above, or v_m at a height of 10 m, determined taking into account the coefficient γ_f.

Let us consider the parameters of the calculated wind flow model according to [21, 23]:

$$\left.\begin{array}{c} v_m(z) = c_r(z)c_o(z)v_b c_{prob} \\ c_r(z) = k_r \ln(z/z_0) \\ k_r = 0.19(z_0/0.05)^{0.07} \\ v_b = c_{dir}c_{season}v_{b,0} \end{array}\right\} \quad (14)$$

$$\left.\begin{array}{c} I(z) = \sigma_v/v_m(z) \\ \sigma_v = k_r v_b k_I \end{array}\right\} \quad (15)$$

$$\left.\begin{array}{c} L(z) = L_t\,(z/z_t)^{\alpha} \\ \alpha = 0.67 + 0.05\ln(z_0) \end{array}\right\} \quad (16)$$

$$z_{min} \le z \le z_{max} \quad (17)$$

where $v_{b,0}$ is the main value of the base wind speed according to wind zoning (normal value);

v_b is the basic value of wind speed;

c_{dir} is wind direction coefficient of 1.0 unless otherwise indicated in the Eurocode national application;

c_{season} is a seasonal coefficient of 1.0, if there are not another indication in the national Euro code application; k_r is area coefficient; $c_r(z)$ is coefficient taking into account the type of terrain; $c_o(z)$ is orographic coefficient equal to 1.0 for an average slope less than 3 ° (approximately 5%); c_{prob} is probabilistic coefficient of 1.0 with 50-year repeatability; σ_v is pulsation standard deviation of wind speed; k_I is turbulence coefficient of 1.0 unless otherwise indicated in the Eurocode national application; L_t is base turbulence scale; z_t is turbulence base height; z_0 is roughness parameter according to type of terrain according to Eurocode (table 2); z_{min} is the minimum height according to the Eurocode locality (Table 2), if $z < z_{min}$ it should be accepted $z = z_{min}$; z_{max} = 200 m is a maximum height for applying formulas.

For comparison, we consider the parameters of the calculated wind flow model according to [22].

$$\left.\begin{array}{c} v_m(z) = v_r c_m(z) \\ c_m(z) = k_r \ln(z/z_0)\, c_t(z) \\ v_r = v_b c_r \end{array}\right\} \quad (18)$$

$$I(z) = 1/\ln(z/z_0)\, c_t(z) \quad (19)$$

$$L(z) = \bar{L}(\mathrm{z}/\bar{\mathrm{z}})^{\kappa} \quad (20)$$

$$z_{min} \le z \le z_{max} \quad (21)$$

where v_b is the base value of wind speed according to wind zoning (standard value); v_r is design value of wind speed; c_r is probability coefficient equal to 1.0 with 50-year repeatability; $c_m(z)$ is wind velocity profile coefficient; k_r is area coefficient; c_t is a topographical coefficient of 1.0 with an average slope less than 5%; $\bar{L}$ = 300 м is base turbulence scale; $\bar{z}$ is turbulence base height; κ – coefficient accepted by table from CNR-DT 207/2008 (Table 2); z_0 is roughness parameter according to type of terrain according to CNR-DT 207/2008 (Table 2); z_{min} is the minimum height according to CNR-DT 207/2008 (table 2), if $z < z_{min}$ it should be accepted $z = z_{min}$; z_{max} = 200 м is a maximum height for applying formulas.

A comparison of the calculated wind models is shown in Figures 2-4 using the example of the I wind region according to Russian standards. Accordingly, the base wind speed is assumed to be 23.0 m/s according to Table 1.

In all variants of the calculated model of wind, wind flow parameters are constant up to a certain z_{min} takes the value from 2 to 12 m, depending on the type of terrain. It is in the section $z < z_{min}$ that the difference in wind models is most noticeable. At $z > z_{min}$, the profiles of the calculated parameters of the wind flow in all models converge.

The averaged velocity profile $v_m(z)$ increases with height (Figure 2). For $z < z_{min}$, Russian norms give the highest estimate of speed.

The turbulence intensity profile $I(z)$ decreases with height (Figure 3). The estimation of the intensity of turbulence using formulas (12) and (13) should be considered as unrepresentative. For $z < z_{min}$, the Eurocode gives the greatest estimate of the intensity of turbulence.

The turbulence scale profile $L(z)$ increases with height (Figure 4). The greatest estimate of the scale of turbulence give Italian standards.

Since the physical characteristics of wind flows in the framework of wind aerodynamics are uniform for the entire prism boundary layer of the Earth, it seems appropriate to use data on the intensity and scale of turbulence borrowed from foreign norms in calculations for the territory of Russia. Namely, on the basis of the Technical Code of Established Practice [23], published in Russian and introduced in the Union State of Belarus. At the same time, the standard wind pressure w_0 should be taken according to wind zoning in accordance with current Russian standards [8–9]. It is advisable to take the profile of average wind speed according to Russian standards as the most conservative.

5. NUMERICAL MODELING OF WIND LOADS AND NORMATIVE BASE

In general, against the background of the progress of CFD-technologies and it widespread use for solving practical engineering problems in many industries, the method of numerical modeling of wind loads and impacts [1, 3] should be considered as formed part of the system of global engineering knowledge. The necessary initial data are fixed in the normative-technical literature of a number of countries [21–22], including Belarus [23]. In Russia and abroad, great experience has been gained in practical calculations of wind loads in real design problems.

The urgency of the tasks of architectural-constructional aerodynamics in modern construction is growing:

- the complicity of buildings' architectural formation increases, that makes it impossible to determine wind loads and impacts analytically according to the engineering methodology of the Rules;
- the use of light facade systems, for which it is important to correctly take into account the actual distribution of peak wind pressure over the facade area, is expanding;
- construction of buildings closes to each other (for example, towers on a common stylobate), and construction in conditions of dense urban development, where the influence of air flow interference on wind loads cannot be neglected, grows;
- high-rise construction is expanding, in particular, Russia owns records for the height of buildings in Europe (the “Federation Tower” with a height of 374 m in the Moscow International Business Center; the Lakhta Center under construction with a height of 462 m in St. Petersburg);
- increasing social and regulatory requirements for comfort, in particular, the assessment of wind pedestrian comfort is provided in [8, 9 and 12].

At the same time, the degree of implementation of computational architectural-construction aerodynamics in real design significantly lags behind existing capabilities and international experience. The main reason for this state of affairs is the lack of a regulatory base, that does not allow us to present the results of numerical

modeling of wind loads as part of the mandatory expertise of the project documentation.

In the Russian system of regulatory documentation, numerical modeling of wind loads and impacts is considered only in GOST R 56728-2015 "Buildings and structures. Method for determining wind loads on enclosing structures" [13]. However, this standard is focused on conducting experimental design studies and provides for numerical simulation exclusively in the formulation of a virtual wind tunnel, when the numerical model reproduces the conditions of an aero physical experiment in a wind tunnel, taking into account the scale of the simulation. Such a statement devaluates the computational and theoretical advantages of numerical simulation, which lies precisely in the simulation on a natural scale under external flow conditions.

In our opinion, the following solutions are necessary for the further development of computational architectural-constructional aerodynamics in Russia.

1. Adopt the Handbook to SP 20.13330.2016 "Loads and Impacts" for calculating wind loads and impacts using the methods of numerical architecture and roof aerodynamics based on the detailed proposals declared in [3]. The manual should contain specific requirements for aerodynamic design schemes and methods of numerical simulation.

In particular, the Manual should contain an algorithm for the purpose of the calculated model of the wind. We believe it is advisable to recommend the use of the algorithm considered in this article, based on the sharing of normative-technical documents in force in Russia and Belarus.

2. To verify the software implementing CFD technology in relation to the determination of wind loads of impacts (similar to the verification of software for strength calculations, which has been carried out at RAACS for a number of years).

3. To supplement GOST R 56728-2015 with the section "Computer (numerical) modeling in the conditions of natural and man-made environment", in which to take into account the specifics of the development of numerical aerodynamic models of cylindrical configuration on a natural scale in the formulation of external flow.

In our opinion, among the common problems, the greatest advantages of numerical simulation of wind loads manifests itself in determining the peak wind load on buildings of ordinary height with light facade and stained glass systems.

CONCLUSIONS

1. The ability to numerically simulate the tasks of architectural-constructional aerodynamics using computational fluid and gas mechanics (CFD technologies) is due to the fundamental theoretical basis and many years of interdisciplinary experience in solving applied engineering problems in a wide range of parameters of the studied currents.
2. The necessary data for the purpose of the design model of the wind flow should be contained in the aggregate of regulatory and technical documents adopted in Russia and Belarus. The standards are available in Russian and, in our opinion, it should be recommended for joint use.
3. The development of the regulatory and technical base for wind loads and impacts, in our opinion, should go along the path of adopting the Handbook for SP 20.13330.2016 "Loads and Impacts" for calculating wind loads and impacts using computational architectural-constructional aerodynamics.

ACKNOWLEDGMENTS

The authors are grateful for the organizational support of the work and the promotion of the implementation of computational architectural-constructional aerodynamics in the real design of V.F. Ivanov, N.A. Clementyev and S.N. Suvorov (Spectrum Group); for useful discussions and valuable advice in preparing the work of N.N. Fedorova and S.A. Valger (Scientific and Educational Center of Computer Modeling

“CADFEM-Sibstrin” at NSACEU); for a series of lectures at MGSU in 2018 within the framework of the author's advanced training program “Strategies for calculating wind influences. System views "M.I. Kazakevich.
Special thanks for the many years of mentoring in the field of computational architectural-constructional aerodynamics, the authors express to S.I. Dubinsky.

REFERENCES

1. **Dubinskii S.I.** Chislennoe Modelirovanie Vetrovyh Vozdejstvij na Vysotnye Zdaniya [Numerical Modeling of Wind Effects on High-Rise Buildings]. Dis. kand. tekhn. nauk (Ph.D Thesis). Moscow, MGSU, 2010 (in Russian).
2. **Poddaeva O.I., Kubenin A.S., Churin P.S.** Arhitekturno-Stroitel'naya Aehrodinamika [Architectural and Building Aerodynamics]. Moscow, MGSU, 2015 (in Russian).
3. **Belostotsky A.M., Akimov P.A., Afanaseva I.N.** Vychislitel'naya Aehrodinamika v Zadachah Stroitel'stva [Computational Aerodynamics in Construction Problems]. Moscow, ASV Publishing House, 2017 (in Russian).
4. **Valger S.A., Fedorova N.N., Fedorov A.V.** Chislennoe Issledovanie Interfe-rencionnyh Effektov, Voznikajushhih v Vozdushnom Potoke pri Obtekanii Kom-pleksa Zdanij Slozhnoj Formy [Numerical Study of the Interference Effects Arising in the Air Flow in the Flow Around a Complex of Buildings of Complex Shape]. // *Thermophysics and Aeromechanics*, 2017, Volume 24, Number 1(103), pp. 35-44 (in Russian).
5. **Valger S.A., Fedorova N.N., Fedorov A.V.** Numerical Study of Atmospheric Air Flow in the Vicinity of Urban Environment. // *AIP Conference Proceedings*, 2016, 1770, Paper No 040017.
6. **Valger S.A., Fedorova N.N., Fedorov A.V.** Struktura Turbulentnogo Otryvnogo Techenija v Okrestnosti Ustanovlennoj na Plastine Prizmy s Kvadratnym Secheniem [Structure of Turbulent Separated Flow in the Neighborhood of a Plate-Mounted Prism of Square Section]. // *Thermophysics and Aeromechanics*, 2015, Vol. 22, No. 1, pp. 29-42 (in Russian).
7. **Khitrykh D.P.** Opyt Modelirovaniya Processov Snegoperenosa i Snegootlozheniya [Experience in the Simulation of Snow Transfer and Snow Deposition]. // *ANSYS Advantage.* Russian Edition, 2013, No. 19, pp. 27-32 (in Russian).
8. SP 20.13330.2016 Nagruzki i Vozdejstvija [Loads and Actions]. Actualized SNiP 2.01.07-85* (in Russian).
9. SP 20.13330.2011. Nagruzki i Vozdejstvija [Loads and Actions]. Actualized SNiP 2.01.07-85* (in Russian).
10. SNiP 2.01.07-85*. Nagruzki i Vozdejstvija [Loads and actions] (in Russian).
11. GOST R 56728-2015. Zdanija i Sooruzhenija. Metodika Opredelenija Vetrovyh Nagruzok na Ograzhdajushhie Konstrukcii [Buildings and Constructions. Method for Determining Wind Loads on the Building Envelope] (in Russian).
12. MDS 20-1.2006. Vremennye Rekomendacii po Naznacheniyu Nagruzok i Vozdejstvij, Dejstvuyushchih na Mogofunkcional'nye Vysotnye Zdaniya i Kompleksy v Moskve [Temporary Recommendations on the Designation of Loads and Impacts Acting on Multifunctional High-Rise Buildings and Complexes in Moscow] (in Russian).
13. **Lyczkowski R.W.** The History of Multiphase Science and Computational Fluid Dynamics. A Personal Memoir. Springer, 2018.
14. **Weinhold I., Parry J.** The Third Wave of CFD. NAFEMS World Congress, Salzburg, Austria, 2013.
15. **Bocharov A.N., Balakirev B.A., Bityurin V.A.** et al. Numerical Simulation as an Important Tool in Developing Novel Hypersonic Technologies. // *Journal of Physics: Conference Series*, 2015, Vol. 653.

16. **Menter F.R., Kuntz M., Langtry R.** Ten Years of Industrial Experience with the SST Turbulence Model. // *Proceedings of the 4th International Symposium on Turbulence, Heat and Mass Transfer*, Begell House Inc., West Redding, 2003, pp. 625-632.
17. **Van der Hoven I.** Power Spectrum of Horizontal Wind Speed in the Frequency Range from 0.0007 to 900 Cycles per Hour. // *J. Meteor.*, 1957, Volume 14, pp. 160–164.
18. **Davenport A.G.** The Spectrum of Horizontal Gustiness Near the Ground in High Winds. // *J. Royal Meteorol. Soc.*, 1961, Volume 87, Issue 372, pp. 194-211.
19. **Popov N.A.** Rekomendacii po Utochnennomu Dinamicheskomu Raschetu Zdanij i Sooruzhenij na Dejstvie Pul'sacionnoj Sostavlyayushchej Vetrovoj nagruzki [Recommendations on the Updated Dynamic Calculation of Buildings and Structures for the Effect of the Pulsation Component of the Wind Load]. Moscow, CNIISK / EVROSOFT, 2000 (in Russian).
20. **Cejtlin A.I., Bernshtejn A.S., Guseva N.I., Popov N.A.** Novaya Redakciya Razdela "Vetrovye nagruzki" glavy SNiP "Nagruzki i vozdejstviya" [New Edition of the Section "Wind Loads" of the Head of SNiP "Loads and Impacts"]. // *Stroitel'naya Mekhanika i Raschet Sooruzhenij*, 1987, No. 6 (in Russian).
21. Eurocode 1: Actions on Structures – Part 1-4: General Actions – Wind actions. EN 1991-1-4:2005.
22. National Research Council of Italy. Advisory Committee on Technical Recommendations for Construction. Guide for the Assessment of Wind Actions and Effects on Structures. CNR-DT 207/2008.
23. Tekhnicheskij Kodeks Ustanovivshejsya Praktiki. TKP EN 1991-1-4-2009. Belorusskaya Redakciya. Evrokod 1. Vozdejstviya na Konstrukcii. Chast' 1-4. Obshchie Vozdejstviya. Vetrovye Vozdejstviya.

СПИСОК ЛИТЕРАТУРЫ

1. **Дубинский С.И.** Численное моделирование ветровых воздействий на высотные здания. Диссертация на соискание ученой степени кандидата технических наук. – М.: МГСУ, 2010.
2. **Поддаева О.И., Кубенин А.С., Чурин П.С.** Архитектурно-строительная аэродинамика. – М.: МГСУ, 2015.
3. **Белостоцкий А.М., Акимов П.А., Афанасьева И.Н.** Вычислительная аэродинамика в задачах строительства. – М.: Издательство АСВ, 2017.
4. **Вальгер С.А., Федорова Н.Н., Федоров А.В.** Численное исследование интерференционных эффектов, возникающих в воздушном потоке при обтекании комплекса зданий сложной формы. // *Теплофизика и аэромеханика*, 2017, том 24, №1 (103), с. 35-44.
5. **Valger S.A., Fedorova N.N., Fedorov A.V.** Numerical Study of Atmospheric Air Flow in the Vicinity of Urban Environment. // *AIP Conference Proceedings*, 2016, Vol. 1770, Paper No 040017.
6. **Вальгер С.А., Федорова Н.Н., Федоров А.В.** Структура турбулентного отрывного течения в окрестности установленной на пластине призмы с квадратным сечением. // *Теплофизика и аэромеханика*, 2015, том 22, №1, с. 29-42.
7. **Хитрых Д.П.** Опыт моделирования процессов снегопереноса и снегоотложения. // *ANSYS Advantage*. Русская редакция, 2013, №19, с. 27-32.
8. СП 20.13330.2016 Нагрузки и воздействия. Актуализированная редакция СНиП 2.01.07-85*.
9. СП 20.13330.2011. Нагрузки и воздействия. Актуализированная редакция СНиП 2.01.07-85*.
10. СНиП 2.01.07-85*. Нагрузки и воздействия.
11. ГОСТ Р 56728-2015. Здания и сооружения. Методика определения ветровых нагрузок на ограждающие конструкции.

12. МДС 20-1.2006. Временные рекомендации по назначению нагрузок и воздействий, действующих на многофункциональные высотные здания и комплексы в Москве.
13. **Lyczkowski R.W.** The History of Multiphase Science and Computational Fluid Dynamics. A Personal Memoir. Springer, 2018.
14. **Weinhold I., Parry J.** The Third Wave of CFD. NAFEMS World Congress, Salzburg, Austria, 2013.
15. **Bocharov A.N., Balakirev B.A., Bityurin V.A.** et al. Numerical Simulation as an Important Tool in Developing Novel Hypersonic Technologies. // *Journal of Physics: Conference Series*, 2015, Vol. 653.
16. **Menter F.R., Kuntz M., Langtry R.** Ten Years of Industrial Experience with the SST Turbulence Model. // *Proceedings of the 4th International Symposium on Turbulence, Heat and Mass Transfer*, Begell House Inc., West Redding, 2003, pp. 625-632.
17. **Van der Hoven I.** Power Spectrum of Horizontal Wind Speed in the Frequency Range from 0.0007 to 900 Cycles per Hour. // *J. Meteor.*, 1957, Volume 14, pp. 160–164.
18. **Davenport A.G.** The Spectrum of Horizontal Gustiness Near the Ground in High Winds. // *J. Royal Meteorol. Soc.*, 1961, Volume 87, Issue 372, pp. 194-211.
19. **Попов Н.А.** Рекомендации по уточненному динамическому расчету зданий и сооружений на действие пульсационной составляющей ветровой нагрузки. – М.: ЦНИИСК/ЕВРОСОФТ, 2000.
20. **Цейтлин А.И., Бернштейн А.С., Гусева Н.И., Попов Н.А.** Новая редакция раздела «Ветровые нагрузки» главы СНиП «Нагрузки и воздействия». // *Строительная механика и расчет сооружений*, 1987, №6.
21. Eurocode 1: Actions on Structures – Part 1-4: General Actions – Wind actions. EN 1991-1-4:2005.
22. National Research Council of Italy. Advisory Committee on Technical Recommendations for Construction. Guide for the Assessment of Wind Actions and Effects on Structures. CNR-DT 207/2008.
23. Технический кодекс установившейся практики. ТКП EN 1991-1-4-2009. Белорусская редакция. Еврокод 1. Воздействия на конструкции. Часть 1-4. Общие воздействия. Ветровые воздействия.

Andrei V. Deineko, Ph.D., assistant professor, head of the center for computer simulation of Spectrum Group of Companies (Spectrum R&D); Building 15, Complex 29, Academica Tupoleva Embankment, Moscow, 105005, Russia; phone: +7 (495) 981-68-88;
E-mail: deineko@spgr.ru;
https://www.spectrum-group.ru.

Aleksey I. Shamshurin, leading engineer of the center for computer simulation of Spectrum Group of Companies (Spectrum R&D); Building 15, Complex 29, Academica Tupoleva Embankment, Moscow, 105005, Russia; phone: +7 (495) 981-68-88; e-mail: shamshurin@spgr.ru; https://www.spectrum-group.ru.

Narek A. Kazaryan, leading engineer of the center for computer simulation of Spectrum Group of Companies (Spectrum R&D); Building 15, Complex 29, Academica Tupoleva Embankment, Moscow, 105005, Russia; phone: +7 (495) 981-68-88; e-mail: nkazaryan@spgr.ru; https://www.spectrum-group.ru.

Дейнеко Андрей Викторович, кандидат технических наук, доцент, руководитель центра компьютерного моделирования ГК «Спектрум» (Spectrum R&D); 105005, Россия, Москва, Наб. Академика Туполева, 15, корп. 29; тел.: +7 (495) 981-68-88;
E-mail: deineko@spgr.ru;
https://www.spectrum-group.ru.

Шамшурин Алексей Игоревич, ведущий инженер центра компьютерного моделирования ГК «Спектрум» (Spectrum R&D); 105005, Россия, Москва, Наб. Академика Туполева, 15, корп. 29;
тел.: +7 (495) 981-68-88; e-mail: shamshurin@spgr.ru;
https://www.spectrum-group.ru

Казарян Нарек Арменович, ведущий инженер центра компьютерного моделирования ГК «Спектрум» (Spectrum R&D); 105005, Россия, Москва, Наб. Академика Туполева, 15, корп. 29; тел.: +7 (495) 981-68-88;
E-mail: nkazaryan@spgr.ru;
https://www.spectrum-group.ru

Table 1. Wind zoning of the territory of Russia.

Wind region	Ia	I	II	III	IV	V	VI	VII
Regulatory wind pressure w_0, Pa	170	230	300	380	480	600	730	850
Regulatory average wind speed v_0, m/s	16.7	19.4	22.2	25.0	28.1	31.4	34.6	37.3
Estimated average wind speed $v_m \approx v_{50}$, m/s	19.8	23.0	26.2	29.5	33.2	37.1	40.9	44.2

Table 2. Approximate compliance of types of terrain according to Russian and foreign norms.

Design codes	Параметры	Типы местности					
Russian design codes SP 20.13330.2011 [9], SP 20.13330.2016 [8]	Type of terrain	—	—	**A**	—	**B**	**C**
	Минимальная высота z_{min}, м	—	—	5	—	5	10
Eurocode EN 1991-1-4:2005 [21]; Belarusian design codes ТКР EN 1991-1-4-2009 [23]	Type of terrain (terrain category)	**0**	**I**	**II**	—	**III**	**IV**
	Roughness parameter z_0, meters	0.003	0.01	0.05	—	0.3	1.0
	Minimum height z_{min}, meters	1	1	2	—	5	10
Italian design codes CNR-DT 207/2008 [22]	Type of terrain (exposure category)	—	**I**	**II**	**III**	**IV**	**V**
	Roughness parameter z_0, meters	—	0.01	0.05	0.1	0.3	0.7
	Minimum height z_{min}, meters	—	2	4	5	8	12
	Area coefficient k_r	—	0.17	0.19	0.20	0.22	0.23
	Table coefficient κ	—	0.44	0.52	0.55	0.61	0.65

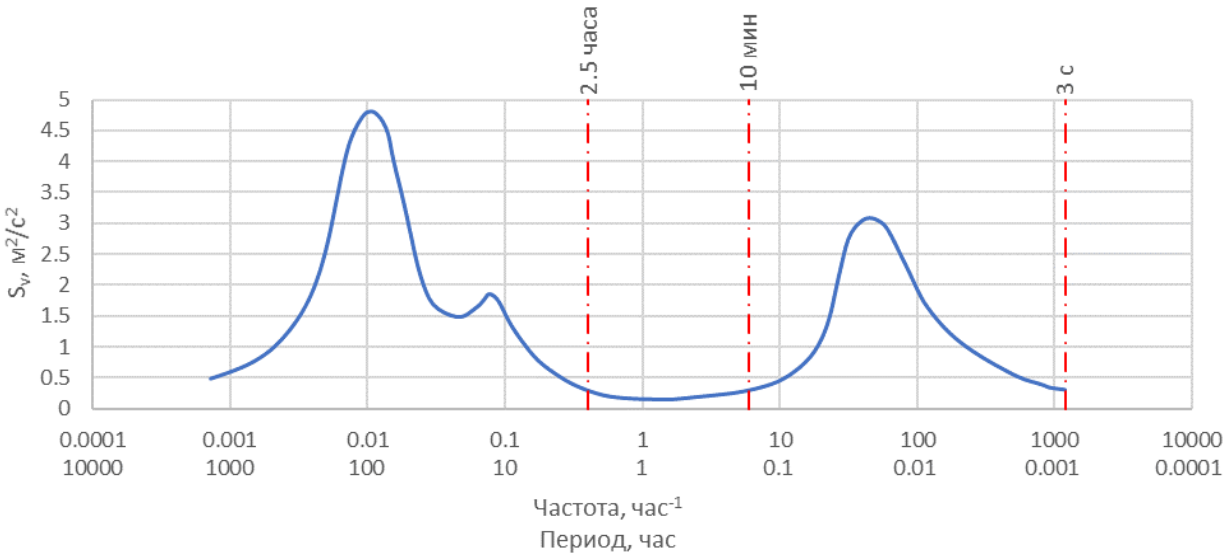


Figure 1. The character of the spectral density of wind speed according to [17].

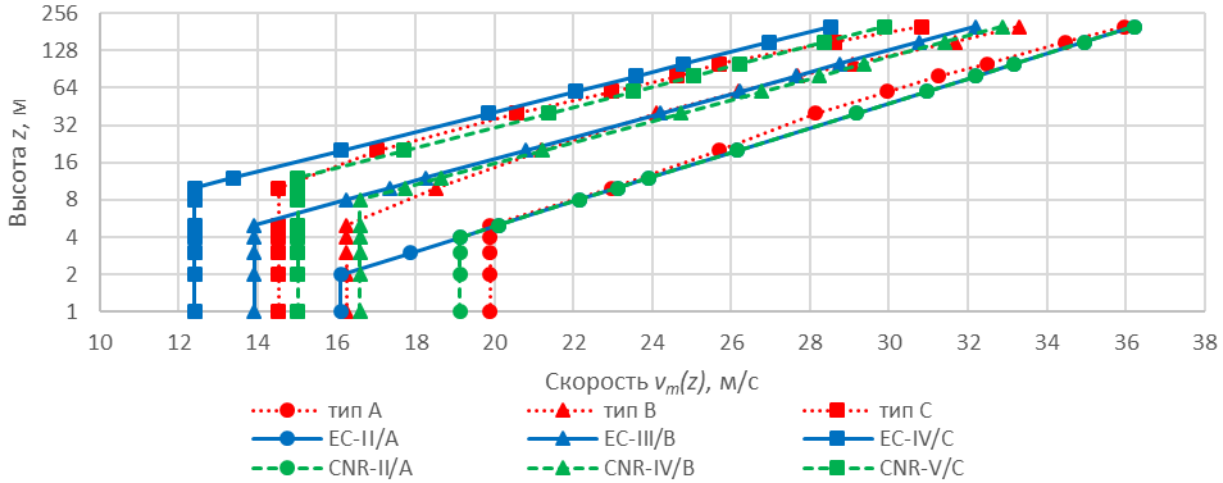


Figure 2. The nature of the profile of the average wind speed $v_m(z)$ in different types of terrain according to Russian and foreign design codes.

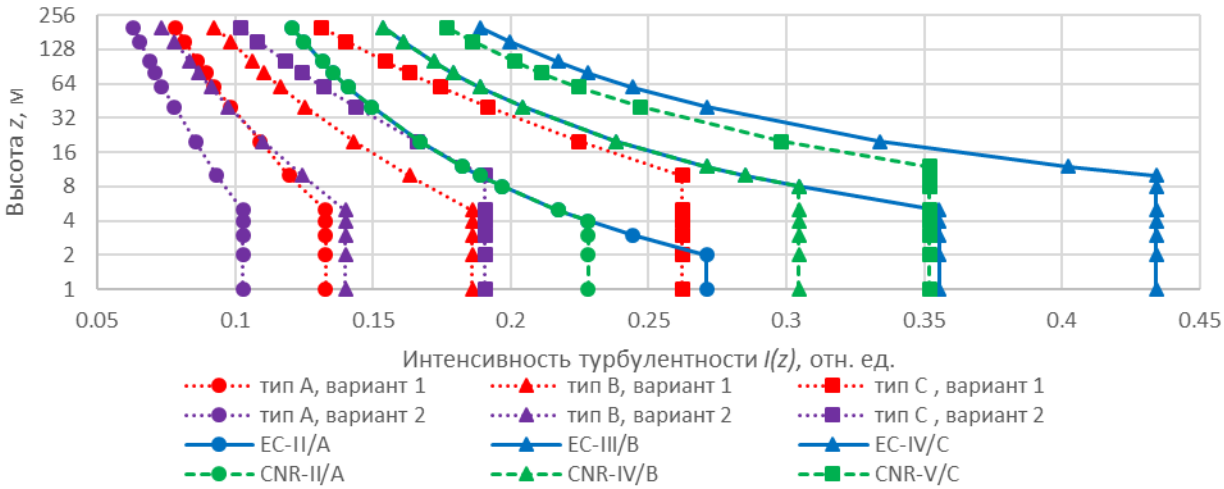


Figure 3. The nature of the profile of the intensity of wind turbulence $I(z)$ in various types of terrain on the modifications of Russian and foreign design codes.

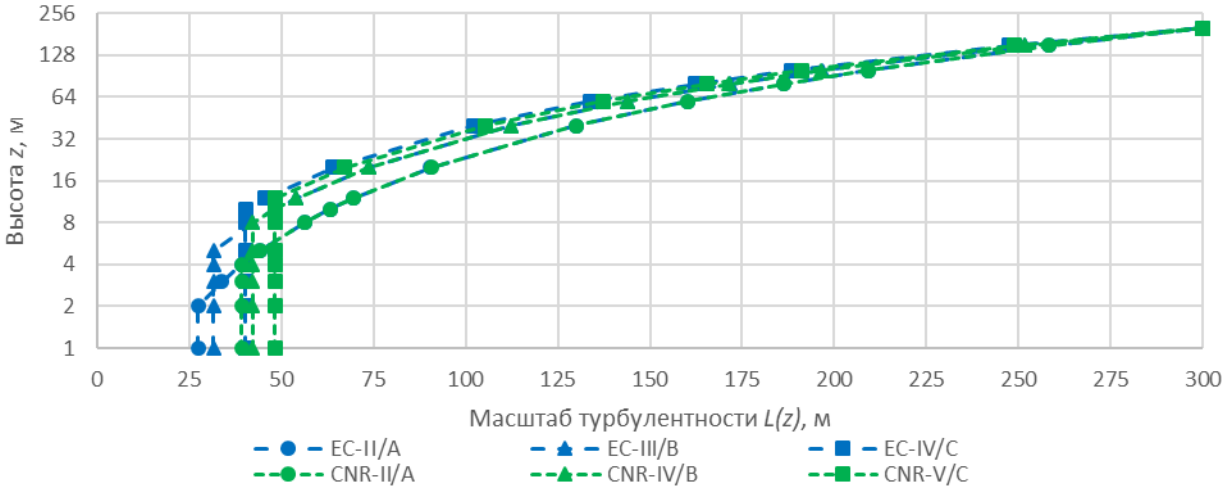


Figure 4. The nature of the profile of the scale of turbulence of the wind $L(z)$ in various types of terrain according to foreign design codes.

TO THE QUESTION OF THE DETERMINATION OF GEOMETRIC CHARACTERISTICS OF THE SECTION OF CORRUGATED BEAMS WITH TRAPEZOIDAL WEBS BASED ON THE SIMULATION RESULTS

Tatiana L. Dmitrieva, Khukhuudei Ulambayar
Irkutsk National Research Technical University, Irkutsk, RUSSIA

Abstract: An algorithm for calculating the geometric characteristics of steel I-beams with plate corrugated webs of arbitrary type is proposed. The algorithm is implemented using the I-beam with plate trapezoid webs as an example. The determination of reduced area and moments of inertia in the axes of the cross section of the trapezoidal profile based on the finite element modeling of the beam with shell elements in calculations for bending and axial compression in the "ANSYS 14.5" software package is described. The verification procedure has been performed for a shell finite element model using the example of an I-beam with a standard flat web. A table has been compiled of geometric characteristics of rod corrugated elements of a trapezoidal profile in order to realize their finite element calculation using a rod diagram. An example of the calculation of a flat frame with a horizontal corrugated element, made in software package "LIRA-SAPR" using a flat rod diagram is given.

Keywords: shell finite element, rod finite element, simulation results, numerical analysis, maximum deflection, moment of inertia, software "ANSYS"

К ВОПРОСУ ОПРЕДЕЛЕНИЯ ГЕОМЕТРИЧЕСКИХ ХАРАКТЕРИСТИК СЕЧЕНИЯ ГОФРОБАЛОК С ТРАПЕЦЕИДАЛЬНЫМИ СТЕНКАМИ НА ОСНОВЕ КОМПЬЮТЕРНОГО МОДЕЛИРОВАНИЯ

Т.Л. Дмитриева, Х.Уламбаяр
Иркутский национальный исследовательский технический университет, г. Иркутск, РОССИЯ

Аннотация: Предложен алгоритм вычисления геометрических характеристик стальных двутавровых балок с пластинчатыми гофрированными стенками произвольного вида. Алгоритм реализован на примере балок с трапецеидальными стенками. Описано нахождение приведенной площади и моментов инерции в осях поперечного сечения трапецеидального профиля на основе конечно-элементного моделирования балки оболочечными элементами в расчетах на изгиб и осевое сжатие в программном комплексе "ANSYS 14.5". Выполнена процедура верификация оболочечной конечно-элементной модели на примере для двутавровой балки со стандартной прямой стенкой. Составлена таблица геометрических характеристик стержневых гофро-элементов трапецеидального профиля с тем, чтобы реализовать их конечно-элементный расчет по стержневой схеме. Приведен пример расчета плоской рамы с горизонтальным гофроэлементом, выполненный в ПК "ЛИРА-САПР" с применением плоской стержневой схемы.

Ключевые слова: компьютерное моделирование, численный анализ, оболочечный конечный элемент, стержневой конечный элемент, момент инерции, программный комплекс «ANSYS»

INTRODUCTION

I-beams with plate corrugated webs have not widely used in the design of buildings and structures until a certain time [1]. In the past decade, it has been recognized that cold-formed steel beams of various corrugation configurations can be effectively used as bearing components of the framework.

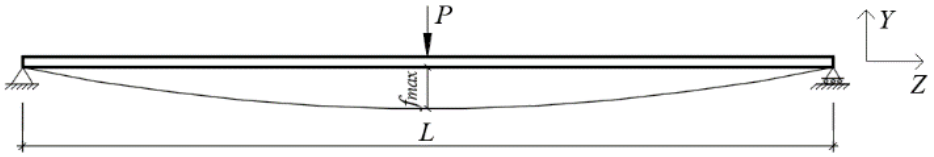


Figure 1. Calculation scheme.

The use of corrugated webs allows the use of thin plates without the need to install stiffeners, which contributes to reducing the weight and cost of the beam [2-4]. Economical expediency of corrugated elements is substantiated in [1, 5-8]. Same source notes main flaws in design of such constructions, which are mainly caused by lack of normative documents, literature and special computation software. The use of such structures is difficult the complexity to analyze their stress-strain state [9-14]. The standard scheme for calculating frameworks of buildings is based on a rod finite element model using geometric characteristics of the cross sections of rod elements. Meanwhile, tabulated values of the geometric characteristics are known for certain corrugation types – triangle [15] and wave types (SIN beams) [16]. For corrugations of an arbitrary profile there are no assortments containing bending, axial and other characteristics of section stiffness. This article proposes an algorithm for determining the geometric characteristics of corrugated beams using the example of beams with corrugated trapezoidal webs.

1. CALCULATION SCHEME MODEL

As an example, consider a single-span model (Figure 1).

The system of differential equations describing the displacement of the beam y (z) has the form given flexural shear

$$\begin{cases} \dfrac{dy(z)}{dz} = -\dfrac{M(z)}{E \cdot I}; \\ \dfrac{dy}{dz} = y(z) + \dfrac{k \cdot P}{G \cdot A_{2f}} \end{cases}, \qquad (1)$$

Substituting from the second equation of system (1) into the first, we obtain the second order equation:

$$\frac{d^2 y}{dz^2} = -\frac{M(z)}{E \cdot I} + \frac{d}{dz} \cdot \left(\frac{k \cdot P}{G \cdot A_{2f}} \right), \qquad (2)$$

where, P is the applied load, E and G are modulus of elasticity and shear modulus, respectively, I is the moment of inertia of the cross section, k is a factor related to the cross section shape, A_{2f} is the area of two flange, M is the bending moment.

The solution of the differential equat.2 taking into account the conditions for fixing the beam is as follows:

$$y = \frac{P \cdot L^2}{16 \cdot E \cdot I} \cdot z - \frac{P}{12 \cdot E \cdot I} \cdot z^3 + \frac{k \cdot P}{G \cdot A_{2f}} \cdot z, \qquad (3)$$

Then, at $z=L/2$, we get at mid-span deflection with allowance for bending and shear deformations:

$$y_{z=L/2} = f_{\max} = \frac{P \cdot L^3}{48 \cdot E \cdot I} + \frac{k \cdot P \cdot L}{2 \cdot G \cdot A}, \qquad (4)$$

From condition (4) we express the moment of inertia:

$$I = \frac{P \cdot L}{48 \cdot E \cdot \left(f_{\max} - \dfrac{k \cdot P \cdot L}{4 \cdot G \cdot A_f} \right)}. \qquad (5)$$

where, A_f is the area of one flange.

This addiction can be used in determining the geometric characteristics of the cross section of steel I-beams with corrugated webs. In this case,

the maximum deflection $f_{\max}$ is determined by automatic calculation using certified software systems that use the spatial model of FE of steel I-beams with corrugated webs.

2. ALGORITHM FOR DETERMINING GEOMETRIC CHARACTERISTICS OF THE CROSS-SECTION OF BEAMS WITH CORRUGATED WEBS OF ARBITRARY TYPE

The algorithm for selecting geometric characteristics of a section for an I-beam with a corrugated web from an arbitrary profile includes the following steps:

- revealing of analytical dependences of displacements from the applied load through stiffness parameters of the beam;
- selection of rational dimensions of the cross sections of beams;
- selection of rational dimensions I-beams with trapezoidal webs;
- definition of deflections based on the finite element model of the shell when bending the beam;
- determination of axial displacement based on shell finite element model under axial compression;
- determination of geometric characteristics of sections of beams with corrugated webs and tabulation of results.

2.1. Analytical dependences of displacements from the stiffness parameters of the beam.

Consider a corrugated beam with trapezoidal webs when loaded with concentrated forces P_x and P_y in the middle of a span in two planes (Figure 2 , Figure 3).

Based on the expression (5), we write down the relations for moments of inertia of cross sections of the beam in two planes.

a. Moment of inertia I_x:

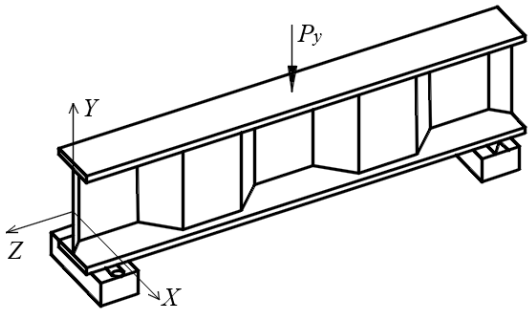


Figure 2. Isometric projection of calculation model with concentrated load at mid-span (in the plane ZOY).

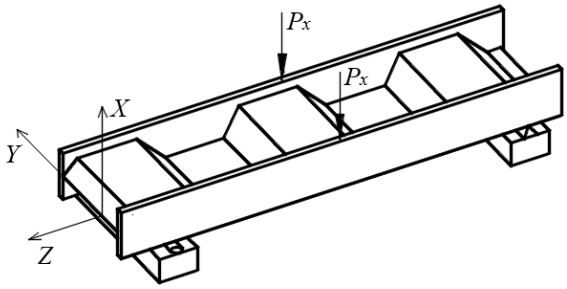


Figure 3. Isometric projection of calculation model with concentrated load at mid-span (in the plane ZOX).

$$I_x = \frac{P_y \cdot L^3}{48 \cdot E \cdot \left(f_{\max,y} - \frac{3 \cdot P_y \cdot L}{20 \cdot G \cdot A_f} \right)}, \qquad (6)$$

b. Moment of inertia I_y:

$$I_y = \frac{P_x \cdot L^3}{48 \cdot E \cdot \left(f_{\max,x} - \frac{3 \cdot P_x \cdot L}{20 \cdot G \cdot A_f} \right)}. \qquad (7)$$

where, P_x and P_y are applied loads, $f_{\max,x}$ and $f_{\max,y}$ are maximum deflections along axis *X* and *Y*.

To determine the reduced area, which is a geometrical parameter under axial impact, the beam is loaded with an axial compressive force P_z (Figure 4).

Formula for determining axial deformation:

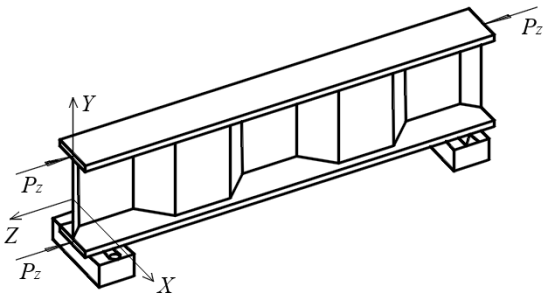


Figure 4. Isometric projection of calculation model with concentrated load along axis Z (in the plane ZOY).

$$\Delta = \frac{P_z \cdot L}{E \cdot A}\ , \qquad (8)$$

where, Δ is amount of Z-axis displacement.
From here, reduced area is determined by the expression:

$$A = \frac{P_z \cdot L}{E \cdot \Delta}. \qquad (9)$$

2.2. Selection of cross-sectional dimensions of beams with corrugated web.

For the study were selected five models of I-beams with trapezoidal webs (BTW1- BTW5). The parameters of the sections of beams were taken in the range of the external height H from 200 to 600 mm with a step of 100 mm (Table 1), which corresponds to assortments of welded I-beams with flat wall.

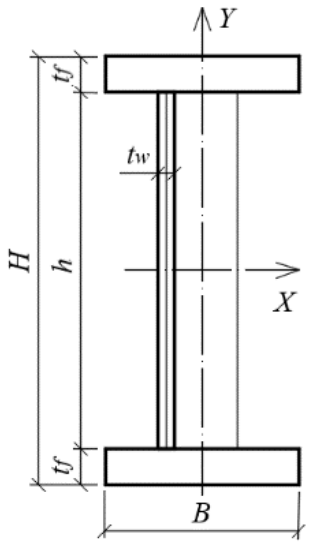


Figure 5. Cross section of models BTW.

Table 1. Parameters of cross section of models BTW.

Accepted models	H, mm	h, mm	B, mm	t_f, mm	t_w, mm
BTW1	200	184	100	8	2
BTW2	300	282	150	9	3
BTW3	400	374	200	13	3
BTW4	500	468	200	16	4
BTW5	600	564	200	18	4

2.3. Selection of trapezoidal webs dimensions for calculation models.

Studies of various trapezoidal profiles were performed in [17,18]. The results of these researches have shown that the most rational in terms of bearing capacity is a beam with a corrugation angle φ = 45%. Optimal sizes of parameters a, b and d were determined on basis of comparative automated calculations. The corrugation parameters corresponding to the accepted models are given in table 2 and in Figure 6.

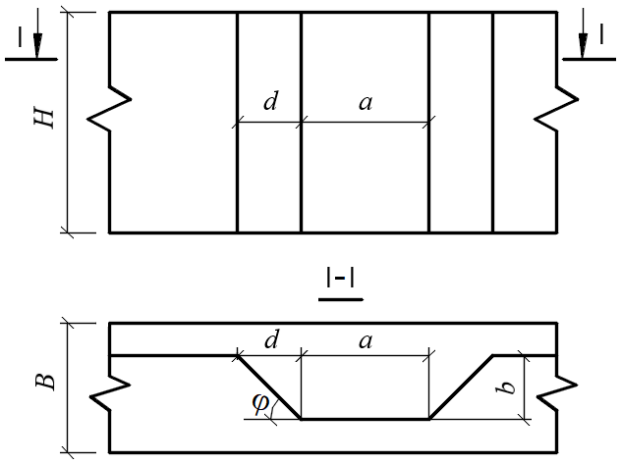


Figure 6. Trapezoidal web dimensions.

Table 2. Parameters of corrugated web beams.

Models	b, mm	a, mm	d, mm	φ,
BTW1	50	180	50	45°
BTW2	76	150	76	45°
BTW3	100	200	100	45°
BTW4	80	200	80	45°
BTW5	100	300	100	45°

2.4. Numerical determination of displacement value based on shell finite element model.

The study consisted in calculation of beams based on shell finite element model. Preliminary verification of this model was performed using a flat wall I-beam as an example and subsequent comparison of results with theoretical values of deflections taking into account the shear deformations. Results obtained by numerical analysis in software package "ANSYS", correlated with the analytical calculation with a maximum error of 0.93%, which is within the limits of permissible (taking into account the fact that errors adopted in the construction design should not exceed 3%).

Next, the calculation was carried out corrugated beams BTW1-5 to determine:

a) maximum deflections in a beam loaded with concentrated forces in two planes (Figure 2 , Figure 3);
b) axial deformation of the beam under axial impact (Figure 4).

The calculation was performed in software package "ANSYS 14.5", where shell finite elements SHELL181 were used. Generation of a grid of quadrangular type was made automatically. The size of finite elements was within 47 mm on long side. Near the junction of webs and flanges, the mesh dimensions were reduced to 7 mm.

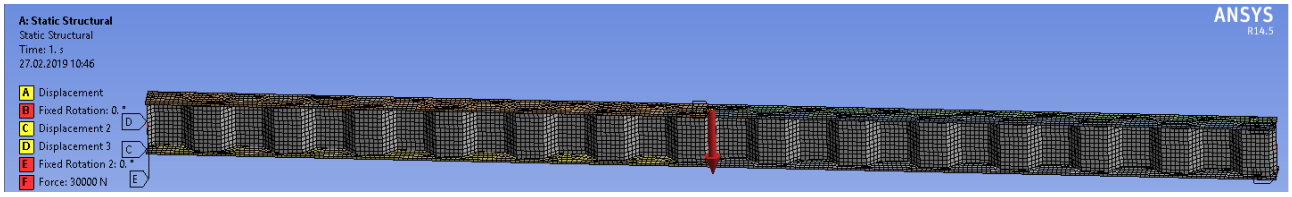


Figure 7. Finite element model of a beam.

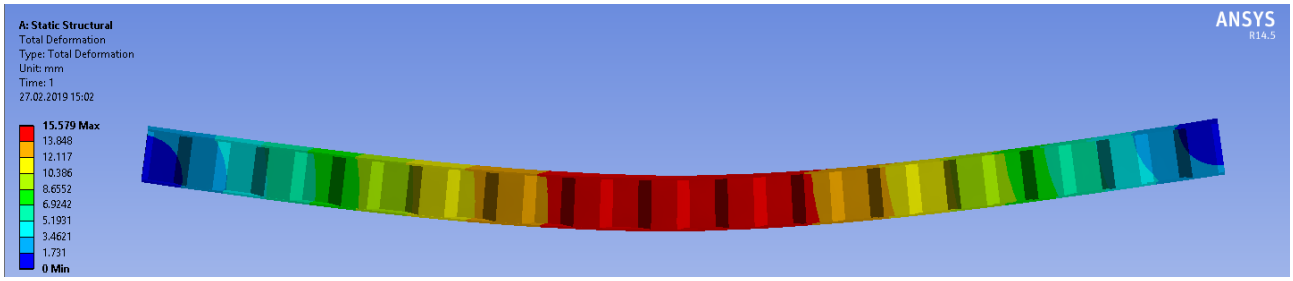
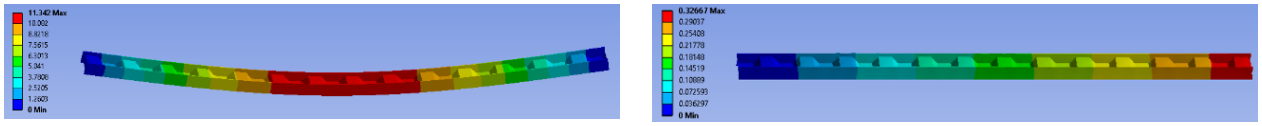


Figure 8. Deformed scheme in YZ plane for the BTW1 model.



a) *b)*

Figure 9. Deformed scheme for the BTW1 model: a) in XZ plane; b) deformed circuit for axial compression.

The maximum axial displacements and deflections obtained in the calculation are shown in Table 3.

Table 3. Results of calculation.

Models	$f_{max,y}$, mm	$f_{max,x}$, mm	Δ, mm
BTW1	15.6	11.34	0.326
BTW2	11.1	12.2	0.25
BTW3	10.45	11.2	0.247
BTW4	19.1	33.7	0.34
BTW5	17.45	43.7	0.38

2.5. Calculations of geometric characteristics. Using obtained maximum deflections ($f_{\max,y}$, $f_{\max,x}$) using the formula (4), moments of inertia about the axes of cross section *X* and *Y* were determined for each model of corrugated beams. Reduced area is determined by formula (9). In calculations were used material characteristics

$$E=200 \text{ kN/mm}^2,\ G=76{,}9 \text{ kN/mm}^2.$$

Determination of moments of resistance and radius of gyration, perform on the basis of well-known analytical formulas for strength of materials [19].

$$W_x = \frac{I_x}{H/2}, \qquad (10)$$

$$i_x = \sqrt{\frac{I_x}{A}}\ . \qquad (11)$$

W_y, i_y - were determined similarly by formulas (10), (11). Static moment of the half-section area relative to the X - axis was calculated by following formula:

$$S_x^{1/2} = \left(\frac{H}{2} - t_f\right)\cdot t_w \cdot \frac{1}{2}\cdot\left(\frac{H}{2} - t_f\right) + B\cdot t_f \cdot \left(\frac{H}{2} - \frac{t_f}{2}\right). \qquad (12)$$

3. RESULTING TABLE OF GEOMETRIC CHARACTERISTICS OF SECTIONS OF BEAMS WITH CORRUGATED WEB

According to research results, was compiled a table of parameters and geometrical characteristics of welded I-beam with a corrugated web (similar to tabulated values standard I-beams). The resulting table can be used to solve the problem of the finite-element analysis of flat frames according to rod diagram, which greatly simplifies the calculation compared to calculation using shell model.

Table 4. Geometric parameters of steel I-beams profiles with corrugated web.

Models	Cross-section specifications, cm					Corrugation specification, cm			
	H	*B*	t_f	t_w	*h*	*b*	*a*	*d*	φ
1	2	3	4	5	6	7	8	9	10
BTW1	20.0	10.0	0.8	0.2	18.4	5.0	10.0	5.0	45°
BTW2	30.0	15.0	0.9	0.3	28.2	7.6	15.0	7.6	45°
BTW3	40.0	20.0	1.3	0.3	37.4	10.0	20.0	10.0	45°
BTW4	50.0	20.0	1.6	0.4	46.8	8.0	20.0	8.0	45°
BTW5	60.0	20.0	1.8	0.4	56.4	10.0	30.0	10.0	45°

Table 5. Geometric parameters of steel I-beams profiles with corrugated web.

Area, cm^2	Mass per 1m, kg	I_x, cm^4	W_x, cm^3	i_x, cm	I_y, cm^4	W_y, cm^3	i_y, cm	$S_x^{1/2}$, cm^3
11	12	13	14	15	16	17	18	19
19.68	16.13	1484.2	148.42	8.68	136	27.2	2.63	85.3
35.46	29.24	5712	380.8	12.7	520	69.3	3.83	226.3
63.22	51.54	18922	946.1	17.3	1765.5	176.6	5.3	555.6
82.72	67.8	38312	1532.48	21.52	2172	217.2	5.13	1212.45
94.56	77.3	61893	2063.1	25.6	2472	247.2	5.11	1763.4

4. CALCULATION OF A FLAT FRAME WITH CORRUGATED ELEMENTS

Using the geometrical characteristics of corrugated beams, it was possible to perform calculations of flat frames according to rod diagram. Let us give an example of the calculation of a flat frame with a horizontal corrugated element, made in software «LIRA-SAPR» using a flat rod diagram.

Example. Consider the frame shown in Fig. 11. For this frame requires: a) build the internal forces diagrams(the axial force *N*, the shear *Q*, and the bending moment *M*); b) determine the maximum normal and stress shearing in the rod of the column and beam.

Initial data: *L=12* m; *q=14* kN/m; *E=200* kN/mm^2.

The cross section of the beam - corrugated beam with plate trapezoidal web (BTW5), columns – the standart I-beam with flat wall (50ШС2). The geometric characteristics of the cross section for the beam are selected from Table 5 and 6.

Calculated geometric characteristics of the cross section of elements: elements 1 and 2: $I=7{,}22 \cdot 10^{-4}$ m^4; $W=29{,}5 \cdot 10^{-4}$ m^3; $A=176{,}25 \cdot 10^{-4}$ m^2; $S_x^{1/2}=16{,}65 \cdot 10^{-4}$ m^3; the element 3: $I=6{,}2 \cdot 10^{-4}$ m^4; $W=2{,}63 \cdot 10^{-4}$m^3; $A=94{,}56 \cdot 10^{-4}$ m^2; $S_x^{1/2}=17{,}63 \cdot 10^{-4}$ m^3.

Assign stiffnesses rod elements: for elements 1 and 2: *EI=144400* kN · m^2; *EA=3525000* kN; for element 3: *EI=124000* kN · m^2; *EA=1891200* kN.

Calculation results

a. The internal forces diagrams, received in software «LIRA-SAPR» shown in Fig. 11, Fig.12.

b. The calculation of normal stresses in rods of column and beam of frame:

$$\sigma_{i,\frac{\max}{\min}} = \frac{N_i}{A_i} \pm \frac{M_i}{W_i}, \qquad (13)$$

where, i = 1, 2, 3 – numbers of rod.

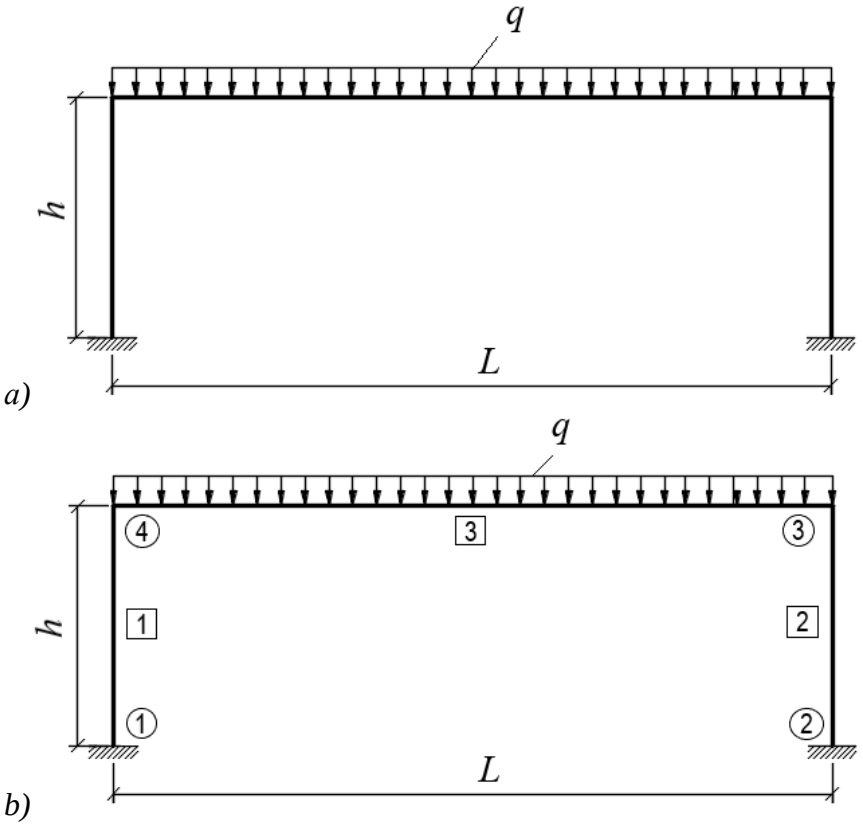


Figure 10. The rod model of a flat steel frame: a) frame geometry; b) calculation scheme.

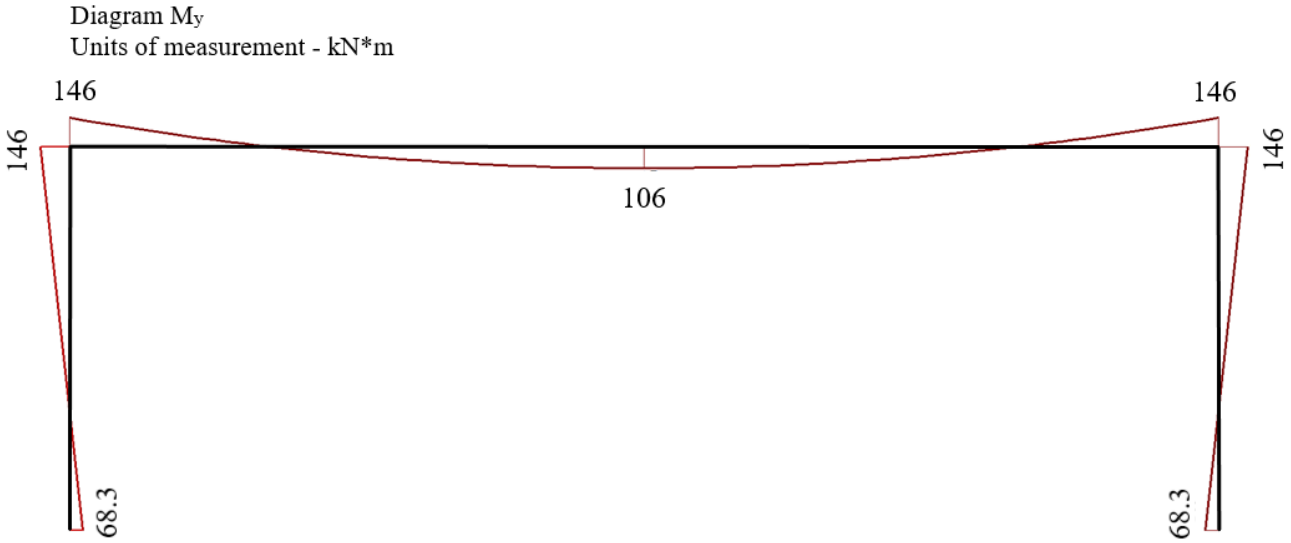


Figure 11. The calculation in Software "LIRA-SAPR": the diagram of bending moment M_y.

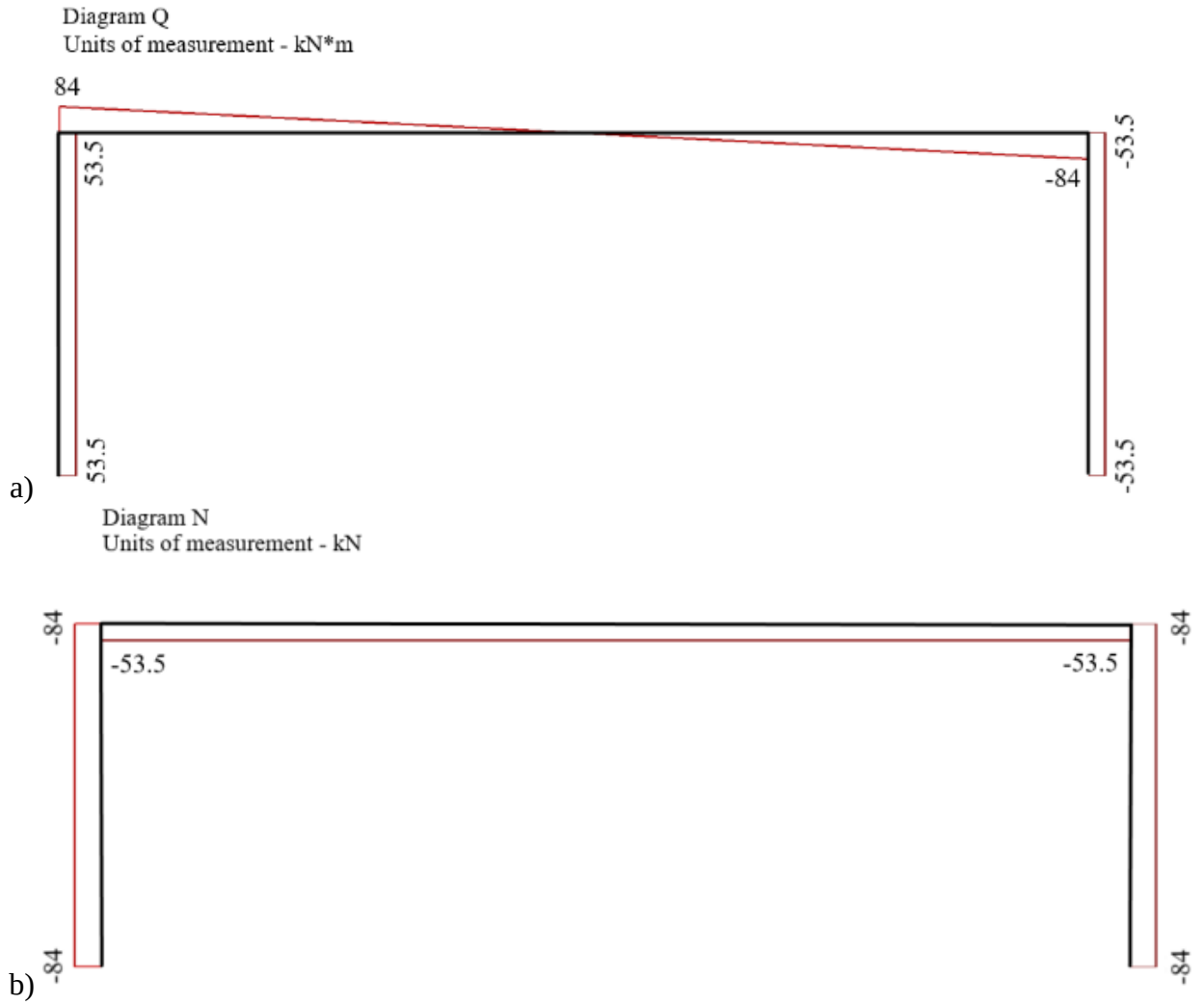


Figure 12. The calculation in Software "LIRA-SAPR": a) the diagram of shear Q ; b) the diagram of axial force N.

Table 6. Results of calculations.

Elements	$\sigma_{i,\max}$, MPa	$\sigma_{i,\min}$, MPa
1	44,7	-54,4
2	44,7	-54,4
3	65,2	-76,43

c. The calculation of stress shearing in rods of column and beam of frame:

$$\tau_i = \frac{Q \cdot S_x^{1/2}}{I_x \cdot t_w}. \qquad (14)$$

Table 7. Results of calculations.

Elements	τ_i , MPa
1	8,23
2	-8,23
3	59,73

CONCLUSION

1. The developed method makes it possible to determine the values of geometric characteristics for corrugated web I-beams with various corrugation configurations.
2. The use of the obtained geometric characteristics makes it possible to carry out the calculation of flat frames with corrugated elements according to the rod scheme.
3. Further research direction involves the generalization of the above method to solving problems of static calculation of spatial rod structures with corrugated elements.

REFERENCES

1. **Dmitrieva T.L., Ulambayar Kh.** Ispolizovanie Balok s Gofrostenkoi v Sovremennom Proektirovanii [Use of Corrugated Beams in Modern Design]. // *Izvestiya Vuzov. Investitsii. Stroitelstvo. Nedvizhimost*, 2015, Vol. 15, No. 4, pp. 132-138 (in Russian).
2. **Limaye A.A., Alandkar P.M.** Strength of Welded Plate Girder with Corrugated Web Olate. // *International Journal of Engineering Research and Applications*, 2013, Vol. 3, Issue 05, pp. 1925-1930.
3. **Bryantsev A.A., Absimetov V.E., Lalin V.V.** Effiktivnosti Primeneniya Dvutavrov s Gofrirovanniimi Stenkami v Proizvodstvenniikh Zdaniyakh [Effective Application of I-beams With Corrugated Webs in the Industrial Building]. // *Construction of Unique Buildings and Structures*, 2017, Vol. 54, No. 3, pp. 93-104 (in Russian).
4. **Lukin A.O., Alpatov V.Yu., Chernyshev D.D.** Sovershensvovanie Konstruktivnogo Resheniya Balki s Gofrirovannoi Stenkoi [Improving Constructive Solution of Beam With Corrugated Wall]. // *Vestnik SGASU. Town Planning and Architecture*, 2016, Vol. 23, No. 2, pp. 4-8 (in Russian).
5. **Akshay Bankar, Pallavi Pasnur.** Experimental Stress Analysis of Trapezoidal Corrugated Steel Web Beam – A Review. // *Imperial journal of Interdisciplinary Research*, 2017, Vol. 3, Issue 06, pp. 621-624.
6. **Jayaraman S., Suresh babu S.** Experimental Investigation on Flexural Behavior of Cold Formed Corrugated Steel Section. // *International Journal for Scientific Research and Development*, 2017, Vol. 5, Issue 02, pp. 1670-1675.
7. **Bondarenko O.S., Kikot A.A.** Analiz Balok s Gofrirovannoi Stenkoi [Corrugated Beam Analysis]. // *Polzunovski Almanakh*, 2016, No. 3, pp. 38-41 (in Russian).
8. **Kudryavtsev S.V.** Raschet Dvutavrovoi Balki s Gofrirovannoi Stenkoi na Izgib v Svoei Ploskosti pod Deistviem Staticheskikh Nagruzok. Rashet Metodom Konechniikh Elementov [Calculation of an I-Beam With a Corrugated Web for Bending in its Plane Under the Action of Static Loads. Calculation Finite Element Method]. Ekaterinburg, GOU BPO UPI, 2007, 11 pages (in Russian).
9. **Basher M.A., Shanmugam N.E., Khalim A.R.** Horizontally Curved Composite Plate Girders With Trapezoidally Corrugated

Webs. // *International Journal of Constructional Steel Research*, 2011, Vol. 67, Issue 06, pp. 947-956.
10. **Wang Z.Y., Wang Q.Y., Jiang R.J.** Finite Element Based Fatigue Assessment of Corrugated Steel Web Beams in Highway Bridges. // *International Journal of Civil Engineering*, 2015, Vol. 13, Issue 04, pp. 419-431.
11. **Revathi N., Satheshkumar G.K., Arunkumar Dr.G.** Numerical Investigation on Flexural Behaviour of Cold Formed Steel I – Section With Triangular Corrugated Web. // *International Journal of Research and Innovation in Engineering Technology*, 2016, Vol. 02, Issue 12, pp. 48-53.
12. **Siddharth R.P., Magdum M.M.** Comparative Study of Innovative Corrugated Hollow Columns and Conventional Column. // *Technical Research Organization India*, 2017, Vol. 04, Issue 07, pp. 30-37.
13. **Arunkumar G., Sampathkumar P., Sukumar S.** Investigation on Cold – Formed Steel Lipped I-Beam With Trapezoidal Corrugation in Web by Varying Depth. // *International Journal of Innovative Research and Development*, 2013, Vol. 02, Issue 05, pp. 938-949.
14. **Denan F., Osman M.H., Saad S.** The Study of Lateral Torsional Buckling Behavior of Beam with Trapezoid Web Steel Section by Experimental and Finite Element Analysis. // *International Journal of Research and Reviews in Applied Sciences*, 2010, Vol. 02, Issue 03, pp. 232-240.
15. **Maksimov Yu.S., Ostrikov G.M.** Sortament Svarniikh Dvutavroviikh Profilei Obiichnogo Tipa i s Gofrirovannimi Stenkami, Sootvetstvuiushie po Prochnostniim Kharakteristikam Prokatniim [Mix of Fabricated I-Beam Sections of Regular Type and With Corrugated Walls Meeting Strength Properties of Rolling Sections]. RDS RK 5.04-24-2006, Astana: Kaz Steel Project, 2007, 22 pages (in Russian).
16. Rekomendatsii po Proektirovaniiu: Balki Dvutavroviie Gofrirovanniie Oblegchenniie [Design Recommendations: Lightweight I-Beams Corrugated] (Sin beams TU U B.2.6-28.1-30653953-007:2007) Kh., et. project, 2013, 110 pages (in Russian).
17. **Prabha V.C., Shalini A., Saravanaganesh S., Selvakumar K.** Study on Behaviour of Cold Formed Built-Up I-Section With Trapezoidal Corrugation in Web by Varying the Aspect Ratio and Angle of Corrugation. // *International Journal of Chemical Sciences*, 2015, Vol. 13, Issue 04, pp. 1935-1946.
18. **Divahar R., Joanna P.S.** Lateral Buckling of Cold Formed Steel Beam With Trapezoidal Corrugated Web. // *International Journal of Civil Engineering and Technology*, 2014, Vol. 05, Issue 03, pp. 217-225.
19. **Alexandrov A.V., Potapov V.D., Derzhavin B.P.** Soprotivlenie Materialov [Mechanics of Materials with Elements of Theory of Linear Elasticity]. Moscow, Visshaya shkola, 2003, 560 pages (in Russian).

СПИСОК ЛИТЕРАТУРЫ

1. **Дмитриева Т.Л., Уламбаяр Х.** Использование балок с гофростенкой в современном проектировании. // *Известия вузов. Инвестиции. Строительство. Недвижимость*, 2015, том 15, №04, с. 132-138.
2. **Limaye A.A., Alandkar P.M.** Strength of Welded Plate Girder with Corrugated Web Olate. // *International Journal of Engineering Research and Applications*, 2013, Vol. 3, Issue 05, pp. 1925-1930.
3. **Брянцев А.А., Абсиметов В.Э., Лалин В.В.** Эффективность применения двутавров с гофрированными стенками в производственных зданиях. // *Строи-*

тельство уникальных зданий и сооружений, 2017, том 54, №03, с. 93-104.

4. **Лукин А.О., Алпатов В.Ю., Чернышев Д.Д.** Совершенствование конструктивного решения балки с гофрированной стенкой. // *Вестник СГАСУ. Градостроительство и архитектура*, 2016, том 23, №02, с. 4-8.
5. **Akshay Bankar, Pallavi Pasnur.** Experimental Stress Analysis of Trapezoidal Corrugated Steel Web Beam – A Review. // *Imperial journal of Interdisciplinary Research*, 2017, Vol. 3, Issue 06, pp. 621-624.
6. **Jayaraman S., Suresh babu S.** Experimental Investigation on Flexural Behavior of Cold Formed Corrugated Steel Section. // *International Journal for Scientific Research and Development*, 2017, Vol. 5, Issue 02, pp. 1670-1675.
7. **Бондаренко О.С., Кикоть А.А.** Анализ балок с гофрированной стенкой. // *Ползуновский альманах*, 2016, №03, с. 38-41.
8. **Кудрявцев С.В.** Расчет двутавровой балки с гофрированной стенкой на изгиб в своей плоскости под действием статических нагрузок. Расчет методом конечных элементов. – Екатеринбург: ГОУ ВПО УПИ. 2007. – 11 с.
9. **Basher M.A., Shanmugam N.E., Khalim A.R.** Horizontally Curved Composite Plate Girders With Trapezoidally Corrugated Webs. // *International Journal of Constructional Steel Research*, 2011, Vol. 67, Issue 06, pp. 947-956.
10. **Wang Z.Y., Wang Q.Y., Jiang R.J.** Finite Element Based Fatigue Assessment of Corrugated Steel Web Beams in Highway Bridges. // *International Journal of Civil Engineering*, 2015, Vol. 13, Issue 04, pp. 419-431.
11. **Revathi N., Satheshkumar G.K., Arunkumar Dr.G.** Numerical Investigation on Flexural Behaviour of Cold Formed Steel I – Section With Triangular Corrugated Web. // *International Journal of Research and Innovation in Engineering Technology*, 2016, Vol. 02, Issue 12, pp. 48-53.
12. **Siddharth R.P., Magdum M.M.** Comparative Study of Innovative Corrugated Hollow Columns and Conventional Column. // *Technical Research Organization India*, 2017, Vol. 04, Issue 07, pp. 30-37.
13. **Arunkumar G., Sampathkumar P., Sukumar S.** Investigation on Cold – Formed Steel Lipped I-Beam With Trapezoidal Corrugation in Web by Varying Depth. // *International Journal of Innovative Research and Development*, 2013, Vol. 02, Issue 05, pp. 938-949.
14. **Denan F., Osman M.H., Saad S.** The Study of Lateral Torsional Buckling Behavior of Beam with Trapezoid Web Steel Section by Experimental and Finite Element Analysis. // *International Journal of Research and Reviews in Applied Sciences*, 2010, Vol. 02, Issue 03, pp. 232-240.
15. **Максимов Ю.С., Остриков Г.М.** Сортамент сварных двутавровых профилей обычного типа и с гофрированными стенками, соответствующие по прочностным характеристикам прокатным РДС РК 5.04-24-2006. – Астана: Каз. сталь проект, 2007. – 22 с.
16. Рекомендации по проектированию: Балки двутавровые гофрированные облегченные (Гофробалки ТУ У В.2.6-28.1-30653953-007:2007). Х.: Мет.проект, 2013. – 110 с.
17. **Prabha V.C., Shalini A., Saravanaganesh S., Selvakumar K.** Study on Behaviour of Cold Formed Built-Up I-Section With Trapezoidal Corrugation in Web by Varying the Aspect Ratio and Angle of Corrugation. // *International Journal of Chemical Sciences*, 2015, Vol. 13, Issue 04, pp. 1935-1946.
18. **Divahar R., Joanna P.S.** Lateral Buckling of Cold Formed Steel Beam With Trapezoidal Corrugated Web. // *International Journal of Civil Engineering*

and Technology, 2014, Vol. 05, Issue 03, pp. 217-225.
19. **Александров А.В., Потапов В.Д., Державин Б.П.** Сопротивление материалов. – М.: Высшая школа, 2003. – 560 с.

Tatiana L. Dmitrieva, Dr.Sc., Professor, Department of Theoretical Mechanics and Strength of Materials, Irkutsk National Research Technical University, Lermontov street, 83, Irkutsk, 664074, Russia; phone/fax: + 7(914)9136125;
E-mail: dmitrievat@list.ru.

Khukhuudei Ulambayar, Ph.D. Student, Department of Automated Systems, Irkutsk National Research Technical University, Lermontov street, 83, Irkutsk, 664074, Russia; phone/fax: + 7(914)8746115;
E-mail: Ulambayar_kh@yahoo.com.

Дмитриева Татьяна Львовна, доктор технических наук, профессор, кафедра теоретической механики и сопротивления материалов, Иркутский национальный исследовательский технический университет, 664074, Россия, г. Иркутск, ул. Лермонтова, 83;
тел. + 7(914)9136125, E-mail: dmitrievat@list.ru.

Хухуудэй Уламбаяр, аспирант, кафедра автоматизированных систем, Иркутский национальный исследовательский технический университет; 664074, Россия, г. Иркутск, ул. Лермонтова, 83, тел. + 7(914)8746115;
E-mail: Ulambayar_kh@yahoo.com.

THE METHOD OF LOCAL AUTOMATIC CONTROL OF THERMOPHYSICAL PARAMETERS OF EXTERNAL WALLS OF BUILDINGS AT THE LOCATIONS OF CONDENSATE LOSS

Sergej V. Fedosov [1], Pavel N. Mureev [2], Vitalij G. Kotlov [2], Aleksandr N. Makarov [2], Andrej V. Ivanov [2]

[1] Ivanovo State Politechnical University, Ivanovo, RUSSIA
[2] Volga State University of Technology, Yoshkar-Ola, RUSSIA

Abstract: Today the buildings of the 60-80th of the XX century do not satisfy to modern requirements for energy saving. The low value of the resistance to heat transfer leads overcooling of the wall surface in the cold period of the year and to overheating in the warm period. In addition, over the years of operation building envelopes subjected to numerous of climatic changes that were not envisaged in the design earlier. The lowering of microclimate parameters in the room negatively affects to the comfort and health of a person. As a result, the specific heat consumption for heating increases, the resistance to heat transfer decreases, and the thermal diffusivity increases. Therefore, a new method for calculating the actual value of the resistance to heat transfer is developed. The problem of providing sanitary and hygienic and thermophysical comfort conditions in the premises of the student hostel of the Volga State University of technology is also being solved. This occurs by controlling the temperature of the internal surface of the outer walls with a heating cable. Such a design will not only keep the difference between the wall surface temperature and the internal air temperature within the limits of the norm, but will also help to solve the problem of condensate precipitation by raising the temperature of the inner surface of the wall above the dew-point temperature. The developed technique takes into account the conditions of the heat transfer regime at a particular time, and also makes a correction to the final value of the design resistance. This makes the technique applicable for processing the results of field experiments and determining the actual resistance to heat transfer. Also results of field experimental researches of external walls of buildings are resulted and the scheme of laboratory installation is shown.

Keywords: internal wall insulation, dew point, temperature, humidity, heat flux, heat transfer resistance, the quasi-stationary mode

СПОСОБ ЛОКАЛЬНОГО АВТОМАТИЧЕСКОГО УПРАВЛЕНИЯ ТЕПЛОФИЗИЧЕСКИМИ ПАРАМЕТРАМИ НАРУЖНЫХ СТЕН ЗДАНИЙ В МЕСТАХ ВЫПАДЕНИЯ КОНДЕНСАТА

С.В. Федосов [1], П.Н. Муреев [2], В.Г. Котлов [2], А.Н. Макаров [2], А.В. Иванов [2]

[1] Ивановский государственный политехнический университет, г. Иваново, РОССИЯ
[2] Поволжский государственный технологический университет, г. Йошкар-Ола, РОССИЯ

Аннотация: В настоящее время здания застройки 60-80-х годов XX века не отвечают современным требованиям по энергосбережению. Низкое значение сопротивления теплопередаче приводит к переохлаждению поверхности стенового ограждения в холодный период года и к перегреву в тёплый период. Кроме этого, за годы эксплуатации ограждающие конструкции зданий испытывают многочисленные климатические изменения, не предусмотренные ранее при проектировании. Снижение параметров микроклимата в помещении негативно воздействует на комфорт и здоровье человека. В результате возрастает удельный расход тепла на отопление, снижается сопротивление теплопередаче, повышается температуропроводность. Поэтому разработана новая методика расчета фактического значения сопротивления теплопередаче. Также решается задача обеспечения санитарно-гигиенических и теплофизических ком-

фортных условий в помещениях студенческого общежития Поволжского государственного технологического университета. Это происходит с помощью регулирования температуры внутренней поверхности наружных стен при помощи нагревательного кабеля. Подобная конструкция позволит не только сохранять перепад между температурой поверхности стены и температурой внутреннего воздуха в пределах нормы, но и будет способствовать решению проблемы выпадения конденсата путем повышения температуры внутренней поверхности стены выше температуры точки росы. Разработанная методика учитывает условия режима теплопередачи в конкретный момент времени, а также вносит поправку в итоговое значение расчетного сопротивления. Это делает методику применимой для обработки результатов натурных экспериментов и определения фактического сопротивления теплопередаче. Также приводятся результаты натурных экспериментальных исследований наружных стен зданий и показана схема лабораторной установки.

Ключевые слова: внутреннее утепление стены, точка росы, температура, влажность, тепловой поток, сопротивление теплопередаче, квазистационарный режим

Currently, the construction of residential buildings in Russia is rising with high speed. As a result, the country's housing stock is being updated. However, a large share in the housing stock still consist of buildings built in the 1960-1980th of the 20th century (up to 45% according to Rosstat). These houses were built by obsolete requirements for today [4]. For such a long period of time, both the external climatic conditions and the operating conditions of the buildings were subject to changes. All these conditions ultimately lead to a significant decrease in the heat-shielding characteristics of the exterior walls of buildings [9,10,11,12]. Under the condition of elevated temperatures and humidity of indoor air in the room, associated with domestic heat generation and insufficient ventilation of air, there are times when the temperature of the internal surface of the wall drops below the dew point temperature, i.e. there is a moment of condensation, which can lead to the formation of mold.

The basis for the development of new methods for determining the actual resistance to heat transfer was the method of V.I. Zuev and co-authors "Method for determining the thermal resistance of a structural element area under non-stationary heat transfer mode" [5], the essence of which is in determining the conditions for the existence of a quasi-stationary heat transfer mode and its criterion θ_{max}. In this method, the negative sides were identified, which were taken into account when developing a new technique.

The aim of this investigation is to develop a new technique that will reduce the calculation of the actual value of the heat transfer resistance to the determination of the minimum measurement time and the correction for thermal resistance ΔR; development of a local automatic room climate control system using a proportional-integral-differential controller.

Due to the fact that the constancy of the heat flux is an insufficient condition for the stationary heat transfer mode, the criterion for determining the quasi-stationarity of the heat transfer mode is the temperature distribution through the thickness of the fence in a straight line from outside to inside temperature.

In the case of a quasi-stationary heat transfer mode, when determining the actual heat transfer resistance, we distinguish two components: the heat transfer resistance $R^{0,92}$ and the ΔR amendment caused by the quasi-stationary heat transfer mode (1):

$$R_{факт} = R^{0,92} + \Delta R = \frac{T_в^{0,92} - T_н^{0,92}}{Q^{0,92}} + \Delta R \qquad (1)$$

where $R_{факт}$ is the fact resistance against heat transfer of the wall's part, $\frac{м^2 \cdot {}^0C}{Вт}$,; $T_в^{0,92}$ is temperature of internal surface with probability of 0,92(0,98), ºC; $T_н^{0,92}$ is temperature of external surface with probability of 0,92(0,98), ºC; $Q^{0,92}$ is heat flow with probability of 0,92(0,98), $\frac{Вт}{м^2}$,;

ΔR is a amendment to heat resistance of the wall's part, $\frac{м^2 \cdot {}^0C}{Вт}$.

Taking the heat transfer mode close to stationary, the value $R^{0.92}$ is calculated by the standard formula with the difference that the value of the temperature of the inner and outer surface and heat flux are taken with a probability of 0.92 (0.98). The amendment to the heat transfer resistance takes into account the quasi-stationarity of the heat transfer mode. The criterion of the stationary mode is the linear temperature distribution in the thickness of the outer wall, therefore, the amendment depends on the deviation of the actual temperature distribution from the theoretical (linear) and heat flux passing through the outer wall (2):

$$\Delta R = \sum_{i=1}^{6} |R_{cp} - R_i| \qquad (2)$$

where

$$R_{cp} = \frac{R^{0.92}}{6}$$

is theoretical resistance to heat transfer of i-th layer, calculated for quasi-stationary mode, $\frac{м^2 \cdot {}^0C}{Вт}$,

$$R_i = \frac{T_{i-1}^{0,92} - T_i^{0,92}}{Q^{0,92}}$$

calculated in accordance sensor readings, $\frac{м^2 \cdot {}^0C}{Вт}$.

In Figure 1, the dashed line shows the theoretical temperature distribution in the thickness of the outer wall, the solid one shows the actual temperature distribution in the thickness of the outer wall.

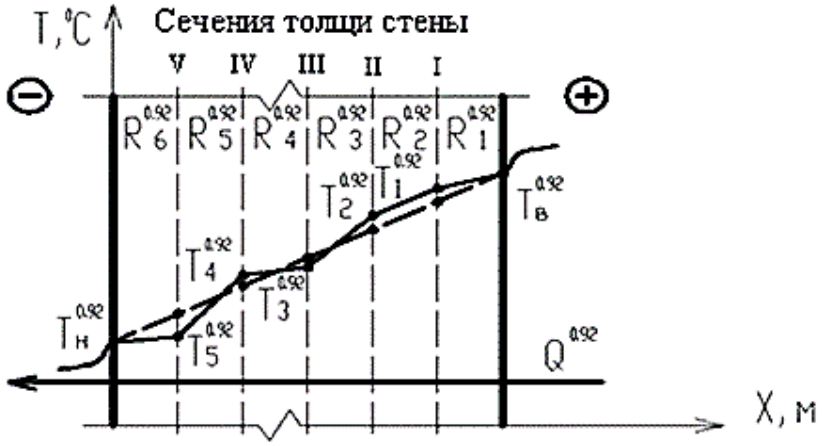


Figure 1. The actual and theoretical temperature distribution in the thickness exterior wall.

In practice, this technique is implemented using software, in which it can be put the selection criteria for the processed time intervals, the value of amendment ΔR in fractions of $R^{0.92}$ or absolute values. Measurements are made during the entire heating period, which allows us to find a set of values with the same criteria for the selection of time intervals. On the basis of the obtained values, the total value is determined with the help of the technique with the required probability, which is recommended to be taken as the actual value of the heat transfer resistance for the heat engineering calculation of the reconstructed buildings.

Using the classical formula to determine the actual resistance to heat transfer without taking into account the amendment ΔR deprives the meaning of the method using this approach for determining $R_{факт}$. In natural conditions it is impossible to create a stationary mode of heat transfer. In some techniques to bring the heat

transfer mode to the stationary it uses the various heating elements, which are located on the inner, outer, or on both surfaces. The use of such heating elements violates the thermal state of the outer wall section, that leads to a large error in the measurement results. Also unknown is there an affecting of these heating elements on the accuracy of data from heat flow and temperature sensors. The only correct solution is to conduct a full-scale experiment without changing the thermal state of the object, taking into account the degree of non-stationarity of the heat transfer mode.

The main conveniently controlled parameter of the stationary mode of heat transfer is the linear distribution of temperatures in the thickness of the outer wall during a time interval not less than the time of thermal inertia of this outer wall. If the temperature distribution in the thickness of the outer wall differs more significant from the linear one, then the degree of quasi-stationarity of the heat transfer mode is greater.

The developed technique takes into account the conditions of heat transfer at a particular point in time, and also amends the final value $R_{факт}$.. This makes the technique applicable for processing the results of experiments and determining the actual resistance to heat transfer.

The decision of wall insulation becomes the structure, which is a heating element mounted in the inner plaster layer of the wall (Fig. 2) [6].

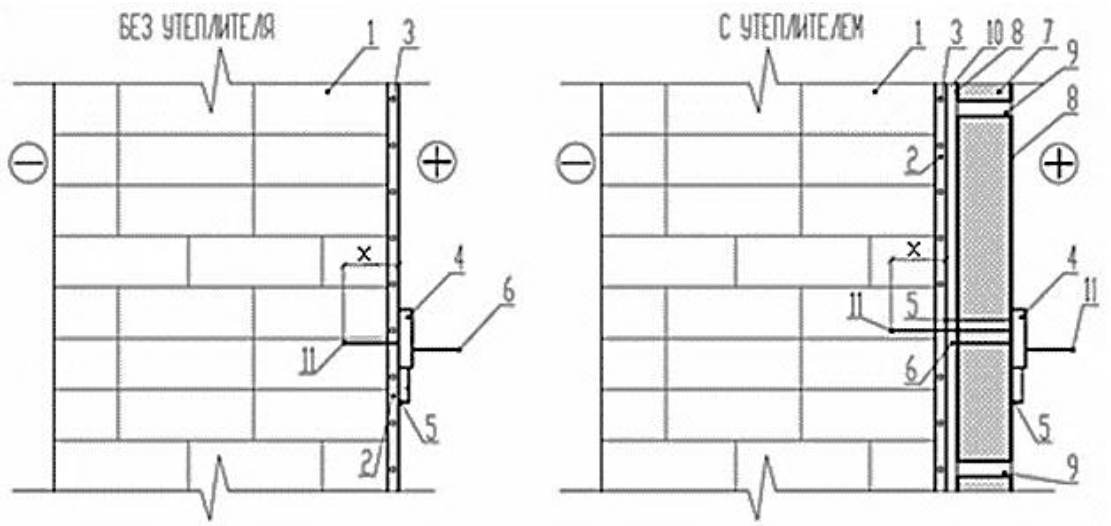


Figure 2. Designed wall fencing with adjustable temperature of the inner surface: 1-outer wall; 2 plastering layer; 3-heating element; 4-thermostat; 5-surface temperature sensor; 6-humidity and air temperature sensors; 7-insulation (mineral wool δ = 100 mm); 8 gypsum plasterboard; 9 products; 10-air gap; 11 temperature sensor.

Such a design not only maintain the difference between the wall surface temperature and the internal air temperature within the normal range (≤40 ° C according to [7]), but also help to solve the problem of condensate by increasing the temperature of the internal wall surface above the dew point temperature. In addition, the design variant with insulation (Fig. 2) increases the resistance to heat transfer of the wall enclosure, while the heating element will prevent the insulation from getting wet by shifting the dew point deep into the wall thickness.

The operation of the thermostat is based on the observance of two parameters: the provision of standardized temperature difference and condensation on the inner surface.

The fulfillment of these tasks will lead to the solution of other important requirements: the prevention of the possibility of mold formation on the inner surface of the walls; exclusion of

the probability of human contact with heated surfaces that are below the level required for a person's comfort; and the obstruction of wetting of the walls and, as a result, the reduction of heat loss through the building envelope.

The mathematical description of the dynamics of the thermal process of heat transfer to building structures are partial differential equations.

For the synthesis of algorithms for automatic control of technological processes, when describing the dynamics of processes, the transfer functions of the ratio of the input signal to the output type (3) are used:

$$W(s) = \frac{X(s)}{Y(s)} \quad (3)$$

where X(s), Y(s) are Laplace transformations of input and output signals respectively.

To determine the transfer functions of the masonry, the physical model of the control object is presented in Figure 3, which schematically depicts a heterogeneous masonry with a built-in heating element in the form of a nickel-chrome alloy heating cable, similar to that used in floor heating systems. In the physical model of the control object (Fig. 3), the following descriptions are adopted: Q_0 is a heat flow in the direction from the heating element to the room; Q_1 is a heat flow in the direction from the heating element to the outside of the building; Q_2 is a heat flow in the direction from the room to the outside of the building; Q_3 is a heat flow in the direction outside the building to the room; t_0 is the indoor temperature; t_1 is the temperature of the inner surface of the building wall; t_2 is the temperature of the outer surface of the building wall.

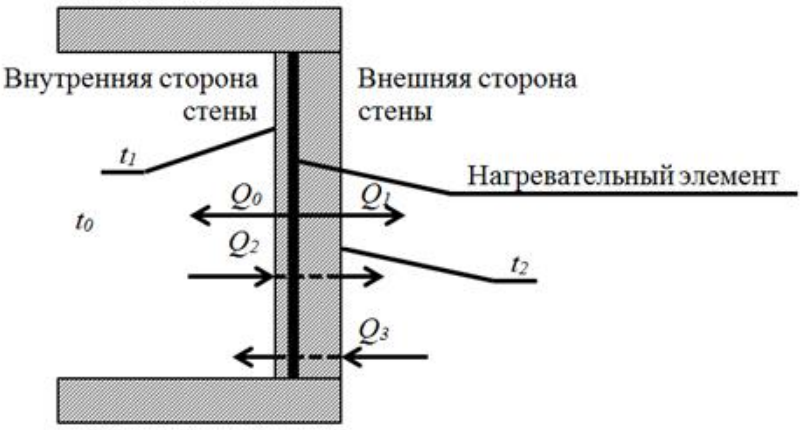


Figure 3. Physical model of the object of control.

V.S. Tkachev, A.V. Kostenko [1,8] proposed to represent the transfer function of heterogeneous masonry in the form of the sum of the transfer functions of its layers, that is, consider the masonry in layers. In this case, in the physical model of a masonry with a heating element, it is possible to distinguish two main layers: 1 is a layer from the heating element into the interior, through which the heat flow Q_0 passes; 2 is layer from the heating element to the outside of the building, through which the heat flux Q_1 passes. Taking into account the small depth of installation of the heating element in the wall relative to the inner side of the wall (no more than 5 cm), this layer can be considered conventionally homogeneous and describe it as one transfer function of the aperiodic link of the first order of the following form (4):

$$W(s) = \frac{1}{Ts+1} \quad (4)$$

where *T* is time constant; *s* is Laplace operator.

The purpose of the operation of the automatic control system is to maintain the temperature difference inside the room t_0 and the temperature of the inner surface of the building wall t_1

at a level less or equal to 40 ° C, which ensures the spatial shift of the dew point inside the building wall [2]. This protects the interior surface of the wall with decorative trimming from condensation, the spread of fungus and ensuring a comfortable location of the person inside the room.

In order to control the indoor temperature t_0 and the temperature of the inner surface of the building wall t_1, it is necessary to install two primary transducers - resistance thermometers. To prevent the possibility of self-oscillations in the automatic control system caused by abrupt changes in the readings of the thermometer of resistance of the internal temperature in the room t_0, it is necessary to ensure its sufficient inertia by using thermal screens or installing away from the main air flow caused by short-term opening of doors or windows in the room. The block diagram of the automatic control system is shown in Figure 4.

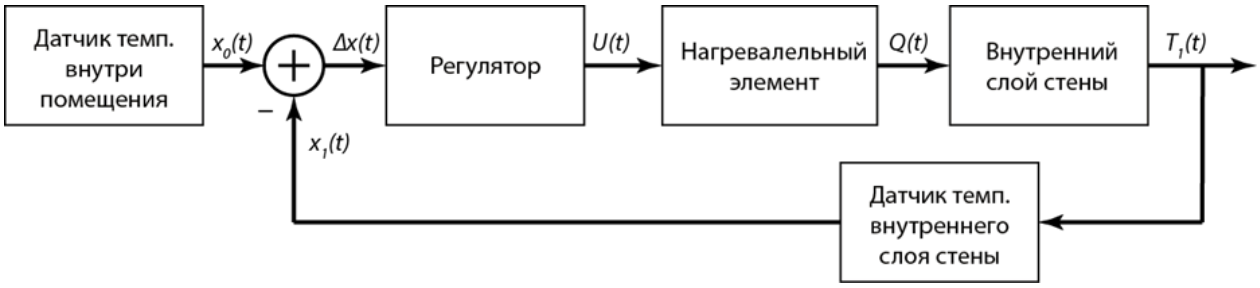


Figure 4. Block diagram of the automatic control system.

The basis of the automatic control system is a controller made according to the scheme of a classical proportional-integral-differential controller (PID controller), the operation of which is described by the expression (5):

$$U(t) = Ke(t) + \frac{1}{T_i} \qquad (5)$$

where t is time, K, T_i, T_d are proportionality coefficient, integration constant and differentiation constant respectively.

A signal on the mismatch Δx (t) of the measured air temperatures inside the room $x_0(t)$ and the inner layer of the wall $x_1(t)$ is sent to the input of the PID controller. The output control signal U(t) is formed according to expression (5), while the proportional coefficient, the integration constant and the differentiation constant are chosen experimentally from the point of view of minimizing the transition process or the overshoot value. The output control signal U (t) is actually the power control signal of the heating element built into the wall and takes values from 0 to 100 as a percentage of the maximum power of the heating element.

The transient graph obtained during simulation in VisSim is shown in Figure 5 and describes the temperature change t_1 of the inner wall surface with an abrupt change in indoor temperature from 20 ° C to 25 ° C at time T = 30 minutes. As can be seen from the graph, the use of the PID controller allows us to significantly reduce the time of the transition process.

For maximum reliability of the results, it is decided to conduct research in natural conditions (Figure 6). A residential dormitory is chosen as an object of study, in the corner rooms of which mold formations are observed.

Characteristics of the dormitory building: year of construction - 1975, number of floors - 9, building volume - 26,708 m3, total area - 6,335.9 m^2, external walls made of silicate bricks of 640 mm thick, plastered on the inside and outside with a cement-sand mortar 20 mm.

To improve the accuracy of the results, experimental facilities were located in several problem dormitory rooms located on the north-west side on different floors of the building (Fig. 7).

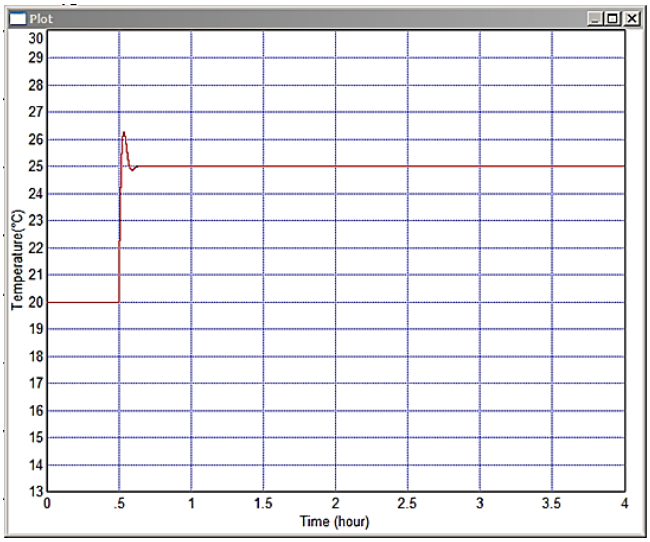


Figure 5. Transient graph of the heating of the inner layer of the wall using the PID controller.

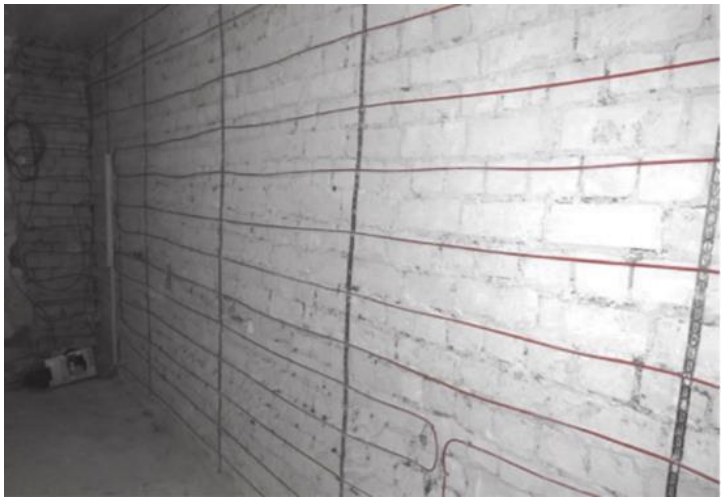


Figure 6. Heating cable on the inner surface of the wall of one of the living rooms of the dormitory.

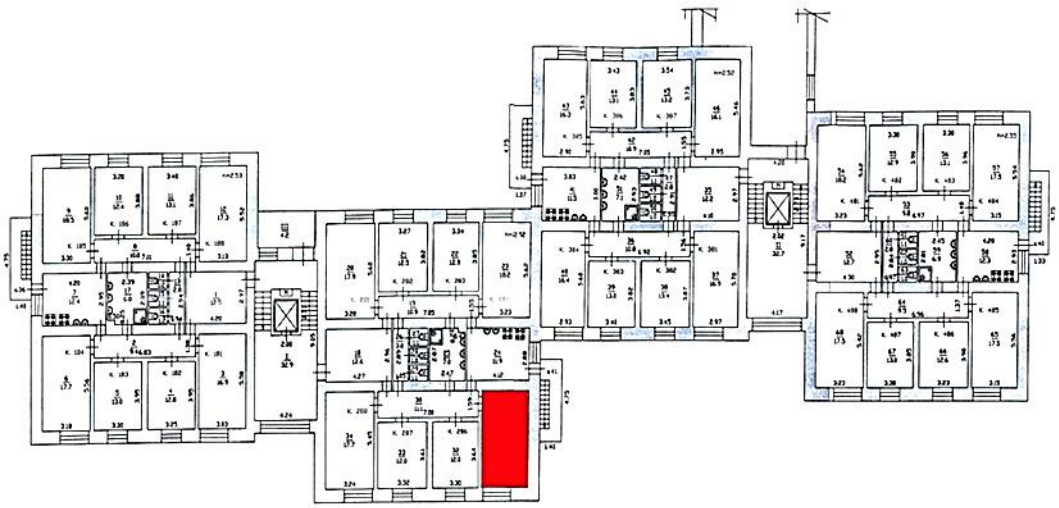


Figure 7. The location of rooms 225, 235, 245, 265 on the floor plan of a typical dormitory (indicated by color).

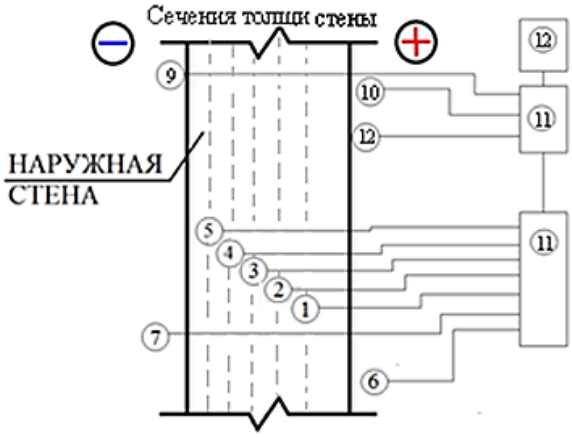


Figure 8. Diagram of the laboratory setup for determining the actual resistance to heat transfer.

The main installation with the control module is located in room number 245 on the fourth floor (Figure 8). The room has two exterior walls, one facing north, the other toward the west, and one window with a PVC profile facing north.

The data obtained from the experimental facilities allow us to track changes in temperature and humidity outside, on the surface and in the thickness of the wall enclosure.

Figure 9 shows a graph of the distribution of temperature fields on the surface and in the thickness of the wall fencing for the heating period of 2014-2015, which has 5 time intervals (I-V), when the difference between the temperatures of the inside air and the inner surface of the wall fencing exceeds the required value of 4 ^{0}C. The total duration of time when $\Delta t \geq 4$ ° C for the heating period 2014-2015 is 68 days, which is about 37% of the total duration of the heating period [3].

The graph (Figure 9) shows that the selected intervals I – V are characterized by a decrease in the values of the outdoor temperature, which indicates a high thermal conductivity of the wall material and a low resistance to heat transfer of the wall enclosure design.

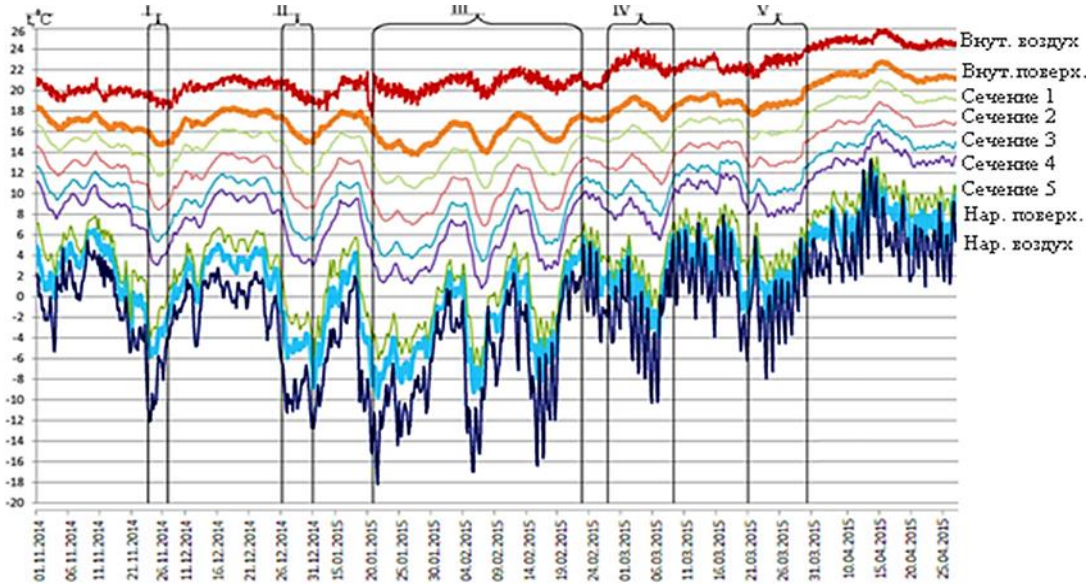


Figure 9. The graph of temperature distribution on the surface and in the thickness of the wall fencing (01.11.14-25.04.15).

Thus, it is visually shown that a low value of heat transfer resistance leads to overcooling of the wall surface in the cold period of the year and to overheating in the warm period, which leads to a person being uncomfortable in the room. The temperature distribution in the section of the wall thickness (Fig. 10) for the point in time when the outdoor temperature assumed the lowest value t_{min} = -19.49 0C (5:00, 01.23.2015) shows that the actual temperature values deviate from the line connecting the temperature of the outer and inner surface, which indicates the non-stationarity of heat transfer.

When analyzing the graph of changes in relative humidity in the thickness of the structure (Fig. 11), it can be seen that the values are not distributed linearly (straight from the inside to the outside of the room), which is clearly shown in Figure 12 at an arbitrary time 02.03.15.

From figures 11 and 12 it can be seen that the relative humidity takes maximum values in 4 sections - at a distance of 1/3 from the outer surface of the wall enclosure.

In one of the time intervals during the measurement period, a moment of condensate was observed on the inner surface of the wall (Fig. 13), when the values of the relative humidity of the internal air reached values of up to 76%, and the maximum temperature of the internal air is 24 ° C, and does not exceed 17 ° C, which is lower than the dew point temperature.

Based on the above, it should be noted that the thermal state of the outer wall during the entire heating period is not constant. The thermophysical characteristics of the material of the outer wall change during the entire heating period, which confirms the need for carrying out field studies for a long time.

Analysis of the experimental data shows that the thermal state of the outer wall during the entire heating period is not constant. The thermophysical characteristics of the material of the outer wall vary throughout the heating period.

To reduce labor and time costs, it is proposed to use a computer-aided design (CAD) system for modeling and forecasting heat fluxes in the thickness of a wall fence. CAD will reduce the number of sensors used to two (on the outer and inner surfaces of the wall). In this case, intermediate values will be determined automatically, taking into account probabilistic characteristics, reflecting the deviation of the actual values of temperatures from the theoretical ones.



Figure 10. The distribution of temperature values in the thickness of the wall at time 5:00 01.23.2015.

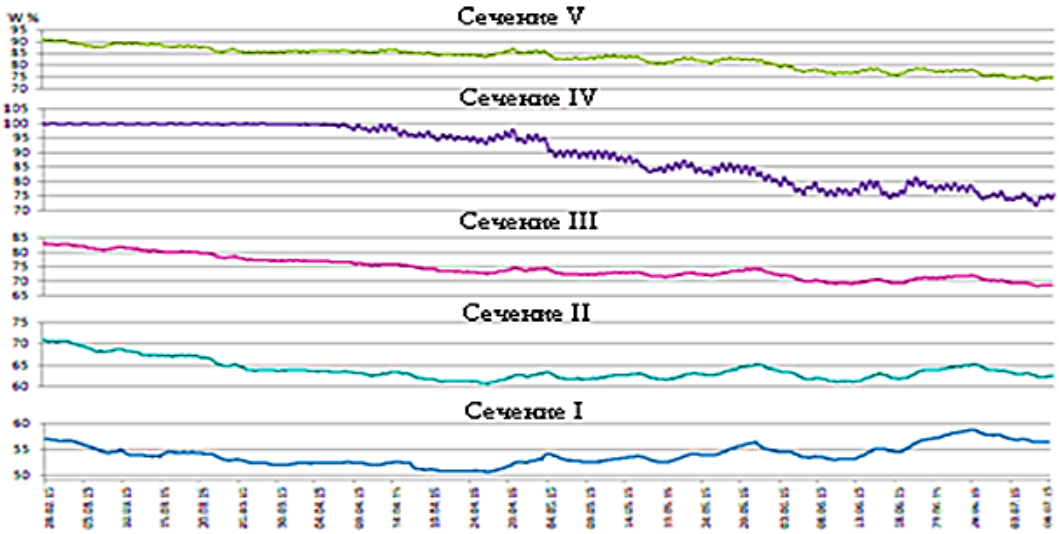


Figure 11. Distribution of the relative humidity values by section of the wall fence.

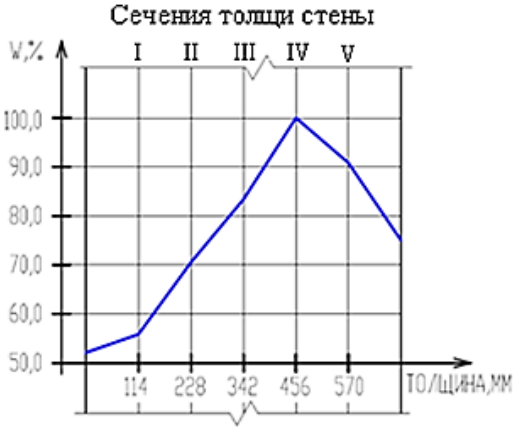


Figure 12. Distribution of values of relative humidity through the thickness of the wall enclosure 02.03.2015.

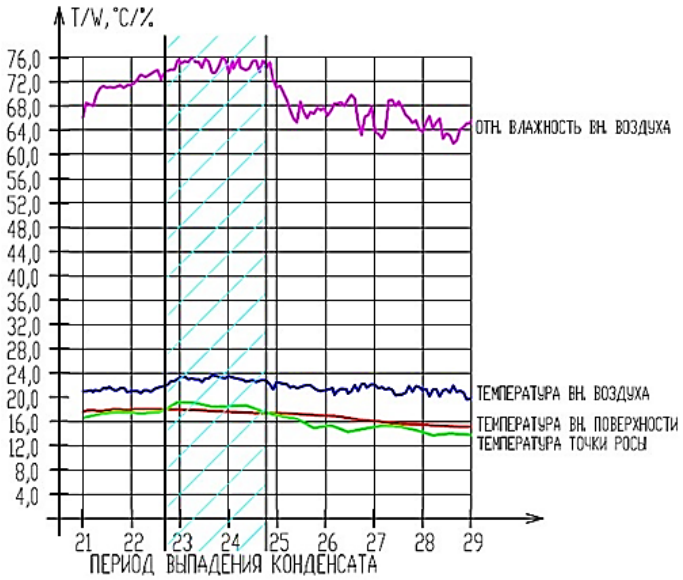


Figure 13. The time interval characterized by condensation on the inner surface of the walls.

Thus, the developed design will allow:
1) Prevent condensation on the inner surface of the wall;
2) Observe the normalized difference (≤4 ° C) between the temperature of the inner surface of the wall and the air temperature in the room.
In the future, it is planned to conduct similar experimental studies on wall fences made of other materials, such as concrete, wood, etc., in order to determine the previously agreed additional coefficients in determining the actual resistance to heat transfer. The need to develop an automated regulator of the heating element with the smallest possible number of unknown parameters and with a more "sensitive" mode of operation has been identified. It is also planned to link the work of the developed design with automated ATP thermal points, which will allow to avoid overheating of the premises and will contribute to energy efficiency.

REFERENCES

1. **Kostenko V., Nikolenko A., Popereka E., Yadrova M., Tymaniuk K.** Information-Measuring System of Control of the Normalized Parameters of Industrial Factors. // Eastern-European Journal Of Enterprise Technologies, 2014, Volume 3, Number 9(69), pp. 51-56.
2. **Makarov A.N.** and etc. Avtomaticheskaya Sistema Upravleniya Mikroklimatom Pomeshchenij [Automatic Control System of Indoor Climate]. // *Aktual'nye problemy ehlektronnogo priborostroeniya*, 2016, Vol. 2, pp. 517-523 (in Russian).
3. **Makarov A.N., Mureev P.N., Makarov R.N.** Analiz Izmeneniya Teplotekhnicheskih Harakteristik Naruzhnyh Kirpichnyh Sten Zdanij Zhiloj Zastrojki. Razrabotka Sposoba Resheniya Problemy Vypadeniya Kondensata na Vnutrennej Poverhnosti Ograzhdayushchih Konstrukcij [Analysis of Changes in the Thermal Characteristics of the Exterior Brick Walls of Residential buildings. Development of a Method for Solving the Problem of Condensate Precipitation on the Internal Surface of Enclosing Structures]. // *Vestnik Povolzhskogo gosudarstvennogo tekhnologicheskogo universiteta. Seriya "Materialy. Konstrukcii. Tekhnologii"*, 2017, No. 4, pp. 57-67 (in Russian).
4. **Mureev P.N., Kotlov V.G., Makarov A.N., Sabantseva I.S., Ivanov A.V.** Issledovanie Teplofizicheskih Svojstv Obrazcov Stenovyh Ograzhdenij pri Pomoshchi Avtomatizirovannogo Laboratornogo Kompleksa v Naturnyh Usloviyah [Investigation of the Thermophysical Properties of Wall Fence Samples Using an Automated Laboratory Complex in Natural Conditions]. // *Trudy Povolzhskogo gosudarstvennogo tekhnologicheskogo universiteta. Ser: Tekhnologicheskaya*, 2015, Vol. 3, pp. 212-216 (in Russian).
5. Patent 2010142067/28 Rossijskaya Federaciya. Sposob Opredeleniya Termicheskogo Soprotivleniya Uchastka Ehlementa Konstrukcii pri Nestacionarnom Rezhime Teploperedachi [The Method for Determining the Thermal Resistance of a Part of a Structure Element in the Non-Stationary Mode of Heat Transfer]. / V.I. Zuev and etc.– No. 2457471; published 14.10.2010, Byul. No. 21 (in Russian).
6. Patent na Izobretenie 2015131657 Rossijskaya Federaciya. Teploizolyacionnaya Konstrukciya Naruzhnoj Steni [Thermal Insulation Design of the Outer Wall]. / A.N. Makarov and etc – No. №2607561; published 10.01.2017, Byul. No. 1 (in Russian).
7. SP 50.13330.2012. Teplovaya Zashchita Zdanij [Thermal Protection of Buildings]. Utv. Prikazom Minregiona Rossii №265 2012-06-30. Moscow, Minregion Rossii, 2012 (in Russian).
8. **Tkachov V.S., Kostenko A.V.** Analiticheskoe Issledovanie Dinamiki Razogreva Odnorodnogo Tela [Analytical Research of Dynamics of Heating of a Homogeneous Body]. // *Bulletin of Phydniprovs'ska State Academy of Civil Engineering and Archi-*

tecture, 2012, No. 11, pp. 21-27 (in Russian).
9. **Fokin K.F.** Stroitel'naya Teplotekhnika Ograzhdayushchih Chastej Zdaniya [Construction Heat Engineering of the Enclosing Parts of the Building]. Moscow, Strojizdat, 2007, 319 pages (in Russian).
10. **Fedosov S.V.** Teplomassoperenos v Tekhnologicheskih Processah Stroitel'noj Industrii [Teplomassoperenos v tekhnologicheskikh protsessakh stroitel'noy industrii [Heat and Mass Transfer in Technological Processes of the Building Industry]. Ivanovo, IPK "PresSto", 2010. 364 pages (in Russian).
11. **Fedosov S.V., Sakharov A.A., Mirozov V.E.** Matematicheskaya Model' Teploprovodnosti i Promerzaniya Ograzhdayushchih Konstrukcij v Okrestnosti Zakladnyh Detalej [Mathematical Model of Heat Conduction and Freezing of Enclosing Structures in the Vicinity of Embedded Parts]. // *Vestnik Grazhdanskih Inzhenerov*, 2013, No. 1, pp. 32-36 (in Russian).
12. **Fedosov S.V.** and etc. Problemy Trekhslojnyh Ograzhdayushchih Konstrukcij [Problems of Three-Layer Enclosing Structures]. // *Zhilishchnoe stroitel'stvo*, 2012, No. 7, pp. 9-12 (in Russian).

СПИСОК ЛИТЕРАТУРЫ

1. **Kostenko V., Nikolenko A., Popereka E., Yadrova M., Tymaniuk K.** Information-Measuring System of Control of the Normalized Parameters of Industrial Factors. // *Eastern-European Journal Of Enterprise Technologies*, 2014, Volume 3, Number 9(69), pp. 51-56.
2. **Макаров А.Н.** и др. Автоматическая система управления микроклиматом помещений. // *Актуальные проблемы электронного приборостроения*, 2016, том 2, с. 517-523.
3. **Макаров А.Н., Муреев П.Н., Макаров Р.А.** Анализ изменения теплотехнических характеристик наружных кирпичных стен зданий жилой застройки. Разработка способа решения проблемы выпадения конденсата на внутренней поверхности ограждающих конструкций. // *Вестник Поволжского государственного технологического университета. Серия: Материалы. Конструкции. Технологии*, 2017, №4, с. 57-67.
4. **Муреев П.Н., Котлов В.Г., Макаров А.Н., Сабанцева И.С., Иванов А.В.** Исследование теплофизических свойств образцов стеновых ограждений при помощи автоматизированного лабораторного комплекса в натурных условиях. // *Труды Поволжского государственного технологического университета. Серия: Технологическая,* 2015, Вып.3, с. 212-216.
5. Патент 2010142067/28 Российская Федерация. Способ определения термического сопротивления участка элемента конструкции при нестационарном режиме теплопередачи. / В.И. Зуев [и др.]. – № 2457471; опубл. 14.10.2010, Бюл. № 21.
6. Патент на изобретение 2015131657 Российская Федерация. Теплоизоляционная конструкция наружной стены. / А.Н. Макаров и др. – №2607561; опубл. 10.01.2017, Бюл. №1.
7. **СП 50.13330.2012.** Тепловая защита зданий. Утв. Приказом Минрегиона России № 265 2012-06-30. – М.: Минрегион России, 2012.
8. **Ткачев В.С., Костенко А.В.** Аналитическое исследование динамики разогрева однородного тела. // *Вестник Приднестровской государственной академии строительства и архитектуры*, 2012, №11, с. 21-27.
9. **Фокин К.Ф.** Строительная теплотехника ограждающих частей здания. – М.: Стройиздат, 2007. – 319 с.
10. **Федосов С.В.** Тепломассоперенос в технологических процессах строительной индустрии. – Иваново: ИПК «ПресСто», 2010. – 364 с.

11. **Федосов С.В., Сахаров А.А., Мизоров В.Е.** Математическая модель теплопроводности и промерзания ограждающих конструкций в окрестности закладных деталей. // *Вестник гражданских инженеров*, 2013, №1, с. 32-36.
12. **Федосов С.В.** и др. Проблемы трехслойных ограждающих конструкций. // *Жилищное строительство*, 2012, №7, с. 9-12.

Федосов Сергей Викторович, академик Российской академии архитектуры и строительных наук (РААСН), доктор технических наук, профессор; советник при ректорате по внешним связям, заведующий кафедрой техносферной безопасности, Ивановский государственный политехнический университет; 153037, Россия, г. Иваново, ул. 8 Марта, д. 20;
E-mail: fedosov-academic53@mail.ru.

Муреев Павел Николаевич, кандидат технических наук, доцент кафедры «Проектирование зданий», Поволжский государственный технологический университет; 424000, Россия, г. Йошкар-Ола, ул. Панфилова, д. 17; e-mail: pavel.mureev@yandex.ru.

Котлов Виталий Геннадьевич, кандидат технических наук, профессор кафедры «Строительные конструкции и водоснабжение», директор института строительства и архитектуры, Поволжский государственный технологический университет; 424000, Россия, г. Йошкар-Ола, ул. Панфилова, д. 17;
E-mail: kotlov.vitaliy@mail.ru.

Макаров Александр Николаевич, главный инженер, Поволжский государственный технологический университет; 424000, Россия, г. Йошкар-Ола, ул. Панфилова, д.17. E-mail: saha240164@mail.ru.

Иванов Андрей Владимирович, ассистент кафедры «Проектирование зданий», Поволжский государственный технологический университет; 424000, Россия, г. Йошкар-Ола, ул. Панфилова, д.17;
E-mail: IvanovAVL@volgatech.net.

Sergey V. Fedosov, Full Member of the Russian Academy of Architecture and Construction Sciences, Professor, Dr.Sc.; Advisor at the University Administration on External Relations, Head of the Department of Technospheric Safety, Ivanovo State Politechnic University; 20, 8 Marta Street, Ivanovo, 153037, Russia;
E-mail: fedosov-academic53@mail.ru.

Pavel N. Mureev, Ph.D., Associate Professor of the Department “Designing Buildings”, Volga State University of Technology; 17, Panfilova Street, 424000, Yoshkar-Ola, Russia; e-mail: pavel.mureev@yandex.ru.

Vitaliy G. Kotlov, Ph.D., Professor of the Department “Building Structures and Water Supply”, Director of the Institute of Construction and Architecture Volga State University of Technology; 17, Panfilova Street, 424000, Yoshkar-Ola, Russia; e-mail: kotlov.vitaliy@mail.ru.

Aleksandr N. Makarov, Chief Engineer, Volga State University of Technology; 17, Panfilova Street, 424000, Yoshkar-Ola, Russia; e-mail: saha240164@mail.ru.

Andrey V. Ivanov, Assistant of the Department of Building Design, Volga State University of Technology; 17, Panfilova Street, 424000, Yoshkar-Ola, Russia;
E-mail: IvanovAVL@volgatech.net

INELASTIC ANALYSIS OF REINFORCED CONCRETE STRUCTURES IN SCAD

Sergiy Yu. Fialko [1, 2]***, Anatolii V. Perelmuter*** [2]
[1] Tadeusz Kościuszko Cracow University of Technology, Krakow, POLAND
[2] IT company SCAD Soft, Kyiv, UKRAINE

Abstract: This paper describes the approach implemented in SCAD for the analysis of behavior of fragments of thin-walled reinforced concrete structures taking into account the elastic-plastic behavior of both concrete and reinforcement.

Keywords: reinforced concrete structures, nonlinear analysis, stress-strain diagram

РЕАЛИЗАЦИЯ НЕУПРУГОГО РАСЧЕТА ЖЕЛЕЗОБЕТОННЫХ КОНСТРУКЦИЙ В ПРОГРАММНОМ КОМПЛЕКСЕ SCAD

С.Ю. Фиалко [1, 2]***, А.В. Перельмутер*** [2]
[1]Краковский технологический университет им. Тадеуша Костюшко, г. Краков, ПОЛЬША
[2] НПО «СКАД Софт», г. Киев, УКРАИНА

Аннотация: Представлен подход, реализованный в программном комплексе SCAD для анализа поведения фрагментов тонкостенных железобетонных конструкций с учетом упруго-пластической работы как бетона, так и арматуры.

Ключевые слова: железобетонные конструкции, неупругий расчет, диаграмма напряжение-деформация

The report describes the features of software implementation and new SCAD [7] modules for nonlinear analysis of thin-walled reinforced concrete structures based on a specially developed method [9].

It should be noted that in this case plastic behavior implies that loading and unloading are performed according to different laws and the residual deformations are taken into account. This is a fundamental difference from some developments where the so-called "physical nonlinearity" was used, which, in fact, reflects not the plastic behavior, but the nonlinear elasticity. Another important point is that all calculations are performed for a structure with specified reinforcement, i.e. we are dealing with a verification analysis (examination of the structural design).

The analysis of reinforced concrete structures taking into account the inelastic behavior of the material is implemented in SCAD by using special finite elements: a bar element, triangular and quadrangular shell elements (Figure 1).

When creating a design model the mode for specifying the reinforcement layout is used (Figure 2). It implies well-defined options for the placement of rebars, both in bar and in shell elements. The latter assume an orthogonal mesh design, the same orientation of the upper and lower reinforcement and the arrangement of rebars consistent with the direction of the alignment of forces N_{x1}.

This corresponds to common cases of reinforcement design, although it narrows the fundamental possibilities of the calculation method, when the number of reinforcement layers in shells can be greater than four and the direction of reinforcement bars in each reinforcement layer can be arbitrary.

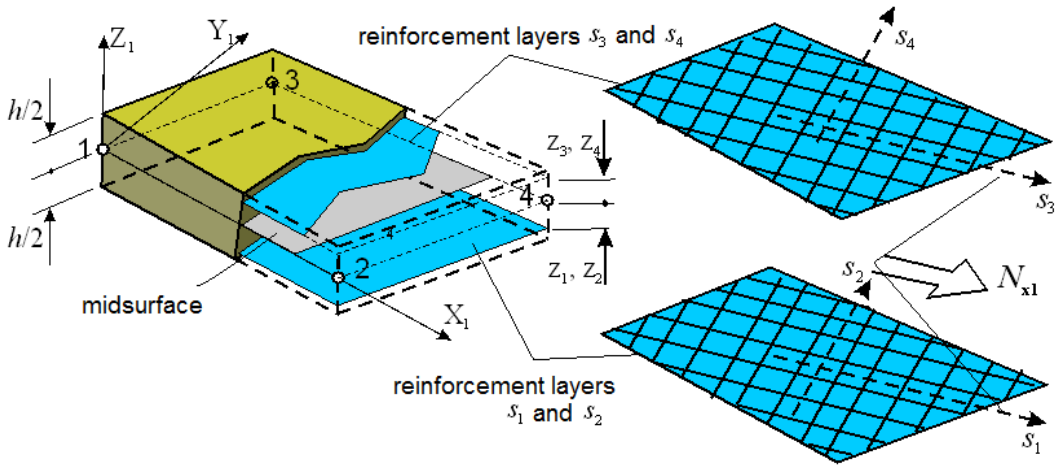


Figure 1. Four-node finite element for the calculation of reinforced concrete structures.

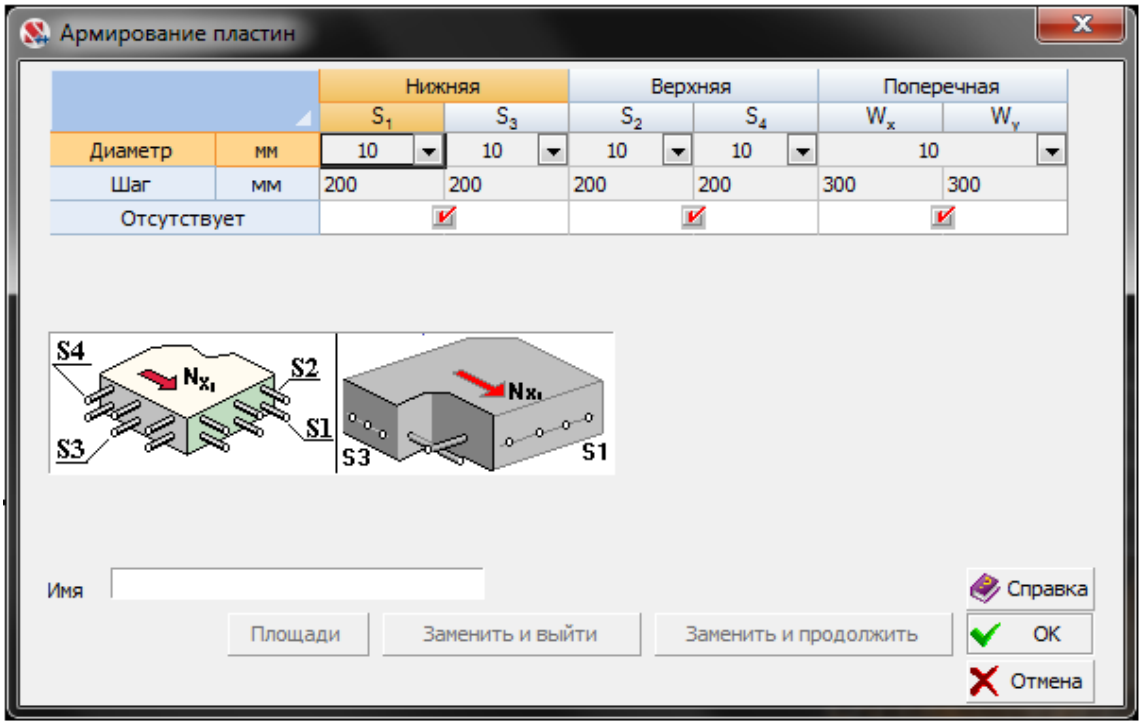


Figure 2. The "Reinforcement of Plates" dialog box.

This calculation mode is invoked by checking the **Physical nonlinearity** checkbox in the **Rigidities** dialog box. If this checkbox is checked, the **Materials** dialog box appears, where you can specify the physical and mechanical properties of the material.

The software provides two options of the plastic behavior of the material:

- according to the strain theory of plasticity;
- according to the theory of plastic flow.

The strain theory of plasticity has given the best agreement with experiment in most tested cases. This option is used by default. In this case only the "stress-strain" diagram is required to describe the behavior of the system. The conditions of the elastic volume change and elastic unloading, as well as the proportionality of the stress deviator and the strain deviator, responsible for the shear and shape changes, respectively, are satisfied.

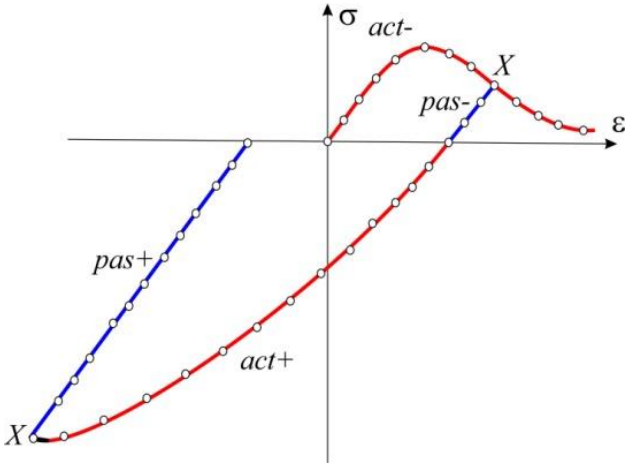


Figure 3. The σ – ε diagram: act- – active loading in the tension area; pas- – unloading in the tension area; act+ – active loading in the compression area; pas+ – unloading in the compression area; X – start of unloading.

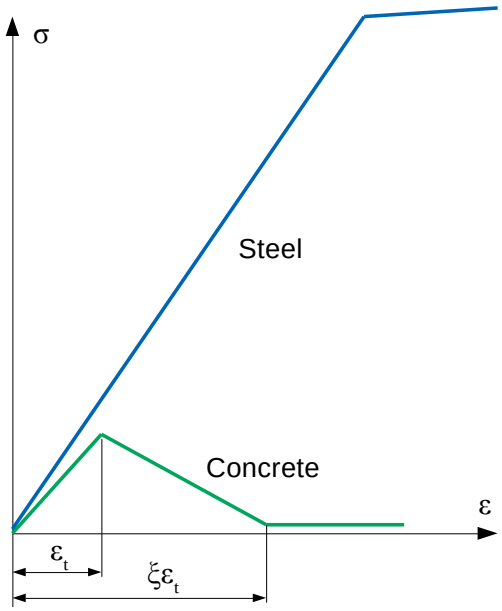


Figure 4. Regularization parameter.

In the second case, the behavior of the system also defines the yield surface, which in the program can be represented either by the Drucker-Prager plasticity condition [1] or by the Genie's plasticity condition [5].

The stress-strain relationship with a descending branch in the tension area can be used to describe the behavior of concrete (Figure 3). The degradation of concrete caused by crack opening is modeled in this way. It is known that the presence of a descending branch of the σ - ε diagram is a source of instability of computational algorithms. The approach implemented in SCAD is based on the fact that only reinforced concrete (and not concrete) structures are considered, and the reinforcement, the σ - ε diagram for which does not have any descending regions, regularizes the numerical solution.

Since in the numerical implementation of a nonlinear problem, an arbitrary assignment of the σ – ε diagram can lead to a lack of convergence (see for example [4]), they are automatically reduced to a form that ensures the stability of the computational process. For this purpose, the parameter ξ is used, which specifies the length of the descending branch (Figure 4).

The role of the parameter ξ is illustrated by a simple example of a tensile reinforced concrete bar (Figure 5).

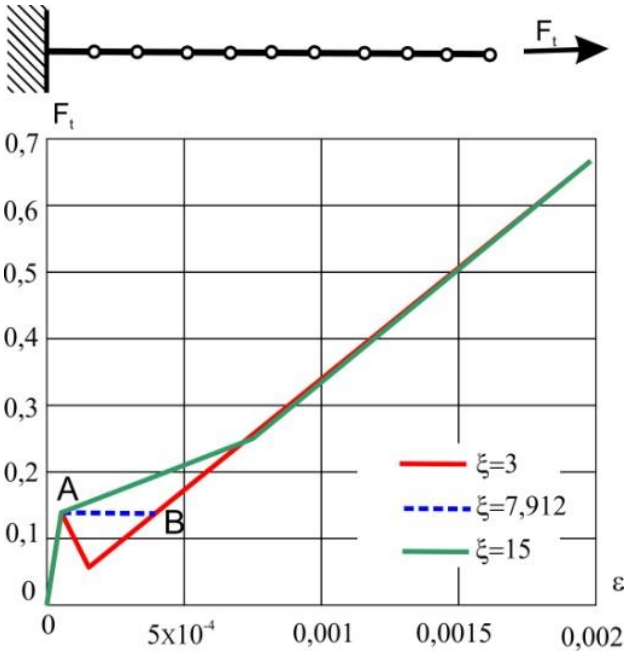


Figure 5. Tension of a reinforced concrete bar.

When ξ = 15 ($\xi > \xi_{min}$) the equilibrium curve increases monotonically and corresponds to stable equilibrium states at all points. When $\xi = \xi_{min} = 7.912$ the equilibrium curve has a plateau.

When $\xi = 3$ ($\xi < \xi_{min}$) a descending region appears on the equilibrium curve, corresponding to unstable equilibrium states. Therefore, a jump occurs from the point A, which corresponds to the beginning of the descending branch of the σ - ε diagram for concrete, to a new stable equilibrium state (point B). Here

$$\xi_{min} = 1 + E/(\mu_s E_s),$$

where $$\mu_s = A_s/A$$

is the reinforcement ratio, A is the concrete area, A_s is the reinforcement area [9].

In the considered simple problem the jump from point A to point B occurs simultaneously for all finite elements when $\xi < \xi$min. However, in real problems such jumps in different finite elements occur at different values of the load parameter. The equilibrium curve contains many regions corresponding to unstable equilibrium states, and obtaining the correct numerical solution for such a problem becomes too time-consuming. Therefore, the program always takes $\xi > \xi$min .

Allowing for the degradation of concrete in the tension area during cracking when obtaining the numerical results for the curve *a* can lead to a time-consuming solution. Obtaining the numerical results for the curves *b* and *c* without taking into account the degradation of concrete and the strength of concrete in the tension area (Figure 6) is significantly less time-consuming.

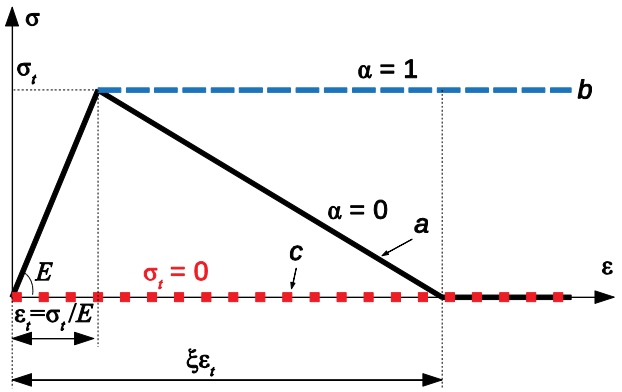


Figure 6. Diagrams for concrete in the tension area.

The performed calculations show that the curve *b* gives an upper-bound estimate of the solution, and the curve *c* gives a lower-bound estimate. If the difference between the curves *b* and *c* turns out to be small, then we can take the curve *c* as the final result, when using the curve *a* leads to considerable computational difficulties.

The work of the program can be illustrated by the analysis of a fragment of a multistory building (Figure 7). The design model was created from triangular and quadrangular shell elements [3].

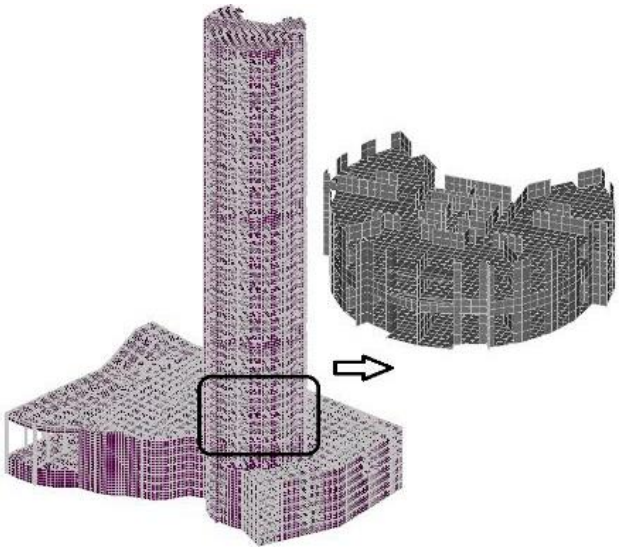


Figure 7. Multistory building fragment.

The results of the calculation enable to detect critical states of finite elements, which in turn indicate that the structure has experienced some irreversible changes. It means that the finite element has reached its limit state, but the system may still be serviceable.

Figure 8 shows critical events in the considered example. Apparently, such states of the structure require close attention. It can only be noted here, that this problem is not solved in the design codes, which consider the plastic redistribution of forces only in particular cases.

Calculations performed when testing the software have indicated some unusual results:

1. When there are developed deformations, some floor slab elements turn out to be tensile! This effect is caused by the fact that strong walls form a closed loop for the floor. The applied vertical load from the weight of the above floors compresses the walls in the vertical direction, simultaneously causing the lateral expansion.

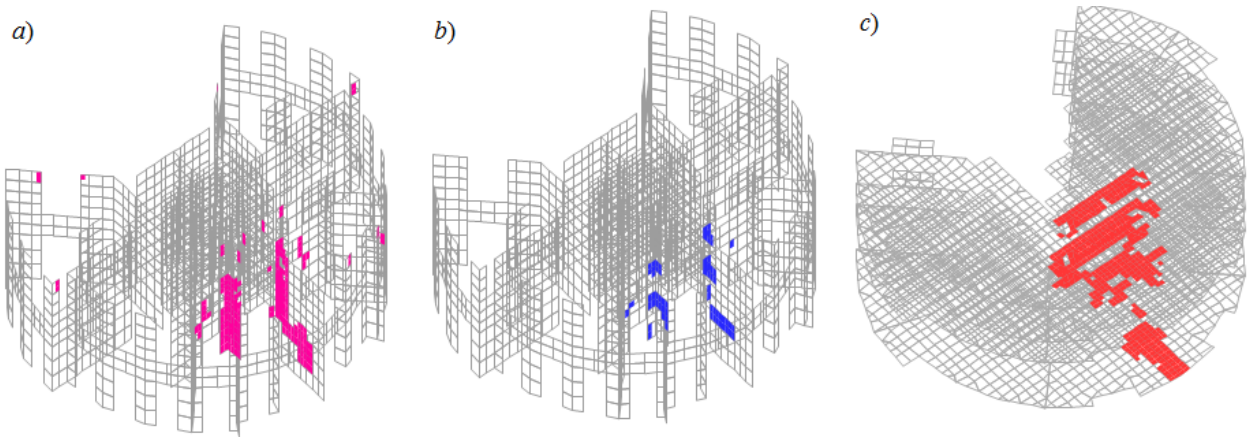


Figure 8. Results of the calculation: a – the reinforcement of the compression area has reached the yield point; b – the concrete of the compression area has reached the yield point; c – the reinforcement of the tension area has reached the yield point.

2. Due to the fact that when plastic deformations develop, the tangential stiffness of concrete is distributed asymmetrically across the section height, and also in the case of asymmetrical reinforcement, nonzero components appear in the stiffness matrix of a finite element relating membrane and bending internal forces.

Tension-compression stresses and shear stresses arise while transverse bending. At the same time when internal forces act at the middle surface the transverse bending is manifested. None of this is true for elastic finite elements from a homogeneous material.

Finally, let us point out some general problems that arise in the nonlinear structural analysis. In particular, the nonlinear analysis can be extremely challenging for the majority of SCAD users since their professional experience is based on linear problems. It should also be noted that there is a contradiction between the results of the refined elastoplastic calculation and the rule for applying the method of design limit states, where the safety factors are justified by the linear probabilistic analysis.

After all, both the distribution of internal forces and the strength parameters are defined by the same diagram of the material behavior, so the question arises about the possibility of their separate consideration (Figure 9).

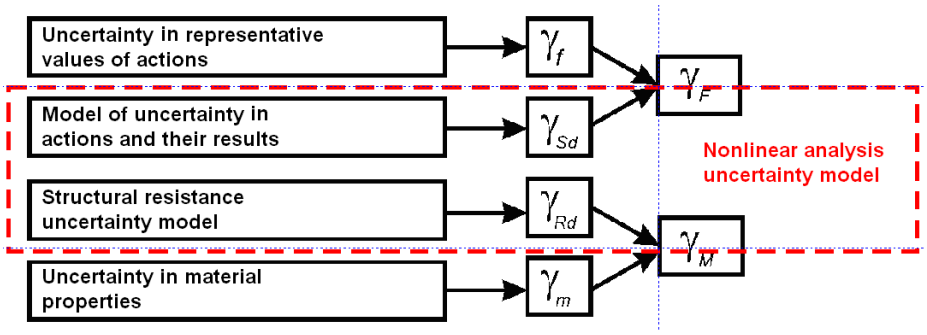


Figure 9. Selection of design factors.

A complete transition to nonlinear analysis is hardly possible due to the fundamental difficulties arising here [8]. And the long history of using the linear calculations, apparently, speaks in favor of the fact that they should not be abandoned yet. Nonlinear analysis should serve as an auxiliary tool to complement and clarify the results of linear calculations.

For example, when designing a high-rise complex “Federation” in Moscow [6], all linear calculations were preliminarily performed, and the peculiarities of the structural behavior were determined. And only then was the behavior of the considered fragments refined taking into account the nonlinear behavior of reinforced concrete.

REFERENCES

1. **Drucker D.C., Prager W.** Soil Mechanics and Plastic Analysis or Limit Design. // *Quaterly of Applied Mathematics*, 1952, Vol. 10, pp. 157-165.
2. **Fialko S.Yu.** Quadrilateral Finite Element for Analysis of Reinforced Concrete Floor Slabs and Foundation Plates. // *Applied Mechanics and Materials*, 2015, Vols. 725-726, pp. 820-835.
3. **Fialko S.Yu., Karpilovskyi V.S.** Triangular and Quadrilateral Flat Shell Finite Elements for Nonlinear Analysis of Thin-Walled Reinforced Concrete Structures in SCAD Software. // *Shell Structures: Theory and Applications*, Vol. 4. (ed. Pietraszkiewicz W. and Witkowski W.) CRC Press Taylor & Francis Group, London, New York. 2017, pp. 367-370.
4. **Kayhan E.** Application of Viscous and Non-Local Integral Type Regularization Schemes for Softening Plasticity. Master’s Thesis. Manufacturing Engineering Atilim University, 2009.
5. **Geniev G.A., Kissyuk V.N., Tupin G.A.** The *T*heory of Plasticity of Concrete and Reinforced Concrete. Moscow. Stroyizdat, 1974. 306 pages (in Russian).
6. **Karpenko N.I., Karpenko S.N., Travush V.I.** O Metodah Rascheta Vysotnyh Zdanij i Sooruzhenij iz Monolitnogo Zhelezobetona na Osnove Poslojnoj Detalizacii [On the Methods for Analysis of High-Rise Buildings and Structures from Monolithic Reinforced Concrete on the Basis of Layered Detailing]. // *Sovremennoe Promyshlennoe i Grazhdanskoe Stroitel'stvo*, 2011, Vol. 7, No. 3, pp. 147-163 (in Russian).
7. **Karpilovsky V.S., Kriksunov E.Z., Malyarenko A.A., Perelmuter A.V., Perelmuter M.A., Fialko S.Yu.** SCAD Office. Versija 21 Vychislitel'nyj Kompleks SCAD++ [SCAD Office. Version 21. SCAD++]. Moscow, SCAD Soft, ASV Publishing House, 2015, 848 pages (in Russian).
8. **Perelmuter A.V., Tur V.V.** Gotovy li My Perejti k Nelinejnomu Analizu pri Proektirovanii? [Whether we are Ready to Proceed to a Nonlinear Analysis at Designing?]. // *International Journal for Computational Civil and Structural Engineering*, 2017, Volume 13, Issue 3, pp. 86-102.
9. **Fialko S.Yu.** Primenenie Metoda Konechnyh Jelementov k Analizu Prochnosti i Nesushhej Sposobnosti Tonkostennyh Zhelezobetonnyh Konstrukcij s Uchetom Fizicheskoj Nelinejnosti [Application of Finite Element Method to Analysis of Strength and Bearing Capacity of Thin-Walled Concrete Structures, Taking into Account the Physical Nonlinearity]. Moscow, SCAD Soft, ASV Publishing House, 2018.

СПИСОК ЛИТЕРАТУРЫ

1. **Drucker D.C., Prager W.** Soil Mechanics and Plastic Analysis or Limit Design. // *Quaterly of Applied Mathematics*, 1952, Vol. 10, pp. 157-165.
2. **Fialko S.Yu.** Quadrilateral Finite Element for Analysis of Reinforced Concrete Floor Slabs and Foundation Plates. // *Applied Mechanics and Materials*, 2015, Vols. 725-726, pp. 820-835.
3. **Fialko S.Yu., Karpilovskyi V.S.** Triangular and Quadrilateral Flat Shell Finite Elements for Nonlinear Analysis of Thin-Walled Reinforced Concrete Structures in SCAD

Software. // *Shell Structures: Theory and Applications*, Vol. 4. (ed. Pietraszkiewicz W. and Witkowski W.) CRC Press Taylor & Francis Group, London, New York. 2017, pp. 367-370.

4. **Kayhan E.** Application of Viscous and Non-Local Integral Type Regularization Schemes for Softening Plasticity. Master's Thesis. Manufacturing Engineering Atilim University, 2009.
5. **Гениев Г.А., Киссюк В.Н., Тюпин Г.А.** Теория пластичности бетона и железобетона. – М.: Стройиздат, 1974. – 316 с.
6. **Карпенко Н.И., Карпенко С.Н., Травуш В.И.** О методах расчета высотных зданий и сооружений из монолитного железобетона на основе послойной детализации. // Современное промышленное и гражданское строительство, 2011, том. 7, №3, с. 147-163.
7. **Карпиловский В.С., Криксунов Э.З., Маляренко А.А., Перельмутер А.В., Перельмутер М.А., Фиалко С.Ю.** SCAD Office. Версия 21 Вычислительный комплекс SCAD++. – М.: Издательство АСВ, 2015. – 848 с.
8. **Перельмутер А.В., Тур В.В.** Готовы ли мы перейти к нелинейному анализу при проектировании? // *International Journal for Computational Civil and Structural Engineering / Международный журнал по расчету гражданских и промышленных конструкций*, 2017, Volume 13, Issue 3, pp. 86-102.
9. **Фиалко С.Ю.** Применение метода конечных элементов к анализу прочности и несущей способности тонкостенных железобетонных конструкций с учетом физической нелинейности. – М.: АСВ, 2018. – 192 с.

Sergey Yu. Fialko, Professor, Dr.Sc., Department of Physics, Mathematics and Applied Computer Science, Cracow University of Technology; 24, ul. Warszawska, Kraków 31-155, Poland; tel. +48 12 628 20 00; fax +48 12 628 20 71; e-mail: sergiy.fialko@gmail.com, sfialko@poczta.onet.pl.

Anatolii V. Perelmuter, Foreign member of the Russian Academy of Architecture and Construction Sciences (RAACS), Doctor of Science, Professor; SCAD Soft Ltd; office 1,2, 3a Osvity street, Kiev, 03037, Ukraine; phone: +38 044 249 71 93 (91), +38 044 248 71 00, +38 044 248 80 60; e-mail: avp@scadsoft.com.

Фиалко Сергей Юрьевич, профессор, доктор технических наук, кафедра физики, математики и прикладных компьютерных наук, Краковский политехнический университет; 24, ul. Warszawska, Kraków 31-155, Poland; тел. +48 12 628 20 00; факс +48 12 628 20 71; e-mail: sergiy.fialko@gmail.com, sfialko@poczta.onet.pl.

Перельмутер Анатолий Викторович, иностранный член Российской академии архитектуры и строительных наук (РААСН), профессор, доктор технических наук; НПО СКАД Софт; 03037, Украина, г. Киев, ул. Просвещения (Освиты), 3а, к. 1,2; тел.: +38 044 249 71 93 (91), +38 044 248 71 00, +38 044 248 80 60; e-mail: avp@scadsoft.com.

THE NEW PHYSICALLY NONLINEAR FINITE ELEMENTS IN SOFTWARE PACKAGE LIRA 10.8

Yuriy D. Geraymovich, Isaak D. Yevzerov, Dmitriy V. Marchenko
LIRA Group of Companies, Kiev, UKRAINE

Abstract: The new physically nonlinear finite elements, based on the theory of elastic plasticity, are proposed for bending rods and plates. These new elements can be used for static and dynamic problems, including seismic. The iterative method is used for static problems, the finite differences method – for dynamic.

Keywords: elastic plasticity, iterative method, finite differences method

НОВЫЕ ФИЗИЧЕСКИ НЕЛИНЕЙНЫЕ КОНЕЧНЫЕ ЭЛЕМЕНТЫ В ПРОГРАММНОМ КОМПЛЕКСЕ ЛИРА 10.8

Ю.Д. Гераймович, И.Д. Евзеров, Д.В. Марченко
Группа компаний «ЛИРА», г. Киев, УКРАИНА

Аннотация: Предлагаются новые физически нелинейные конечные элементы изгибаемых стержней и пластин, основанные на теории упруго-пластичности. Эти новые элементы могут применяться как для статических, так и для динамических расчетов, в том числе и для решения задач сейсмики. В статической задаче применяется шагово-итерационный метод, в динамической – метод конечных разностей.

Ключевые слова: упруго-пластичность, итерационный метод, метод конечных разностей

INTRODUCTION

In the previous versions of the LIRA software package (SP LIRA), physically nonlinear finite elements (FE) for bending rods and plates, based on the nonlinear theory of elasticity, were realized. These FE are successfully used for static calculations, but are not applicable to dynamics problems. Then, two-dimensional and three-dimensional physically nonlinear FE, based on the theory of elastic-plasticity, were developed. These elements are used for both static and dynamic calculations, but they do not solve bending problems. In the version of SP LIRA 10.8 new physically nonlinear FE of bending rods and plates are proposed, based on the theory of elastic-plasticity. These new elements have all the possibilities that physically nonlinear bending elements have – the same set of loads, shear calculation, the presence of an elastic basis, which can be one-sided. New elements can be used for both static and dynamic calculations, including seismic problems. The stepwise iteration method is used in the static problem, the finite difference is applied in the dynamic problem the finite difference method is applied. Convergence is proved in [1].

Dependences between stresses and strains in the theory of elastic-plasticity are studied in [2]. Let us introduce in stress space

$$\sigma = \{\sigma_{ij}\}$$

a closed convex set K, which contains point O, determined by inequality

$$\Phi(\sigma) \le 0,$$

where $\Phi(\sigma)$ – continuous convex function. Denote as $P_K(\sigma)$ nearest to σ point of set K,

$$g(\sigma) = \sigma - \mathrm{P}_{\mathrm{K}}(\sigma),$$

where $g(\sigma) = 0$ if $\sigma \in \mathrm{K}$. Assume that the strains ε_{ij} are sums of elastic and plastic deformations, where elastic deformations satisfy Hooke's law, whereas velocities of plastic deformations are equal to vector $g(\sigma)$. Inequalities, which determine set K, are formulated in terms of main stresses $\sigma_i, i = 1,2,3$, $\sigma_1 \geq \sigma_2 \geq \sigma_3$, or invariants

$$S_1 = \sigma_1 + \sigma_2 + \sigma_3,$$
$$S_2 = \sqrt{(\sigma_1 - \sigma_2)^2 + (\sigma_2 - \sigma_3)^2 + (\sigma_3 - \sigma_1)^2}.$$

Prandtl model

$$R_c \leq \sigma_i \leq R_s$$

for rods and Geniev model

$$\Phi(\sigma) = -(R_c + R_s)S_1/3 + S_2^2 + R_c * R_s$$

for plates are used, $R_c \leq 0 \leq R_s$ are uniaxial compression and tension limits.

EXAMPLES

Examples of static and dynamic problems solution with new physically nonlinear finite elements of bending rods and plates, based on the nonlinear theory of elasticity, are given.

An example of solving a static problem.
As an example, demonstrating the differences in the work of physically nonlinear and elastically plastic FE, a cantilever beam loaded with a uniformly distributed load of intensity q=12 tf/m is considered and then unloaded by a uniformly distributed load of the same intensity. Simulation was performed by both rod and shell FE. The rod (FE 210) and shell (FE 244) physically nonlinear FE and rod (FE 510) and shell (FE 544) elastic-plastic FE were used. The calculation scheme consists of 5 elements (Figure 1). All the dimensions in figure 1 are given in millimeters. The cross-section of the cantilever beam is reinforced with one rod 56 mm in diameter, installed as shown in Figure 1.
Diagrams of work and numerical values describing the law of deformation for concrete and reinforcement are shown in figure 2 and Figure 3.
The load is selected so that approximately 10 percent does not reach the limit moment. In Figure 4, vertical displacements (Z) of the free edge of the console are superimposed in the case of simulation by the rod (FE 210) and shell (FE 244) physically nonlinear FE.
In Figure 5, vertical displacements (Z) of the free edge of the console are superimposed in the case of modeling by elastic (FE 510) and shell (FE 544) elastic-plastic FE.
The static task is considered in the above example. The first part of the graph (from 0 to 1) is the process of loading the calculation scheme, the second part of the graph (from 1 to 2) is the process of unloading the calculation scheme. It is easy to see that under load the results for physically nonlinear and for elastic-plastic finite elements are very close. When unloading, there are residual deformations in elastic-plastic elements (figure 5).

An example of solving a dynamic problem.
The solution of the dynamic problem and comparison with the results obtained in the ANSYS finite element analysis package are given below. Here, too, a cantilever beam of square cross section was considered for a seismic action given in the form of an accelerogram of an earthquake (Figure 6).
The damping was represented by a damping matrix in the Rayleigh form $C = \alpha \cdot M + \beta \cdot K$, with the following parameter values $\alpha = 0.0\ sec^{-1}$, $\beta = 0.0023016\ sec$.

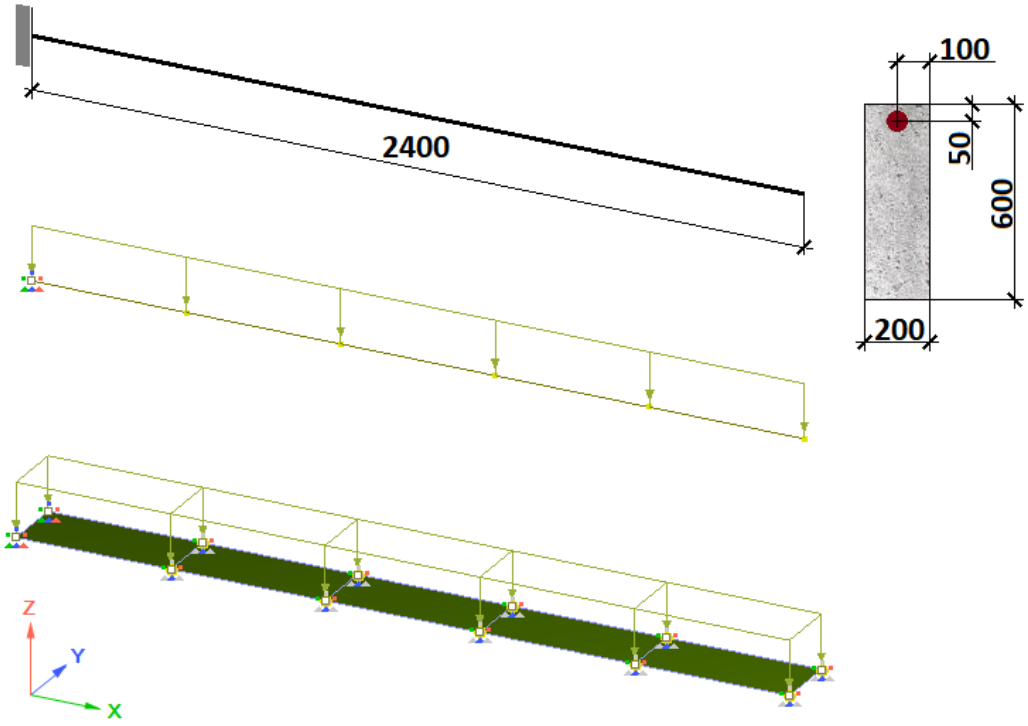


Figure 1. Calculation scheme of the static problem.

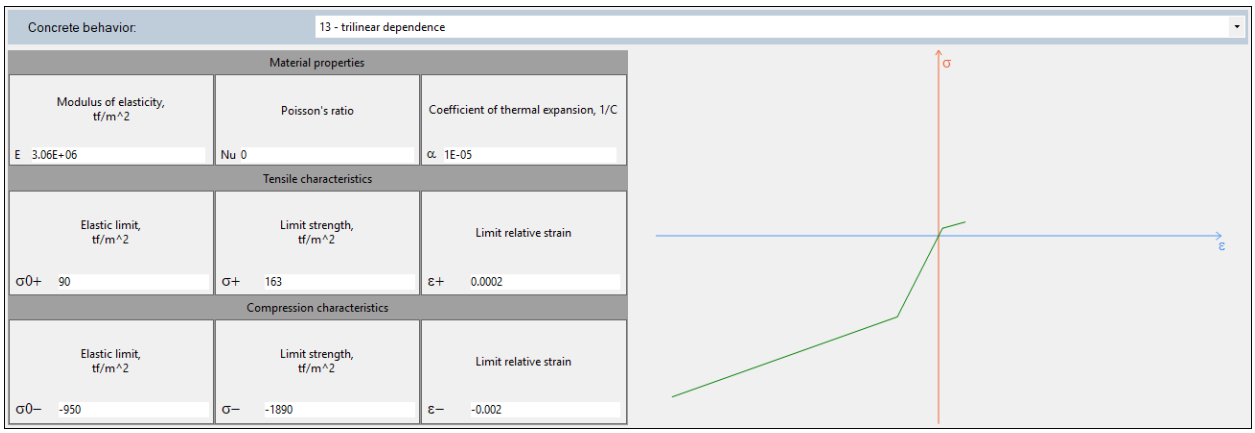


Figure 2. The diagram of the work of concrete.

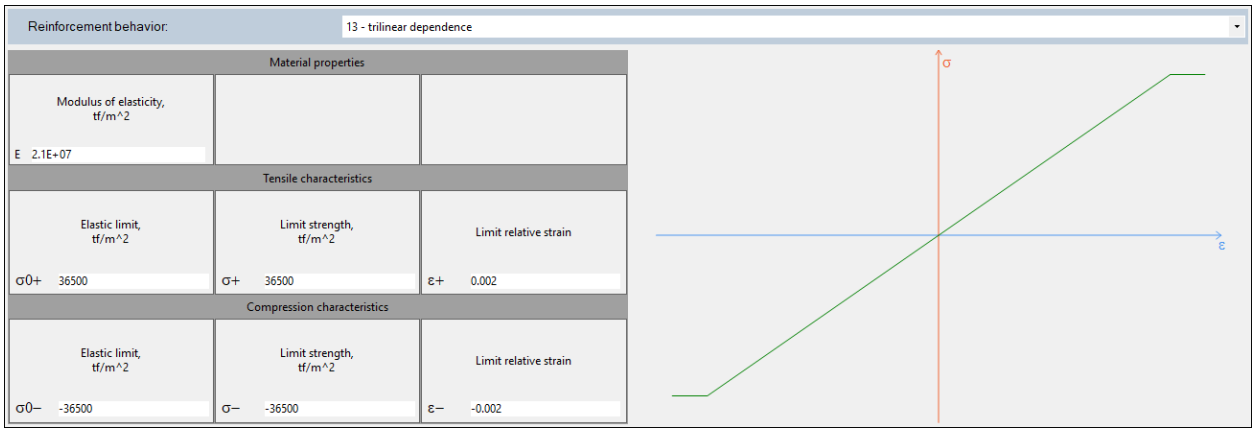


Figure 3. The diagram of the work of reinforcement.

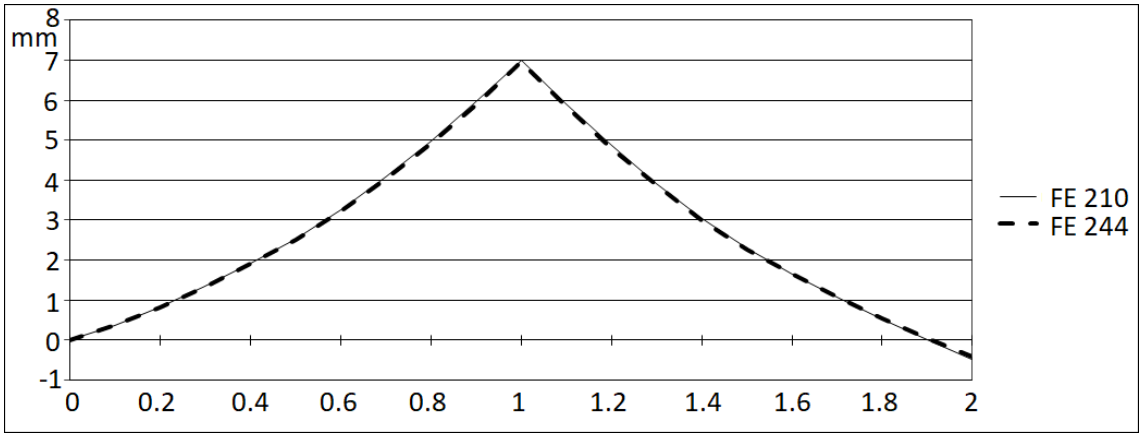


Figure 4. Displacements of the free edge when modeling physically nonlinear FE.

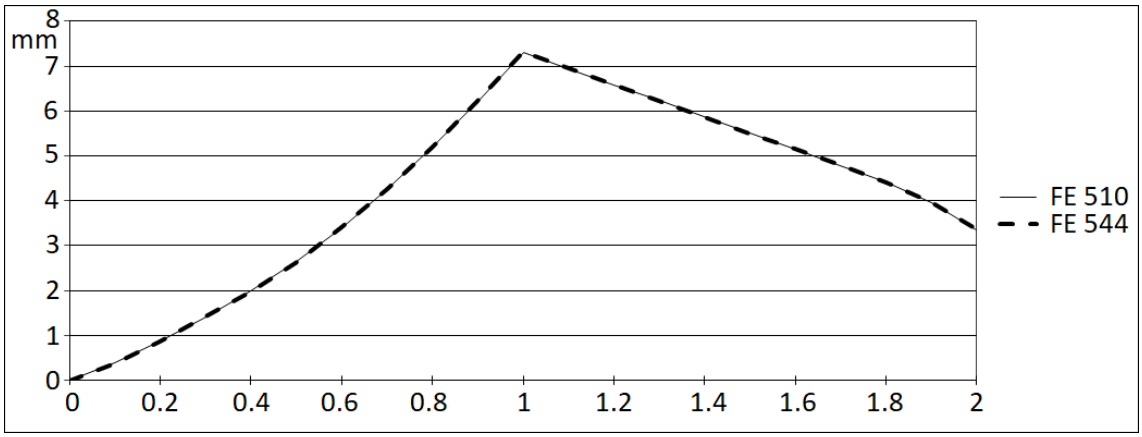


Figure 5. Displacements of the free edge when modeling elastic-plastic FE.

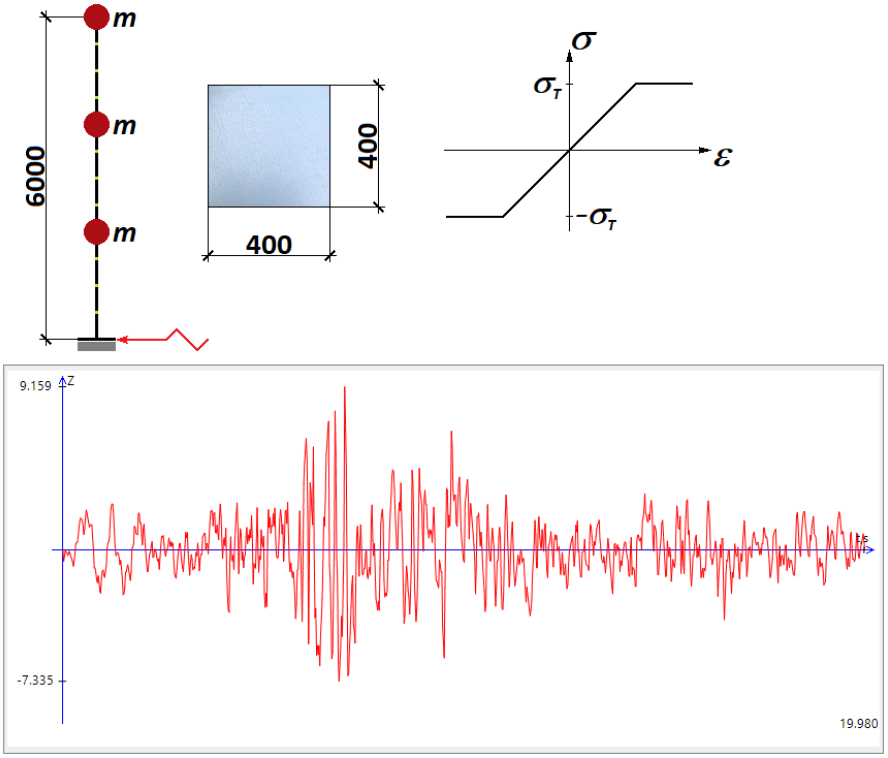


Figure 6. Calculation scheme of the dynamic problem.

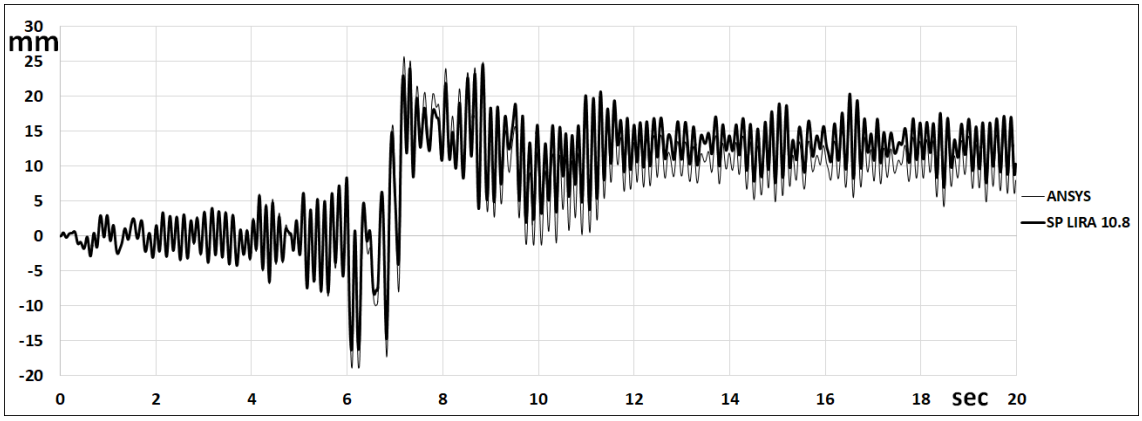


Figure 7. Comparison of the X displacements of the upper node.

The initial modulus of elasticity is equal to

$$E = 2.0e7\,\frac{tf}{m^2},$$

yield strength

$$\sigma_T = 2000\,\frac{tf}{m^2}.$$

All the dimensions in Figure 6 are given in millimeters.

First, a linear dynamic problem was solved, the results of which showed a complete coincidence between the SP LIRA 10.8 and ANSYS. Next, we solved a nonlinear dynamic problem, whose results are shown in Figure 7, in the form of graphs of the time variation of the X displacements of the upper node.

Thanks to the new nonlinear FE, based on the theory of elasticity, the developers of SP LIRA 10.8 (http://www.lira10.com) provided an opportunity for the practical use of direct dynamic calculation by design engineers. The structure of the SP LIRA 10.8 includes a specialized calculation and graphic system DYNAMICS+ for calculating structures for arbitrary dynamic effects by the method of direct integration of the equations of motion in linear and nonlinear formulations. Below is a brief description of the capabilities of this system:

- setting of time-dependent loads, such as polyline with equidistant and variable steps, harmonic load, accelerogram and earthquake seismogram;
- animation of the integration process;
- plotting of graphs as time functions for displacements and stress components in selected nodes and elements;
- visualization of diagrams, mosaics and isofields for the components of displacements and stresses in selected nodes and elements at the current time;
- tables of the results of the values of the displacement and stress components in the selected nodes and elements.

REFERENCES

1. **Gorbovets A.V., Yevzerov I.D.** Priblizhennyye Skhemy Dlya Statsionarnykh i Nestatsionarnykh Zadach s Odnostoronnimi Ogranicheniyami [Approximate Schemes for Stationary and Non-Stationary Problems with One-Sided Constraints]. // *Vychislitel'nyye Tekhnologii*, 2000, Vol. 5, No. 6, pp. 33-35 (in Russian).
2. **Duvaut G., Lions J.-L.** Les Inequanionsb en Mecanique en Physique. Paris, Dunod, 1972, 383 pages.

СПИСОК ЛИТЕРАТУРЫ

1. **Горбовец А.В., Евзеров И.Д.** Приближенные схемы для стационарных и нестационарных задач с односторонними ограничениями. // Вычислительные технологии, 2000, том 5, №6, с. 33-35.

2. **Duvaut G., Lions J.-L.** Les Inequanionsb en Mecanique en Physique. Paris, Dunod, 1972, 383 pages.

Yurii D. Heraimovych, Cand. Sc. (Tech.), PRIME CAD LLC, executive director, office 216, 6-A, Kadetskiy Gay str., 03048, c. Kiev, Ukraine, phone +38 (044) 246-16-20,
E-mail: mdv@lira.com.ua

Isaak D. Ievzerov, Dr. Sc. (Tech.), VEGA CAD LLC, director, office 209, 6-A, Kadetskiy Gay str., 03048, c. Kiev, Ukraine, phone +38 (044) 520-05-23,
E-mail: ide@lira.com.ua

Dmytro V. Marchenko PRIME CAD LLC, lead engineer, office 216, 6-A, Kadetskiy Gay str., 03048, c. Kiev, Ukraine, phone. +38 (044) 246-16-20,
E-mail: yury@lira.com.ua

Гераймович Юрий Дмитриевич, кандидат технических наук, старший научный сотрудник; ООО ПРАЙМ КАД, исполнительный директор, оф. 216, 6а, ул. Кадетский Гай, 03048, г. Киев, Украина,
тел. (+38 044) 246-16-20; E-mail: mdv@lira.com.ua.

Евзеров Исаак Данилович, доктор технических наук, старший научный сотрудник; ООО ВЕГА КАД, директор, оф. 209, 6а, ул. Кадетский Гай, 03048, г. Киев, Украина, тел. (+38 044) 520-05-23;
E-mail: ide@lira.com.ua.

Марченко Дмитрий Владимирович, ООО ПРАЙМ КАД, ведущий инженер, оф. 216, 6а, ул. Кадетский Гай, 03048, г. Киев, Украина, тел. (+38 044) 246-16-20;
E-mail: yury@lira.com.ua.

INVESTIGATION OF HEAT-HUMIDITY TRANSFER IN HIGH-POROUS GAS-FILLED POLYMERS TO CALCULATE ITS HEAT CONDUCTIVITY

Vladimir V. Gur'ev [1]***, Vadim I. Nikitin*** [2]***, Valeriy A. Kofanov*** [3]
[1] Federal Centre for Regulation, Standardization and Technical Assessment in Construction, Moscow, RUSSIA
[2] Pope John Paul II State School of Higher Education, Biała Podlaska, POLAND
[3] Brest State Technical University, Brest, BELARUS

Abstract: A method for calculating the effective thermal conductivity of moisture-containing highly porous foamed polymers is proposed. In this method a non-additive scheme for taking into account the effect of steam diffusion on heat transfer is used. The sequential binary systems (interstitial substance from a liquid and a vapor-gas mixture, as well as a polymer skeleton and an intra-porous substance) are described by models of structures with interpenetrating components and isolated inclusions. The conditions for the transition from one model of structure to another are defined and there is not necessity to define empirical coefficients. A geometric model of wet foamed polymer has been developed, that allows us to find a way to determine the value of the boundary moisture content of pores or wetting angle at which the transition from partial wetting of the surface of the pores with liquid to full wetting and vice versa occurs. A mathematical description of the process of heat transfer in the model structure of a wet foamed polymer has been made, taking into account the diffusion of water vapor in the pore space.

Keywords: effective heat conductivity, interpenetrating components, high-porous gas-filled polymers, polyurethane foam, vapor diffusion, wetting angle

ИССЛЕДОВАНИЕ ТЕПЛОВЛАГООБМЕНА В ВЫСОКОПОРИСТЫХ ГАЗОНАПОЛНЕННЫХ ПОЛИМЕРАХ ПРИМЕНИТЕЛЬНО К РАСЧЕТУ ИХ ТЕПЛОПРОВОДНОСТИ

В.В. Гурьев [1]***, В.И. Никитин*** [2]***, В.А. Кофанов*** [3]
[1] Федеральный центр нормирования, стандартизации и технической оценки соответствия в строительстве Минстроя России, г. Москва, РОССИЯ
[2] Государственная высшая школа имени Папы Римского Иоанна Павла II, г. Бяла Подляска, ПОЛЬША
[3] Брестский государственный технический университет, г. Брест, РЕСПУБЛИКА БЕЛАРУСЬ

Аннотация: В данной работе предлагается метод расчета эффективной теплопроводности влагосодержащих высокопористых пенопластов, в котором используется неаддитивная схема учета влияния диффузии пара на перенос тепла. Приведена разработанная геометрическая модель влажного пенопласта, позволяющая найти способ определения значения граничного влагосодержания пор или краевого угла смачивания, при которых происходит переход от частичного смачивания поверхности пор жидкостью к полному смачиванию и наоборот. Расчетами показано, что такой переход сопровождается скачкообразным изменением теплопроводности пенопластов. Выполнено математическое описание процесса переноса тепла в модельной структуре влажного пенопласта с учетом диффузии водяного пара в поровом пространстве. Расчетным путем установлено заметное влияние влагосодержания и средней температуры пенопласта на его эффективную теплопроводность при аддитивной и неаддитивной схемам учета диффузионной составляющей теплопроводности.

Ключевые слова: тепловлагообмен, высокопористые газонаполненные полимеры, расчет теплопроводности, диффузия пара, угол смачивания

INTRODUCTION

Rigid polymeric foams (foamed polymers) are widely used in construction and other industries as an effective thermal insulation of buildings and structures. A generalized characteristic of the complex process of heat conduction in foamed polymers is the effective thermal conductivity coefficient λ, used to determine the heat-shielding properties of thermal insulation structures.

It is obvious that the thermal conductivity coefficient of foamed polymers depends on the thermal conductivity of the dense polymer skeleton and the interporous substance, which in moisture-containing materials consists of a vapor-gas mixture and water. When determining the thermal conductivity of such an interporous substance, it is necessary to take into account the influence of a diffusive flow of steam-like moisture moving in the direction of heat flow and accompanied by phase transformations of moisture in the pores (evaporation in the warm zone and condensation in the cold) [1, 2, 3, 4]. At the same time, due to condensation of the diffusing vapor, the thermal conductivity of wet materials and, above all, of highly porous foamed polymers, may significantly increase.

Evaluation of the influence of steam diffusion on heat transfer is currently performed using additive and non-additive schemes. Thus, in [4], the effective thermal conductivity of a wet foamed polymer consists of heat conduction due to condensation of diffusing steam, which is determined using the relation that is similar to the Fourier law for heat flux, recommended for use in the temperature range from 20 to 90 ° C and containing empirical coefficients, and thermal conductivity of the wet material, determined by the Krischer formula, also containing the empirical coefficient. The presence of empirical coefficients imposes certain restrictions on the use of these dependencies in the calculations.

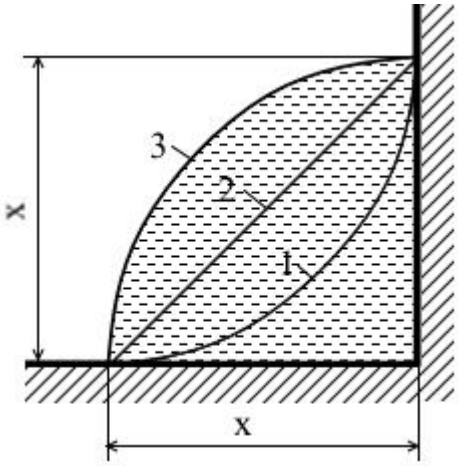
The authors of [3] estimate the effect of vapor diffusion on heat transfer by using a non-additive calculation scheme, simulating a wetted material by a structure with interpenetrating components. An analysis of a three-component system containing a polymer skeleton, liquid moisture and a vapor-gas mixture was carried out using the method of sequential reduction of a multicomponent system to a binary one. First, the effective thermal conductivity of the pore space containing the liquid and the vapor – gas mixture (binary system with interpenetrating components) was determined, and then the effective thermal conductivity of the wet material consisting of the polymer skeleton and the inter-porous substance was determined. The thermal conductivity of the vapor – gas mixture was represented as the sum of the thermal conductivity of dry gas and the thermal conductivity of steam, caused by diffusive transfer of steam in the pore space.

In highly porous foamed polymers, liquid moisture wets the surface of the pores partially (more often) or completely (less often). In the first case, the pore space model should be represented in the form of a binary system with isolated inclusions, and in the second case, in the form of a binary system with interpenetrating components. When changing the moisture content of the pores or the wetting angle, it is possible transition from one binary system to another. In this case we need to know the value of the boundary (critical) moisture content or wetting angle. However, the described calculation schemes do not take into account this important feature.

STRUCTURE'S MODEL OF WET FOAMED POLYMER AND ITS CALCULATIONAL RELATIONSHIPS

When developing the model of wet foamed plastic, the real cellular structure of the polymer skeleton is replaced by an adequate model with an ordered rod structure consisting of identical elementary cells of a cubic form. This form of the unit cell is fairly reasonable and the simplest. In order to assess the character of the distribution of liquid moisture in this cell, it is necessary to take into account the moisture content of the material ψ and the wetting angle Θ formed at the boundary of the solid, liquid and gas. From the analysis

of the results of numerous experimental studies that carried out in laboratory and natural conditions and partially presented in [4, 5, 6], it follows that at constant contact with the environment for which humidity and temperature are changing, the volume moisture content of polyurethane and phenolic foamed polymers can reach $\psi = 0.06–0.07$ m^3 / m^3. To determine the wetting angle Θ, it is used the method of a large drop of liquid (3-4 cm^3) wetting the flat horizontal surface of the polymer [7]. After five independent measurements of the wetting angle with water of a polyurethane surface at a temperature of 20 ° C, it turned out that the measured random variable is characterized by an arithmetic average value $\overline{\theta}$ =56 ° and a sample standard deviation s=3.2 °.



1 – Θ = 0°; 2 – Θ = 45°; 3 – Θ = 90°

Figure 1. View of the liquid surface in the dihedral angle at various wetting angles.

Figure 1 shows the nature of the distribution of a very small amount of liquid in the form of a strip of constant cross section in a two-sided angle formed by two mutually perpendicular half-planes at different wetting angles. If we start from the average cell sizes of polyurethane foams given in [8], it can be assumed that the size x in Figure 1 does not exceed 200 μm. In this case, under normal conditions, gravity will not be able to distort the surface of the liquid (water) shown in Figure 1, since the values of the gravitational forces are no more than 0.5% of the values of the surface tension forces. Then it is not difficult to imagine the nature of the distribution of fluid in the unit cell. As an example, Figure 2 shows the eighth part of a unit cell containing an isolated fluid inclusion at a wetting angle Θ = 45 °.

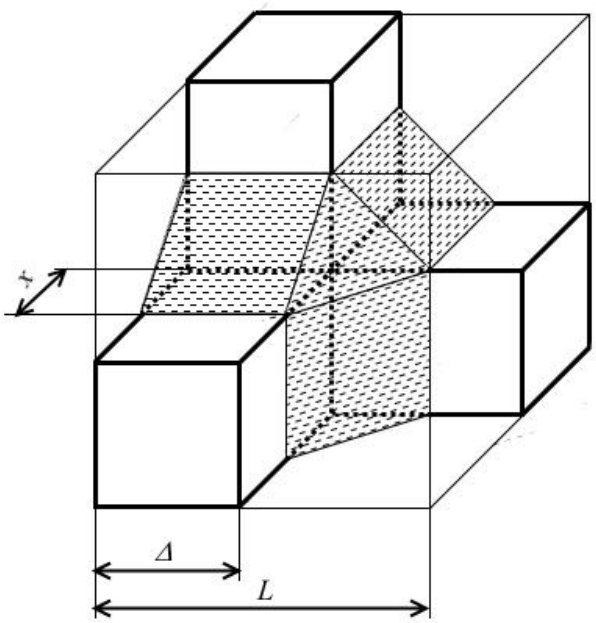


Figure 2. The nature of the distribution of isolated inclusion of liquid in the unit cell at a wetting angle Θ = 45°.

With an increase in moisture content, the size x (Figure 2) increases and at

$$x = L - \Delta$$

isolated fluid inclusions merge and porous space should be considered as a binary system with inter-penetrating components. Thus, when calculating the thermal conductivity of the pore space, it is necessary to know its boundary moisture content, at which the binary system with isolated inclusions transforms to the system with inter-penetrating components and vice versa.

The volume moisture content of pores ψ_p is related to the volume of a liquid V_w and pores V_p by a ratio

$$\psi_p = V_w / V_p$$

or to the volume moisture content of a material ψ and its porosity *m* by ratio

$$\psi_p = \psi / m .$$

From Figure 2 it follows that

$$V_w = 3 \cdot x^2 \cdot \Delta / 2 + x^6 / 6 .$$

Pore volume

$$V_p = (L - \Delta)^3 + 3 \cdot \Delta \cdot (L - \Delta)^2 .$$

Accepting $x = L - \Delta$, after simple transformations, we obtain the volumetric boundary moisture content of pores at a wetting angle $\Theta = 45°$

$$\psi_p^{'} = \frac{1 + 8 \cdot c}{6 \cdot (1 + 2 \cdot c)};\ c = \Delta / L . \qquad (1)$$

Analogically for wetting angle value Θ=90° we obtain

$$\psi_p^{'} = \frac{\pi \cdot (1 + 3.5 \cdot c)}{6 \cdot (1 + 2 \cdot c)}. \qquad (2)$$

For wetting angle value Θ=0° the unknown value of moisture content is determined by formula

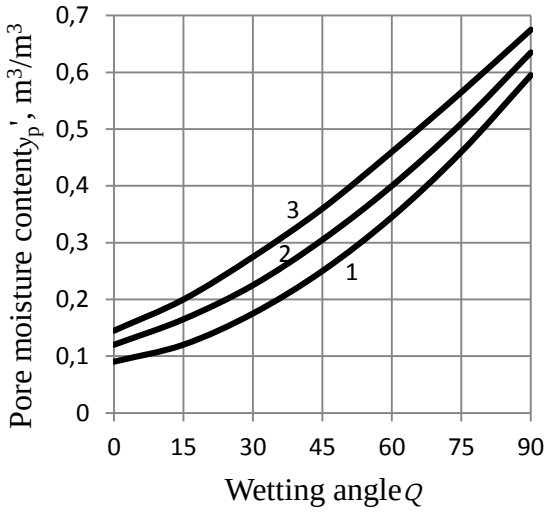
$$\psi_p^{'} = \frac{(4 - \pi) \cdot (1 + 14 \cdot c)}{20 \cdot (1 + 2 \cdot c)}. \qquad (3)$$

Using formulas (1), (2) and (3), it can be determined the relationship for pore moisture content $\psi_p^{'}$ from wetting angle Θ for different values of the rods' relative sizes $c = \Delta / L$ of elementary cell. This relationship is illustrated in Figure 3.

The relative size of the rods is calculated using the ratio [9]:

$$c = 0.5 + \sin\left[\frac{\arcsin(2 \cdot m_i - 1)}{3}\right], \qquad (4)$$

where m_i is concentration of the i-th component (i = 1, 2), for which the value c should be determined.



1 – c=0.1; 2 – c=0.2; 3 – c=0.3

Figure 3. The relationship between boundary moisture content of the pores $\psi_p^{'}$ and the wetting angle Θ at different relative sizes of the rods of the unit cell c.

In order to determine effective heat conductivity for binary system with known components' concentrations m_1, m_2 and its heat conductivities λ_1, λ_2, let us apply relationships, turned out on the basis generalized conductivity theory [3].

For the structure with interpenetrating components, the dependence obtained by G.N. Dulnev in 1965 is used.

$$\lambda = \lambda_1 \cdot [c^2 + \nu \cdot (1 - c)^2 + 2 \cdot \nu \cdot c \cdot (1 - c) \cdot (\nu \cdot c + 1 - c)^{-1}, \qquad (5)$$

where $\nu = \lambda_2 / \lambda_1$.

The components of this structure are geometrically equal and in the calculations it does not matter which of the two components is taken as the first.

For the structure with closed inclusions, the following dependence is chosen:

$$\lambda = \lambda_1 \cdot \frac{1 + (\nu - 1) \cdot (1 - m_2^{2/3}) \cdot m_2^{1/3}}{\nu - (\nu - 1) \cdot m_2^{1/3}}, \qquad (6)$$

where m_2 is volumetric inclusion's concentration, $\nu = \lambda_2 / \lambda_1$.

In this case, the components of the structure are geometrically unequal and the continuous component is always the first with the concentration m_1.

When calculating the thermal conductivity of wet foamed polymer, let us consider the vapor-air mixture as one of the continuous components, since during the operation of the thermal insulation structures there is a diffusion replacement of gas, formed in the pores of the foamed plastics during its manufacture, by air and water vapor. According to [1, 2, 3], the thermal conductivity of the vapor – air mixture λ_{va} equals to the sum of the thermal conductivities of air λ_a and vapor λ_v. Thermal conductivity of steam λ_v, caused by diffusive vapor transfer in the pore space, can be determined by the formula [3]

$$\lambda_v = \frac{D}{\mu} \cdot \frac{M}{R \cdot T} \cdot \frac{P_{va}}{P_{va} - P_v} \cdot \frac{dP_v}{dT} \cdot q_t, \qquad (7)$$

where D is coefficient of water vapor diffusion in still air, m^2/s; μ is coefficient of resistance to vapor diffusion through the pore space; M is molecular weight of steam, kg/mole; R is universal gas constant, J/(mole·K); T is vapor temperature, K; P_{va} is total vapor and air pressure, Pa; P_v is vapor partial pressure, Pa; q_t is specific heat of vaporization at temperature T, J/kg.

In determining the coefficient D, it is widely used dependence, which was justified by R. Schirmer [10] in 1938

$$D = \frac{2.305 \cdot 10^{-5} \cdot P_o}{P_{va}} \cdot \left(\frac{T}{273} \right)^{1.81}, \quad P_o = 101323 \text{ Pa}. \qquad (8)$$

The experimental value of the coefficient μ is determined from the ratio

$$\mu = D / \delta_v, \qquad (9)$$

where δ_v is vapor permeability coefficient of the porous medium, m^2/s.

Experiments can be avoided if it is possible to choose the most suitable formula for the described material from a large number of the proposed formulas. A preliminary analysis showed that, for wet foamed polymers with an open-cell structure, for the concentration of the vapor-air mixture

$$m - \psi \geq 0.93,$$

it can be suggested a simple formula [4]

$$\mu = \frac{1}{0.57 \cdot (m - \psi)}, \ \psi \leq \psi_p \cdot m. \qquad (10)$$

For values

$$m - \psi < 0.93$$

it can be applied dependence [11]

$$\mu = \tau^2 / (m - \psi), \qquad (11)$$

where τ is the tortuosity coefficient, which according to [9] is proposed to be found from the relationship:

$$\tau = (m - \psi) / c^2. \qquad (12)$$

Here the parameter c is determined by the formula (4) for

$$m_1 = m - \psi.$$

Substituting the relation (12) in (11) we finally obtain

$$\mu = (m - \psi) / c^4 \qquad (13)$$

It seems to be expedient to begin the calculation of the diffusion component of thermal conductivity λ_v of foamed polymers when a moisture content is not less than the maximum gyroscopic one

ψ_h and constant at a given temperature and pressure of the saturated vapor p_{vh}.

SCHEME OF A CALCULATION

Let us illustrate the recommended calculation scheme using the example of calculating the effective thermal conductivity of a foamed polymer specimen with a porosity of $m = 0.93$, a density of $\rho = 80$ kg / m3, moisture content $\psi = 0.06$ m^3 / m^3 that is close to the largest operating value, average temperature $t = 20$ ° C and wetting angle $\Theta = 60$ °.

At the beginning, using the formula (7), we calculate the diffusion component of thermal conductivity at λ_v, T = 293 K, $P_{va}=10^5$ Pa. According to reference data we find $M = 0.018$ kg / mol, $R = 8.3144$ J / (mol · K), $P_v=P_{vh}=0.02338\cdot10^5$ Pa,

$$\frac{dP_{vh}}{dT} = 148 \text{ Pa / K (for } dT = 1 \text{ K)},$$

$q_t = 2.38\cdot10^6$ J / kg. According to the formula (8), we determine the diffusion coefficient of vapor in the air $D = 2.65\cdot10^{-5}$ m^2 / s. To calculate the coefficient μ, we use formula (13) with the volume concentration of the vapor-air mixture and the parameter c = 0.7743, found by formula (4) for $m_1 = m = 0.87$. Then we have $\mu = 2.42$.

As a result, we obtain $\lambda_v = 0.03$ W / (m · K) and, taking into account the thermal conductivity of dry air, $\lambda_v = 0.0257$ W / (m · K), the thermal conductivity of the vapor-air mixture is

$$\lambda_{va} = \lambda_v + \lambda_a = 0.0557 \text{ W / (m · K)}.$$

The volume moisture content of the pore space is equal to

$$\psi_p = \psi / m = 0.06 / 0.93 = 0.0645 \text{ m}^3 / \text{m}^3.$$

At a wetting angle $\Theta = 60$ ° and the parameter c = 0.1614, calculated by the formula (4) with a polymer volume concentration of $m_1 = 0.07$, using Figure 3, the boundary moisture content of pores $\psi_p' = 0.38$ m^3 / m^3 was found, which exceeds the actual $\psi_p = 0.0645$ m^3 / m^3 almost 6 times. In this case, the pore space containing the vapor-air mixture and water is considered as a binary system (structure) with isolated inclusions. The first component of this system is a vapor-air mixture with a volume concentration of $m_1 = 0.9355$ and thermal conductivity

$$\lambda_1 = \lambda_{va} = 0.0557 \text{ W / (m · K)},$$

and the second one is water with a volume concentration of $m_2 = 0.0645$ $(m_1 + m_2 = 1)$ and thermal conductivity

$$\lambda_2 = \lambda_w = 0.596 \text{ W / (m · K)}.$$

Now, using the formula (6) with the ratio

$$\nu = \lambda_2 / \lambda_1 = 0.596 / 0.0557 = 10.7,$$

we calculate the effective thermal conductivity of the pore substance

$$\lambda_{12} = 0.0608 \text{ W / (m · K)}.$$

At the final stage of calculation, using formula (5) for a structure with equal interpenetrating components, we determine the effective thermal conductivity λ of a wet foamed polymer. As the first component, we consider the inter-porous substance, for which we have

$$m_1 = m = 0.93, \ \lambda_1 = \lambda_{12} = 0.0608 \text{ W / (m · K)}$$

and the parameter $c = 0.8386$, obtained by formula (4). The second component is a polymer skeleton characterized by $m_2 = 0.07$ and $\lambda_2 = 0.25$ W / (m · K). Then we have a relationship

$$\nu = \lambda_2 / \lambda_1 = 0.25 / 0.0608 = 4.1118.$$

For the obtained values of parameters c and ν, we calculate the effective thermal conductivity of

the wet foamed polymer $\lambda = 0.068$ W / (m · K) using formula (5).

For comparison, according to the considered scheme, a calculation is performed in which, when determining the thermal conductivity of the pore substance λ_{12}, the heat transfer due to condensation of the diffusing vapor λ_v is not taken into account. In this case, the value of the effective thermal conductivity of the wet foamed polymer is $\lambda' = 0.0354$ W / (m · K), that is almost two times less than the result of the previous calculation. If we use the additive calculation scheme and determine the effective thermal conductivity of the wet foamed polymer as a sum, we get the result

$$\lambda = 0.0354 + 0.03 = 0.0654 \text{ W / (m · K)},$$

which is only 3.8% less than the result calculated by the non-additive scheme. Let us note that, when implementing another additive calculation scheme using the formulas recommended in [4] and containing empirical coefficients, the effective thermal conductivity is obtained equal to $\lambda = 0.0745$ W / (m · K), which is 9.6% higher than the value calculated from proposed non-additive calculation scheme. Exactly the same result is given by the proposed calculation scheme using the value of the vapor diffusion coefficient $\mu = 2.016$, which is obtained using formula (10).

NUMERICAL EXPERIMENT AND ITS RESULTS

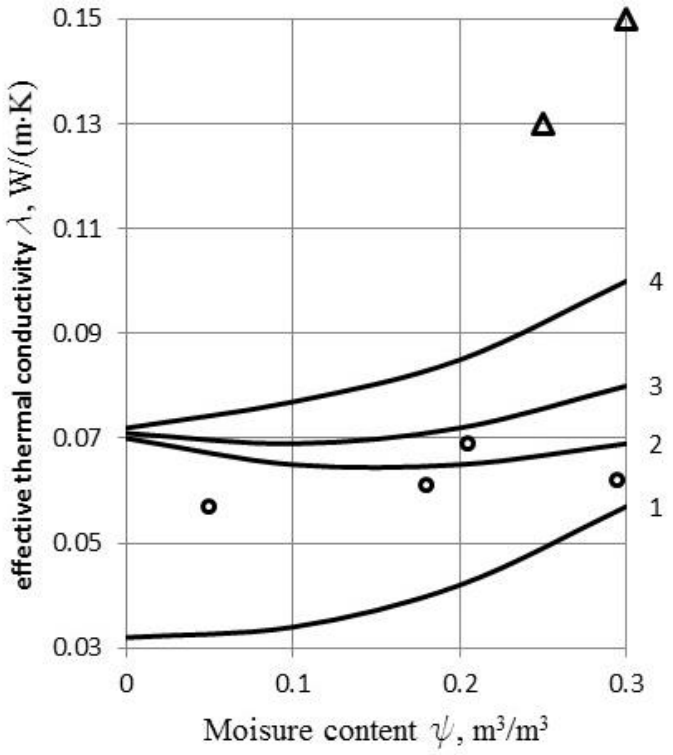
A numerical experiment is carried out to assess the effect of moisture content ψ and the average temperature t of the considered foam plastic on its thermal conductivity λ. To this end, the presented example of calculating λ, which takes into account different approaches to estimating λ, was repeated for other values of moisture content for the range from 0.01 to 0.3. According to the results of repeated calculations, graphs are constructed reflecting various dependencies of λ on ψ, that are shown in figure 4 together with experimental data taken from [4]. Comparing dependence 1 in figure 4 with the other dependences, it follows that the diffusion component of thermal conductivity λ_v for various ways of taking it into account makes a significant contribution to the effective thermal conductivity λ of wet foamed polymer. Using formula (10) to determine the vapor diffusion resistance coefficient μ instead the formula (13) we obtain noticeable differences (qualitative and quantitative) in calculating the effective thermal conductivity λ (dependences 3 and 4). Comparison of dependences 2 and 3 shows that the additive and non-additive schemes for taking the diffusion component λ_v into account when determining the effective thermal conductivity of the foamed polymer gives similar results within the maximum operating moisture content of $\psi \leq 0.07$. In this case, the results of the non-additive calculation exceed the results of the additive calculation no more than 4%. With an increase in the moisture content of the material to $\psi = 0.3$, this difference increases to 15%.

From figure 4 it can be seen that for the same material with moisture holding $\psi > 0.2$, the experimental data of some authors (triangles) exceed the experimental data of other authors (circles) approximately two times, and the calculated curve 3 obtained using the recommended calculation schemes, well predicted by experimental data, indicated by circles. It was also experimentally established [3] that the thermal conductivity of the same material with the same moisture content may differ several times. First of all, this can be explained by the fact that at the same moisture content, but different wetting angles, the moisture can wet the surface of the pores fully or partially.

For the considered foamed plastic (m = 0.93 and $\psi = 0.3$), we have a moisture content of pores

$$\psi_p = \psi / m = 0.323,$$

which corresponds to the boundary wetting angle $\theta' = 52°$ (figure 3).



○, Δ are experimental data obtained by various authors

Figure 4. Dependence of effective thermal conductivity λ on moisture content ψ for foamed plastic with porosity m = 0.93 at a temperature of 20 ° C and wetting angle Θ = 60 ° and various ways of accounting for thermal conductivity of water vapor λ_v due to its diffusion:
1 - excluding; 2 - additive; 3, 4 - non-additive with different formulas for calculating the coefficient of resistance to vapor diffusion.

At wetting angles Θ <52 ° and moisture content ψ = 0.3, the surface of the pores is completely wetted with water and the pore space can be represented as a binary system with interpenetrating components, the thermal conductivity of which is determined by formula (5). In this case, the value of the effective thermal conductivity of a wet foamed polymer is

$$\lambda = 0.136 \text{ W} / (\text{m} \cdot \text{K}),$$

that exceeds the value of thermal conductivity calculated for the same foam with partial water wetting of the pore surface (Θ> 52 °), 1.71 times. It accurately predicts the experimental value

$$\lambda = 0.15 \text{ W} / (\text{m} \cdot \text{K})$$

presented in Figure 4. For another moisture content ψ = 0.25 (ψ_p = 0.269) and a wetting angle Θ <45 °, the calculated value

$$\lambda = 0.121 \text{ W} / (\text{m} \cdot \text{K})$$

is close to another experimental value

$$\lambda = 0.13 \text{ W} / (\text{m} \cdot \text{K}) \text{ (Figure 4).}$$

Thus, with the correct quantitative assessment of the wetting of the surface of the pores with a liquid (partially or completely), determined using the parameters ψ and Θ, the proposed method for calculating the thermal conductivity of foamed polymers λ can satisfactorily predict experimental data.
The calculations confirm the well-known effect of increasing the heat conductivity of a wet foamed polymers with an increase in its average temperature.

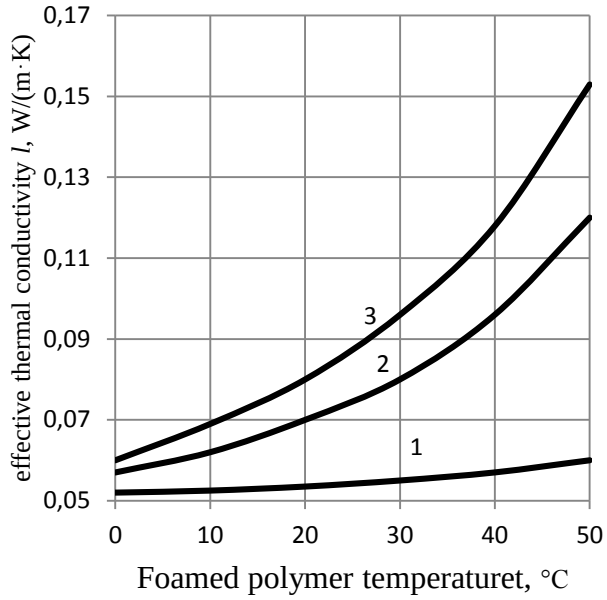


Figure 5. Dependence of the effective thermal conductivity λ on the average temperature of the foamed polymer with a porosity of m = 0.93 with a moisture content of ψ = 0.3 and a wetting angle of Θ = 60 ° and various ways of accounting for the thermal conductivity of water vapor λ_v due to its diffusion
1 - excluding; 2 - additive; 3 - non-additive.

At the same time, within the limits of the operational moisture content of the material $\psi \leq 0.07$, the difference between the values of thermal conductivity calculated by additive and non-additive calculation schemes does not exceed 4%. With an increase in the moisture content of the material to $\psi = 0.3$, this difference increases, that is shown by dependences 2 and 3 in figure 5.

CONCLUSIONS

A geometric model of wet foamed polymer has been developed, that allows us to find a way to determine the value of the boundary moisture content of pores or wetting angle at which the transition from partial wetting of the surface of the pores with liquid to full wetting and vice versa occurs. Calculations have shown that such a transition is accompanied by an abrupt change in the thermal conductivity of foamed polymers. A mathematical description has been made for the process of heat transfer in the model structure of a wet foamed polymer, taking into account the diffusion of water vapor in the pore space. By calculation, a significant influence of the moisture content and average temperature of the foamed polymer on its effective thermal conductivity with additive and non-additive schemes for accounting for the diffusion component of thermal conductivity has been established. Comparison of the calculation results with experimental data revealed its rather exact coincidence.

REFERENCES

1. **Lykov A.V.** Teplomassoobmen [Heat and Mass Transfer]. Moscow, 1971, 560 pages (in Russian).
2. **Missenard A.** Conductivité Thermique des Solides, Liquides, Gaz et de Leurs Mélanges, Paris, Éditions Eyrolles, 1985, 340 pages.
3. **Dul'nev G.N., Novikov V.V.** Protsessy Perenosa v Neodnorodnykh Sredakh

[Transport Processes in Inhomogeneous Media]. Leningrad, 1991, 248 pages (in Russian).
4. **Gur'ev V.V., Zholudov V.S., Petrov-Denisov V.G.** Teplovaya Izolyatsiya v Promyshlennosti. Teoriya i Raschet. [Thermal Insulation in Industry. Theory and Calculation]. Moscow, 2003, 416 pages (in Russian).
5. Thermal Insulation Materials Made of Rigid Polyurethane Foam (PUR/PIR): Report No. 1 (October) / BING: Federation of European Rigid Polyurethane Foam Associations. Brussels, 2006, 33 pages.
6. **Petrov-Denisov V.G., Maslennikov L.A.** Protsessy Teplo- i Vlagoobmena v Promyshlennoy Izolyatsii [Processes of Heat and Moisture Exchange in Industrial Insulation]. Moscow, 1983, 193 pages (in Russian).
7. **Gur'ev V.V., Nikitin V.I., Golubova G.A.** Sposob Opredeleniya Kraevogo Ugla Smachivaniya Polimernykh Kompozitsiy [Method for Determining the Contact Angle of Wetting of Polymer Compositions]. Patent. RU 2025710 /. Published 30.12.1994 (in Russian).
8. **Collishaw P.G., Evans J.R.G.** An Assessment of Expressions for the Apparent Thermal Conductivity of Cellular Materials. // *Journal of Materials Science*, 1994, Vol. 29, pp. 486-498.
9. **Nikitsin V.I., Backiel-Brzozowska B.** Determination of Capillary Tortuosity Coefficient in Calculations of Moisture Transfer in Building Materials // *International Journal of Heat and Mass Transfer*, 2013, Vol. 56, pp. 30-34.
10. **Scheffler G.A., Plagge R.** A Whole Range Hygric Material Model: Modelling Liquid and Vapour Transport Properties in Porous Media. // *International Journal of Heat and Mass Transfer*, 2010, Vol. 53, pp. 286-296.
11. **Epstein N.** On Tortuosity and the Tortuosity Factor in Flow and Diffusion Through Porous Media. // *Chemical Engineering Science*, 1989, Vol. 44, No 3, pp. 777-779.

СПИСОК ЛИТЕРАТУРЫ

1. **Лыков А.В.** Тепломассообмен. – М.: Энергия, 1971. – 560 с.
2. **Missenard A.** Conductivité Thermique des Solides, Liquides, Gaz et de Leurs Mélanges, Paris, Éditions Eyrolles, 1985, 340 pages.
3. **Дульнев Г.Н., Новиков В.В.** Процессы переноса в неоднородных средах. – Л.: Энергоатомиздат. Ленинградское отделение, 1991. – 248 с.
4. **Гурьев В.В., Жолудов В.С., Петров-Денисов В.Г.** Тепловая изоляция в промышленности. Теория и расчет. – М.: Стройиздат, 2003. – 416 с.
5. Thermal Insulation Materials Made of Rigid Polyurethane Foam (PUR/PIR): Report No. 1 (October) / BING: Federation of European Rigid Polyurethane Foam Associations. Brussels, 2006, 33 pages.
6. **Петров-Денисов В.Г., Масленников Л.А.** Процессы тепло- и влагообмена в промышленной изоляции. – М.: Энергоатомиздат, 1983. – 193 с.
7. Способ определения краевого угла смачивания полимерных композиций : пат. RU 2025710 / В.В. Гурьев, В.И. Никитин, Г.А. Голубова. Опубл. 30.12.1994.
8. **Collishaw P.G., Evans J.R.G.** An Assessment of Expressions for the Apparent Thermal Conductivity of Cellular Materials. // *Journal of Materials Science*, 1994, Vol. 29, pp. 486-498.
9. **Nikitsin V.I., Backiel-Brzozowska B.** Determination of Capillary Tortuosity Coefficient in Calculations of Moisture Transfer in Building Materials // *International Journal of Heat and Mass Transfer*, 2013, Vol. 56, pp. 30-34.
10. **Scheffler G.A., Plagge R.** A Whole Range Hygric Material Model: Modelling Liquid and Vapour Transport Properties in Porous Media. // *International Journal of Heat and Mass Transfer*, 2010, Vol. 53, pp. 286-296.

11. **Epstein N.** On Tortuosity and the Tortuosity Factor in Flow and Diffusion Through Porous Media. // *Chemical Engineering Science*, 1989, Vol. 44, No 3, pp. 777-779.

Vladimir V. Gur'ev, Advisor of the Russian Academy of Architecture and Construction Sciences, Professor, Dr.Sc.; Federal Centre for Regulation, Standardization and Technical Assessment in Construction; Floor 2, Building 3, Str. 1, Orlikov Pereulok, Moscow, 107139, Russia;
phone: +7 (495) 133-01-57; e-mail: info@faufcc.ru.

Vadim I. Nikitin, Professor, Dr.Sc., Pope John Paul II State School of Higher Education; Rzeczpospolita Polska, 21-500, woj. Lubelskie, Biała Podlaska, ul. Sidorska, 95/97;
phone: +48 83 344 99 00; fax: +48 83 344 45 90,
E-mail: psw@pswbp.pl.

Valeriy A. Kofanov, Associate Professor, Ph.D., Brest State Technical University; 267, Moskovskaya Str., Brest, 224017, Belarus; phones: + 375 162 42-33-93;
+ 375 162 42-40-84; fax: + 375 162 42-21-27;
E-mail: canc@bstu.by.

Гурьев Владимир Владимирович, советник РААСН, профессор, доктор технических наук; Россия, 107139, Москва, Орликов пер., 3, стр. 1; тел. +7(495) 133-01-57;
E-mail: info@faufcc.ru.

Никитин Вадим Иванович, профессор, доктор технических наук, Государственная высшая школа имени Папы Римско-го Иоанна Павла II; Rzeczpospolita Polska, 21-500, woj. Lubelskie, Biała Podlaska, ul. Sidorska, 95/97; тел. +48 83 344 99 00;
факс +48 83 344 45 90, e-mail: psw@pswbp.pl.

Кофанов Валерий Анатольевич, доцент, кандидат технических наук, Брестский государственный технический университет; ул. Московская 267, 224017, Брест, Республика Беларусь; тел.: +375 162 32-17-32;
факс: +375 162 32-17-55; e-mail: canc@bstu.by.

USING THE CRITERION OF THE MINIMUM MATERIAL CAPACITY OF RODS UNDER STABILITY RESTRICTIONS FOR THE CASE OF MULTIPLE CRITICAL LOAD

Leonid S. Lyakhovich [1], ***Pavel A. Akimov*** [1, 2, 3, 4], ***Anatoly P. Malinowski*** [1]
[1] Tomsk State University of Architecture and Civil Engineering, Tomsk, RUSSIA
[2] Russian Academy of Architecture and Building Sciences, Moscow, RUSSIA
[3] Scientific Research Center "StaDyO", Moscow, RUSSIA
[4] Peoples' Friendship University of Russia, Moscow, RUSSIA

Abstract: As it is known, special criteria are formulated to evaluate the obtained solution of some optimization problems. In particular, we formulate a criterion that allows us to estimate the proximity of the decision on the rod of the lowest weight and the restrictions on the resistance to the minimum material-intensive for rectilinear rods for certain types of cross sections. The criterion is based on the analysis of stresses from bending moments arising from the loss of stability. If the least critical force is not a multiple, then the form of loss of stability and the corresponding diagram of moments are the only ones. At multiplicity of the least critical load there are multiple forms of loss of stability, and any of their linear combination is also its own form. To estimate the obtained solution, it is necessary to form a combination of multiple forms of buckling and the corresponding diagram of bending moments, which will serve as the basis for the use of the criterion. This paper proposes an approach that allows to determine such a combination of multiple forms, which will be the basis for the application of the criterion of proximity of the obtained solution to the minimum material-intensive.

Keywords: optimization, system minimal consumption of materials, stability, critical force, buckling, bending moments, multiplicity, tension, evaluation criteria for solutions of optimal problems

ИСПОЛЬЗОВАНИЕ КРИТЕРИЯ МИНИМАЛЬНОЙ МАТЕРИАЛОЕМКОСТИ СТЕРЖНЕЙ ПРИ ОГРАНИЧЕНИЯХ ПО УСТОЙЧИВОСТИ ДЛЯ СЛУЧАЯ КРАТНОЙ КРИТИЧЕСКОЙ НАГРУЗКИ

Л.С. Ляхович [1], ***П.А. Акимов*** [1, 2, 3, 4], ***А.П. Малиновский*** [1]
[1] Томский государственный архитектурно-строительный университет, г. Томск, РОССИЯ
[2] Российская академия архитектуры и строительных наук, г. Москва, РОССИЯ
[3] Научно-исследовательский центр СтаДиО, г. Москва, РОССИЯ
[4] Российский университет дружбы народов, г. Москва, РОССИЯ

Аннотация: Как известно, для оценки полученного решения некоторых задач оптимизации сформулированы специальные критерии. В частности, сформулирован критерий, позволяющий оценить для прямолинейных стержней при определенных типах поперечных сечений близость решения о стержне наименьшего веса и ограничениях по устойчивости к минимально материалоемкому. Критерий основан на анализе напряжений от изгибающих моментов, возникающих при потере устойчивости. Если наименьшая критическая сила не кратная, то форма потери устойчивости и соответствующая ей эпюра моментов единственные. При кратности наименьшей критической нагрузки возникают кратные формы потери устойчивости, и любая их линейная комбинация также является собственной формой. Для оценки полученного решения необходимо сформировать комбинацию кратных форм потери устойчивости и соответствующую ей эпюру изгибающих моментов, которая и будет служить основой для использования критерия. В данной статье предлагается подход, позволяющий определять такую комбинацию кратных форм, которая станет основой для применения критерия близости полученного решения к минимально материалоемкому.

Ключевые слова: оптимизация, системы минимальной материалоемкости, устойчивость, критическая сила, формы потери устойчивости, изгибающие моменты, кратность, напряжения, критерии оценки решений оптимальных задач

The theoretical foundations of the creation of rods of the lowest weight, prone to buckling, originate from the research works of Lagrange [1], T. Clausen [2], EL. Nikolai [2] and later N.G. Chentsova [4]. J.L. Nudelman [5], A.F. Smirnov [6], A.I. Vinogradov [7], N. Olkhoff [8] and other authors.

In the contemporary literature, the considering problem is normally formulated in terms of nonlinear mathematical programming.

Let us consider a centrally compressed straight line rod (for example, shown in Figure 1, although the boundary conditions in the planes of inertia may be different).

If $F(x)$ is the cross-sectional area of the rod, P is the acting force, $P1_{kp}[1]$ and $P2_{kp}[1]$ are the minimum critical forces in the main inertia planes of the section, then we need to find an expression $F(x)$ at which the rod would remain stable and the volume of the material of the rod V would be minimal. Thus, the objective function can be written as

$$V = \int_0^l F(x)dx, \qquad (1)$$

Besides, we have the following restrictions

$$P \le P1_{kp}[1] = P2_{kp}[1]. \qquad (2)$$

There are a considerable number of methods for solving this problem. Most of them use finite-dimensional approaches. The process of optimization within the implementation of such methods most often stops at a stage when the objective function in the adjacent search steps decreases less than a predetermined value. Such a criterion for stopping the process of searching for a minimum in most cases gives an acceptable result. However, it does not allow researcher to confidently estimate the proximity of the solution obtained to the solution of minimum material consumption (minimum material-intensive solution).

As a result of several research works [1, 2, 3] for rectilinear centrally compressed rods with certain types of cross sections (for example, those in which the moment of inertia is proportional to the square of the section area), a criterion was formulated to estimate the proximity of the solution to the solution of minimum material consumption.

In [3], it was shown that in the considering case, *the rod of the smallest volume will be a bar of equal resistance with respect to the moment diagram arising in the event of loss of stability*. Thus, with a loss of stability with a rod of the smallest volume, the normal stresses in the extreme fibers of the rod, found from the resulting moment diagrams, should be the same in all sections. That is, for the case when the loss of stability occurs in the two main planes of inertia, the criterion is written as

$$\sigma 1(x) = const; \quad \sigma 2(x) = const. \qquad (3)$$

Under conditions (3), $\sigma 1(x)$ and $\sigma 2(x)$ are the absolute values of the normal stresses in the extreme fibers of the rod determined from the diagrams of the moments that occurred in the corresponding principal planes of inertia during loss of stability.

Since the buckling modes and the corresponding moment and stress diagrams are determined to within a constant factor, $\sigma 1(x)$ and $\sigma 2(x)$ are normalized. If the corresponding normalization is made so that the largest values of $\sigma 1(x)$ and $\sigma 2(x)$ would be equal to one, then the proximity of the obtained solution to the solution of minimum material consumption is estimated by the proximity of $\sigma 1(x)$ and $\sigma 2(x)$ to unity.

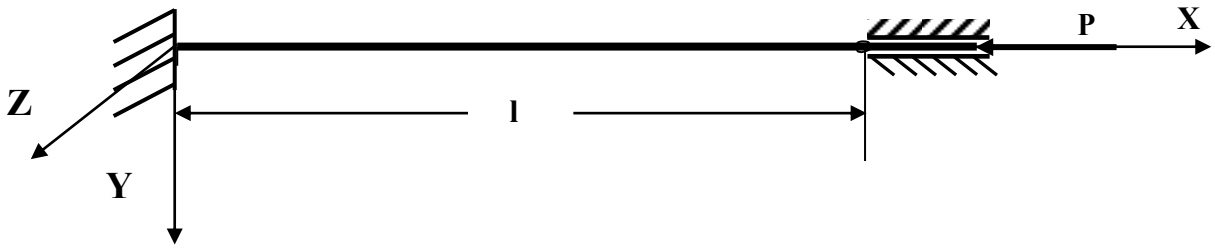


Figure 1. Considering centrally compressed straight line rod.

If the first critical force is not a multiple, then the moment diagram that occurs when stability is lost is unique. In this case, criterion (3) can be used on the basis of this diagram, including in combination with some other restrictions (see, for example, [9]).

If the first critical force is multiple, then multiple buckling modes and the corresponding moment diagrams appear. It is also known that any linear combination of multiple buckling modes will also be proper.

The multiplicity of critical forces that occurs when minimizing the volume of the rod for rigidly restrained rods was identified in [8]. However, the multiplicity of critical forces also occurs in other cases, for example, when optimizing the volume under constraints on the stability of some continuous beam schemes.

In these cases, it is necessary to establish a linear combination of bending moments diagrams corresponding to multiple buckling modes. This combination will serve as the basis for the use of the criterion (3).

Let us consider an approach to determination of such combination. We represent the approach for one main plane of inertia and threefold critical force. For the second plane and the other multiplicity of critical forces, all actions will be similar.

Let it be required to estimate the closeness of the search stage for the solution of the considering optimization problem to the minimum material-intensive one.

At the estimated stage of the search, in the considered main plane of inertia, the first critical forces in $P1_{cr}[1]$, $P1_{cr}[2]$ and $P1_{cr}[3]$ are found, the corresponding forms of buckling and the estimated optimal cross-section sizes and their moments of resistance $w(x)$.

The following steps are performed in the following order:

1. Using the three first forms of buckling found at the estimated stage of the research, the corresponding diagrams of the absolute values of the bending moments $M_1(x)$, $M_2(x)$ and $M_3(x)$ are constructed. Plots are normalized, for example, so that

$$\int_0^l [M_1(x)]^2 dx = 1; \quad \int_0^l [M_2(x)]^2 dx = 1;$$

$$\int_0^l [M3(x)]^2 dx = 1.$$

2. On the basis of the assumption about the optimality of the found dimensions of the cross-sections, a conditionally optimal diagram of the absolute values of the bending moments $M_0(x)$ is constructed, according to which relation (3), that is, the condition,

$$\sigma 1(x) = \frac{M_0(x)}{w(x)} = 1$$

must be fulfilled. Thus, we have $M_0(x) = w(x)$. The plot is also normalized.

3. If the considering solution is optimal, then the combination of arising diagrams

$$M_{00}(x) = a * M_1(x) + b * M_2(x) + c * M_3(x)$$

should coincide with $M_0(x)$. The equations for finding the coefficients a, b and c will be obtained from the minimum condition of the quadratic deviation of the diagram $M_{00}(x)$ from $M_0(x)$. That is, from the minimum condition of the integral

$$\Delta M(a,b) = \int_0^l [M_0(x) - aM_1(x) - bM_2(x) - cM_2(x)]^2 dx,$$

we get three equations

$$\frac{\partial \Delta M(a,b,c)}{\partial a} = 0; \quad \frac{\partial \Delta M(a,b,c)}{\partial b} = 0$$
$$\frac{\partial \Delta M(a,b,c)}{\partial c} = 0.$$

After solution of the system, we can find the coefficients a, b and c.

4. From the

$$M_{00}(x) = aM_1(x) + bM_2(x) + cM_3(x)$$

plot, we can determine

$$\sigma 1(x) = \frac{M_0(x)}{w(x)}$$

and normalize it, and by the proximity of the stress $\sigma 1(x)$ in sections and its average value along the length of the rod

$$\Delta\sigma 1 = [\int_0^{\partial} \sigma 1(x)dx]/l$$

to one, we estimate the optimality of the solution.

5. Besides, the optimality of the considering solution can also be evaluated by the proximity of the diagrams of $M_0(x)$ and $M_{00}(x)$. The proximity is estimated by the values of the differences

$$\Delta M_0(x) = M_0(x) - M_{00}(x)$$

in the sections and the average value of their absolute values along the length of the rod

$$\Delta M_{00} = \{\int_0^l \mathrm{sgn}[\Delta M_0(x)]\Delta M_0(x)dx\}/l.$$

6. If the multiplicity of critical forces for the considering system is not known in advance, then its presence or absence is revealed in the process of optimization. If the multiplicity is detected, then the differences

$$\Delta P1 = \{P1_{kp}[2] - P1_{kp}[1]\}/P1_{kp}[1]\cdot 100\%;$$
$$\Delta P2 = \{P1_{kp}[3] - P1_{kp}[1]\}/P1_{kp}[1]\cdot 100\%$$

in the limit tend to zero. Let us give an illustration of the described approach with samples.

7. For a rod whose scheme is shown in Figure 1, the doubling of the critical force was considered in detail in [8]. Although the possibility of using of the criterion (3) was not considered in [8], taking into account the detailed analysis in [8] of the doubly critical load of a rigidly clamped rod, it seems appropriate to illustrate the proposed approach using other examples. Two numerical samples are considered. The first one deals with two-time critical force, and the second one deals with three-time critical force.

The first numerical sample. Let us consider a rectilinear square rod, compressed by a centrally applied longitudinal force with supporting conditions in both main planes of inertia of sections, shown in Figure 2.

A preliminary analysis showed that the critical force will be twofold.

Let $l = 9$ *meters* be width of span, $P = 3000000\ N$ be magnitude of force;

$E = 206000MPa$ be the modulus of elasticity of the material. The analysis was performed on the basis of a discrete model ([10]) of 41 fragments.

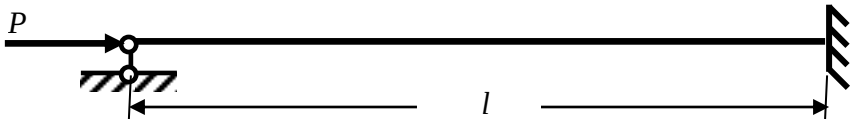


Figure 2. The first numerical sample.

For a discrete model, the objective function (1) is written as

$$V = \sum_{1}^{n} F[i](l/n) = \sum_{1}^{n} (b[i])^2 (l/n), \qquad (4)$$

where $b[i]$ is the size of the square section of the rod; n is dimension of a discrete model.

Diagrams of $M_1(x)$, $M_2(x)$, $M_0(x)$, $M_{00}(x)$, $\Delta M_0(x)$ are represented by $M_1[i]$, $M_2[i]$, $M_3[i]$, $M_{00}[i]$, $\Delta M_0[i]$.

Since the boundary conditions in both main planes of inertia are the same, and the critical forces are assumed to be twofold, the stability constraints are written as

$$P \le P1_{kp}[1] = P1_{kp}[2]. \qquad (5)$$

Criterion (3) for the discrete model in this case takes the form

$$\sigma[i] = const. \qquad (6)$$

Optimization was performed by one of the variants of the method of random search. The estimation of the proximity of the solution to the minimum material-based on criterion (6) was carried out at several stages of the computing (Tables 1 and 2).

Four stages were considered. The results of each stage are presented in the corresponding columns of Tables 1 and 2. Stage 0 corresponds to the results corresponding to the first access to the boundary of the allowable area for a rod of constant square cross-sectional length. The remaining columns show the results, respectively, at 300, 1300 and more than 40,000 tests of the random search method. Table 1 shows the cross-section dimensions $b[i]$ for each stage. The bottom five lines show the values of the objective function – $V, meters^3$; the magnitudes of its decrease compared with stage 0 – ΔV, %; the difference between the first two critical forces – ΔP, %; the values of the coefficients a and b.

Table 2 shows the values of the differences

$$\Delta M_0[i] = M_0[i] - M_{00}[i]$$

and stresses $\sigma[i]$, and in the last line the average values for each stage are the values of these quantities ΔM_{00} and $\Delta\sigma 1$.

Analysis of the data in tables 1 and 2 shows that despite the small difference in the values of the objective function in the last two stages, the difference in cross sections between the values of differences $\Delta M_0[i]$ and stresses $\sigma[i]$ at these stages of the search is more significant. At the last stage, in almost all cross sections, the differences $\Delta M_0[i]$ are close to zero, and the stresses $\sigma[i]$ to unity.

The result obtained confirms that, even with a double critical force, criterion (3) can estimate the proximity of the obtained solution to the minimum material-intensive one.

Let us consider one more example, in which, according to preliminary calculations during optimization, the critical force turns out to be threefold.

Let us consider a rectilinear square rod, compressed by a centrally applied longitudinal force with supporting conditions in both main planes of inertia of sections, shown in Figure 3.

Table 1. Results of analysis.

	b[*i*] by stages of search for optimum			
t	0	300	1300	>40000
1	2	3	4	5
1	0.0915	0.0626	0.0420	0.0426
2	0.0915	0.0655	0.0600	0.0596
3	0.0915	0.0789	0.0696	0.0692
4	0.0915	0.0784	0.0761	0.0761
5	0.0915	0.0835	0.0806	0.0813
6	0.0915	0.0821	0.0855	0.0854
7	0.0915	0.0927	0.0878	0.0888
8	0.0915	0.0883	0.0921	0.0916
9	0.0915	0.0949	0.0943	0.0938
10	0.0915	0.0984	0.0966	0.0957
11	0.0915	0.0949	0.0960	0.0971
12	0.0915	0.0924	0.0985	0.0982
13	0.0915	0.0944	0.0982	0.0990
14	0.0915	0.1110	0.0987	0.0995
15	0.0915	0.0975	0.1000	0.0997
16	0.0915	0.1010	0.0990	0.0997
17	0.0915	0.0995	0.1000	0.0993
18	0.0915	0.0929	0.0987	0.0986
19	0.0915	0.1189	0.0988	0.0977
20	0.0915	0.1021	0.0967	0.0964
21	0.0915	0.1053	0.0944	0.0948
22	0.0915	0.0833	0.0925	0.0927
23	0.0915	0.0998	0.0905	0.0902
24	0.0915	0.0799	0.0877	0.0872
25	0.0915	0.0857	0.0829	0.0834
26	0.0915	0.0787	0.0784	0.0787
27	0.0915	0.0806	0.0724	0.0728
28	0.0915	0.0654	0.0639	0.0647
29	0.0915	0.0743	0.0522	0.0523
30	0.0915	0.0701	0.0255	0.0049
31	0.0915	0.0730	0.0524	0.0518
32	0.0915	0.0603	0.0644	0.0640
33	0.0915	0.0636	0.0731	0.0719
34	0.0915	0.0793	0.0776	0.0777
35	0.0915	0.0736	0.0828	0.0823
36	0.0915	0.0834	0.0852	0.0859
37	0.0915	0.0966	0.0899	0.0888
38	0.0915	0.1000	0.0917	0.0912
39	0.0915	0.0911	0.0924	0.0931
40	0.0915	0.0889	0.0944	0.0946

1	2	3	4	5
41	0.0915	0.0852	0.0956	0.0957
V, $meters^3$	0.07539	0.06904	0.06492	0.06476
ΔV	0.00%	8.43%	13.89%	14.10%
ΔP	195.00%	130.49%	17.74%	0.03%
a	0.48987	0.83099	1.01063	1,02480
b	0.49986	0.13279	-0.01283	-0,02805

Table 2. Results of analysis.

	$\Delta M_0[i]$ by stages of search for optimum				σ by stages of search for optimum			
t	0	300	1300	>40000	0	300	1300	>40000
1	2	3	4	5	6	7	8	9
1	0.1396	0.0388	0.0008	0.0000	0.076842	0.135799	0.978754	0.9988
2	0.1070	0.0284	0.0019	0.0001	0.228466	0.301949	0.893968	0.9973
3	0.0757	0.0202	0.0024	0.0000	0.373973	0.476454	0.902065	0.9984
4	0.0465	0.0256	0.0019	0.0000	0.509501	0.441546	0.913346	0.9986
5	0.0202	0.0003	0.0010	0.0000	0.631502	0.597886	0.923345	0.9985
6	0.0025	0.0103	0.0032	0.0000	0.736850	0.541898	0.952999	0.9988
7	0.0210	0.0334	0.0064	0.0000	0.822944	0.718689	0.971152	0.9988
8	0.0350	0.0815	0.0001	0.0000	0.887779	0.941500	0.930939	0.9987
9	0.0441	0.0678	0.0041	0.0000	0.930011	0.827215	0.910997	0.9990
10	0.0481	0.0215	0.0091	0.0000	0.948989	0.662066	0.889453	0.9990
11	0.0472	0.0239	0.0144	0.0000	0.944770	0.514969	1.000000	0.9987
12	0.0415	0.0293	0.0056	0.0000	0.918104	0.487964	0.907040	0.9989
13	0.0312	0.0782	0.0094	0.0001	0.870409	0.867698	0.973216	0.9991
14	0.0169	0.1005	0.0105	0.0000	0.803706	0.381801	0.977651	0.9987
15	0.0010	0.0407	0.0069	0.0000	0.720548	0.468211	0.902845	0.9987
16	0.0218	0.0869	0.0025	0.0000	0.623928	0.350193	0.921093	0.9986
17	0.0448	0.0572	0.0006	0.0001	0.517169	0.765660	0.929211	0.9991
18	0.0347	0.0903	0.0021	0.0001	0.564413	0.924885	0.940865	0.9990
19	0.0191	0.1114	0.0039	0.0000	0.636604	0.402981	0.914728	0.9988
20	0.0061	0.1037	0.0092	0.0001	0.697070	0.312453	0.888763	0.9984
21	0.0038	0.0158	0.0016	0.0000	0.743026	0.556928	0.923710	0.9985
22	0.0101	0.0800	0.0006	0.0001	0.772075	1.000000	0.928379	0.9992
23	0.0123	0.0377	0.0066	0.0000	0.782309	0.485707	0.894467	0.9988
24	0.0101	0.0041	0.0022	0.0001	0.772383	0.572689	0.918233	0.9982
25	0.0035	0.0387	0.0057	0.0000	0.741573	0.416936	0.973638	0.9984
26	0.0077	0.0122	0.0055	0.0000	0.689821	0.669361	0.979892	0.9989
27	0.0232	0.0177	0.0015	0.0000	0.617743	0.497582	0.915495	0.9984
28	0.0428	0.0142	0.0031	0.0000	0.526627	0.744256	0.982150	0.9985
29	0.0661	0.0478	0.0002	0.0000	0.418400	0.256604	0.938477	0.9988
30	0.0723	0.0574	0.0035	0.0000	0.389795	0.110365	0.055568	-0.0546
31	0.0772	0.0454	0.0007	0.0000	0.366997	0.255342	0.910506	1.0000
32	0.0843	0.0037	0.0032	0.0000	0.333614	0.644771	0.880962	0.9992
33	0.0933	0.0282	0.0051	0.0000	0.292105	0.915174	0.876885	0.9992

1	2	3	4	5	6	7	8	9
34	0.0969	0.0431	0.0044	0.0000	0.275390	0.343807	0.971364	0.9987
35	0.0660	0.0390	0.0017	0.0000	0.418961	0.881604	0.919258	0.9988
36	0.1541	0.0365	0.0028	0.0001	0.554891	0.412768	0.950408	0.9995
37	0.1713	0.0655	0.0045	0.0000	0.679382	0.384630	0.905781	0.9986
38	0.1864	0.0676	0.0004	0.0001	0.788944	0.399366	0.929533	0.9985
39	0.1994	0.0502	0.0013	0.0001	0.880504	0.402443	0.938544	0.9992
40	0.2099	0.0156	0.0064	0.0000	0.951507	0.661024	0.899818	0.9987
41	0.2179	0.0131	0.0077	0.0001	1.000000	0.657937	0.968563	0.9983
Σ / n	0.0408	0.0435	0.0040	0.0000	0.6449	0.5461	0.9094	0.9731

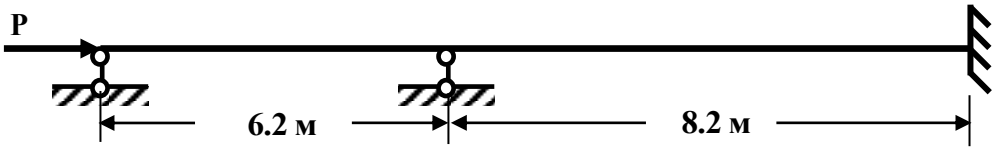


Figure 3. The second numerical sample.

The second numerical sample. Let us consider a rectilinear square rod, compressed by a centrally applied longitudinal force with supporting conditions in both main planes of inertia of sections, shown in Figure 3. The analysis was performed on the basis of a discrete model ([10]) of 41 fragments.

Since the boundary conditions in the two main planes of inertia are the same, and the critical forces are assumed to be threefold, the stability constraints are written as

$$P \le P1_{cr}[1] = P1_{cr}[2] = P1_{cr}[3]. \qquad (7)$$

In the same way as in the first sample, optimization was performed by one of the variants of the random search method. The estimation of the proximity of the solution to the minimum material-based on criterion (6) was carried out at several stages of the calculation (Tables 3 and 4). Similarly to the first sample, four stages of finding the optimal solution were considered.

The results are presented in the corresponding columns of Tables 3 and 4. The designations in these tables are the same as in the first sample. In addition, Table 3 also lists the values of the coefficient c and the difference $\Delta P2$.

Analysis of the data in Tables 3 and 4 shows that in the last two stages of the search, the objective functions differ little.

However, at the same time, differences $\Delta M_0[i]$ and reduced stresses $\sigma[i]$ show that, despite the small difference in the values of the objective function in the last two stages, the difference between the values of differences $\Delta M_0[i]$ and stresses $\sigma[i]$ at these stages of the search is more significant. At the last stage, in almost all cross sections, the differences $\Delta M_0[i]$ are close to zero, and the stresses $\sigma[i]$ to unity. In sections 16 and 31, the stresses are far from unity. This is due to the significantly smaller compared with the other sizes of sections, which in such cases reduces the accuracy of the selected model.

From Table 3 it can be seen how the critical forces approach each other in stages. So, if at stage number 0 the difference $\Delta P1$ is 102.54%, and $\Delta P2$ – 236.62%, then at the last stage these differences are 0.01% and 0.03%.

Table 4 shows how the mean values of differences ΔM_{00} and stresses change $\Delta\sigma 1$.

Table 3. Results of analysis.

	b[*i*] by stages of search for optimum			
t	0	300	1300	>40000
1	2	3	4	5
0.0893	0.0500	0.0503	0.0513	0.0893
0.0893	0.0724	0.0711	0.0705	0.0893
0.0893	0.0745	0.0818	0.0808	0.0893
0.0893	0.0865	0.0882	0.0875	0.0893
0.0893	0.0972	0.0925	0.0920	0.0893
0.0893	0.0936	0.0951	0.0950	0.0893
0.0893	0.1072	0.0967	0.0968	0.0893
0.0893	0.0991	0.0987	0.0976	0.0893
0.0893	0.0968	0.0950	0.0973	0.0893
0.0893	0.0980	0.0951	0.0960	0.0893
0.0893	0.0990	0.0930	0.0936	0.0893
0.0893	0.0901	0.0913	0.0898	0.0893
0.0893	0.0779	0.0848	0.0842	0.0893
0.0893	0.0807	0.0765	0.0759	0.0893
0.0893	0.0637	0.0631	0.0623	0.0893
0.0893	0.0477	0.0260	0.0057	0.0893
0.0893	0.0557	0.0609	0.0618	0.0893
0.0893	0.0748	0.0758	0.0753	0.0893
0.0893	0.0872	0.0832	0.0834	0.0893
0.0893	0.0881	0.0894	0.0889	0.0893
0.0893	0.0908	0.0925	0.0925	0.0893
0.0893	0.0879	0.0943	0.0947	0.0893
0.0893	0.0967	0.0959	0.0958	0.0893
0.0893	0.0898	0.0947	0.0958	0.0893
0.0893	0.0869	0.0941	0.0947	0.0893
0.0893	0.0963	0.0922	0.0925	0.0893
0.0893	0.0867	0.0888	0.0888	0.0893
0.0893	0.0811	0.0831	0.0834	0.0893
0.0893	0.0798	0.0757	0.0753	0.0893
0.0893	0.0604	0.0622	0.0618	0.0893
0.0893	0.0457	0.0242	0.0057	0.0893
0.0893	0.0676	0.0611	0.0602	0.0893
0.0893	0.0785	0.0733	0.0731	0.0893
0.0893	0.0807	0.0811	0.0806	0.0893
0.0893	0.0884	0.0849	0.0854	0.0893
0.0893	0.0957	0.0880	0.0883	0.0893
V, meters^3	0.1149	0.1003	0.0978	0.0973
ΔV	0.00	12.69	14.90	15.35
$\Delta P1$	102.54	31.20	5.72	0.01
$\Delta P2$	236.62	71.35	9.42	0.03

1	2	3	4	5
a	0.2813	0.8000	0.8283	0.5434
b	0.3571	0.1761	0.1846	0.4334
c	0.3932	0.0045	-0.0101	0.0516

Table 2. Results of analysis.

	$\Delta M_0[i]$ by stages of search for optimum				σ by stages of search for optimum			
t	0	300	1300	>40000	0	300	1300	>40000
1	2	3	4	5	6	7	8	9
1	0.1302	0.0087	0.0043	0.0000	0.1554	0.4562	0.9797	0.9995
2	0.0610	0.0332	0.0035	0.0000	0.4501	0.4111	0.8332	0.9992
3	0.0029	0.0161	0.0075	0.0000	0.6979	0.5343	0.8202	0.9991
4	0.0385	0.0139	0.0031	0.0002	0.8741	0.6878	0.8815	0.9974
5	0.0591	0.0696	0.0043	0.0002	0.9623	0.4408	0.8482	0.9998
6	0.0578	0.0032	0.0030	0.0000	0.9565	0.6429	0.8547	0.9988
7	0.0355	0.0852	0.0131	0.0000	0.8616	0.4575	0.9148	0.9988
8	0.0042	0.0033	0.0048	0.0000	0.6924	0.6418	0.8495	0.9987
9	0.0319	0.0418	0.0144	0.0001	0.5743	0.5161	0.9224	0.9984
10	0.0299	0.0824	0.0012	0.0001	0.5827	0.4106	0.8710	0.9992
11	0.0391	0.0502	0.0028	0.0001	0.5436	0.7646	0.8545	0.9995
12	0.0111	0.0683	0.0133	0.0001	0.6630	0.8699	0.8078	0.9984
13	0.0007	0.0358	0.0067	0.0000	0.7133	0.8247	0.8294	0.9985
14	0.0055	0.0431	0.0063	0.0000	0.6869	0.4253	0.8194	0.9989
15	0.0292	0.0192	0.0029	0.0000	0.5859	0.4439	0.8273	0.9990
16	0.0505	0.0094	0.0007	0.0000	0.4952	0.8522	1.0000	0.5329
17	0.0533	0.0249	0.0017	0.0000	0.4831	1.0000	0.8408	0.9987
18	0.0199	0.0160	0.0038	0.0000	0.6253	0.5361	0.8372	0.9989
19	0.0013	0.0875	0.0052	0.0002	0.7048	0.2975	0.8363	1.0000
20	0.0002	0.0171	0.0114	0.0000	0.7092	0.5696	0.8127	0.9988
21	0.0053	0.0234	0.0053	0.0001	0.6877	0.5537	0.8886	0.9984
22	0.0104	0.0662	0.0010	0.0000	0.7544	0.8805	0.8702	0.9989
23	0.0077	0.0523	0.0051	0.0000	0.7430	0.4862	0.8467	0.9988
24	0.0115	0.0459	0.0006	0.0000	0.6612	0.7939	0.8686	0.9986
25	0.0213	0.0236	0.0032	0.0001	0.6193	0.5421	0.8790	0.9983
26	0.0129	0.0406	0.0087	0.0000	0.7653	0.7485	0.9035	0.9990
27	0.0305	0.0474	0.0042	0.0001	0.8400	0.4487	0.8862	0.9996
28	0.0275	0.0163	0.0098	0.0001	0.8275	0.7107	0.9236	0.9993
29	0.0028	0.0230	0.0039	0.0001	0.7223	0.5182	0.8358	0.9979
30	0.0422	0.0090	0.0020	0.0000	0.5305	0.7365	0.8940	0.9990
31	0.0851	0.0091	0.0020	0.0000	0.3474	0.3901	0.3920	0.1702
32	0.0945	0.0139	0.0011	0.0000	0.3074	0.5187	0.8505	0.9981
33	0.0855	0.0221	0.0006	0.0000	0.3460	0.7489	0.8712	0.9984
34	0.0183	0.0742	0.0054	0.0000	0.6321	0.9912	0.8322	0.9989
35	0.0349	0.0245	0.0016	0.0001	0.8589	0.7232	0.8750	0.9993

1	2	3	4	5	6	7	8	9
36	0.0680	0.0961	0.0004	0.0000	1.0000	0.3548	0.8682	0.9987
Σ / n	0.0339	0.0366	0.0047	0.0001	0.6572	0.6091	0.8535	0.9629

So, if in the first three stages the average value of the differences ΔM_{00} is far from zero. Besides, the average stress $\Delta\sigma 1$ is far from one. Thus we have $\Delta M_{00} = 0.0001$ and $\Delta\sigma 1 = 0.9993$ at the last stage.

The result obtained in this sample confirms that with a triple critical force criterion (3) can estimate the closeness of the obtained solution to the minimum material-intensive one.

The approach proposed in this paper is based on using the criterion (3) of estimating the proximity of a solution for optimizing rods with constraints on resistance to the least material-intensive. This approach can be extended to cases of multiplicity of critical forces.

REFERENCES

1. **Lagrange J.-L.** Sur la Figure Des Collonnes. // Mescellanea Taurinensia, 1770-1773, Vol. 5, pp. 123.
2. **Clausen T.** Uber die Form Architektonischer Säulen. // Bull. cl. physico-raath. Acad. St.-Petersbourg, 1851, Vol. IX, pp. 371-380.
3. **Nikolay E.L.** Zadacha Lagranzha o Naivygodnejshem Ochertanii Kolonny [Lagrange's Problem About the Most Advantageous Outline of a Column]. // *News. Of St. Petersburg Polytechnic Institute*, 1907, Vol. VIII (in Russian).
4. **Chentsov N.G.** Stojki Naimen'shego Vesa [Stands of a Minimum Weight]. // *Trudy TSAGI*, 1936, Vol. 265 (in Russian).
5. **Nudelman Ya.L.** Metody Opredelenija Sobstvennyh Chastot i Kriticheskih Sil Dlja Sterzhnevyh Sistem [Methods for Determining Natural Frequencies and Critical Forces for Rod Systems]. Moscow, Gostekhizdat, 1949, 175 pages (in Russian).
6. **Smirnov A.F.** Ustojchivost' i Kolebanija Sooruzhenij [Stability and Oscillations of Structures]. Moscow, Transzheldorizdat, 1958 (in Russian).
7. **Vinogradov A.I.** Problema Optimal'nogo Proektirovanija v Stroitel'noj Mehanike [The Problem of Optimal Design in Structural Mechanics]. Kyiv, Vyscha Shkola Publishing House in Kharkiv University, 1973, 167 pages (in Russian).
8. **Olhoff, N, Rasmussen S.Kh.** O Prostyh i Dvuhkratnyh Optimal'nyh Kriticheskih Nagruzkah Poteri Ustojchivosti Dlja Zashhemlennyh Sterzhnej [On Simple and Two-Fold the Optimal Critical Load of Buckling for the Clamped Rods]. // *Mechanics. New in Foreign Science. Optimal Design of Structures*, 1981, Vol. 27, pp. 139-154 (in Russian).
9. **Lyakhovich L.S.** Osobye Svojstva Optimal'nyh Sistem i Osnovnye Napravlenija ih Realizacii v Metodah Rascheta Sooruzhenij [Special Properties of Optimal Systems and the Main Directions of Their Implementation in the Methods of Calculation of Structures]. Tomsk, Tomsk State University of Architecture and Construction, 2009, 372 pages (in Russian).
10. **Malinovsky A.P.** Chislennyj Metod Rascheta Sterzhnej na Prochnost', Ustojchivost' i Kolebanija [A Numerical Method of Calculation of the Studs for Strength, Stability and Fluctuations]. // Studies in Structures and Structural Mechanics. Tomsk: Publishing House of TSU, 1978, pp. 85-96 (in Russian).

СПИСОК ПУБЛИКАЦИЙ

1. **Lagrange J.-L.** Sur la Figure Des Collonnes. // Mescellanea Taurinensia, 1770-1773, Vol. 5, pp. 123.
2. **Clausen T.** Uber die Form Architektonischer Säulen. // Bull. cl. physico-raath.

Acad. St.-Petersbourg, 1851, Vol. IX, pp. 371-380.
3. **Николаи Е.Л.** Задача Лагранжа о наивыгоднейшем очертании колонны. // *Известия Санкт-Петербургского политехнического института*, 1907, т. VIII.
4. **Ченцов Н.Г.** Стойки наименьшего весаю // *Труды ЦАГИ,* 1936, Вып. 265.
5. **Нудельман Я.Л.**, Методы определения собственных частот и критических сил для стержневых систем. – М.: Гостехиздат, 1949. – 175 с.
6. **Смирнов А.Ф.** Устойчивость и колебания сооружений. – М.: Трансжелдориздат, 1958.
7. **Виноградов А.И.** Проблема оптимального проектирования в строительной механике. – Харьков: Вища школа, Издательство при Харьковском университете, 1973. – 167 с.
8. **Ольхофф Н, Расмуссен С.Х.** О простых и двухкратных оптимальных критических нагрузках потери устойчивости для защемленных стержней. // *Механика. Новое в зарубежной науке. Оптимальное проектирование конструкций*, 1981, №27, с. 139-154.
9. **Ляхович Л.С.** Особые свойства оптимальных систем и основные направления их реализации в методах расчета сооружений. – Томск: Издательство Томского государственного архитектурно-строительного университета, 2009. – 372 с.
10. **Малиновский А.П.** Численный метод расчета стержней на прочность, устойчивость и колебания. // Исследования по строительным конструкциям и строительной механике. – Томск: Издательство ТГУ, 1978, с. 85-96.

Ляхович Леонид Семенович, академик Российской академии архитектуры и строительных наук (РААСН), профессор, доктор технических наук, профессор кафедры строительной механики, Томский государственный архитектурно-строительный университет; 634003, Россия, г. Томск, Соляная пл. 2;
E-mail: lls@tsuab.ru

Акимов Павел Алексеевич, академик Российской академии архитектуры и строительных наук (РААСН), профессор, доктор технических наук; главный ученый секретарь Российской академии архитектуры и строительных наук; заместитель генерального директора по науке ЗАО «Научно-исследовательский центр СтаДиО»; профессор Департамента архитектуры и строительства Российского университета дружбы народов; профессор кафедры строительной механики Томского государственного архитектурно-строительного университета; 107031, г. Москва, ул. Большая Дмитровка, д. 24, стр. 1; тел. +7(495) 625-71-63;
факс +7 (495) 650-27-31; email: akimov@raasn.ru, pavel.akimov@gmail.com.

Малиновский Анатолий Павлович, доцент, кандидат технических наук, и.о. заведующего кафедрой строительной механики, Томский государственный архитектурно-строительный университет; 634003, Россия, г. Томск, Соляная пл. 2; e-mail: bat9203@gmail.com.

Leonid S. Lyakhovich, Full Member of the Russian Academy of Architecture and Construction Sciences (RAACS), Professor, Dr.Sc., Head of Department of Structural Mechanics, Tomsk State University of Architecture and Building; 634003, Russia, Tomsk, Solyanaya St., 2; e-mail: lls@tsuab.ru

Pavel A. Akimov, Full Member of the Russian Academy of Architecture and Construction Sciences (RAACS), Professor, Dr.Sc.; Executive Scientific Secretary of Russian Academy of Architecture and Construction Sciences; Vice-Director for Science Activities, Scientific Research Center “StaDyO”; Professor of Department of Architecture and Construction, Peoples’ Friendship University of Russia; Professor of Department of Structural Mechanics, Tomsk State University of Architecture and Building; 24, Ul. Bolshaya Dmitrovka, 107031, Moscow, Russia;
phone +7(495) 625-71-63; fax: +7 (495) 650-27-31;
E-mail: akimov@raasn.ru, pavel.akimov@gmail.com.

Anatoly P. Malinowski, Associate Professor, Ph.D, H.T. Head of Department of Structural Mechanics, Tomsk State University of Architecture and Building; 634003, Russia, Tomsk, Solyanaya St., 2;
E-mail: bat9203@gmail.com.

BEARING CAPACITY OF DEEP PILE FOUNDATION FOR HIGH-RISE FACILITY ON WEAK SOILS: COMPARING OF ANALYSIS RESULTS AND EXPERIMENTAL DATA

Rashid A. Mangushev [1], ***Nadezhda S. Nikitina*** [2]
[1] Saint-Petersburg State Architecture and Construction University, Saint-Petersburg, RUSSIA
[2] National Research Moscow State University of Civil Engineering, Moscow, RUSSIA

Abstract: The results of static testing of the pile and comparative results of analytical and numerical calculations for the experimental deep pile (length 65 m, diameter 1.2 m) under the high-rise building, designed in the area of a large thickness of weak soils, are presented in the paper. At the same construction site, an experimental barrette pile of rectangular cross-section with a size of 3.3 × 1.1 and a length of 65 m with the location of the base in solid Proterozoic clays was made. This pile was tested with the use of Osterberg cells, for which strain gauges were mounted in its reinforcement cage at 9 levels. In the first stage, a standard test of the entire experimental barrette pile in the top-down direction was conducted; in the second, after reaching the maximum possible load, the tests were carried out using the "O-cells" located at a depth of 50 m in the thickness of solid clays and transmitting the load in two directions (up and down). A General assessment of the bearing capacity of the barrette pile obtained by three methods is given.

Keywords: bearing capacity, analytical methods, numerical methods, experimental studies, pile, high-rise building, weak soils

НЕСУЩАЯ СПОСОБНОСТЬ СВАЙНОГО ФУНДАМЕНТА ГЛУБОКОГО ЗАЛОЖЕНИЯ ДЛЯ ВЫСОТНЫХ ОБЪЕКТОВ НА СЛАБЫХ ГРУНТАХ: СОПОСТАВЛЕНИЕ РЕЗУЛЬТАТОВ РАСЧЕТА И ЭКСПЕРИМЕНТАЛЬНЫХ ДАННЫХ

Р.А. Мангушев [1], ***Н.С. Никитина*** [2]
[1] Санкт-Петербургский государственный архитектурно-строительный университет,
г. Санкт-Петербург, РОССИЯ
[2] Национальный исследовательский Московский государственный строительный университет,
г. Москва, РОССИЯ

Аннотация: В настоящей статье представлены результаты статических испытаний и соответствующие сравнительные результаты аналитических и численных расчетов для опытной глубокой сваи (длина – 65 метров, диаметр – 1.2 метра) под высотным зданием, спроектированным в зоне большой толщи слабых грунтов. На той же строительной площадке была изготовлена опытная свая-баретта прямоугольного сечения размером 3.3 × 1.1 метра и длиной 65 метров с расположением основания в твердых протерозойских глинах. Эта свая была испытана с использованием ячеек Остерберга. Для этого при устройстве сваи в ее арматурном каркасе были установлены тензодатчики на девяти уровнях. Испытание опытной сваи-баретты проводилось с два этапа. Так, на первом этапе было выполнено стандартное испытание всей сваи в направлении сверху вниз, а на втором этапе, после достижения максимально возможной нагрузки, испытания проводились с использованием ячеек "O-cell", которые располагались на глубине 50 метров в толще твердых глин, передающих нагрузку в двух направлениях (вверх и вниз). Дана общая оценка несущей способности сваи-баретты на основе трех методов.

Ключевые слова: несущая способность, аналитические методы, численные методы, экспериментальные исследования, свая, высотные здания, слабые грунты

1. INTRODUCTION

Modern large-scale underground construction in a cramped town planning and a sharp increase in the number of facilities' storeys requires careful consideration of the pile construction affecting (especially in weak soils) and changes in soil properties directly under the foundation and in the surrounding area under the influence of man-made factors that appear during construction process. It is the most important to consider such changes in complex geotechnical conditions. An important aspect in this case is the assessment of the bearing capacity of piles by analytical methods. Therefore, it is very valuable to compare reliability of such analytical methods with full-scale tests.

A large number of analytical methods for calculating the bearing capacity of a single pile, taking into account pile geometric dimensions and the characteristics of the surrounding soil [1], is known. Unfortunately, often the calculated values differ significantly from the natural ones obtained when loading such piles with vertical load. Especially acute this problem arises with a large length of piles and their production under the protection of a clay mortar or casing pipe. Comparing of the differences between results of calculations for Building Codes of the Russian Federation SNiP 24.13330 [2] and SP 50-102-2003 [3] and results of standard tests for vertical load according to Standard of the Russian Federation GOST 5686 [3] show that the first, as a rule, is much smaller for first ones than the second. In addition, the anthropogenic impact on the soil under the foundation can be local and general (territorial) in nature and differs depending on the adopted technology [1,2].

In accordance with the mentioned above, relevant assessments and comparisons carried out with respect to pile foundations of high-rise buildings in the conditions of their construction on weak soils are of interest.

The mentioned problem was investigated during of design work on the building of "Okhta-Center" (height 396 m). In order to determine the total bearing capacity of bored piles and barrette piles, as well as, separately of bearing capacity on the lateral surface and the base, two experimental bored piles under the protection of a casing pipe with a diameter of 1.2 m and a length of 52.8 m (piles BN), and five experimental barrette piles with a size of 3.3 × 1.0 m and a length of 65 m (piles SB) were built and tested.

2. ENGINEERING GEOLOGICAL CONDITIONS OF THE TEST SITE

According to the results of drilling to a depth of 170 m, the ground sediments were revealed at the base, kinds and average characteristics of which are given in the table 1.

3. EVALUATION OF BEARING CAPACITY OF EXPERIMENTAL PILE BN

In accordance with the regulatory documents of the Russian Federation [1, 2] the calculated bearing capacity of friction piles is determined by the formula

$$F_d = \gamma_c \left[\gamma_{cR} R A + u \sum \gamma_{cf} f_i h_i\right], \qquad (1)$$

where γ_c is coefficient of working conditions of a pile in a ground, which takes the value for driving piles $\gamma_c = 1$; R is design resistance of the soil under the lower end of the pile; A is area of pile cross section, m^2; u is perimeter of the pile cross section; f_i is design resistance of i–th soil layer along the lateral surface of the pile, kPa; h_i is thickness of i-th soil layer surrounding the pile surface, m, that should be $h_i \le 2$ m; γ_{cR}, γ_{cf} are the coefficients of working conditions of the ground under the lower end of the pile and surround the pile surface respectively which take in account affecting of the pile production technology.

Tests of piles BN were conducted using hydraulic jacks until a maximum load of 3500 T (35000 kN; Production and testing of bored piles were carried out by the company “Geoizol” in 2009).

Table 1. Characteristics of soil.

A name of soil	Geological index	γ, *kN/m^3*	W	e	IL	E, *MPa*	φ, *degree*	c, *MPa*
Bulk soil	tg IV	17.5	-					
Marine and lake sediments	m,lIV	19.6	0.256	0.683	0.71	14	24	0
Upper glacial lake sediments (upper sediments) of the Baltic glacial lake	lg IIIb	18.6	0.360	0.980	1.1	4.5	7	0.006
Lower glacial lake sediments of the Luga moraine (lower sediments)	lgIIIz	20.4	0.220	0.600	0.87	10.5	17	0.030
Moraine sediments of the Luga moraine	gIIIlz	21.5	0.160	0.43	0.25	17	22	0.036
Dislocated Vendian clays	Vkt2	21.4	0.176	0.503	-0.35	16	14	0.130
Undislocated Vendian clays	Vkt2	22.3	0.129	0.367	-0.79	113	22	0.840



Figure 1. General view of loading system for testing of BN pile under static vertical load.

Table 2. Results of assessment of BN pile overall bearing capacity by different methods.

Method for determining the bearing capacity of a pile	*Overall bearing capacity of the BN experimental pile, kN*
Calculation by the formula (1), $F_{d,calc}$	8320 (- 301%)
Calculation by PC PLAXIS 3D, $F_{d,PLAXIS}$	11000 (- 227%)
Experimental data, $F_{d,site}$	25000

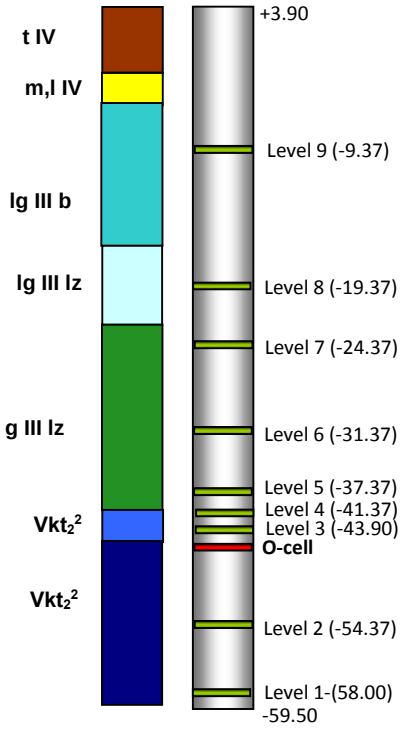


Figure 2. Situation scheme of O-cell element and strain gauges in the experimental barrette pile.

In order to provide these tests, a special loading platform of cross beams, based on a system of 33 drilling-injection anchors of the "Titan" type (Fig. 1), was arranged.

According to [4] the overall pile bearing capacity was assessing by the value of load for which pile gets vertical deformation Δ =20 mm that in the considered case corresponds to loading $F_{d,site}$ = 25000 kN.

Calculation by the formula (1) gave the value of overall bearing capacity of the experimental pile $F_{d,calc}$ = 8320 kN, that includes 5985 kN (71%) under the tip and only 3145 kN (29%) on the lateral surface.

The value of overall bearing capacity obtained by [2, 3] is similar to analysis result of pile under vertical load in PC PLAXIS 3D ($F_{d,PLAXIS}$ = 11000 kN).

Results of assessment of BN pile overall bearing capacity by different methods are given in table 2.

4. EVALUATION OF BEARING CAPACITY OF EXPERIMENTAL BARRETTE PILE SB

At the mentioned building site it was provided experimental testing of barrette pile with length of 65 m and cross section of 3.3 x 1.0 m. The pile was immersed into Vendian clays layer (Vkt2). During the tests, it was used Osterberg cells (O-cells) and strain gauges the situation scheme of which is presented in Figure 2.

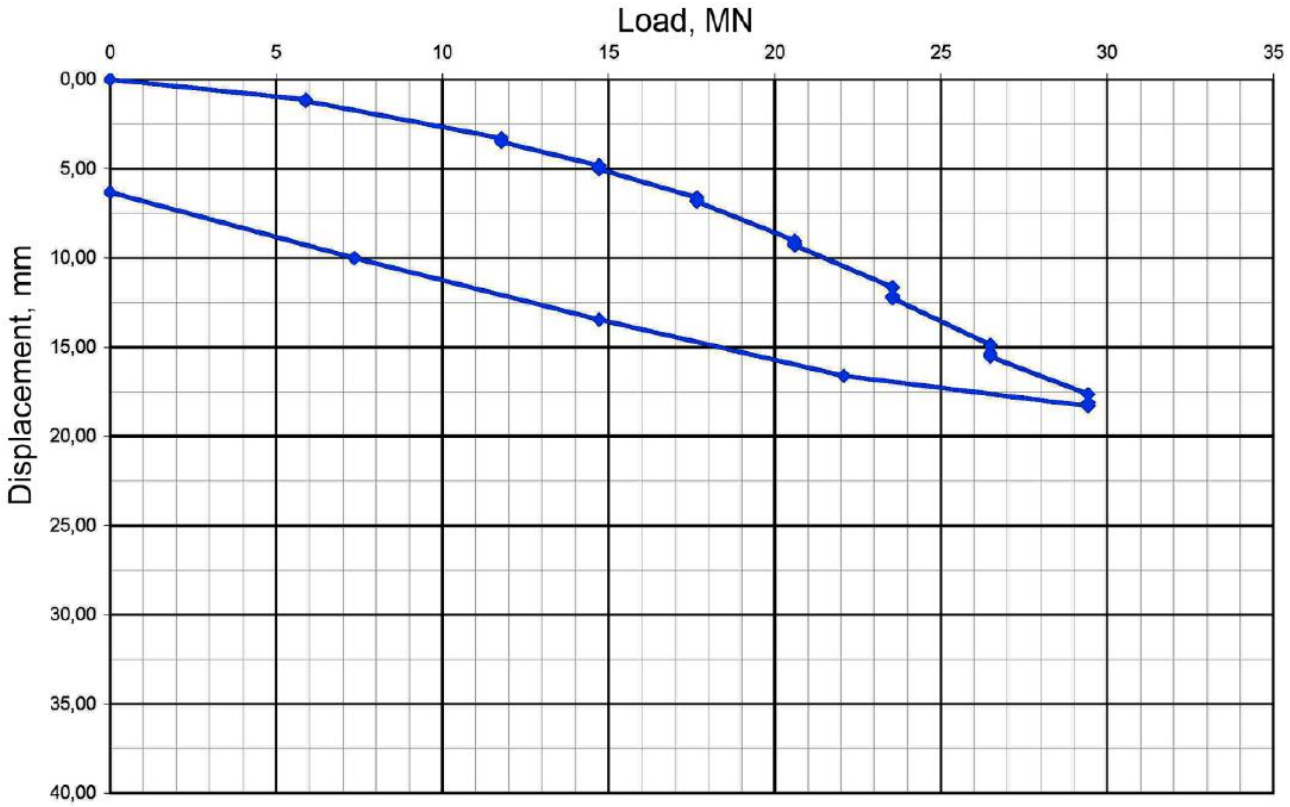


Figure 3. Load-deformation diagram for barrette pile under vertical loading.

Tests of the pile under vertical static load were conducted in two stages: first one is standard test under vertical load applied Top-down; second one is test conducted when load reached its maximum value with usage of O-cell at depth value -45.00 m. Using O-cell, the loading was transmitted in two direction: up and down [5].

The test results for experimental barrette at first stage by Top-down method are shown in Figure 3. At the maximum load 35000 kN deformation does not exceed 20 mm.

Extrapolation of load-deformation diagram until horizontal line corresponding to Δ =20 mm allows assessing overall bearing capacity of the experimental barrette pile at it first loading by $F_{d,Top\text{-}Down}$ = 32000 kN.

An analytical calculation of the experimental barrette pile by the formula (1) [2, 3] gives value of the overall bearing capacity $F_{d,calc}$ = 31244 kN, that is enough close to test results obtained by Top-down method.

Calculational results obtained by PC PLAXIS 3D give value of the overall bearing capacity $F_{d,PLAXIS}$ = 27800 kN (Figure 4) that is smaller than results of Top-down experimental method.

The results of the tests using the Osterberg O-cell, performed after the Top-down loading are shown in Figure 5.

The upper curve corresponds to the bottom-up test of the upper part of the pile and makes it possible estimating the bearing capacity of the barrette on the lateral surface; the lower curve reflects the tests from top to bottom of the pile and allows estimating the bearing capacity of the barrette base.

Extrapolation of the upper curve to the intersection with the horizontal axis corresponding to the value of Δ = -20 mm gives the opportunity to evaluate the bearing capacity of the lateral surface of pile $F_d{}^f{}_{,o\text{-}cell}$ =29500 kN, and the bottom graph allows evaluating the bearing capacity under the tip of barrett which is not less than $F_d{}^R{}_{,o\text{-}cell}$ =13000 kN. The total bearing capacity of the pile according to the described test method is not less than $F_{d\ ,o\text{-}cell}$ = 42500 kN.

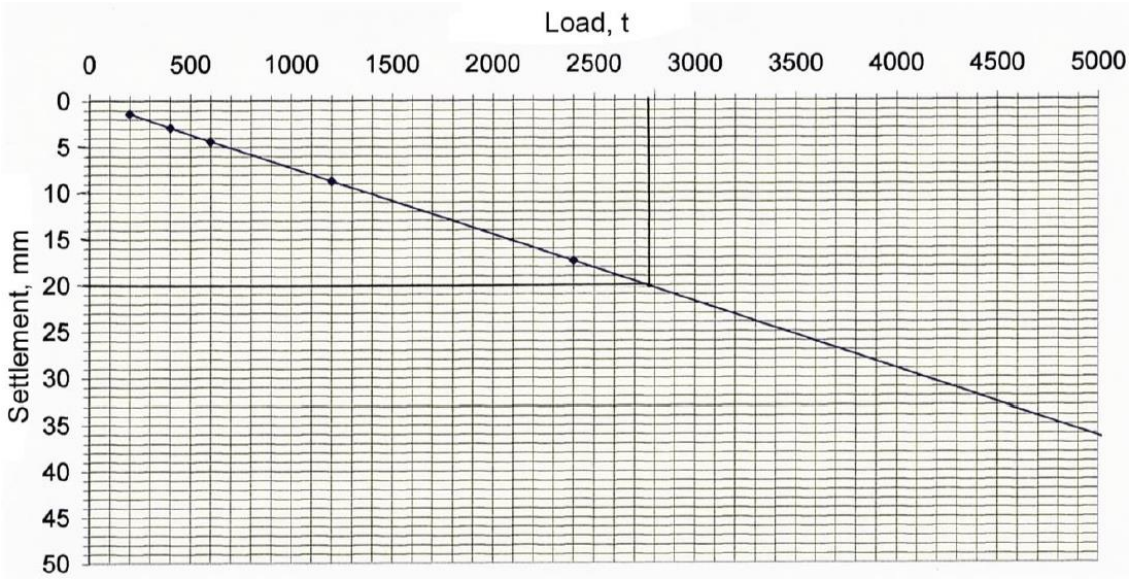


Figure 4. Calculational results obtained by PC PLAXIS 3D for experimental barrette pile under vertical loading.

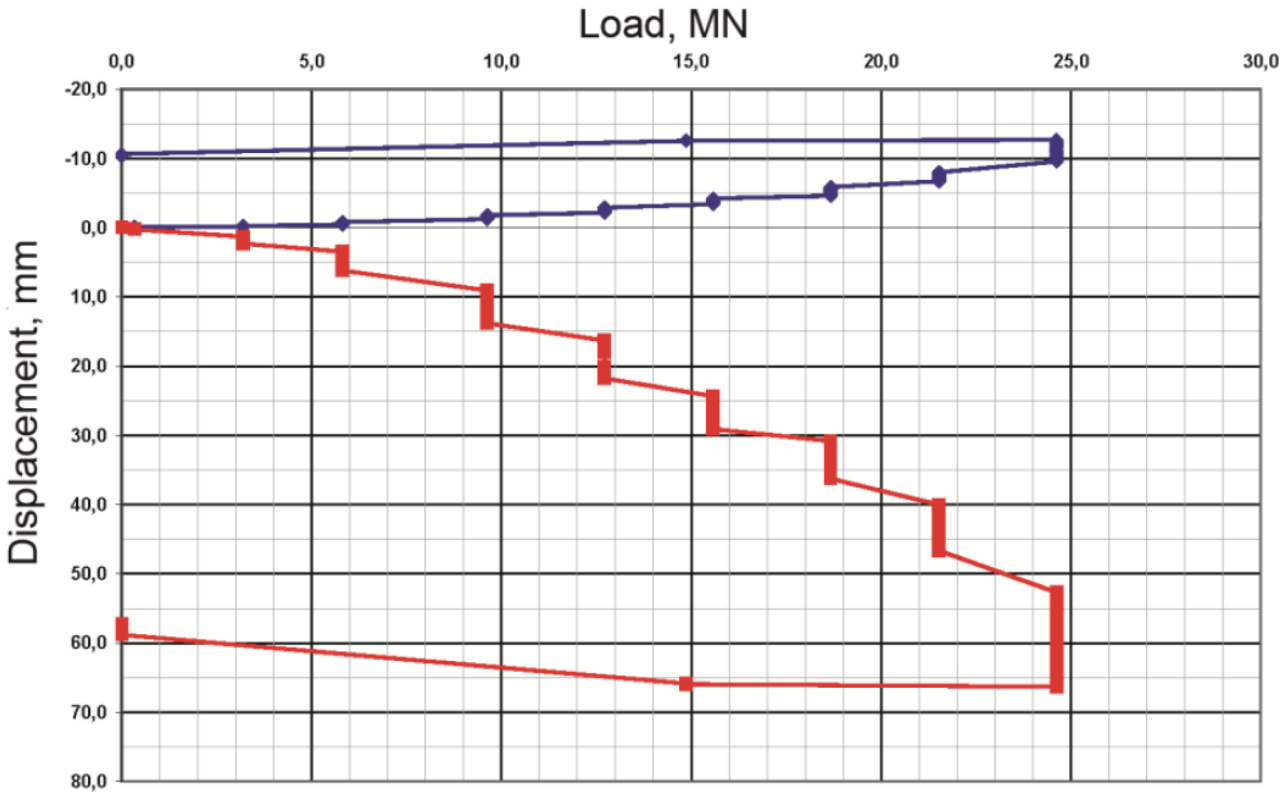


Figure 5. Displacement diagram for pile under vertical loading by O-cell method.

As expected, the total bearing capacity of the barrette pile under repeated loading by the "O-cell" method is higher than under primary loading by the "Top-down" method (more than 30%).

Table 3 summarizes the test results by the method of "O-cell" and analytical calculations of bearing capacity of the barrette piles.

Table 3. Summary of test results by the method of "O-cell" and analytical calculations of bearing capacity of the barrette piles.

Method of bearing capacity determining for barrette pile	*Total of bearing capacity of the experimental barrette pile F_d, κH*
Calculation by the formula (1), $F_{d,calc}$	31244 (-2,5%)
Calculation by PLAXIS 3D, $F_{d,PLAXIS}$	27800 (-15%)
Natural tests' result by *Top-Down method* (primary loading), $F_{d,Top\text{-}Down}$	32000
Natural tests' result «O-cell» *method* (secondary loading),	
$F_{d\ ,o\text{-}cell}$	42500
$F_d{}^{f}{}_{,o\text{-}cell}$	29500
$F_d{}^{R}{}_{,o\text{-}cell}$	13000

5. CONCLUSIONS

1. The bearing capacity of the experimental piles with a diameter of 1.2 m and a length of 52.8 m according to the test results is significantly higher (more than 200%) than the calculated values according to Russian standards [2,3] and the PLAXIS 3D program.
2. The bearing capacity of the experimental pile-barrette with a length of 65 m and a cross section of 3.3 × 1.0 m according to the results of full-scale tests is very close to the calculated values according to Russian standards [1,2] (deviation of 2,5%) and the program PLAXIS 3D (deviation of 15%).
3. The bearing capacity of the soil on the tip (13000 kN) equals half value of one's on the lateral surface (29000 kN), despite the presence of a large thickness of weak soils along the trunk of the barrette pile.

REFERENCES

1. **Mangushev R.A., Gotman A.L., Znamenskiy V.V., Ponomarev A.B. Svai i** Svaynyye Fundamenty. Konstruktsii, Proyektirovaniye i Tekhnologii [Piles and pile Foundations. Constructions, Design and Technology]. Moscow, ASV Publishing House, 2015, 320 pages (in Russian).
2. Building Code of the Russian Federation SNiP 24.13330.2011. Svod Pravil. Svaynyye fundamenty. Aktualizirovannaya Redaktsiya SNiP 2.02.03-85 [Pile Foundations. Updated Version of SNiP 2.02.03-85] (in Russian).
3. Building Code of the Russian Federation SP 50-102-2003. Proyektirovaniye i ustroystvo svaynykh fundamentov [Design and Installation of Pile Foundations] (in Russian).
4. Standard of the Russian Federation GOST 5686-2012. Grunty. Metody polevykh ispytaniy svayami [Soils. Field Test Methods by Piles] (in Russian).
5. **Kolodiy Ye.V.** Sravnitel'nyy analiz sovremennykh metodov otsenki nesushchey sposobnosti svay (na primere svai-baretty v inzhenerno-geologicheskikh usloviyakh Sankt-Peterburga) [Comparative analysis of modern methods for assessing the carrying capacity of piles (using the example of a pile-barette in the engineering-geological conditions of St. Petersburg)]. // Sb. trudov nauchn.-tekhn. konferentsii «Aktual'nyye voprosy geotekhniki pri reshenii slozhnykh zadach novogo stroitel'stva i rekonstruktsii» [Proc. of scientific and technical conf. Actual issues of geotechnics in solving complex problems of new construction and reconstruction"], SPbGASU, Saint Petersburg, 2010. Pp. 87-95 (in Russian).

СПИСОК ЛИТЕРАТУРЫ

1. **Мангушев Р.А., Готман А.Л., Знаменский В.В., Пономарев А.Б.** Сваи и свайные фундаменты. Конструкции, проектирование и технологии. – М.: АСВ, 2015. –320 с.
2. СНиП 24.13330.2011. Свод правил. Свайные фундаменты. Актуализированная редакция СНиП 2.02.03-85. Утв. Приказом Минрегиона РФ от 29.12.2011. № 635/2.
3. 3. СП 50-102-2003. Проектирование и устройство свайных фундаментов. – М.: Стройиздат, 2004. 81 с.
4. ГОСТ 5686-2012. Грунты. Методы полевых испытаний сваями. – М., 2013.
5. **Колодий Е.В.** Сравнительный анализ современных методов оценки несущей способности свай (на примере сваи-баретты в инженерно-геологических условиях Санкт-Петербурга). // Сборник трудов научно-технической конференции «Актуальные вопросы геотехники при решении сложных задач нового строительства и реконструкции». – СПб.: СПбГАСУ, 2010, с. 87-95.

Mangushev Rashid Abdullovich, Corresponding Member of the Russian Academy of Architecture and Construction Sciences, Professor, Doctor of Technical Sciences; Head of Geotechnical Department, Saint-Petersburg State Architecture and Construction University, Director of Scientific and Consulting Centre of Geotechnologies, Russia, Saint-Petersburg, 2-ya Krasnoarmeyskaya 4;
E-mail: ramangushev@yandex.ru.

Nadezda Sergeevna. Nikitina, PhD, Professor, Department of “Soil Mechanics and Geotechnical”, National Research Moscow State University of Civil Engineering (National Research Univer-sity), 26, Yaroslavskoe Shosse, Moscow, 129337, Russia; phone/fax: +7(495) 287-49-14;
E-mail: nsnikitina@mail.ru.

Мангушев Рашид Абдуллович, член-корреспондент РААСН, профессор, доктор технических наук; заведующий кафедрой геотехники Санкт-Петербургского государственного архитектурно-строительного университета (СПбГАСУ), директор научно производственного консалтингового центра геотехнологий СПбГАСУ. Рос-сия, Санкт-Петербург, 2-я Красноармейская 4;
E-mail: ramangushev@yandex.ru.

Никитина Надежда Сергеевна, профессор кафедры «Механики грунтов и геотехники», Национальный исследовательский Московский государственный строительный университет, г. Москва, Россия, 129337, Ярославское шоссе, д.26,тел./факс: +7(495) 287-49-14;
E-mail: nsnikitina@mail.ru.

RESTABILIZATION OF THE POSTCRITICAL EQUILIBRIUM OF ELASTIC SYSTEMS

Gaik A. Manuylov, Sergey B. Kosytsyn, Maxim M. Begichev
Russian University of Transport (MIIT), Moscow, RUSSIA

Abstract: The application of the Appel-Vozlinsky theorem on the stability or instability conditions for bifurcation points of conservative elastic systems with a symmetric bifurcation diagram to evaluate restabilization possibility of structures under loads substantially larger than the first critical force. It is shown that restabilization is possible if the first eigenvalue of the Hesse matrix is a continuous alternating function of the load parameter, and the remaining eigenvalues are sign-definite quantities. The examples of the systems with restabilization are given: a high Mises girder and an elastic system composed of compressible rods.

Keywords: equilibrium, restabilization, bifurcation point, stability

О ВОЗМОЖНОСТИ РЕСТАБИЛИЗАЦИИ ЗАКРИТИЧЕСКОГО РАВНОВЕСИЯ НЕКОТОРЫХ УПРУГИХ СИСТЕМ

Г.А. Мануйлов, С.Б. Косицын, М.М. Бегичев
Российский университет транспорта (МИИТ), г. Москва, РОССИЯ

Аннотация: Рассматриваются особенности применения теоремы Аппеля-Возлинского об условиях устойчивости или неустойчивости точек бифуркации консервативных упругих систем с симметричной бифуркационной диаграммой, к вопросам возможной рестабилизации при нагрузках, существенно больших первой критической. Показано, что рестабилизация возможна, если первое собственное значение матрицы Гессе есть непрерывная знакопеременная функция от параметра нагрузки, а остальные собственные значения – знакопостоянные величины. Приведены примеры систем с рестабилизацией: высокая ферма Мизеса и упруго сочлененная система, составленная из сжимаемых стержней.

Ключевые слова: равновесие, рестабилизация, точка бифуркации, устойчивость

1. SYMMETRIC SYSTEMS, SYMMETRIC DIAGRAMS OF BIFURCATION AND APPEL – VOZLINSKY THEOREM

Appel-Vozlinsky theorem formulates stability (or instability) conditions of bifurcation points for so-called “entirely symmetric systems”. Such systems include all elastic systems with symmetric bifurcation diagram as it is shown in Figure 1. Usually, these systems have two plane (two directions) of symmetry (rods, plates, flat and spatial frames or trusses, symmetric arches, some symmetric shells and another structures). Let us note two important moments:

1) Changing of the stability character of the basic equilibrium always is caused by reaching of the first bifurcation point (at $P_{kp\ min}=P_{bif1}$), and it not always occurs at reaching of high bifurcation points.
2) Stability character of “new” equilibrium forms, branching out from the basic equilibrium in the bifurcation point, is determined by stability or instability of this bifurcation point in accordance with V.T. Stability character of “new” equilibriums branching out from the basic one in the bifurcation point is determined by stability or instability of this bifurcation point (W. T. Koiter [1]).

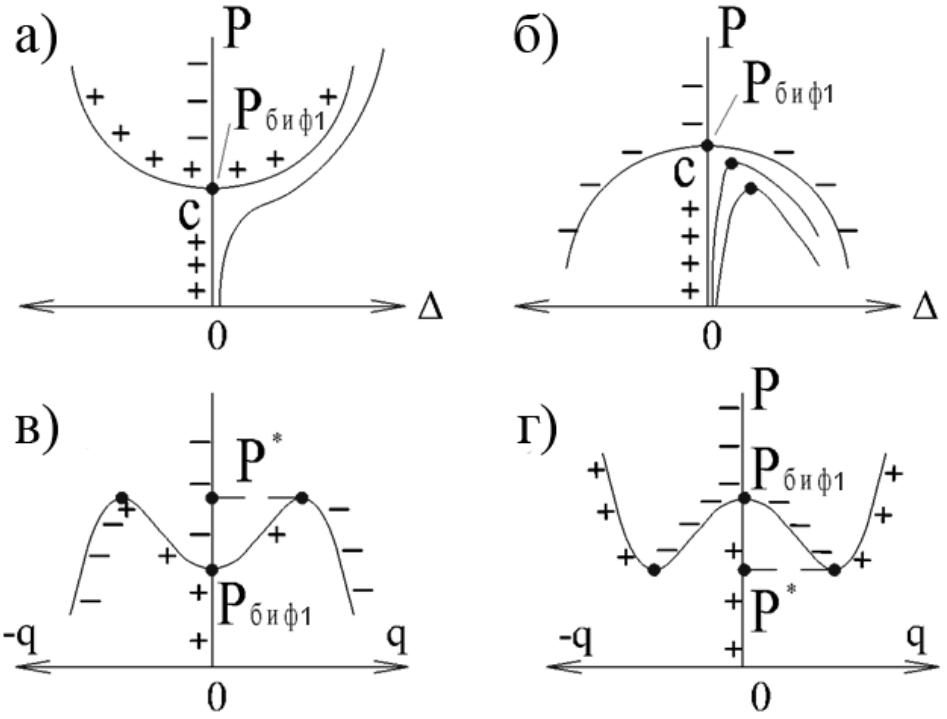


Figure 1. Bifurcation diagrams for scenarios "fold" and "butterfly": a, c) standard "butterfly" and "fold"; b, d) dual "butterfly" and "fold"; P is critical load in the ultimate point.*

Further, let us note that symmetric bifurcation point appears if decomposition of full potential energy to power series by bifurcation coordinate corresponds to features of the failure type "fold":

$$V \approx q^4 + \varepsilon_2 q^2 + \varepsilon_1 q,$$

or standard "butterfly" type [2]:

$$V \approx q^6 + \varepsilon_4 q^4 + \varepsilon_3 q^3 + \varepsilon_2 q^2 + \varepsilon_1 q.$$

The stability of the "first" bifurcation points at load $P = P_{биф1}$ is determined by positive branches of these features ($+q^4$ and $+q^6$). Negative signs of branches ($-q^4$ and $-q^6$) give instability symmetric diagrams. Types of symmetric diagrams which presented in figures 1 (a) and 1(b) corresponds to features of "fold" as well as feature of "butterfly" at some combination of managing parameters ($\varepsilon_1 - \varepsilon_4$). Here the distinctive feature is existing of only two "new" postbifurcation half-branches of equilibrium states. However, in the case of "butterfly" feature it is possible such combination of parameters, when near bifurcation point an elastic system have not two, but four "new" equilibrium states at some range of load P values as it is shown in figures 1 (c) and 1 (d). In accordance with diagrams in figure 1 the system has 4 "new" states of postcritical equilibrium at the range of loads P_{bif} - P^*(that is until ultimate points will be reached). There are only two ($P < P_{bif1}$, figure 1 c, and $P > P_{bif1}$, figure 1 d) or none post critical equilibriums (figure 1 c at $P > P^*$, and figure 1 d at $P < P^*$) beyond the boundary of these "new" postcritical equilibriums' ranges.

Appel-Vozlinsky theorem [3-5] allows us to predict a character of the closest bifurcation point: stability of symmetric bifurcation point is determined by stability single equilibrium half-branch closing to it (from the side of load values, that smaller ($P < P_{bif}$) or larger ($P > P_{bif}$) than bifurcation load.

Presented in figures 1 (a) and 1 (c) single half-branch, closing to bifurcation point, is sustainable branch of OC. Hence, the first bifurcation point at load P_{bif1} is sustainable. Also growing

"new" branches of postbifurcation equilibriums are sustainable.

On the contrary, single half-branches of systems with bifurcation diagrams by types presented in figures 1 b and 1 d are unsustainable the basic postbifurcation equilibriums (at $P > P_{bif1}$). Consequently, bifurcation point is unsustainable as well as new branching out equilibriums "falling" by load. Unsustainable equilibrium branches are signed as "-".

Let us note, that bifurcation diagrams P = P(q) are intersection line for surfaces of equilibriums near bifurcation curvature $(dV/dq = 0)$ and plane POq (at null value of initial imperfection parameter $\xi_1(\xi_1 = 0)$). Possible variants of symmetric sustainable diagrams, that have simple bifurcation points for systems with co-dimension less or equal 4 (number of managing parameters), are bounded by diagrams as it is shown in figures 1 (a) – 1 (d). However, Appel-Vozlinsky theorem also is acceptable to symmetric system with large (even) number of managing parameters.

Let us note for system with two or in some cases 4 managing parameters, that sufficient condition of simple symmetric bifurcation point stability (figures 1 a, 1 c) is singularity and stability of under critical equilibrium.

Necessary stability condition is geometric symmetry of system and symmetry of acting loads. However, this condition is not sufficient.

The sufficient instability condition for simple symmetric bifurcation point is singularity and instability of initial (basic) postbifurcation equilibriums' half-branch (figure1 b).

It should be noted, that V.I. Vozlinsky formulated and proved theorem of stability (instability) of symmetric bifurcation point in 1967 [3]. However, formulation of the same theorem can be found in the paper of P. Appel [5], the original of which appeared in 1932. There it was written "… Stability character in the curvature with vertical tangential is the same if it would be in half-branch of "intersecting" curvature that is not bounded by branches of the first ones (that is singular).

2. ENERGY MEANING OF BIFURCATION POINTS AND CHANGING STABILITY CHARACTER OF THE BASIC EQUILIBRIUM STATE

In accordance with energy position the bifurcation point of the basic equilibrium appears then and only then, when there is orthogonal in energy aspect non-null addition component D. Reaching of bifurcation point by load (or kinematic compression) proves that basic subcritical stress-strain state exhausts possibilities to accumulate growing energy of an elastic deformation, caused by load rising, in the form, specified by initial (sub bifurcation) stress-strain state.

System self-organizes to have possibility to continue loading. It switches on additional accumulators to absorb new portions of potential energy of elastic deformation. Such additional forms are "new" equilibrium forms, that do not exist at subcritical equilibrium but exist in non-null addition D, that have spoken before. If such addition is null (D = 0), then bifurcation loss of stability becomes impossible. This aspect is determined by form of the first null Eigen vector W_1^0, calculated for subcritical equilibrium ($P = P_{cr} - 0$). If this vector is orthogonal to external load vector [5]

$$\vec{W}_1^{\,0} \perp \vec{P} \Rightarrow \left(\vec{P} \cdot \vec{W}_1^{\,0}\right) = 0,$$

then critical point is bifurcation point, the initial stress-strain state of which is filled by new components [6]. It principally allows to continue loading of the system.

If reduced scalar product is not equal to zero, then loss of stability occurs at ultimate point. For this point, the "null" eigen vector $(\vec{W}_1^{\,0})$ of subcritical equilibrium usually is similar to form of such equilibrium [7]. Therefore, there is not any postcritical addition of subcritical equilibrium at reaching ultimate point. Critical equilibrium is unsustainable and system searching for a new sustainable equilibrium transforms to dynamic splash state.

However, at bifurcation case or reaching of ultimate point a “new” initial postcritical equilibrium $W_{i/postcr}$ is a sum of subcritical equilibrium W_{subcr} and “null” eigen vector, taken with scale factor ξ:

$$W_{н/пкр} = W_{предкр} + \xi W_1^0$$

3. CHANGING OF STABILITY FORM AT BIFURCATION POINT AND RESTABILIZATION OF THE BASIC EQUILIBRIUM

It is believed that at the reaching of the bifurcation point there is always a change in the quality of the equilibrium: the sustainable equilibrium existing before bifurcation point reached becomes unsustainable after the bifurcation point exceeds this value (at load $P = P_{bif} + \xi$). In general, this is always true only for the first bifurcation point (or for the first point on the "new" postcritical equilibrium branch of the secondary bifurcation). There are many systems for which, when passing by the basic equilibrium of the second, third, ..., m-th bifurcation point (m=2,3, ... m, ...), the instability property acquired by this equilibrium as a result of the first bifurcation point does not change after passing the higher bifurcation points. In other words, the stability of the basic equilibrium under load above the first bifurcation is not restored. An example of a such situation is an ordinary Eulerian rod (Figure 2), for which the "new" compressed-curved forms of equilibrium branching out in the second, third and subsequent points of bifurcation-increasing by load and unsustainable equilibrium. After loss of stability at passing of the first bifurcation point, further the basic linear equilibrium remains unsustainable (Fig. 2) at all load values, exceeding the first critical one ($P > P_{bif1}$). In the figure 2, unsustainable branches of postcritical equilibrium are marked with crosses; sustainable forms are shown by solid lines.

Sustainable postbifurcation equilibrium is compressed-curved equilibrium (at $P > Pcr1$) branching out at the first point of bifurcation. At "higher" "curved" forms of "new" equilibriums that branch out from the main linear equilibrium at

$$P_{кр2} = 2\pi^2 EI / l^2,$$
$$P_{кр3} = 3\pi^2 EI / l^2, \ldots$$
$$P_{кр m} = m\pi^2 EI / l^2,$$

all of these equilibriums may really exist and can be observed, if we input additional cross hinge supports at nodes (or equivalent points of bend). Then the higher critical load $P_{кр2}$, $P_{кр3}$,…, P_{crm}, acquire a certain "optimization" meaning. For example, the second critical load of P_{cr2} is the highest critical load for a double-hinged rod with one intermediate support.

If this support is placed in the middle point of the rod, it divides rod into two identical and equal-sustainable parts, each of which does not affect the stability margin of the neighbor one. Equal-stability property gives

$$\max P_{кр} = 4\pi^2 EI / l^2.$$

Strict energy proof of the instability of all "higher" buckling forms of the compressed Eulerian rod was given by E. Reyes [6]. He showed that at the same norms (the same values for all forms of the sinusoid amplitudes) the values of the full potential energy for the first form V_1 and the higher forms of buckling V_2, ..., V_n form a steadily increasing sequence.

$$V_1 < V_2 < V_3 < \ldots < V_m < \ldots$$

All members of this sequence are greater than the value of the first member V_1 corresponding to the potential energy of the stable first form of the post-bifurcation equilibrium. Therefore, if you compress the Euler rod by load, exceeding the third critical load (for system with additional hinge supports), and further remove the supports, the compressed-curved s-form will instantly become unsustainable and "switch" on the first sustainable post-critical form of Euler elastics, corresponding to value of acting load.

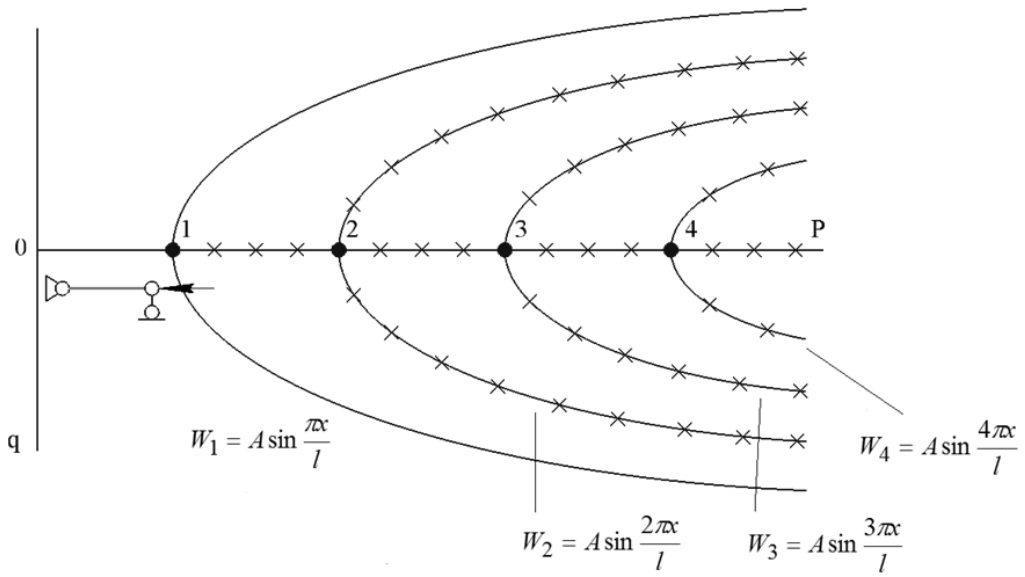


Figure 2. Sustainable (first) and unsustainable (all following) branches of the "new" compressed-curved equilibriums that bifurcate from the basic linear equilibrium of a Eulerian rod in the first and higher bifurcation points.

In accordance with the above, it should be note that the "new" higher forms of post-bifurcation equilibrium growing by load are not always forms of sustainable equilibrium. The equilibrium curve should grow by load to achieve condition when it consists of points corresponding to sustainable equilibrium. But this requirement is only a necessary but not sufficient sign of the stability of the mentioned above equilibriums. An additional requirement is that the load-increasing equilibriums have a minimum potential energy. Just considered the highest forms of post-critical equilibrium of Euler rod are a good "reverse" illustrations to this provisions. At the same time, the "falling " (descending) branches of equilibrium are always unsustainable.

Theorem 1. For systems with a symmetric bifurcation diagram, it is possible to restabilize the basic equilibrium after passing an even number of the bifurcation point (2nd, 4th, etc.) if:

a) at each point of bifurcation the basic equilibrium changes the nature of stability;

b) "new" equilibriums branching out from this point of bifurcation (m=2,3,4...) are rising and unsustainable (Fig. 3).

Without reducing the generality of reasoning, let us consider a symmetric system with two degrees of freedom, which has a bifurcation diagram, as it is shown in Figure 3, and the basic equilibrium loses its stability when P > Рбиф1 and it becomes unsustainable in the interval of loads $P_{bif1} < P \le P_{bif2}$. These equilibriums under loads $P < P_{bif2}$ form a single half-branch suitable to the second bifurcation point from the left. Therefore, according to theorem Appel-Vozlisky, the second bifurcation point "is not sustainable"; the branching out at this point the "new" equilibriums, increasing by the load, also are unsustainable. According to the condition, the change in the nature of the stability of the basic equilibrium after passing the second bifurcation point, this equilibrium should become sustainable at $P > P_{bif2}$. This theorem has been proved.

Note that the nature of stability of "new" equilibriums branching out at the first bifurcation point (at $P = P_{bif1}$) does not affect the conditions of this theorem. But if we assume that the "new" equilibriums branching out at the second bifurcation point (at $P = P_{bif2}$) form unsustainable "falling" branches (Fig. 3), then the basic equilibrium under load $P > P_{bif2}$ should also be unsustainable. But this provision contradicts the condition of changing the nature of the stability of the basic equilibrium in the bifurcation points. Therefore, there is not restabilization in this case.

For conservative systems, the possibility of restabilization of the basic equilibrium is determined by the behavior of the eigenvalues μ1(P), μ2(P),..., μn(P) of the Hesse matrix of the total potential energy as a function of the parameter P. If the numbers are monotonically decreasing functions of P

$$(\frac{d\mu_1}{dp}<0,\frac{d\mu_2}{dp}<0,...,\frac{d\mu_n}{dp}<0)$$

and each function passes through zero (from positive values to negative) to its point of bifurcation, then restabilization of the basic (initial) equilibrium at loads greater than the first critical ($P>P_{cr1}=P_{bif1}$) is impossible (example - elastic frame system).

If the degeneration of the Hessian matrix at the bifurcation points is associated with zero padding only one function μ1 (P) (in this case it must be alternating), and all other numbers are positive functions (Fig. 4), then the basic equilibrium can be restabilized in the intervals loads of $P_{bif2} \le P \le P_{bif3}$, $P_{bif4} < P < P_{bif5}$ and so on.

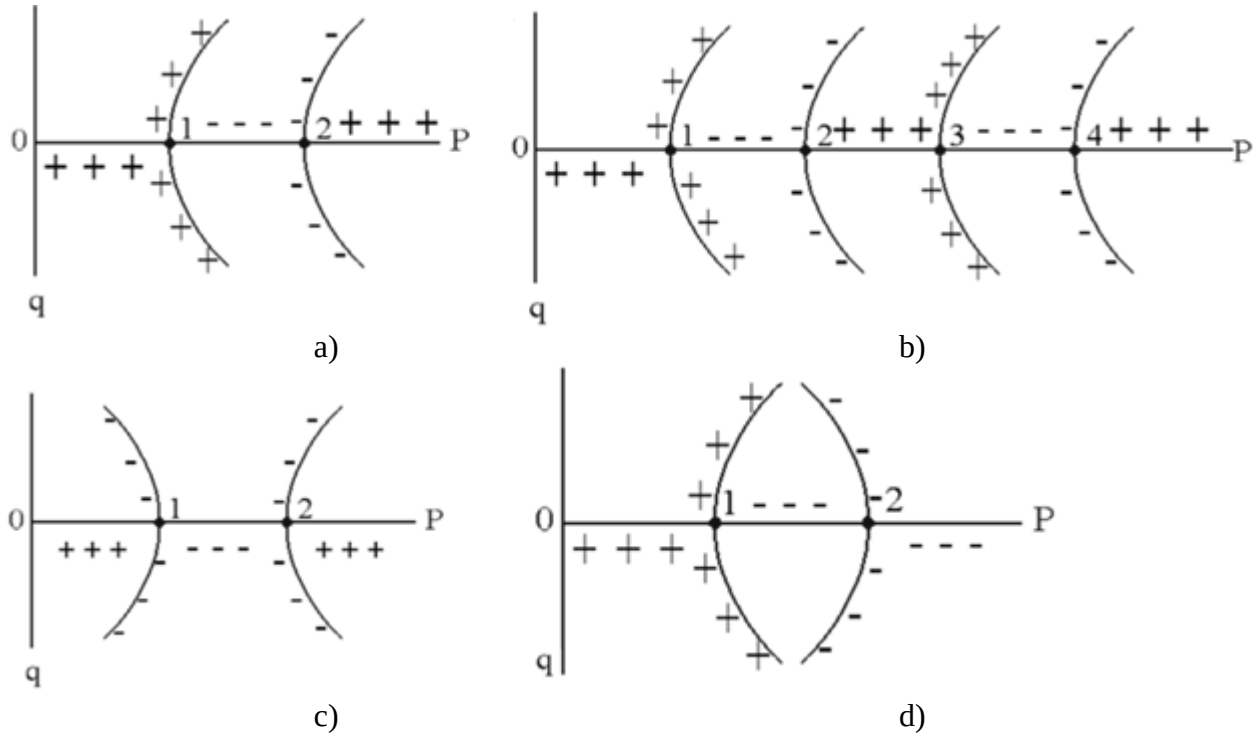


Figure 3. An illustration of Theorem 1 on the conditions for re-stabilization.

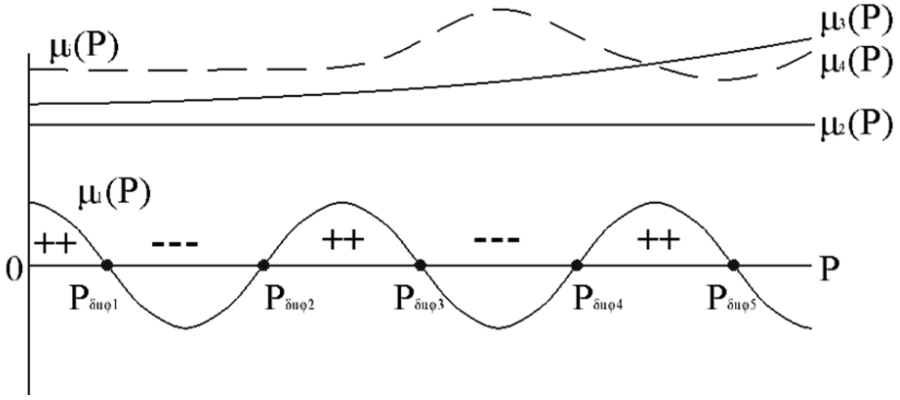


Figure 4. The graph of changes in the eigenvalues of the matrix NE: - μ1 (P) periodic function.

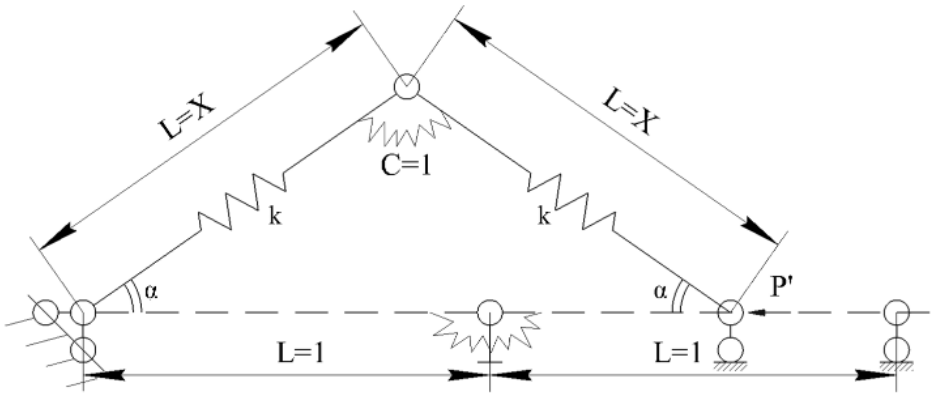


Figure 5. To the problem of the stability of straight-linear equilibrium of a system of 2 compressible rods connected by an elastically-flexible hinge.

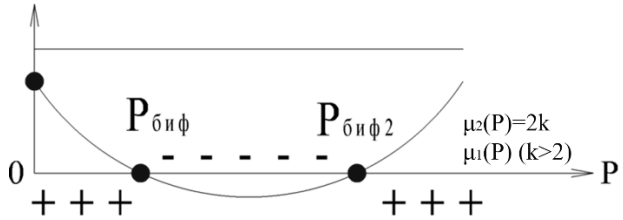


Figure 6. Curves of the trajectories of eigenvalues μ1 (P) and μ2 (P) and the stability region of the rectilinear equilibrium of the system in Fig. 10.

4. SAMPLES OF SYSTEMS WITH RESTABILIZATION

Let us consider a system with the re-stabilization of the main equilibrium under loads P> Pbif2 (Fig. 5). It consists of two compressible rods connected by an elastic-flexible hinge with a spring of rigidity c = 1. The initial lengths of the compressible rods are L = 1, the relative longitudinal rigidity is K, the initial unbuckled equilibrium is rectilinear and horizontal. The stability of one such compressible rod with an "elastic" hinge was studied in detail by V.I. Theodosiev [8]. He constructed characteristic graphs of post-critical equilibrium curves for the state of the observing rod and investigated it stability at various combinations of stiffness and geometric parameters. T. Poston and I. Stewart [2] investigated this system heuristically to demonstrate some properties of the butterfly failure. The system was considered in more detail by M. Golubitsky and D. Schaeffer [9]. However, in their work, the curves of the post-critical ("broken") equilibriums near the point of the secondary bifurcation were constructed inaccurately.

Our interest in this system is determined by the desire to show the non-monotonic behavior of the eigenvalue μ1 (P) of the Hesse matrix, which allows us to obtain a re-stabilization of the rectilinear equilibrium under loads of large loads of the second bifurcation (P> $P_{bif\,2}$, as it is shown Figure 6).

Let α is the angle of deflection of the rods from the horizontal, X is the value of the current length of the compressible rod, P is the compressive load,

$$X = \left(P \diagup k\right)\cos\alpha\,.$$

Potential energy of the system:

$$V(k,P,\alpha,X) = k(X-1)^2 + \frac{1}{2}\alpha^2 + 2PX\cos\alpha$$

Equilibrium equations:

$$\frac{\partial V}{\partial \alpha} = \alpha - 2PX\sin\alpha = 0$$
$$\frac{\partial V}{\partial X} = 2(\alpha - 1)k - 2P\cos\alpha = 0$$

Hesse matrix (or the Jacobi matrix of the system of equilibrium equations):

$$H_V = \begin{vmatrix} \frac{\partial^2 X}{\partial \alpha^2} & \frac{\partial^2 V}{\partial \alpha \partial X} \\ \frac{\partial^2 V}{\partial X \partial \alpha} & \frac{\partial^2 V}{\partial X^2} \end{vmatrix} = \begin{bmatrix} 1 - 2PX\cos x & -2P\sin\alpha \\ -2P\sin\alpha & 2k \end{bmatrix}$$

For the initial rectilinear equilibrium (α = 0), this matrix takes the diagonal form:

$$H(x=0) = \begin{vmatrix} 1-2PX & 0 \\ 0 & 2k \end{vmatrix}$$

Consequently, the eigenvalues of this matrix (or stability coefficients) are

$$\mu_1(P) = 1 - 2PX = 1 - 2P(1 - \frac{P}{k}) = 1 - 2P + 2\frac{P^2}{k};$$
$$\mu_2(P) = 2k = const$$

From these expressions it follows that only one eigenvalue μ1 (P) depends on the load; the second eigenvalue μ2 (P) = 2k does not depend on the load and is a constant number. The conditions for the equality to zero of the first eigenvalue μ1 (P) = 0 determine the bifurcation points of the basic (initial) rectilinear equilibrium of the system:

$$\mu_1(P) = 0 \to P_{биф1,2} = \frac{1}{2}(k \pm \sqrt{k^2 - 2k})$$

The basic equilibrium is sustainable at loads lower than the first critical one, as well as at loads greater than the second critical one:

$$P < P_{биф1} = \frac{1}{2}(k - \sqrt{k^2 - 2k}),$$
$$P > P_{биф2} = \frac{1}{2}(k + \sqrt{k^2 - 2k})$$

(state of re-stabilization).

A square parabola describing the dependence of μ1 (P) can have either two real roots (ie, two bifurcation points) or none.

The last case occurs when k < 2. When k = 2, the two points of the bifurcation merge into one ($P_{bif\ (2)}$ = 1). Graphs of the functions μ1 (P) and μ2 (P) are shown in fig. 6.

Curves of "broken" equilibriums (initial sections) for some characteristic values of the compressibility parameter K are given in Fig. 7.

The study of the bifurcation points of the basic equilibrium shows that

$$k > 2\frac{2}{3}$$

at symmetric points of the bifurcation, two curves of “broken” equilibriums, that grow by load, branch out (Fig. 7a). However, only one branch is stable, branching out at P = P_{Bif1}. The equilibriums that are branched out at the second point of the bifurcation P_{bif2}, although growing, but are unsustainable. If

$$k = 2\frac{2}{3},$$

then on the curve of the primary “broken” equilibriums at the point of the first bifurcation, the curvature becomes zero, and further at

$$k < 2\frac{2}{3}$$

it becames negative. This means that at

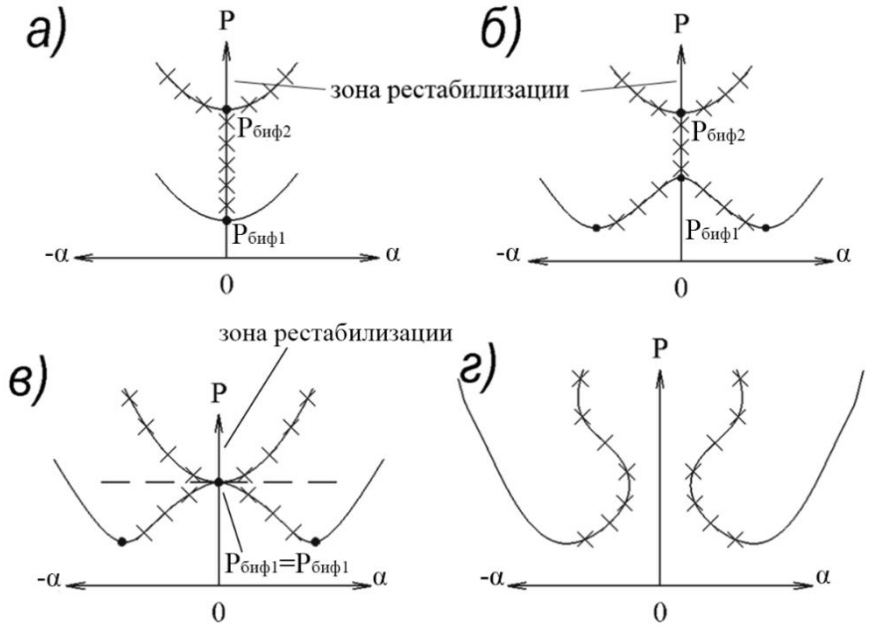


Figure 7. Sustainable state curves and areas of it stability for a two-rod system with various combinations of its stiffness and geometrical parameters:

a) $k > 2\frac{2}{3}$ *; b)* $2 < k < 2\frac{2}{3}$ *; c)* $k=2$*; г)* $k<2$.

$$k < 2\frac{2}{3}$$

the number of equilibriums of the system at P * <P <P_{bif} there is five equilibrium points (initial and four "new" equilibriums) instead one (initial). In this case, the first point of the bifurcation from a sustainable one transforms to an unsustainable one. Consequently, at the initial part the post-bifurcation "broken" equilibriums are also unsustainable (up to the achievement of the lower ultimate point P * (Fig. 7b)).

At k value decreasing, the two points of the bifurcation approach to each other and at k = 2 it converges into one point $P_{bif\ 1} = P_{bif\ 2} = 1$ (Fig. 7c). When k < 2, the original rectilinear equilibrium is sustainable for all compressive loads. Any bifurcation load values disappear ("compressibility" win the aspire to loss of stability). "Broken" equilibria exist by themselves, and do not intersect with straight-line equilibria (Fig. 7c). At the same time, the branches of these equilibria that are closest to the original (α = 0) are the branches of unsustainable saddle equilibria and form a "watershed" between the sustainable basic rectilinear equilibrium and the far equilibrium (but sustainable!) in the extreme parts of the isolated branches.

Another example of a system having zones of postcritical restoration is the "high" Mises truss (Fig. 8) with an initial angle of inclination of the rods $\alpha_0 > 67°,36$ (Fig. 8, b). For the Mises truss in the paper of V.I. Slivker and A.V. Perlmuther [10] the Hesse matrix is calculated. This matrix has the following eigenvalues:

$$\mu_{биф}(P) = 2\left(1 - \frac{tg\alpha}{(1+tg^2\alpha)^{\frac{3}{2}}\cos\alpha_0}\right),$$

$$\mu^*(P) = 2\left(1 - \frac{1}{(1+tg^2\alpha)^{\frac{3}{2}}\cos\alpha_0}\right),$$

α=α(P).

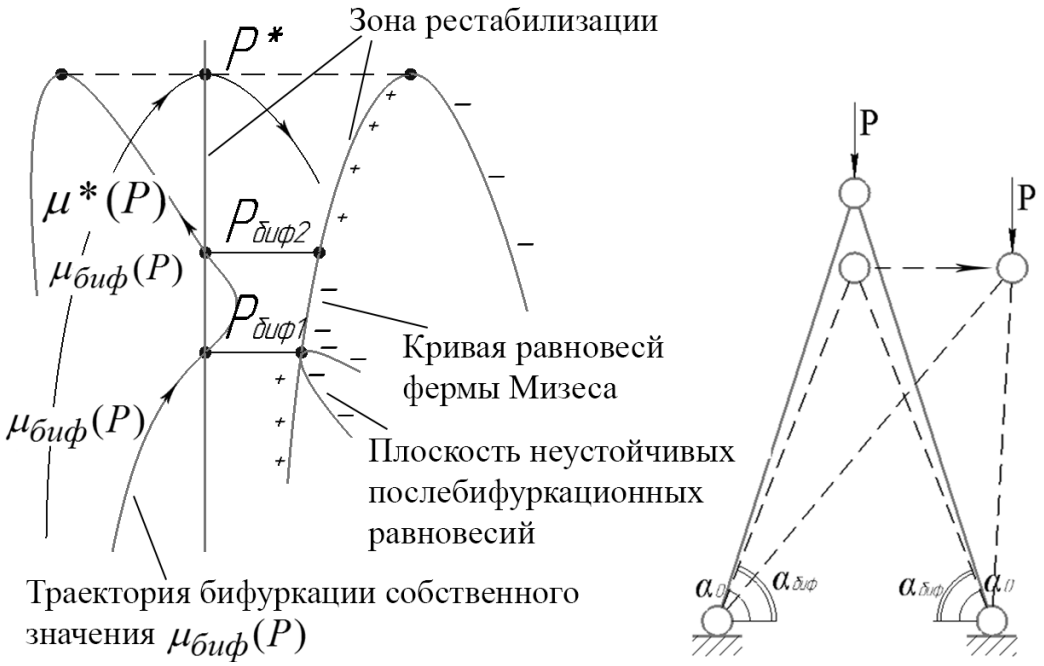


Figure 8. Equilibrium re-stabilization of the high Mises truss.

Here, the first number $\mu_{bif}(P)$ determines the stiffness of the truss node against horizontal perturbations, the second number $\mu^*(P)$ determines stiffness against vertical ones. The case, when stiffness $\mu_{bif}(P)$ becomes zero, corresponds to the moment of the bifurcation of symmetric equilibrium. The second number $\mu^*(P)$ equals to zero at the limit point. The bifurcation loss of stability of the Mises truss is possible only if the truss is sufficiently high ($\alpha_0 > 67°,36$). At this value of α_0, a double bifurcation point appears on the equilibrium curve, which then at large α_0 angles splits into two simple bifurcation points.

These points are on the ascending branch of equilibria (i.e. before reaching the limit point) if the initial tilt angle α_0 is in the range of $67°,36 < \alpha_0 < 69°,22$.

Until the load angle $\alpha > \alpha_{bif1}$, the both numbers $\mu(P) > 0$, $\mu^*(P) > 0$ and the symmetrical equilibrium of the truss is sustainable. When $\alpha = \alpha_{bif1}$, the load is $P = P_{bif1}$ and the eigenvalue $\mu_{bif}(P)$ passes through zero from positive to negative values. Symmetrical form equilibrium becomes unsustainable. However, when $\alpha = \alpha_{bif2}$ and, accordingly, the second critical load $P = P_{bif}$, the eigenvalue $\mu_{bif}(P)$ again passes through zero (from negative values to positive values). Since, in this case, the second eigenvalue $\mu^*(P)$ does not change its sign and remains positive, (until to reaching the ultimate point), then at loads $P > P_{bif2}$, the both eigenvalues $\mu_{bif}(P)$ and $\mu^*(P)$ are positive, the Hesse matrix is positively defined, and the Mises truss is again sustainable (at loads of $P_{bif\ 2} < P < P^*$) (as it is shown in Fig. 8). So, for a truss with an initial angle $\alpha_0 = 68°$, 5 critical values of the tilt angles of the rods are $\alpha_{bif1} = 61°,903$, $\alpha_{bif2} = 47°.347$. These values are determined by solving the equation $\cos^3\alpha - \cos\alpha + \cos\alpha_0 = 0$. The corresponding bifurcation loads are calculated by the formula

$$P_{bif} = 2cl\,(\sin\alpha_{bif} - \cos\alpha_0 \cdot \mathrm{tg}\alpha_{bif}),\ c = EA / l.$$

For the critical load at the ultimate point is $P^* = 2cl \cdot \sin^3\alpha^*$, where the tilt angle α^* is determined from the relation $\cos^3\alpha^* = \cos\alpha_0$. At $\alpha_0 = 68°,5$ this angle is $\alpha^* = 44°,305$.

The eigenvalue of the Hesse matrix is μ_{bif} at $\alpha = 47° > \alpha_{bif1}$ ($\mu_{bif}(47°) = 0.1437$; at $\alpha = 55°$ ($\alpha_{bif} = 47°,347 < \alpha = 55° < \alpha_{bif1} = 61°,9$) eigenvalue is negative ($\mu_{bif}(55°) = -1.886$); at $\alpha = 47°$ ($\alpha^* = 44°,305 < 47° < \alpha_{bif2} = 47°.347$) it is again positive. The re-stabilization interval is determined by the tilt angles $44°,305 < \alpha < 47°.347$, since in this range $\mu_{bif}(P) > 0$ and $\mu^*(P) > 0$. The ap-

pearance of the re-stabilization zone and the non-monotonous nature of the dependence of the eigenvalue μ_{bif} under the load P is unexpected [10, p. 377]. In our opinion, the non-monotonicity of the function μ_{bif} (P) is explained by the fact that there are three points of critical equilibriums for trusses with initial angles α_0 (67°.36 < 0 <69°.22) on the ascending branch of symmetric equilibriums: two points of bifurcation and one ultimate point. Meanwhile, the Hesse matrix takes a second order, and, therefore, there are only two continuous by load P functions of eigenvalues μ_{bif} (P) and μ^*(P). The function μ^*(P) within the ascending branch is positive and zero padding at the ultimate point (at P = P *). For existing of two bifurcation points at loads 0 < P <P*, the continuous function μ_{bif} (P) must two times "go over" through zero values: the first time from plus to minus, and the second time from minus to plus. Therefore, it cannot be monotonous, as discussed in paragraph 3. And it explains the existence of a re-stabilization zone for such forms.

REFERENCES

1. **Koiter W.T.** Elastic Stability and Post-Buckling Behavior. // Proc. Symp. Nonlinear Problems. Madison University Press, 1963, 257 pages.
2. **Poston T., Stuart I.** Teoriya Katastrof i Yeye Prilozheniya [Catastrophe Theory and its Applications]. Moscow, Mir, 1980, 366 pages (in Russian).
3. **Vozlinskiy V.I.** Ob Ustoychivosti Tochek Vetvleniya Ravnovesiy [On the Stability of the Branch Points of Equilibria] // *PMM*, 1978, Vol. 42, pp. 259-267 (in Russian).
4. **Vozlinskiy V.I.** O Chislennoy Otsenke Oblasti Ustoychivosti. Voprosy Ustoychivosti Tochek Vetvleniya Ravnovesiy [On the Numerical Estimate of the Stability Domain. Questions of Stability of Branch Points of Equilibria]. // Teoriya ustoychivosti i yeye prilozheniya. Novosibirsk, Nauka, 1978, pp. 94-100 (in Russian).
5. **Appel P.** Figury Ravnovesiya Vrashchayushcheysya Odnorodnoy Zhidkosti [Equilibrium Figures of a Rotating Homogeneous Fluid]. Moscow, Leningrad, ONTI, 375 pages (in Russian).
6. **Reyyes E.** Poterya Ustoychivosti Kolonny – Elementarnyy Primer Bifurkatsii [Loss of Column Stability – An Elementary Example of Bifurcation]. // Teoriya Vetvleniya i Nelineynyye Zadachi na Sobstvennyye Znacheniya. Moscow, Mir, 1974, pp. 9-18 (in Russian).
7. **Manuylov G.A., Kositsyn S.B., Begichev M.M.** O Kriticheskikh i Posle-kriticheskikh Ravnovesiyakh v Zadachakh Ustoychivosti Uprugikh Sistem. // *Stroitel'naya Mekhanika Inzhenernykh Konstruktsiy i Sooruzheniy*, 2015, No. 5, pp. 47-54 (in Russian).
8. **Feodosyev V.I.** Izbrannyye Zadachi i Voprosy po Soprotivleniyu Materialov [Selected Problems and Questions of the Strength of Materials]. Moscow, Nauka, 1967, 376 pages (in Russian).
9. **Golubitsky M., Schaeffer D.** A Theory for Imperfect Bifurcation via Singularity Theory // *Communications on Pure and Applied Mathematics*, Vol. XXXII, pp. 21-97.
10. **Perelmuter A.V., Slivker V.I.** Ustoychivost' Ravnovesiya Konstruktsii i Rodstvennyye Problemy. Vol. 1. Moscow, SCAD Soft, 2007, 655 pages.

СПИСОК ЛИТЕРАТУРЫ

1. **Koiter W.T.** Elastic Stability and Post-Buckling Behavior. // Proc. Symp. Nonlinear Problems. Madison University Press, 1963, 257 pages.
2. **Постон Т., Стюарт И.** Теория катастроф и ее приложения. – М.: Мир, 1980.–366 с.
3. **Возлинский В.И.** Об устойчивости точек ветвления равновесий. // ПММ, 1978, том 42, с. 259-267.

4. **Возлинский В.И.** О численной оценке области устойчивости. Вопросы устойчивости точек ветвления равновесий. // Теория устойчивости и ее приложения. Новосибирск: Наука, 1978, с. 94-100.
5. **Аппель П.** Фигуры равновесия вращающейся однородной жидкости. – М.:-Л.: ОНТИ, 1936. – 375 с.
6. **Рейес Е.** Потеря устойчивости колонны – элементарный пример бифуркации // Теория ветвления и нелинейные задачи на собственные значения. – М.: Мир, 1974, с. 9-18.
7. **Мануйлов Г.А., Косицын С.Б., Бегичев М.М.** О критических и послекритических равновесиях в задачах устойчивости упругих систем. // *Строительная механика инженерных конструкций и сооружений*, 2015, №5, с. 47-54.
8. **Феодосьев В.И.** Избранные задачи и вопросы по сопротивлению материалов. – М.: Наука, 1967. – 376 с.
9. **Golubitsky M., Schaeffer D.** A Theory for Imperfect Bifurcation via Singularity Theory // Communications on Pure and Applied Mathematics, Vol. XXXII, pp. 21-97.
10. **Перельмутер А.В., Сливкер В.И.** Устойчивость равновесия конструкции и родственные проблемы. Том 1. – М.: SCAD Soft, 655 с.

Мануйлов Гайк Александрович, кандидат технических наук, доцент, доцент кафедры «Строительная механика» Российского университета транспорта (МИИТ); 127994, г. Москва, ул. Образцова, 9, стр. 9; тел./факс +7(499) 972-49-81.

Косицын Сергей Борисович, советник РААСН, доктор технических наук, профессор, заведующий кафедрой «Теоретическая механика» Российского университета транспорта (МИИТ); 127994, г. Москва, ул. Образцова, 9, стр. 9; тел./факс +7(499) 978-16-73;
E-mail: kositsyn-s@yandex.ru, kositsyn-s@mail.ru.

Бегичев Максим Михайлович, кандидат технических наук, доцент кафедры «Теоретическая механика» Российского университета транспорта (МИИТ); 127994, г. Москва, ул. Образцова, 9, стр. 9; тел./факс +7(499) 978-16-73; E-mail: noxonius@mail.ru.

Gaik A. Manuylov, Ph.D., Associate Professor, Department of Structural Mechanics, Russian University of Transport (MIIT); 127994, Russia, Moscow, 9b9 Obrazcova Street; phone/fax +7(499)972-49-81.

Sergey B. Kosytsyn, Dr.Sc., Professor, Head of Department of Theoretical Mechanics, Russian University of Transport (MIIT); 127994, Russia, Moscow, 9b9 Obrazcova Street; phone/fax: +7(499) 978-16- 73;
E-mail: kositsyn-s@yandex.ru, kositsyn-s@mail.ru.

Maxim M. Begichev, Ph.D., Associate Professor, Department of Theoretical Mechanics, Russian University of Transport (MIIT); 127994, Russia, Moscow, 9b9 Obrazcova Street; phone/fax: +7(499) 978- 16-73;
E-mail: noxonius@mail.ru.

FIRE DESIGN OF STEEL STRUCTURES

Anatolii V. Perelmuter
SCAD Soft, Kyiv, UKRAINE

Abstract: This paper describes new software features for the fire design of steel structures. This analysis is performed according to Eurocode. An example is used to demonstrate the role of secondary effects and show that the estimation based on the critical temperature may differ significantly from the revised calculation.

Keywords: fire design, thermal properties, critical temperature, secondary effects

РАСЧЕТ ОГНЕСТОЙКОСТИ СТАЛЬНЫХ КОНСТРУКЦИЙ

А.В. Перельмутер
НПО «СКАД Софт», г. Киев, УКРАИНА

Аннотация: Приводятся сведения об особенностях программной реализации модулей расчета стальных конструкций на огнестойкость. Методика расчета следует указаниям Еврокода. На примере демонстрируется роль вторичных эффектов и показывается, что оценка по критической температуре может существенно отличаться от уточненного расчета.

Ключевые слова: огнестойкость, теплотехнические свойства, критическая температура, вторичные эффекты

1. BASIS OF FIRE DESIGN

A structure is fire resistant when the necessary safety margin can be provided for a certain period of time. It is also necessary to take into account the variation of the thermal and mechanical properties of steel under the fire heating of the structure along with the mechanical actions.

Evaluation of fire resistance includes:

- determination of structural heating – a thermal analysis performed in order to predict the temperature (select the fire type) and structural heating patterns;
- strength analysis, which takes into account the variation of physical properties of the material under the action of high temperature.

The calculation is performed for one of the four standard variants of the temperature variation during a fire (Figure 1).

Thermal analysis of steel structures is greatly simplified due to the fact that high thermal conductivity of steel and relatively small thickness of bearing structures allow us to accept the hypothesis of a uniform temperature in the cross-section, which makes it possible to use analytical relationships between temperature, thermal conductivity $\lambda(T)$, specific heat $c(T)$ of steel and external temperature T (Figure 2).

Moreover, it is assumed that the temperature of the element is constant along its length.

The strength analysis takes into account the variation of the mechanical properties of the material (Figure 3).

Since the structure was designed to take all active loads, and only dead and long-term loads are taken into account in the fire analysis, there is a certain safety margin characterized by the degree of utilization μ.

The critical temperature can be determined for any degree of utilization μ as:

$$\theta_{crit} = 39,19 \ln\left(\frac{1}{0,9674\mu^{3,833}} - 1\right) + 482 .$$

Moreover, it is important to determine the time it takes to reach this temperature, so that it could be compared with the fire resistance time.

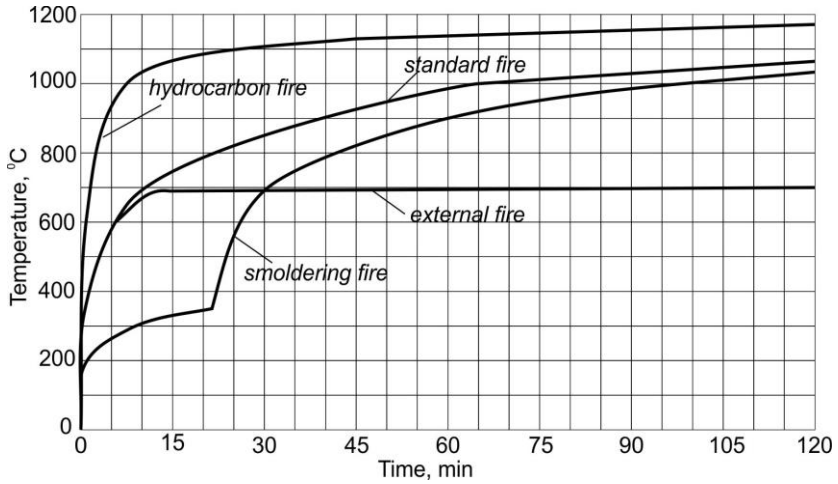


Figure 1. Temperature-time curve.

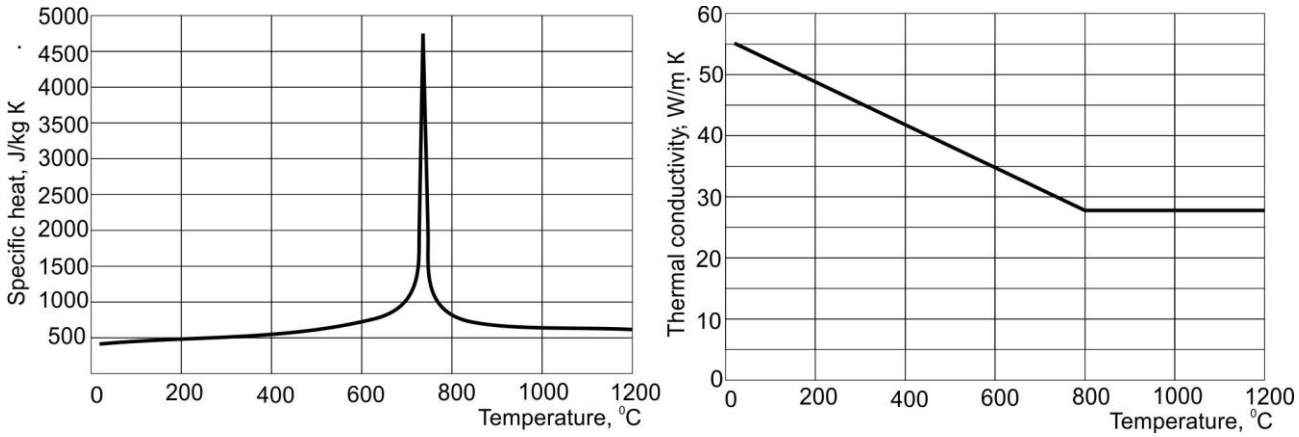


Figure 2. Variation of the thermal properties of steel.

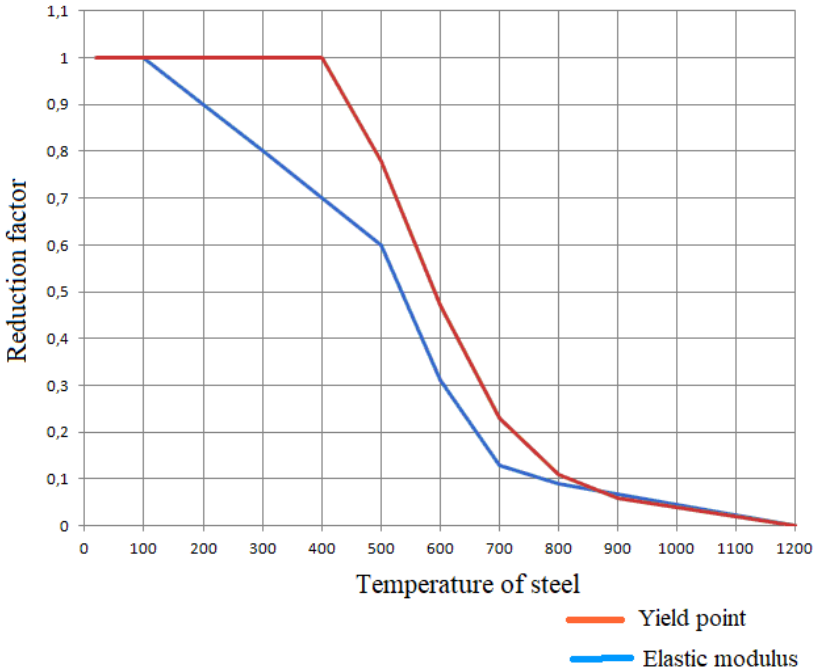


Figure 3. Effect of heating on the mechanical properties of steel.

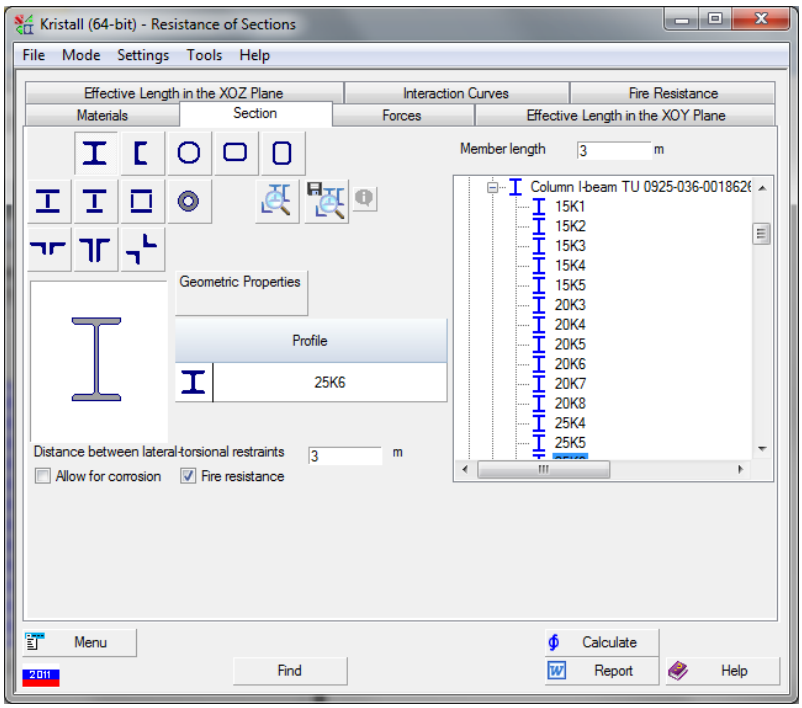


*Figure 4. The **Resistance of Sections** dialog box with an active fire test mode.*

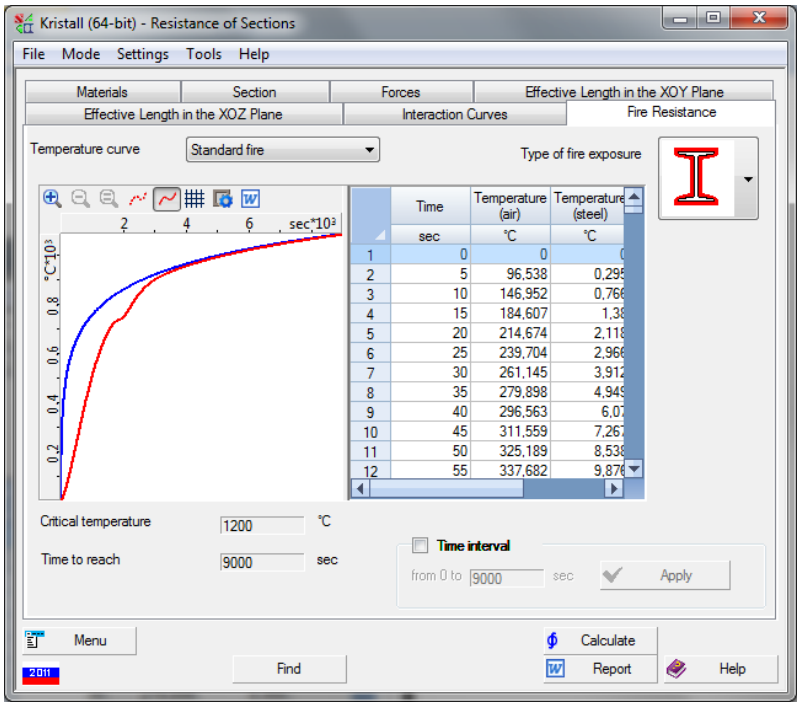


Figure 5. Results of the calculation.

2. SOFTWARE INTERFACE

Kristall enables to perform the fire design if the respective option is enabled in the **Resistance of Sections** mode (Figure 4).
The results of the calculation include (Figure 5):

- graph of the temperature increase for the selected fire;
- graph of the temperature variation of the structure;
- critical temperature;
- time to reach the critical temperature.

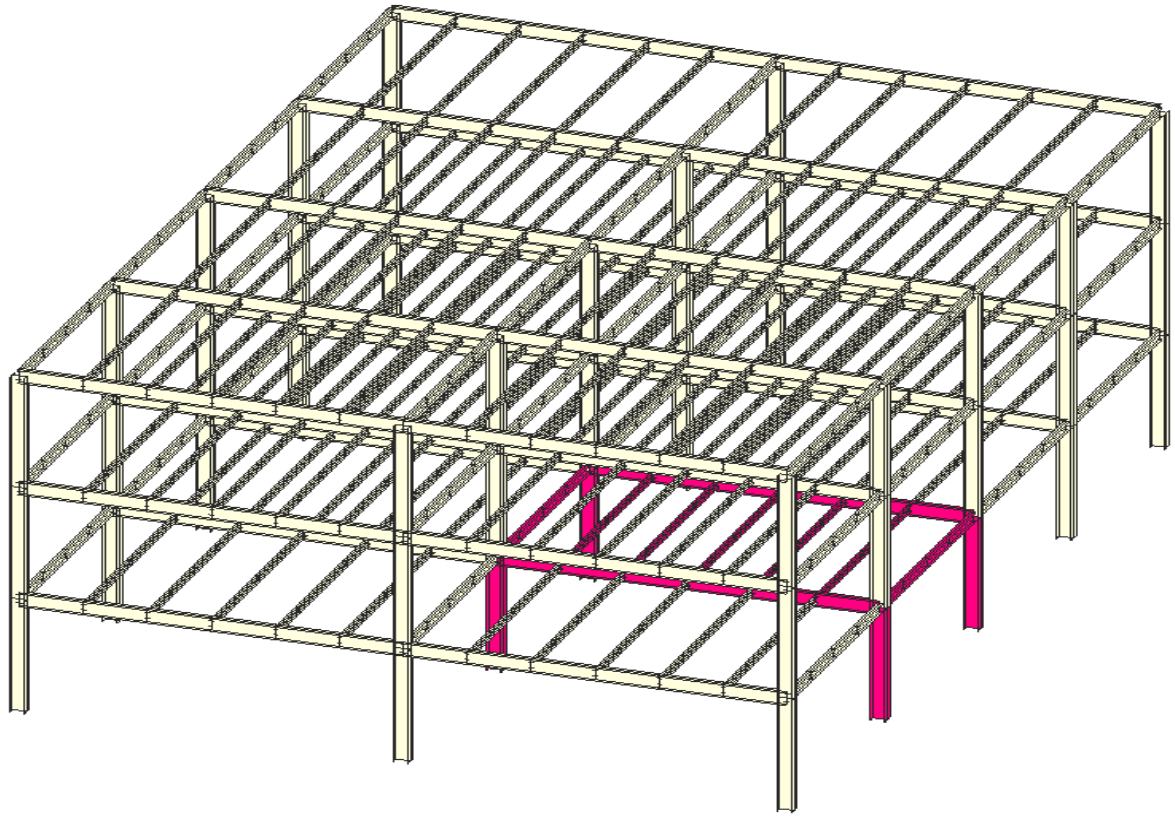


Figure 6. Frame.

3. SECONDARY EFFECTS

The role of secondary effects is demonstrated by an example. Let's consider a three-story building (Figure 6) with steel columns, beams, and minor beams. The floor is simply-supported on minor beams and only transfers the load to them without taking it. The fire action is applied in a section of the first floor shown in color in Fig. 6
The column cross-section is an I-beam 35K1, GOST 26020-83, the beam cross-section is an I-beam 46B1, GOST 26020-83, and a minor beam cross-section is an I-beam No. 20, GOST 8239-89.
The floor is assumed to be sufficiently fire-resistant and therefore the columns are heated from 4 sides, and beams and minor beams from 3 sides.
The dead load on the floor is G =150 kg/m^2, the live load is Q = 400 kg/m^2. The live load factor is taken as 0,25.

A standard fire is considered when the temperature in the fire compartment varies according to the following equation

$$\theta_g = 20 + 345\,lg\left(8t + 1\right),$$

where t is time in minutes. The heating of steel structural elements was calculated in increments, which was determined according to the following formula for the time interval Δt

$$\Delta\theta_a = \left(\frac{A_m}{V}\right)\frac{1}{c_a\rho_a}\left\{25\left(\theta_g - \theta_a\right) + \right.$$
$$\left. +5{,}67\cdot 10_{-8}\left[\left(\theta_g + 273\right)^4 - \left(\theta_a + 273\right)^4\right]\right\}\Delta t\,,$$

where ρ_a = 78590 kg/m^3 is the density of steel.
The results of the thermal analysis are given in the Table 1. This table also provides the values of the reduction factors for the elastic modulus

and design resistance caused by the heating (Figure 7 and Figure 8).

Table 1. The results of the thermal analysis.

Time from the start of the fire, min	Temperature, °C			Reduction factor E			Reduction factor R_y		
	Column	Beam	Minor beam	Column	Beam	Minor beam	Column	Beam	Minor beam
0	20	20	20	1,000	1,000	1,000	1,000	1,000	1,000
1	41	44	64	1,000	1,000	1,000	1,000	1,000	1,000
2	72	80	133	1,000	1,000	1,000	1,000	1,000	1,000
3	99	112	200	1,000	1,000	1,000	1,000	1,000	1,000
4	134	152	277	1,000	1,000	0,897	1,000	1,000	1,000
8	291	326	625	0,878	0,832	0,297	1,000	1,000	0,510
10	374	419	794	0,767	0,709	0,210	1,000	0,930	0,187
12	461	514	947	0,653	0,560	0,131	0,830	0,770	0,116
15	592	658	1128	0,333	0,280	0,037	0,522	0,344	0,033

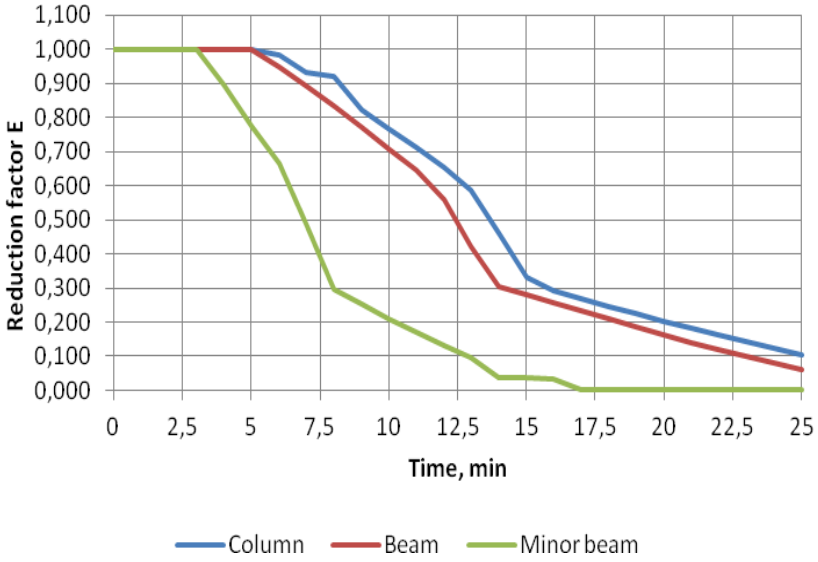


Figure 7. Reduction of the elastic modulus.

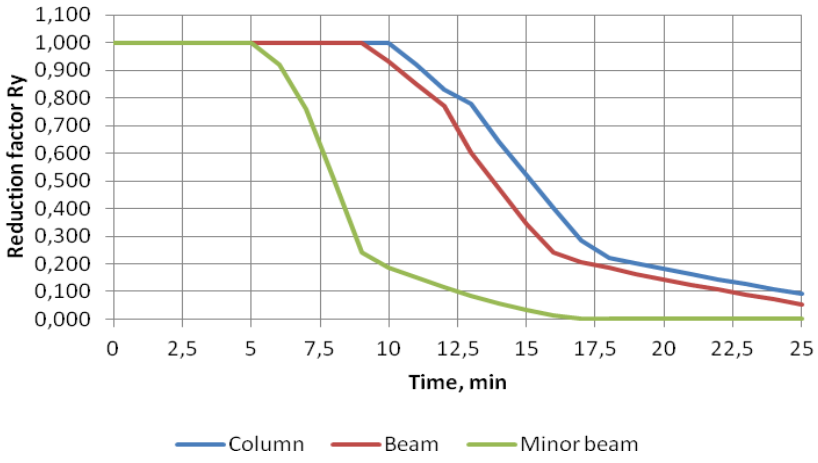


Figure 8. Reduction of the design resistance.

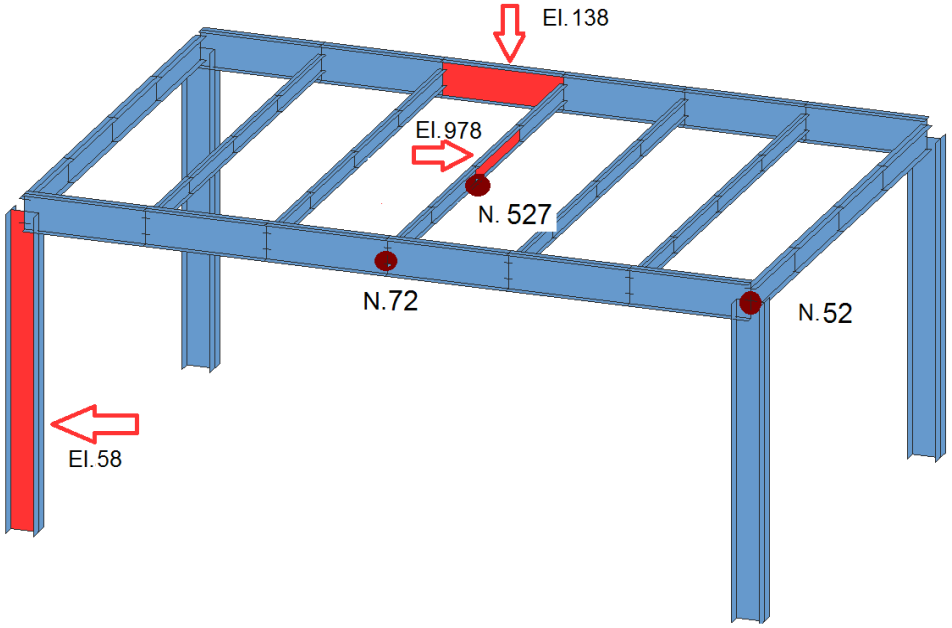


Figure 9. Controlled elements.

Table 2. The results of the calculation.

Time, min	Displacements, node 52			Displacements, node 72			Displacements, node 527		
	X	Y	Z	X	Y	Z	X	Y	Z
0	0,18	0,01	-0,97	-0,01	0,01	-10,28	-0,02	0,00	-11,06
4	0,85	-2,09	4,94	-0,39	-1,52	-13,74	-0,21	-0,41	-23,39
8	1,14	-2,00	11,11	-1,02	-1,33	-15,73	-0,81	-0,57	-23,42
10	1,30	-2,25	13,86	-1,20	-1,50	-20,42	-0,95	-0,67	-29,14
12	1,34	-1,81	16,52	-1,31	-1,19	-25,31	-1,10	-0,63	-32,21
15	1,86	-0,53	17,32	-0,42	-0,42	-38,06	-0,34	-0,24	-42,18

The strength analysis was performed in **SCAD** (the **Erection** mode) for the state of the structure at the beginning of the fire and on the 4-th, 8-th, 10-th, 12-th and 15-th minute from the start of the fire. The results of the calculation are given below.

Internal forces are tracked in columns (finite element 58), the middle of the beam (finite element 138), and the middle of the minor beam (finite element 978). These elements are shown in Figure 9.

Control nodes 52, 72 and 527 are selected to track the displacements. They are shown in Figure 9 as well.

The results of the calculation are given in the Tables 2 and 3.

Beam strength failure occurs between 4-th and 8-th minutes, minor beams fail on the 4-th minute, and columns fail between 8-th and 10-th minutes, although their temperature is far from the critical value (Fig. 10). The critical time is about 16 minutes for columns, 14 minutes for beams, and 11 minutes for minor beams.

The strong discrepancy is caused by a fundamental change in the type of the stress-strain state (drastic difference in eccentricities). In this example, the so-called secondary effects have created large longitudinal forces in the elements some of which were considered as only flexural. The fact that the fire area was a section of the floor turned out to be less favorable for the columns. If all columns on the floor were equally

heated, the critical temperature estimate would be closer to the design behavior of the structure.

Table 3. The results of the calculation.

Time, min	Forces in the element 58			Forces in the element 138			Forces in the element 978		
	N, t	M, tm	Q, t	N, t	M, tm	Q, t	N, t	M,tm	Q, t
0	-72.90	0.00	0.00	-72.70	0.00	0.00	8.57	2.34	1.25
4	-251.29	-6.85	4.50	-250.69	2.15	4.50	-276.01	10.58	4.83
8	-331.76	-10.45	6.66	-330.96	2.87	6.66	-489.23	12.52	5.62
10	-655.95	-17.30	11.16	-654.36	5.02	11.16	-756.67	25.44	11.70
12	-481.76	-8.09	5.07	-480.56	2.03	5.07	-514.84	13.64	6.15
15	-541.81	-1.58	0.97	-540.41	0.34	0.97	-327.65	9.89	4.22

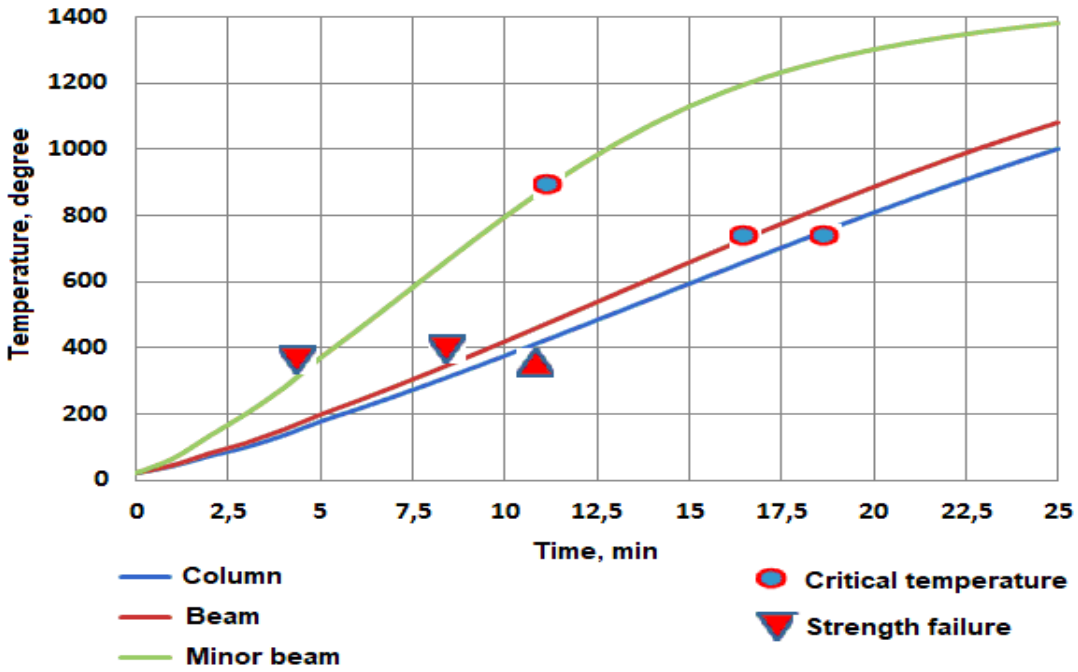


Figure 10. Comparison of results.

4. CHALLENGING ISSUES

All the above calculations are based on the strength check performed according to the codes (but taking into account changes in the yield strength and elastic modulus of steel). In other words, plasticity has been practically ignored.

If we assume deep plastic deformation, then additional forces from thermal heating can drop rapidly. This is evidenced by experiments carried out at the University of Sheffield (UK) by Allam A.V., Burgess I.W., Plank R.J. (Figures 11 and 12).

Moreover, it is necessary to answer the following important questions:

1. A building has different structural components with various fire resistance limits. The following question arises: should the calculation of the entire structure be performed to the minimum or to the maximum limit? This problem is not considered in European fire regulations, where fire resistance requirements are set not for individual components, but for the whole structure.

2. It is not clear how to simulate a fire – which fire area should be considered when a structure is not divided into fire compartments.

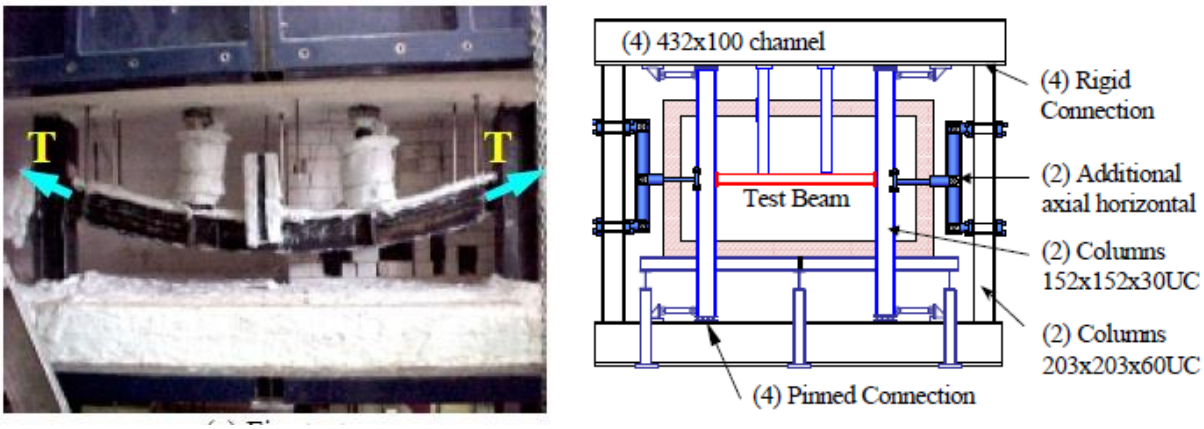


Figure 11. Experimental setup.

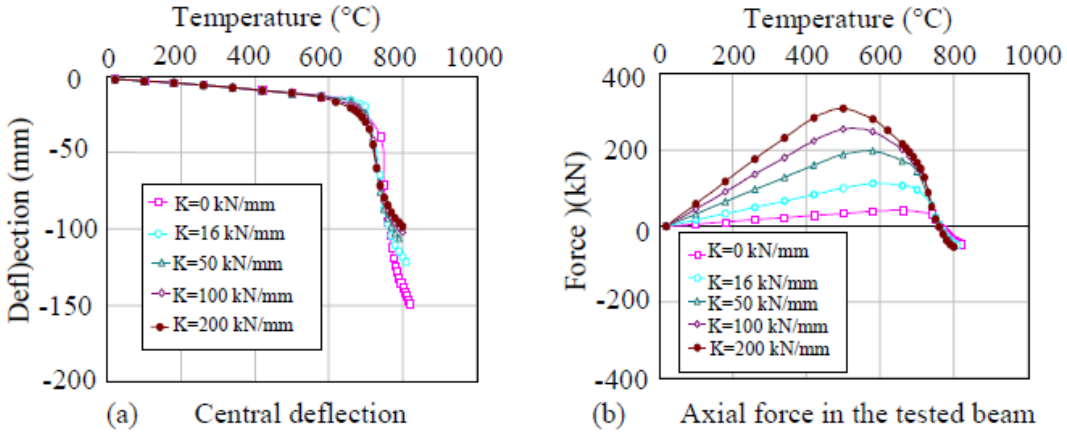


Figure 12. Fire test results.

REFERENCES

1. **Allam A.M., Burgess I.W. and Plank R.J**. Performance-Based Simplified Model for a Steel Beam at Large Deflection in Fire. // *Proc. 4th International Conference on Performance-Based Codes and Fire Safety Design Methods*, Melbourne, Australia, 2002.
2. **Bailey C.G., Burgess I.W. and Plank R.J.** Computer Simulation of a Full-Scale Structural Fire Test. // *The Structural Engineer*, 1996, Vol. 74, No. 6, pp. 93-100.
3. **EN 1993-1-2. Eurocode 3:** Design of steel structures. General rules – Structural fire design. Brussels, CEN, 2010.
4. **Poklonsky V.G., Fesenko O.A,, Tarasyuk V.G. et al.** Fire Design of Reinforced Concrete Structures According to Eurocode 2. Kiev, Intertekhnologiya, 2016, 83 pages.
5. **Fedorov V.S., Levitsky V.E., Molchadsky I.S., Aleksandrov A.V.** Ognestojkost' i Pozharnaja Opasnost' Stroitel'nyh Konstrukcij [Fire Resistance and Fire Hazard of Building Structures]. Moscow, ASV, 2009 (in Russian).

СПИСОК ЛИТЕРАТУРЫ

1. **Allam A.M., Burgess I.W. and Plank R.J**. Performance-Based Simplified Model for a Steel Beam at Large Deflection in Fire. //

Proc. 4th International Conference on Performance-Based Codes and Fire Safety Design Methods, Melbourne, Australia, 2002.
2. **Bailey C.G., Burgess I.W. and Plank R.J.** Computer Simulation of a Full-Scale Structural Fire Test. // The Structural Engineer, 1996, Vol. 74, No. 6, pp. 93-100.
3. **EN 1993-1-2. Eurocode 3:** Design of steel structures. General rules – Structural fire design. Brussels, CEN, 2010.
4. **Poklonsky V.G., Fesenko O.A,, Tarasyuk V.G. et al.** Fire Design of Reinforced Concrete Structures According to Eurocode 2. Kiev, Intertekhnologiya, 2016, 83 pages.
5. **Федоров В.С., Левитский В.Е., Молчардский И.С., Александров А.В.** Огнестойкость и пожарная опасность строительных конструкций. – М.: АСВ, 2009. – 408 с.

Anatolii V. Perelmuter, Foreign member of Russian Academy of Architecture and Construction Sciences, Doctor of Science, Professor; SCAD Soft, Ltd; Kiev 03037, Ukraine, 3a Osvity street, office. 1,2;
phones: +38 044 249 71 93 (91), +38 044 248 71 00,
+38 044 248 80 60; e-mail: avp@scadsoft.com.

Перельмутер Анатолий Викторович, иностранный член РААСН, доктор технических наук, профессор; НПО СКАД Софт, 03037, Украина, г. Киев, ул. Просвящения, 3а, Офис 2; тел. +38 044 249 71 93 (91),
+38 044 248 71 00, +38 044 248 80 60;
E-mail: avp@scadsoft.com.

SIMULATION OF A DEFECTLESS LIFECYCLE OF UNIQUE UNDERGROUND STRUCTURES OF THE SEWAGE SYSTEM AT THE STAGE OF THEIR CONSTRUCTION IN DIFFICULT SOIL CONDITIONS

Nickolai A. Perminov
Emperor Alexander I Saint-Petersburg State Transport University, Saint-Petersburg, RUSSIA

Abstract: Simulation of the parameters of a defectless lifecycle of large caissons at the stage of their plunging into heterogeneous soil milieu allows considerable expansion of the area of rational use of underground areas of megacities for deep transport facilities and engineering infrastructure due to provision of structural safety and sustainable operation of a special underground structure. Mega sizes of an RC caisson allow creating open underground areas, unique in volumes and deepness. The analysis of behavior of a massive gravitational fencing caisson at its incrementing and plunging into heterogenenous soil milieu allowed identifying the nature of its non-linear and unsteady behavior. Unsteadiness of the processes of interaction of a large structure and soil milieu accompanied by geometrical changeability causes the necessity to create methods of adaptive control of strain-stress behavior of the system "gravitational large body – heterogeneous host medium" for decreasing aggravating influence of these effects on strength, deformability and reliability of the structure at the subsequent stages of its lifecycle. Due to joint step-by-step implementation of geotechnical and structural calculations a history of the processes of caisson-soil milieu interaction is modeled and the parameters of adaptive control of strain-stress behavior are predicted, thus providing conditions of controlled lowering. The paper demonstrates results of consistent implementation of the given concept at the lifecycle stages of the unique caissons for the sewage system of the megacity beginning from numerical modeling during design to computer models of control of strain-stress behavior of the system "large caisson – soil bulk" using the methods of geotechnology with subsequent monitoring provision of the defectless stage of construction.

Keywords: simulation, unique underground structure, heterogeneous soil milieu, geometrical changeability, non-linear models, control of strain-stress behavior of the system, structural safety, defectless lifecycle

МОДЕЛИРОВАНИЕ БЕЗДЕФЕКТНОГО ЖИЗНЕННОГО ЦИКЛА УНИКАЛЬНЫХ ПОДЗЕМНЫХ СООРУЖЕНИЙ СИСТЕМЫ ВОДООТВЕДЕНИЯ НА СТАДИИ ИХ ВОЗВЕДЕНИЯ В СЛОЖНЫХ ГРУНТОВЫХ УСЛОВИЯХ

Н.А. Перминов
Государственный университет путей сообщения Императора Александра I, г. Санкт-Петербург, РОССИЯ

Аннотация: Моделирование параметров бездефектного жизненного цикла крупногабаритных оболочек на стадии их погружения в неоднородные грунтовые среды позволяет за счет обеспечения конструкционной безопасности и устойчивого функционирования специального подземного сооружения существенно расширить область рационального использования подземного пространства мегаполисов для объектов транспортной и инженерной инфраструктуры . Мега размеры железобетонной оболочки позволяют создавать открытые подземные пространства уникальными по объемам и глубинами заложения. Анализ поведения массивной гравитационной ограждающей оболочки при постепенном ее наращивании и погружении в неоднородную грунтовую среду среды позволили выявить характер их нелинейного и нестационарного поведения. Нестационарность процессов взаимодействия массивного сооружения с грунтовой средой, сопровождаемая геометрической изменчивостью, вызывает необходимость создания методов адаптивного управления напряженно-деформированным состоянием системы «гравитационное крупногабаритное тело – неоднородная вмещающая среда» для уменьшения

осложняющего влияния этих эффектов на прочность, деформируемость и надежность сооружения на последующих стадиях его жизненного цикла. Посредством совместного пошагового выполнения геотехнических и конструкторских расчетов моделируется история процессов взаимодействия оболочки с грунтовой средой и прогнозируются параметры адаптивного управления НДС системы, обеспечивая условия регулируемого погружения. В статье представлены результаты последовательной реализации изложенной концепции на стадиях жизненного цикла уникальных опускных сооружений системы водоотведения мегаполиса от численного моделирования при проектировании до компьютерных моделей управления с помощью методов геотехнологии напряженно-деформируемым состоянием системы «крупногабаритная оболочка – грунтовый массив» с последующим мониторинговым обеспечением бездефектной стадии строительства.

Keywords: моделирование, уникальное подземное сооружение, неоднородная грунтовая среда, геометрическая изменчивость, нелинейные модели, управление напряженно-деформируемым состоянием системы, конструкционная безопасность, бездефектный жизненный цикл.

1. NON-LINEAR AND UNSTEADY PROCESSES OF INTERACTION OF A LARGE CAISSON IN THE CONDITIONS OF SIMULTANEOUS INCREMENTING AND PLUNGING OF THE STRUCTURE

Characteristic parameters and indicators, according to which underground structures of the sewage system of large cities can be regarded as the unique ones, first and foremost, include abnormal depth of more than 70 m as well as a high degree of requirements to their ecological safety. Special requirements to preservation of structural integrity during long-tem exploitation should be set for these structures as particulary dangerous facilities accumulating and transporting agressive sewage discharge through their internal culverts under residential urban areas.

Structural integrity of an underground sewage structure means the capacity of its resistance to decrepit and corrosive damages at all stages of its lifecycle. One can achieve these conditions only by means of joint gradual solution of geotechnical and structural problems when pre-limit stress-strain states of an RC culvert during its interaction with a soil bulk are modeled and predicted at the stage of design of its life cycle, then using the methos of geotechnology and monitoring they are provided at the stage of construction of a structure, and later applying the same or modified monitoring system they are supported at the stage of long-term operation under the conditions of technically generated effects. There is a need to consider another factor which defines the category of structure uniqueness as a particular and specific one. It implies limited or complete unavailability of repair of underground structures of this type. Firstly, it is associated with the fact that according to the present schemes of sewage, which exist in megacities nowadays, these facilities cannot virtually be put out of operation without a threat of violating sustainment of the city engineering infrastructure.

Therefore, in order to provide safe and sustainable operation of large underground structures of the sewage system it is necessary to provide internal integrity of fencing structures with high degree of water resistance at all stages of their lifecycle.

The existing norms and sets of regulations envisage verification calculations of caisson underground structures for the stages of construction and exploitation. However for large-size caisson structures due to specific conditions of their interaction with a soil bulk and inclusion the large scale effect (factor): according to hyper sizes of the area of lateral surface of a culvert interacting with heterogeneous soil and a super large weight, which creates a powerful kinetic impulse at instant, often sudden drops of a caisson structure, joint manifestation of these factors causes specific non-linear behavior of the structure at its driving and the embedding soil

bulk. Strength and deformability of a large-size massive structure, its geometrical variability should be calculated not only for the final stage of construction but also for a whole history of driving considering a history of caisson-soil bulk interaction at driving, and, consequently the effect of gradual inheritance of stress-strain state, that is possible to make only using solutions of non-linear problems, non-linear models and computer non-linear simulation.

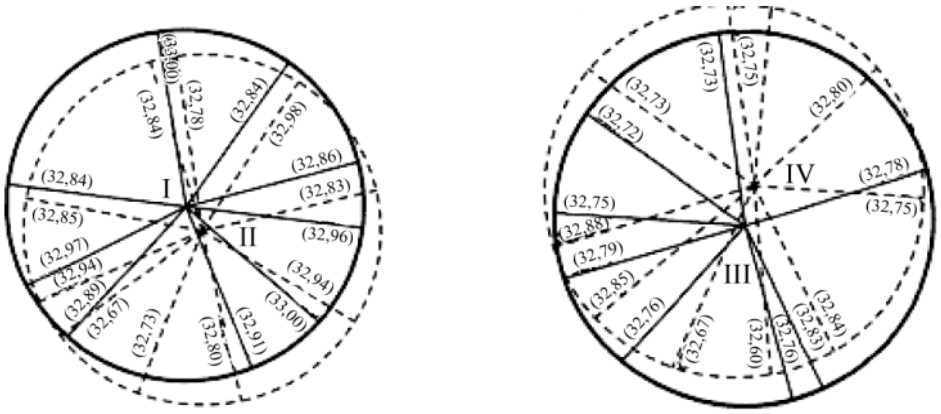
The analysis of test and experimental results presented in the paper showed that the main defects leading to violation of culvert integrity and crack occurrence emerged in the period of construction of the underground part in the soil bulk. Therefore, the main task is reduced to provision of operation of a structure at pre-limit states at the stage of construction of its lifecycle. In order to implement these conditions the decisive role is played by evaluation of real work of structures with account of the process of their gradual construction in the soil bulks and non-linear properties of structural materials and soil. Consideration of these conditions allows constructing an adequate model of the process of culvert interaction at its stage-by-stage embedment into the soil bulk. Calculation substantiation of a range of pre-limit changes of the stress-strain state of a megamassive culvert at its embedment into heterogeneous soils provides defectless operation of the lifecycle of an underground structure at the stage of its construction [1]. The analysis of the processes of caisson loading at the stage of its construction with account of the effect of inherited stress-strain behavior allows creating an adequate calculation-analytical model of an underground structure and selecting a rational method of calculation to predict dynamics and spatial borders of changing stress-strain state of an RC caisson structure providing defectlessness of the structure at all stages of its driving.

The methodological approach proposed in the paper allows transferring from the earlier accepted methods of calculation of underground sewage caisson structures to the concept of simulation and prediction of defectless lifecycle at the stage of construction. The results of experimental and theoretical research, which are given in the paper, substantively prove that modeling and calculative substantiation of schemes and parameters of preventive protection of an underground structure at the stage of its construction using geotechnical methods provides its safety and resistance against technically generated impacts at the subsequent stages of the lifecycle during its long-term regime operation.

2. THE ANALYSIS OF INTERACTION OF A LARGE CAISSON WITH HETEROGENEOUS SOIL MILIEU AT THE STAGE OF ITS PLUNGING

In order to provide stable and safe operation of large caisson structures there is a need to ensure internal integrity of fencing structures with high degree of waterproofness at all stages of their life cycle.

The existing standards [1] and regulations [2] envisage checking calculations of underground structures to be lowered for the stages of their construction and operation. However, based on the experience one can say that in case of large caisson structures it is not enough due to specific conditions of their interaction with a soil bulk and inclusion the effect (factor) of a large scale: hyper sizes of an area of lateral surface of the shell, which interacts with heterogeneous soil, and its super large weight, which creates a powerful kinetic impulse during instant, often sudden subsidence, cause a beyond-design situation for a caisson structure. Joint actions of these factors stipulate specific non-linear behavior of the structure at lowering as well as the host soil bulk.

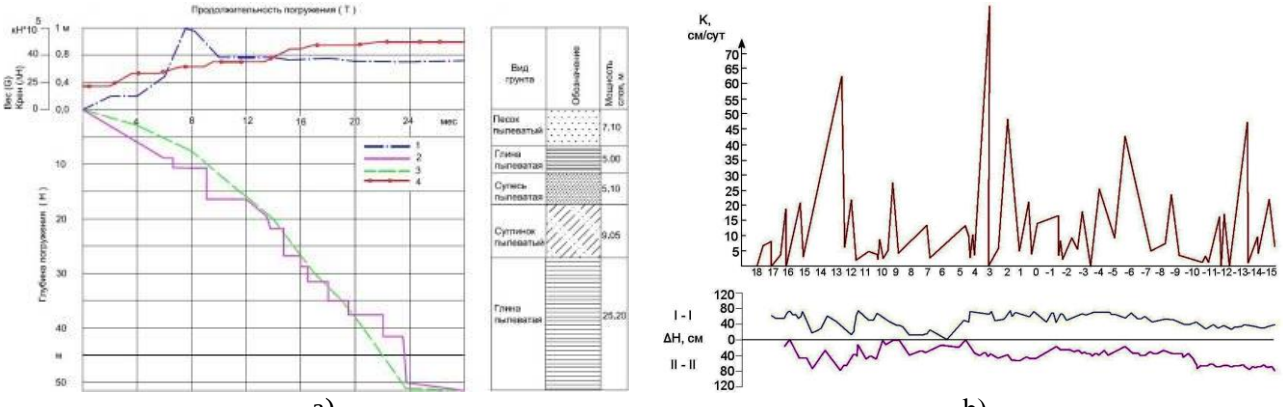


a) b)

Figure 1. The measurement of a radius R and displacement of the center of circle O during its lowering to a depth H: a, b – respectively I –for H = 17 m; II – for H = 29 m; III – for H = 25 m; IV – for H = 29 m; O (I–II) = 0.108 m; O (III–IV) = 0.234 m.

Due to strength and deformability of the large massive structure, its geometric changeability it is necessary to calculate not only the final stage of construction but also the whole history of lowering taking into account a history of the process of shell-soil bulk interaction during caisson lowering and, consequently, the effect of gradual inheritance of stress-strain behavior. These problems could be solved only by tackling non-linear problems, non-linear models and computer non-linear simulation [3,4,5].

The analysis of the results of in situ and calculation-experimental works and the data of the comprehensive system of geotechnical monitoring (fig. 1) of lowering large shells showed the features of their interaction with heterogeneous soil milieu [6]. The geotechnical profile for the monitored facilities is characterized as follows: the upper layer is represented by Quaternary strata down to the depth of 14.0–25.0 m (saturated silty sands of medium density, E = 11 MPa, C = 0 MPa, φ = 30°; plastic silty clayey sands, E = 4 MPa, C = 0.01 MPa, φ= 15°; liquid-plastic silty sandy clays, E = 9 MPa, C = 0.025 MPa, φ = 16°; semi-solid silty sandy clays with gravel and pebbles, E = 14 MPa, C = 0.028 MPa, φ = 28°), the lower level represents the bed of dislocated solid Proterozoic clays (E= 19 MPa, C = 0.04…0.06 MPa, φ = 18…21°).



a) b)

Figure 2. Graphs of shell lowering: a – D=51 m, H= 53 m (1 – tilt graph; 2 – an elevation of lower plane; 3 – soil elevation; 4 – increase of shell weight); b – the diagram of deviation of the shell from the vertical axis.

The monitoring identified a very important phenomenon: the peak values of horizontal stresses exceed the calculation values 2.3–2.5 times, and it is observed at deviation of the shell from the vertical axis and changes of its geometry (Figure 1, 2). It can be the reason of suspension of the process of lowering the massive shell with a subsequent sudden, conditionally instant drop. Based on the analysis of the graph of lowering (fig. 2a) it can be seen that a value of drop reaches 1.5 m and more. The shell structure takes impact beyond-design loads by creating a powerful kinetic impulse by its drop to the soil bulk of a pit bottom [7], that can cause occurrence of microcracks in concrete of the structure and inevitably leads to violation of the structural hydro insolation. This phenomenon has been identified after 10–15-year-long operation of the gas and pumping station complex of the water treatment facilities of St. Petersburg [8].

Geomonitoring showed unsteadiness of the processes of interaction of the external contour of the massive structure [9]. Complex and, as a rule, uncontrolled character of the processes during conditionally instant embedment of the shell into the host heterogeneous milieu as well as the environment, that has physical and genetic non-linearity [10], demonstrate that the study of stain-stress behavior of the shell and soil bulk can be carried out only on the basis of computer modeling of this process using geotechnical and structural software complexes.

3. THE SIMULATION OF CONDITIONALLY INSTANT DROPS OF THE MASSIVE SHELL DURING ITS LOWERING INTO HETEROGENEOUS SOIL MILIEU

The analysis of behavior of the caisson structure during its sudden uncontrolled sliding (drop) to the bottom of an open soil cavern from the height 1.3 – 1.5 m with the angles of deviation from the vertical axis 0.5°-5°C was conducted with a help of the software complex Autodesk Robot Structural Analysis Professional [11].

While developing the calculation model (figure 3) it was considered that the shell structure consists of two cylinders, one stands on the other: the upper cylinder: the external radius R = 36 m, the internal radius R = 30.5 m, the height H1 = 46 m; the lower cylinder: the external radius R = 36 m, the internal radius R = 30 m, the height H2 = 25 m. Therefore, the external diameter of the shell was D = 72 m, the height of the shell was H = 71 m. Concrete grade - B30.

In order to simulate a value of impact force at dropping the shell in the model the cylinder fell from the height H = 150-250 cm under the action of its own weight with the tilt angle 0.5°-5° to a flexible soil (green-gray clay: φ = 21°, C = 0.04 MPa, E = 19 MPa). A spatial calculation scheme of the shell was modelled: the weight G = 210000 tons; the amount of nodes 16944; the amount of volumetric finite elements 12496; the amount of static degrees of freedom 50828; the amount of loadings 27; the acceleration of gravity g = 9.81 m/kV.s; the time of drop

$$t = \sqrt{2 * H / g}\ ;$$

Δt=0.30-0.54 s. Due to the tilt angle friction forces were applied in the upper part of the caisson from one side and in the lower part – from the opposite one.

As the simulation of the processes of drop at different angles of deviation of the shell from the axis -α and falling heights –ΔH was made in quite a large range, table 1 gives only the most typical results, which were taken for the analysis. The total calculation table of the results of integration of motion equation for the shell during the drop (falling) at speeds VZ, VX, VY (cm/s), acceleration AZ, AX, AY(cm/s2) and displacements UZ, UX, UY (cm) included 186385 lines.

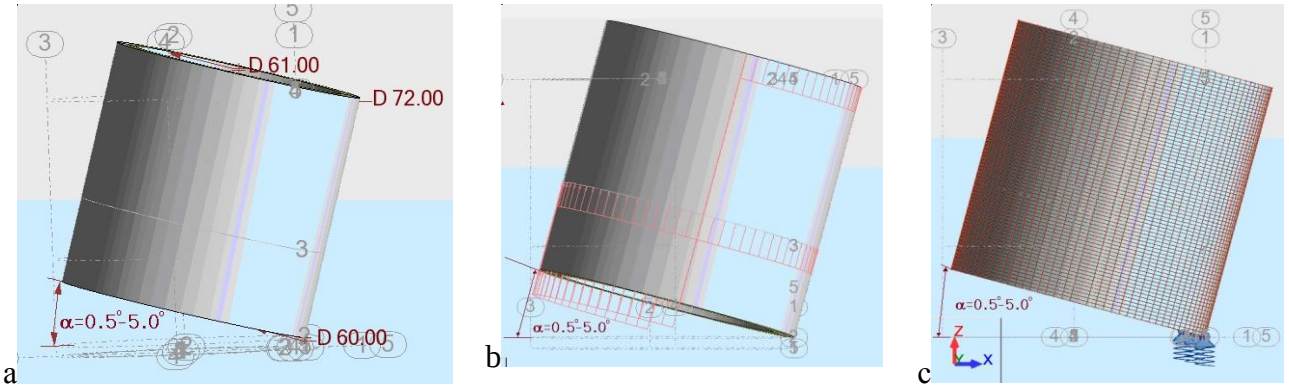
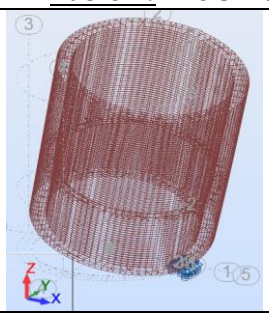
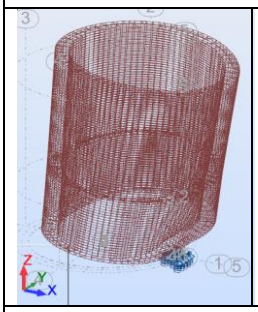
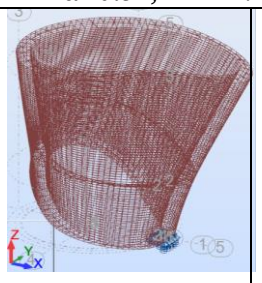
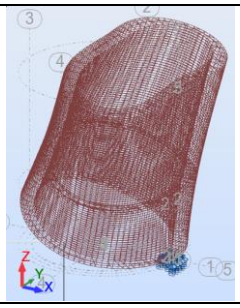


Figure 3. The schemes of calculation models of the lowered shell at different angles of its deviation from the vertical axis: a- static support at tilt; b,c — drop and sliding at tilt (deviation from the vertical axis).

Table 1. The simulation results.

 n^0=0.21 Δ^0_{max}= 0.0cm	 n^2=0.56 Δ^2_{max}= 3.1cm	 n^4=0.97 Δ^4_{max}= 26.1cm
The initial position α=0.5°; ΔH=0 m	Shape 2 Pre-limit strain-stress behavior α=0.5°; ΔH=1.25 m	Shape 4 Limit strain-stress behavior α=1°; ΔH=1.25 m
 n^{11}=1.94 Δ^{11}_{max}= 43.5cm	 n^{17}=3.68 Δ^{17}_{max}= 62.3cm	 n^{22}=8.47 Δ^{22}_{max}= 183.4cm
Shape 11 Post-limit strain-stress behavior α=2.5°; ΔH=1.25 m	Shape 17 Post-limit strain-stress behavior α=2.5°; ΔH=2.5 m	Shape 22 Post-limit strain-stress behavior α=3.5°; ΔH=2.5 m

Based on the simulation results (Figure 4) there were set admissible parameters of spatial location of the shell and the ranges of its conditionally instant drops, which provide pre-limit strain-stress behavior of the shell.

The simulation results show that for the large shell the recommendations of regulatory documents [12] have limited application and are needed to be confirmed via calculative modeling.

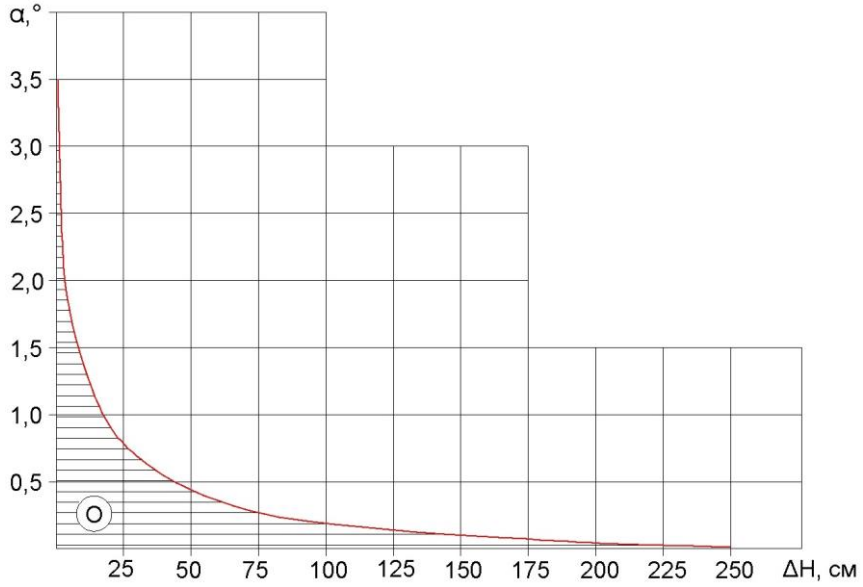


Figure 4. The area of limit admissible values of conditionally instant drops ΔH of the shell, D=61m, height H=71m, weight G=210000 tons, at different angles of deviation of the structure from the vertical axis a°(Concrete B30; φ = 21°, C = 0.04 MPa, E = 19 MPa)

4. THE SIMULATION OF CONTROLLED REGIMES OF LOWERING THE MASSIVE SHELL INTO A SOIL OF DIFFERENT STRENGTHS USING THE METHODS OF GEOTECHNOLOGY

Taking into account the results of the previous steps of modeling, at this stage the problem of geotechnical simulation of the process of lowering the shell into the soil bulk in a controlled mode was solved. The geotechnical methods served as external impacts on the "shell-soil bulk" system.

An incremental model of deformation type was used as the calculation soil model for solving the non-linear problem. A stress-strain connection in the model was taken separately for volumetric and shear components of a stress tensor

$$\left.\begin{aligned} dS_{ij} &= 2G^T \cdot de_{ij} \\ d\delta_{cp} &= 3K^T \cdot d\xi_{cp} \end{aligned}\right\} \quad (1)$$

where: dS_{ij} and de_{ij} are increments of deviatoric components of stress and strain tensors, respectively; $d\delta_{cp}$ and $d\xi_{cp}$ are increments of average stress and strain; G^T and K^T – tangent moduli of deformation of shape and volume.

Tangent moduli of deformation G^T and K^T were approximated according to linear polynomial of the second degree with one variable:

$$\left.\begin{aligned} G^T &= G\left(S_{ij};\delta_{\text{ср}}\right) = A_0 + A_1\delta_{cp} + AS_{ij} \\ K^T &= K\left(\delta_{cp}\right) = B_0 + B_1\delta_{cp} + B_2\delta_{cp}^2 \end{aligned}\right\} \quad (2)$$

Approximating dependencies (2) are experimentally substantiated on the example of stabilometer triaxial tests (STT) [1,2].

The model considers the conditions of loading and unloading according to the following criteria:

$$\left.\begin{aligned} \text{loading -}\ & dS_{ij} > Ø; d\delta_{cp} > Ø \\ \text{unloading -}\ & dS_{ij} < Ø; d\delta_{cp} < Ø \end{aligned}\right\} \quad (3)$$

In order to fulfill the condition of "loading" tangent moduli K_H^T and G_H^T were calculated according to formulae (2) in compliance with the current stress-strain behavior. For fulfilling the condition of "unloading" K_P^T and G_P^T were defined according to other dependencies (4).

$$K_P^T = const; \mathrm{G_P^T} = A_0 + A_1\delta_{cp} \qquad (4)$$

The parameters of the calculation model A0; A1; A2; Kp; B0; B1; B2 were defined based of the data of STT. The medium-grained sandy soil of the density Pd=1.65g/cm3 and water content W=10% was used as the tested soil. All calculations were made using the numerical method of finite elements with a help of geotechnical software "PCK". The procedure of solving the non-linear problem was reduced to the well-known method of variable rigidity [13], according to which the matrix of rigidity was transformed at each step of the solution in accordance with the current level of stress-strain behavior and orientation of the vector of additional loading.

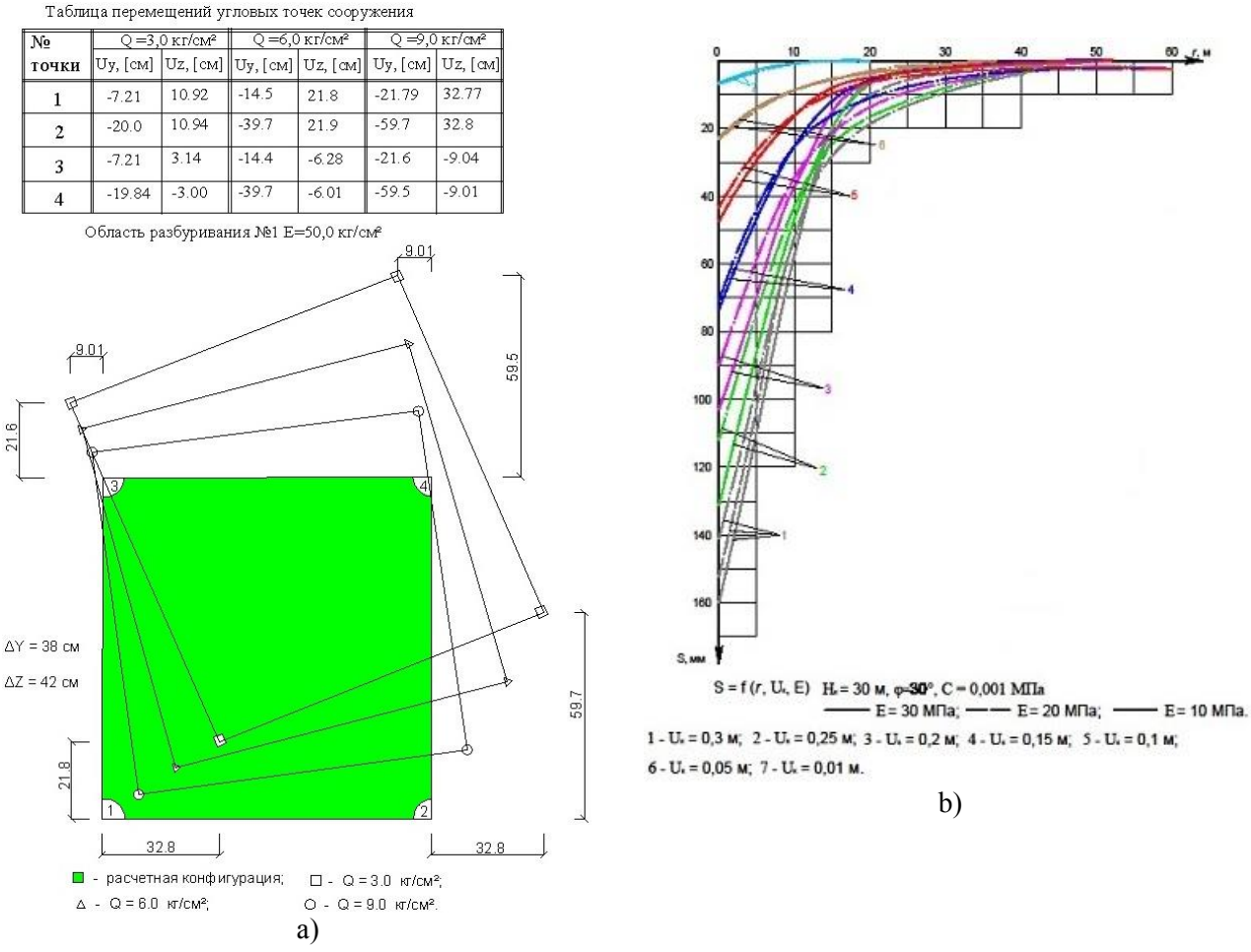


Figure 5. The displacement of the shell contour in continuous milieu: a - at correction of tilt under the conditions of action of a lateral additional load Q = 0.3- 0.9 MPa; b – the influence of a value of the shell contour displacement Ux on settlements of the soil surface at correction of tilt.

Figure 5a shows a characteristic graph of the shell contour displacement to the design position with inclusion of a geotechnical impact on strain-stress behavior of the surrounding soil

bulk into the calculation. The results of simulation show (Figure 5b) that rectification of the shell contour displacement almost to the design position (from 32.8 cm to 9.01 cm) allows decreasing an area of distribution and a value of settlement of the soil bulk around the shell several times (the area of distribution reduces from 45 m to 9 m; the value of settlement, respectively, from 150 cm to 8 cm).

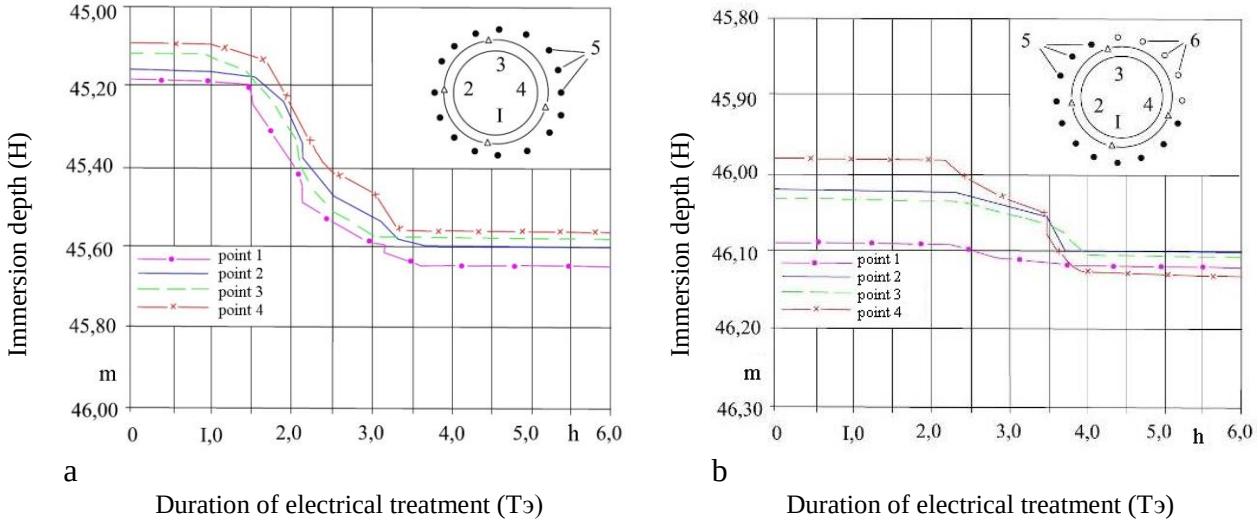


Figure 6. Electroosmosis deeping diagram phragments: a - even deeping; b - bank correction; 1,2,3,4 - fixed points; 5,6 - electrodes (catodes and anodes).

The control of strain-stress behavior of the system "large caisson – heterogeneous host medium" to provide structural safety of an RC structure in the range of design parameters [4,7] is achieved with a help of the methods of geotechnology [8], which are accompanied by the interactive system of monitoring of the lifecycle at the stage of construction. Figure 6 shows the graphs of defectless plunging of a large 57-m caisson at the elevation of 46 m in the mode of electroosmosis-controlled lowering into heterogeneous soils (E1 = 45 MPa; E2 = 240MPa), which calculation regimes were elaborated on the basis of step-by-step computer modeling.

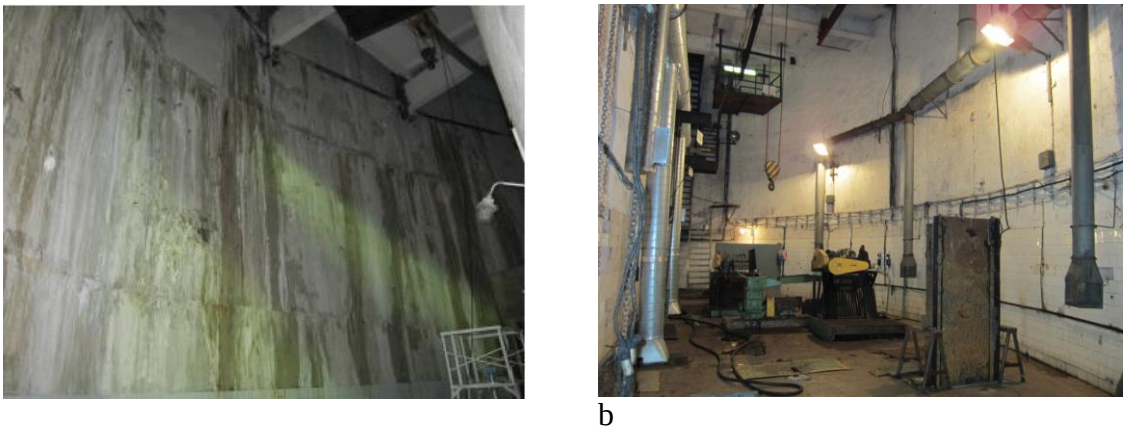


Figure 7. Examples of defectless and defective lifecycles of caissons at the stage of operation: a – 'in the conditions of simulation and monitoring of the plunging process, b – without simulation of the process at the drop of structures.

The defectless lifecycle of a large massive caisson at the stage of its construction is demonstrated by its integrity and water resistance of its structure after long-term operation (fig.7a, b). Fig.7a and fig.7b - show comparatively a caisson which was plunged into heterogeneous soils without geotechnical support. Both long-operating structures belong to the system of underground sewage facilities.

5. CONCLUSIONS

The analysis of behavior of the massive gravitational fencing shell during its gradual increasing and lowering into the heterogeneous soil milieu allowed identifying a number of factors, which characterize its non-linear behavior in the conditions of joint interaction.

Physical non-linearity is caused by behavior in the elasto-plastic area of the soil bulk, which contacts with the lateral surface, during deviation of the structure from the vertical axis. Geometric non-linearity manifests itself when its geometry changes asymmetrically during instant-stepwise drops of the massive shell.

Unsteadiness of the processes of interaction of the massive structure with the soil milieu as well as itself causes the necessity of creating methods of adaptive control of the stress-strain behavior of the system “gravitational large body – heterogeneous host milieu".

Due to joint step-by-step making geotechnical and structural calculations a history of the processes of shell-soil milieu interaction is simulated, the parameters of the adaptive control of the system of strain-stress behavior, which are implemented with a help of external geotechnical impacts at the stage of construction of the structure, are predicted.

The results of the considered concept are applied at geotechnical support of a lifecycle of the unique underground structures of the sewage system of St. Petersburg at the stage of construction of large caisson shells during simultaneous lowering and increasing of the structure.

REFERENCES

1. **Perelmuter A.V.** The Formation and Development of Concepts About the Design Scheme of Structures. // *International Journal for Computational Civil and Structural Engineering*, 2018, Volume 14, Issue 4, pp. 109-129
2. **Ilichev V.A. and Mangushev R.A.** Spravochnik Geotehnika. Osnovanija, Fundamenty i Podzemnye Sooruzhenija [The Reference Book of a Geotechnical Engineer. Soils, foundations and underground structures]. Moscow, ASV Publishing House, 2016, 1034 pages (in Russian).
3. SP 43.13330.2012. Sooruzhenija Promyshlennyh Predprijatij [Structures of Industrial Enterprises]. An updated version. Construction Code 2.09.03-85. Moscow, National standard, 2012, 101 pages (in Russian).
4. **Perminov N.A.** Unsteady Interaction Simulation of a Large RC Shell With Heterogeneous Soil Milieu for a Gradually Increasing Caisson Structure. // *IOP Conf. Ser.: Mater. Sci. Eng.*, 2018, Vol. 465, 012059.
5. **Barabash M.S.** Modelirovanie Zaproektnyh Vozdejstvij pri Issledovanii Zhiznennogo Cikla Konstrukcij Zdanij i Sooruzhenij [Simulation of Beyond-Design Impacts at Studying the Lifecycle of Buildings and Structures]. // *International Journal for Computational Civil and Structural Engineering*, 2016, Volume 12, Issue 3, pp. 15-25 (in Russian).
6. **Ilichev V.A.** Ploskaja Zadacha o Shtampe na Uprugom Osnovanii s Uchetom Tehnologii Ego Vozvedenija [A Flat Problem of a Plate on Elastic Subsoil With Account of a Technology of its Construction]. // *Soils, Foundations and Soil Mechanics*, 2008, Volume 4, pp. 12-16 (in Russian).
7. **Perelmuter A.V., Kabantsev O.V.** Analiz Konstrukcij s Izmenjajushhejsja Raschetnoj

Shemoj [The Analysis of Structures With a Changing Calculation Scheme]. Moscow, SCAD Soft, ASV Publishing House, 2015, 148 pages (in Russian).

8. **Perminov N.A.** Comprehensive Geotechnical Support for the Construction of Large Edifices as a Part of St. Petersburg. // Geotechnical Engineering for the Preservation of Monuments and Historic Sites (Viggiani (ed.) Balkema, Rotterdam, 1997, pp. 1074-1081.
9. **Perminov N.A., Perminov A.N.** Geotehnicheskie Aspekty Obespechenija Bezopasnosti Dlitel'no Jekspluatiruemyh Ob#ektov Inzhenernoj Infrastruktury Krupnyh Gorodov v Slozhnyh Gruntovyh Uslovijah [Geothermal Aspects of Providing Safety of Long-Operating Facilities of Engineering Infrastructure of Large Cities in Difficult Soil Conditions]. // *The Journal of Perm Research University*, 2014, Volume 4, pp. 111-128 (in Russian).
10. **Perelmuter A.V., Slivker V.I.** Raschetnye Modeli Sooruzhenij i Vozmozhnost' ih Analiza [Calculation Models of Structures and a Possibility of Their Analysis]. Moscow, SCAD Soft, DMK Press Publishing House, 2011, 710 pages (in Russian).
11. SP 22.13330.2016 Osnovanija Zdanij i Sooruzhenij [Foundations of Buildings and Structures]. An updated version. Construction Code 2.02.01-83*. Moscow, National standard, 2016, 172 pages (in Russian).
12. **Carmody Y., Sterling R.L.** Underground space design. A guide to subsurface utilization and design for people in underground spaces. New York, VNR, 1993, 328 pages.
13. **Ponomaryov A.B., Kaloshina S.V., Zakharov A.V., Bezgodov M.A., Shenkman R.I., Zolotozubov D.G.** Results of Geotechnical Modeling of the Influence of Construction of the Large Foundation Ditch on the Existing Historical Building. // Japanese Geotechnical Society Special Publication: *The 15th Asian Regional Conf. on Soil Mechanics and Geotechnical Engineering: Geotechnical Heritage*. Part 2 (TC 301/ATC 19 Session) Volume 78, 2015, pp. 2676-2679.

СПИСОК ЛИТЕРАТУРЫ

1. **Perelmuter A.V.** The Formation and Development of Concepts About the Design Scheme of Structures. // *International Journal for Computational Civil and Structural Engineering / Международный журнал по расчету гражданских и строительных конструкций)*, 2018, Volume 14, Issue 4, pp. 109-129.
2. **Ильичев В.А. и Мангушев Р.А.** Справочник геотехника. Основания, фундаменты и подземные сооружения. – М.: Издательство АСВ, 2016. – 1034 с.
3. СП 43.13330.2012 Сооружения промышленных предприятий/ Актуализированная редакция. СНиП 2.09.03-85. – М.: Национальные стандарты, 2012. – 101 с.
4. **Perminov N.A.** Unsteady Interaction Simulation of a Large RC Shell With Heterogeneous Soil Milieu for a Gradually Increasing Caisson Structure. // *IOP Conf. Ser.: Mater. Sci. Eng.*, 2018, Vol. 465, 012059.
5. **Барабаш М.С.** Моделирование запроектных воздействий при исследовании жизненного цикла конструкций зданий и сооружений. // *International Journal for Computational Civil and Structural Engineering / Международный журнал по расчету гражданских и строительных конструкций)*, 2016, Volume 12, Issue 3, pp. 15-25.
6. **Ильичев В.А.** Плоская задача о штампе на упругом основании с учетом технологии его возведения. // *Основания, фундаменты и механика грунтов*, 2008, №4, с. 12-16.

7. **Перельмутер А.В., Кабанцев О.В.** Анализ конструкций с изменяющейся расчетной схемой. – М.: СКАД СОФТ Издательство АСВ, 2015. – 148 с.
8. **Perminov N.A.** Comprehensive Geotechnical Support for the Construction of Large Edifices as a Part of St. Petersburg. // Geotechnical Engineering for the Preservation of Monuments and Historic Sites (Viggiani (ed.) Balkema, Rotterdam, 1997, pp. 1074-1081.
9. **Перминов Н.А. и Перминов А.Н.** Геотехнические аспекты обеспечения безопасности длительно эксплуатируемых объектов инженерной инфраструктуры крупных городов в сложных грунтовых условиях. // *Вестник ПНИПУ. Строительство и архитектура*, 2014, №4, с. 111-128.
10. **Перельмутер А.В., Сливкер В.И.** Расчетные модели сооружений и возможность их анализа. – М.: СКАД СОФТ, Издательство ДМК Пресс, 2011. – 710 с.
11. СП 22.13330.2016 Основания зданий и сооружений / Актуализированная редакция. СНиП 2.02.01-83*. – М.: Минстрой России, 2016. – 172 с.
12. **Carmody Y. and Sterling R.L.** Underground space design. A guide to subsurface utilization and design for people in underground spaces. New York, VNR, 1993, 328 pages.
13. **Ponomaryov A.B., Kaloshina S.V., Zakharov A.V., Bezgodov M.A., Shenkman R.I., Zolotozubov D.G.** Results of Geotechnical Modeling of the Influence of Construction of the Large Foundation Ditch on the Existing Historical Building. // Japanese Geotechnical Society Special Publication: *The 15th Asian Regional Conf. on Soil Mechanics and Geotechnical Engineering: Geotechnical Heritage*. Part 2 (TC 301/ATC 19 Session) Volume 78, 2015, pp. 2676-2679.

Nicolay A. Perminov, C.T.Sc., Chief specialist of the Institute SUE "Lengiproingproekt", docent «Emperor Alexander I St. Petersburg State Transport University», 9, Moskovsky prospect, St. Petersburg, 190031, Russia; phone +7 (812) 315-26-21; fax: +7 (812) 315-26-21;
E-mail: perminov-n@mail.ru.

Перминов Николай Алексеевич, кандидат технических наук, главный специалист института ГУП «Ленгипроинжпроект», доцент «Петербургского государственного университета путей сообщения Императора Александра I»; 190031, Россия, г. Санкт-Петербург, пр. Московский, д. 9, тел. +7 (812) 315-26-21; факс +7 (812) 315-26-21;
E-mail: perminov-n@mail.ru.

TO THE ASSESSMENT OF VERTICAL CRANE LOAD

Sergii F. Pichugin, Yulia E. Patenko
Poltava National Technical Yuri Kondratyuk University, Poltava, UKRAINE

Abstract: The problems of analytical and statistical modeling of the travelling cranes loads are carried out in the paper. The analytical model was expanded by the consideration of influence of the approach of cranes trolley, consideration of zero realization areas and crane impact zones which allowed to precise the statistical characteristics of the vertical crane loads. The numerical modeling which takes into account the accidental position of the crane bridge and position of the trolley on the crane bridge was used for the calculation the vertical crane loads from the four-wheel cranes. Comparison of the results showed that the design value of the vertical load per wheel is rarely realized. This fact should be used to clarify the crane load combination factors.

Keywords: cranes loads**,** analytical model, numerical modeling, combination factor

К ОЦЕНКЕ ВЕРТИКАЛЬНОЙ КРАНОВОЙ НАГРУЗКИ

С.Ф. Пичугин, Ю.Э. Патенко
Полтавский национальный технический университет имени Юрия Кондратюка, г. Полтава, УКРАИНА

Аннотация: В статье рассмотрены проблемы аналитического и статистического моделирования нагрузок мостовых кранов. Аналитическая модель была расширена за счет учета влияния сближения тележек кранов, учета областей нулевой реализации и зон воздействия кранов, что позволило уточнить статистические характеристики вертикальных крановых нагрузок. Численное моделирование, которое учитывает случайное положение мостового крана и положение тележки на мостовом кране, использовалось для расчета вертикальных нагрузок от воздействия четырехколесных кранов. Сравнение результатов показало, что расчетное значение вертикальной нагрузки на колесо реализуется редко. Этот факт следует использовать для уточнения коэффициента сочетания крановых нагрузок.

Ключевые слова: крановые нагрузки, аналитическая модель; численное моделирование, коэффициент сочетания

INTRODUCTION

The overhead travelling cranes which operate in real workshops transmit on the structures the complex loads. The determination of this loads by the full scale investigations in a real industrial building is very complicated due to the great complexity of tests. In this regard, statistical modeling of crane loads is justified for the clarification the reliability estimations of structures. Vertical loads from the influence of bridge cranes on the constructions under real-life conditions have a number of features, such as the close connection with the technological process of industrial buildings (IB), the specificity of the transmission on the structure, the dynamic nature, the probabilistic nature, etc. The paper considers some specific features of the realization of crane loads.

1. ANALYSIS OF RECENT RESEARCHES AND PUBLICATIONS

The problems of overhead travelling cranes actions which operate in the IB were examined in the monograph [1] and in work [2]. The detailed description of crane loads through the different probabilistic techniques were done in [3-5], where also the quantitative estimation of reliability of steel structures under crane loads were performed. Comparative analysis of

different travelling crane producers was done in the paper [6].

Further development the probabilistic models and the calculation of numerical characteristics values from vertical and horizontal crane loads is done in [7]. The values of mathematical expectation, variance and standard for vertical and horizontal components of crane load were received analytically. The time factor, stochastic nature of loads and the strength of steel were taken into account to reveal an effect of different parameters (cranes capacity and mode of cranes, columns step, type of connection the column and girder, type of roofing, wind and snow loads) on the reliability of steel frameworks of IB [8, 9]. A moderate number of random variables were taken into account in the work [10]. Notwithstanding, some random factors weren't taken into account. The random factors such as position of the crane bridge and position of the trolley on the crane bridge were considered in statistical modelling [11] where were suggested to include load combination factors into the calculation formulas using the temporary load with combinational value which should be reduced by the particular load combination factor for each new temporary load.

2. INFLUENCE OF THE APPROACH OF CRANES TROLLEY

In case of the permanent equipment placement in the workshop is unchanged, the vertical load can be determined taking into account the actual location of the crane maintenance zones and the actual approach of the trolley to the columns.

Vertical pressure of the crane wheel, could be calculated by:

$$\tilde{F}\left[\frac{G_{cr}}{2}\left(\tilde{Q}G_{crab}\right)\frac{\tilde{a}}{L_{cr}}\right]\frac{1}{n_0}, \qquad (1)$$

where G_{cr} – weight of crane; $\tilde{Q}$ – accidental value of lifting capacity of crane; G_{crab} – weight of crab; $\tilde{a}$ – accidental value of maximum closure of the crane hook to the column; L_{cr} – crane span; n_0 – number of crane wheels.

The random pressure of the wheel $\tilde{F}$ is a function of two accidental arguments $\tilde{Q}$ and $\tilde{a}$, which are multiplied in (1). As a result, the distribution $f(\tilde{F})$ may vary depending on the distribution of the arguments $f(\tilde{Q})$ and $f(\tilde{a})$, and their correlation.

We will consider the distribution of the expression

$$Z = XY$$

of random variables, one of which X is distributed by the normal distribution law, another Y – by the uniform law:

$$f(X) = \frac{1}{\hat{X}\sqrt{2\pi}} exp\left[-\frac{X^2}{2\hat{X}^2}\right];$$
$$-\infty < X < \infty, \bar{X} = 0;$$
$$f(Y) = \frac{1}{\beta-\alpha}, \alpha \leq Y \leq \beta. \qquad (2)$$

The distribution function $F(z)$ is defined as:

$$F(z) = P\left((X,Y)CD\right) =$$
$$= \int_{(D)}\int f(X,Y)dXdY.$$

The domain of integration is in this case a band of width $\beta-\alpha$, which extends from $-\infty$ to the intersection with a hyperbola $Z = XY$, at the same time the projection of the section of the intersection on the X axis has a length $\frac{z}{\beta} - \frac{z}{\alpha}$.

$$F(Z) = \int_{-\infty}^{Z/\beta} dX \int_{\alpha}^{\beta} \frac{1}{\beta-\alpha}\frac{1}{\hat{X}\sqrt{2\pi}} exp\left(-\frac{X^2}{2\hat{X}^2}\right)dy +$$
$$+ \int_{-\infty}^{Z/\beta} dX \int_{\alpha}^{i/X} \frac{1}{\beta-\alpha}\frac{1}{\hat{X}\sqrt{2\pi}} exp\left(-\frac{X^2}{2\hat{X}^2}\right)dy.$$

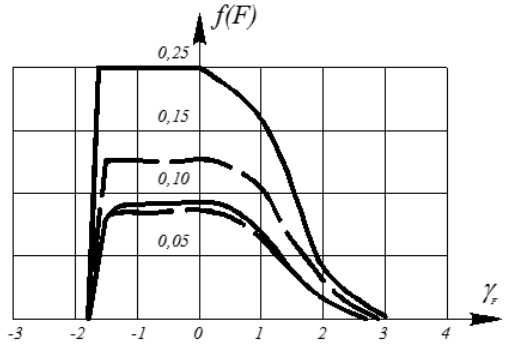
For $f(Z) = F(Z)$, after the reduction we obtain the expression:

$$f(Z) = \frac{1}{\hat{X}\sqrt{2\pi}(\beta - \alpha)} \times \times \int_{\frac{z}{\beta}}^{Z/\propto} \frac{1}{X} exp\left(-\frac{X^2}{2\hat{X}^2}\right) dX. \quad (3)$$

Using this expression for the vertical load (1), we obtain for the density of distribution:

$$f(F) = \frac{L_{cr} n_0}{\sqrt{2\pi}(\beta - \alpha)\hat{F}} \times \times \int_b^a \frac{1}{Q} exp\left[-\frac{(Q - \bar{Q} - G_T}{2\hat{G}^2}\right] dQ. \quad (4)$$

a)



b)

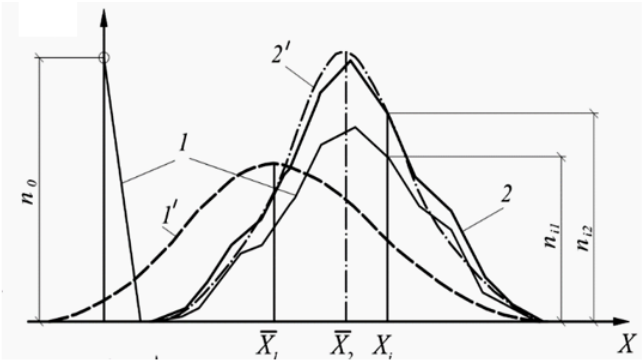


Figure 1. Distribution of vertical crane loads:
a) vertical pressure on a wheel of cranes of different load-carrying capacity;
b) ordinates of crane load processes.
Legend: 1 and 1 '– empirical and normal distributions for the process;
2 and 2' – the same for a process without zeros.

Boundaries of integration:

$$a = \left(F - \frac{G_M}{2n_0}\right)\frac{L_{cr} n_0}{\propto} - G_T;$$
$$b = \left(F - \frac{G_M}{2n_0}\right)\frac{L_{cr} n_0}{\beta} - G_T.$$

An example of load distribution on a crane wheel, constructed according to the derived expression (4), is shown in Fig. 1, a.

On the basis of the theorem on the numerical characteristics of the product of random variables were determined:

– wheel pressure mathematical expectation:

$$\bar{F} = \left[\frac{G_M}{2} + (\bar{Q} G_T)\frac{(\propto + \beta)}{2L_{cr}}\right]\frac{1}{n_0}; \quad (5)$$

– wheel pressure standard:

$$\hat{F} = \hat{Q}^2 \frac{(\beta - \alpha)^2}{12{L_{cr}}^2 {n_0}^2}(\bar{Q} + G_T)^2 \times \times \frac{(\beta + \alpha)^2}{12{L_{cr}}^2 {n_0}^2} + \frac{(\beta + \alpha)^2}{4{L_{cr}}^2 {n_0}^2}. \quad (6)$$

The reducing coefficient for the taking into account the limitation of the trolley crane approach is proposed for the calculation the vertical load:

$$l = \frac{F^H(p)}{F^H}, \quad (7)$$

where $F^H(p)$ and F^H are the standard pressures with the same probability $[P]$, respectively, with the passport approaching to the considered range of columns y_0 and with the limitation of approaching $y_{min} = y_0 + pL_{cr}$.

In case of impossibility of approaching to a range of columns at a distance y_{min} actual and nominal load on the column and crane beam the considered row:

$$F_{max}^{fact} = \left[\frac{G_{cr}}{2} + \left(\frac{Q + G_{crab}}{0{,}5n}\right)\frac{L_{cr} - y_0}{L_{cr}}\right]\sum Y;$$

$$F_{max} = \left[\frac{G_{cr}}{2} + \left(\frac{Q + G_{crab}}{0{,}5n}\right)\frac{L_{cr} - y_{min}}{L_{cr}}\right]\sum Y,$$

where G_{cr} and G_{crab} – respectively the weight of the crane and crab; n – number of wheels of the crane; y_0 – passport minimum trolley approximation to the row of columns considered; $\sum Y$ – the sum of the ordinates of the influence lines.

We designated the ratio

$$k = \frac{Q + G_T}{G_M}$$

and took into account the expression

$$y_{min} = y_0 + pL_{cr}$$

we obtained:

$$l = 1 - \frac{pkL_{cr}}{2L_{cr} + k(L_{cr} - y_0)}. \quad (8)$$

It is considered that the statistical picture of the change of vertical loads with limited approach of cranes and in usual cases with the absence of approaches – remains unchanged. This assumption goes to the safety margin, which leads to an increase of the factor *l* in comparison with the actual values. Expression (8) defines a minimum limit for reducing the vertical load and provides a significant reduction of loads in a number of cases (on average, the load is reduced by 10 ... 12%). The values of the coefficients *l* = 0,76 ... 0,94 were recommended for practical calculations when *p* = 0,1 ... 0,4.

3. CONSIDERATION OF ZERO REALIZATION AREAS

Realization of crane influences on a structure usually takes into account breaks in loading – zero areas. Such character of loads influences on the numerical characteristics of crane loads. Below is shown the analytical approach to taking into account zero areas of implementation of vertical loads of bridge cranes.

In the case of statistical processing of continuous realization of crane loads, the stationary random process $\tilde{X}_1(t)$ is divided into time intervals Δt, which gives, after framing, the bimodal distribution of the process ordinates, the estimation of the statistical mean $\bar{X}_1$ and the dispersion $\hat{X}_1$. The normal distribution constructed according to these characteristics does not correspond to the experimental distribution, therefore, it is interesting to pass to the random process $\tilde{X}_2(t)$ without zero sections with numerical characteristics $\bar{X}_2$ and $\hat{X}_2$, for which the ordinates of distribution are close to the normal law.

Thus, the detailed characteristics of the random process $\tilde{X}_1(t)$ for the vertical loads of bridge cranes with a flexible suspension were detailed:

$$\bar{X}_1 = (1 - n_0)(0{,}66 - 0{,}243\eta);$$

$$X_1 = (1 - n_0) \times \times [0{,}017 + +n_0(,66 - 0{,}243\eta)^2];$$

$$\hat{X}_1 = \sqrt{(1 - n_0)[0{,}017 + n_0(,66 - 0{,}243\eta)^2]}.$$

4. CONSIDERATION OF THE CRANE IMPACT ZONES

The value of n_0 may be considered as a possibility of the absence of a bridge crane in the considered zone of influence and defined as $n_0 = 1 - p_1$, where p_1 – is the probability of a crane stay in the zone of influence under the condition of its operation.

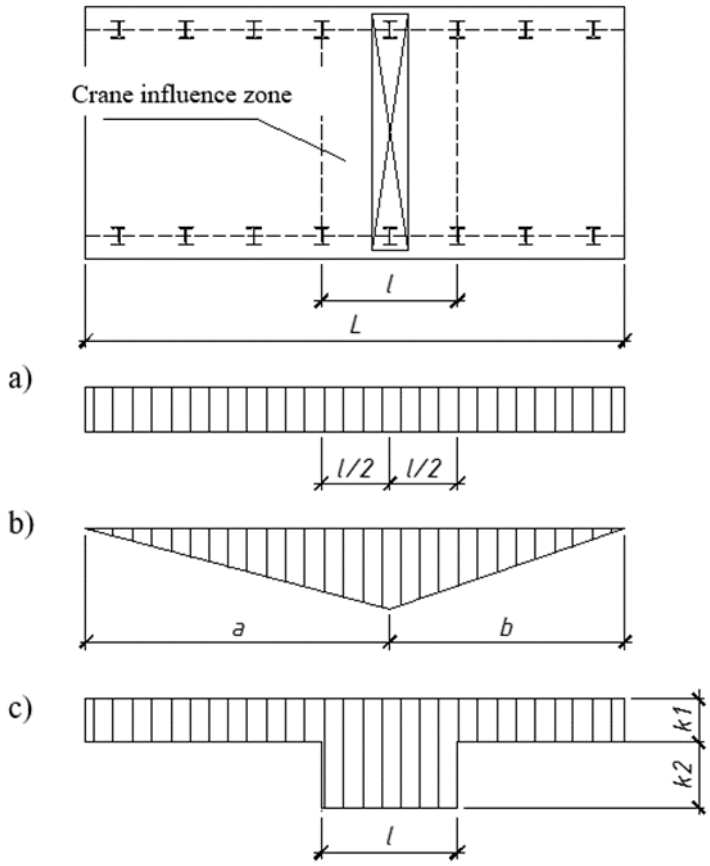


Figure 2. To determination of the probability of crane stay in the zone of influence: a) 1-st scheme of intensity of work; b) 2-th scheme of intensity of work; c) 3-rd scheme of intensity of work.

Value p_1 depends on the peculiarities of the technological process in the span of the IB. The three schemes of intensity of work of bridge cranes practically completely cover possible technological situations in spans, shown in Fig. 2.
The first scheme – is described by a uniform distribution (Fig. 2, a). In this case, the probability of staying the crane in the zone of influence is defined as $p_1 = l/L$, where l – the length of the zone of influence; L – total length of the crane zone.
Then the frequency of zero load values is defined as:

$$n_0 = 1 - \frac{l}{L} = \frac{L - l}{L}.$$

The second scheme is described by a triangular distribution (Fig. 2, b). The probability of a crane stay in the zone of influence is determined as follows:
Then the expression for the desired frequency will look like:

$$n_0 = \frac{b(a + 0{,}5l)^2 + a(b + 0{,}5l)^2}{aL}.$$

If $a = b = 0{,}5l$ the values p_1 and n_0 will be follows:

$$p_1 = 2\frac{l}{L} - \left(\frac{l}{L}\right)^2, \qquad n_0 = \frac{(L - l)^2}{L^2}.$$

The third scheme is described by a uniform distribution, and the intensity of the technological process in the zone of influence is k times higher than outside (Fig. 2, c). Ordinaries of density on areas are:

$$k_1 = \frac{1}{(k+1)(L-l)};$$
$$k_2 = \frac{k}{l(1+k)}.$$

Thereby the probability of a crane in the zone of influence is:

$$p_1 = k_2 l = \frac{k}{1+k}.$$

Then the frequency is:

$$n_0 = k_1(L-l) = \frac{1}{1+k}.$$

5. NUMERICAL MODELLING OF CRANE LOADS

Recent numerical studies [11] have shown that these combination factors of loads are too high. Due to the low probability of implementing the most disadvantageous position of all bridge cranes with maximum loads, it is possible to reduce the combination factors of efforts.

Modern programs allow to take into account many variables. Such an approach is realized by prof. A.V. Perelmuter in the development of a load calculation program [11]. This program was used for the calculations the loads of bridge cranes with a payload of 32/16,5t. Accidental values for each of the bridge cranes were:

- the position of the cranes on the crane girders;
- the load weight;
- the position of the trolleys on the bridge of the crane.

The distributions obtained by the modelling were close to the distributions constructed by the analytical method (Fig. 1, a). Load values were calculated at different positions of the crane with different weight of the load (Fig. 3, items 1-6):

- 1 – a crab without a load near the right range of columns;
- 2 – a crab with a load, near the right range;
- 3 – a crab without a load, near the left range;
- 4 – a crab with a load, located in the middle of the span;
- 5 – a crab with a load, near the left range, the weight is equal to the average load-carrying capacity Qav;
- 6 – a crab with a load near the left range, the weight is Qav + 2.5Qst (Qst - the standard load-carrying capacity);
- 7 – a crab with a weight, near the left range, the weight is Qav + 3.5Qst.

The polygons of vertical loads on the crane wheel, normalized by the value $Q + G_{cr} + G_{crab}$, showed that most of the values of the polygon are concentrated between the estimated values of positions 2 and 4 (Fig. 3). The characteristic value of the vertical load, calculated in accordance with the requirements of the norms DBN [12] (position 5), is in the zero zone, that shows, the characteristic value is rarely realized.

In addition, the vertical loads on the column of the IB with span 22,5 m were numerically modeled. The length of the building is 120 meters, the span of crane girder is 6 meters. Crane base is 5,1 meters, the overall dimension of crane is 6,3 meters, minimum approach to the column is 1,5 meters. The polygons of vertical loads on the crane wheel and the column of the IB which were received by the numerical modelling (Fig. 2) are similar to the above-described distributions of the ordinates of crane load processes with zero zones (Fig. 1, b):

- Cr 1 Fnom – vertical load on the crane wheel;
- Cr 1 N – vertical load on the column from the influence of one crane;
- Cr 2 N – vertical load on the column from the influence of two cranes;
- Cr 2 N2 – vertical load on the column from the influence of four cranes.

The comparative loads were put on the abscissa axis. The comparative loads are the modelling loads (q) which were divided by the design load values (q_d). The ordinate axis was trimmed for the better visualization.

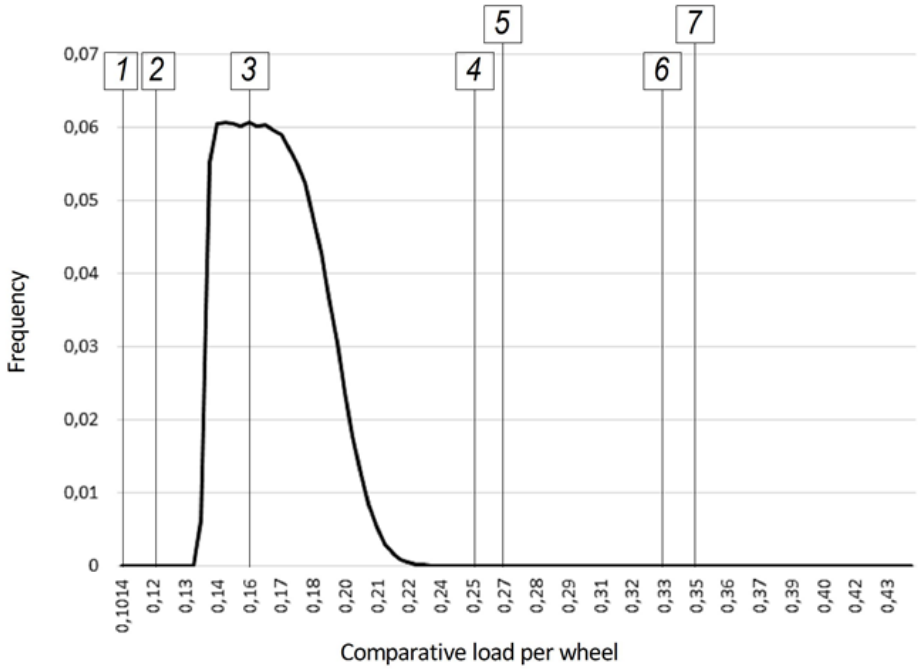


Figure 3. Polygon of the vertical loads on the wheel.

The resulting vertical load on the crane wheel (Fig. 4) are within the range of 0,4 ... 0,6 of the calculated load, while the loads on the column from one, two and four cranes have values from 0 to 0,4 of the calculated load on column. The greater part of the vertical load on the column (up to 87 % of the tests) have zero values.

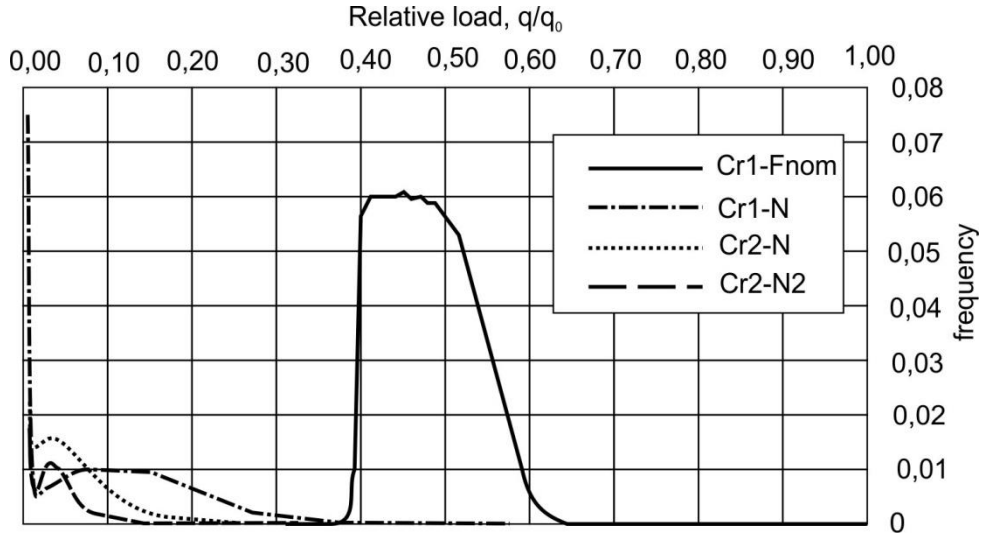


Figure 4. Vertical loads polygons on the wheel and on the IB column.

6. CONCLUSIONS

Due to the great difficulty of experimental investigations of the crane loads, which have the complicated statistical nature, it is possible to consider analytically such special features of these loads as a trolley approximation, zero crane operation zones and crane impact zones. Nowadays statistical computer modelling can take into account a greater number of variable

parameters (position of the cranes in the span, position of the crab on the bridge crane, crane position relative to each other). Comparison of polygons of vertical load on the crane wheel with the analytical results showed that design value of load, calculated according codes DBN realizes very rarely. The further numerical modeling of loads arises an interest for obtaining a more precise definition of the load combination factors and efforts in the structures of industrial buildings.

REFERENCES

1. **Pichugin S.F.** Kranovyye Nagruzki na Stroitel'nyye Konstruktsii [Crane Loads on Building Structures]. Poltava, OOO "ASMI", 2014 (in Russian).
2. **Gordeyev V.N., Lantukh-Lyashchenko A.I., Makhin'ko A.V., Pashinskiy V.A., Perel'muter A.V., Pichugin S.F.** Nagruzki i Vozdeystviya na Zdaniya i Sooruzheniya [Loads and Impacts on Buildings and Structures]. Moscow, SCAD Soft, ASV, 2011, 514 pages (in Russian).
3. **Pichugin S.F., Demchenko N.A.** Reliability of Crane Loads. Poltava, PNTU, 2005, 91 pages.
4. **Pichugin S.** Analysis of Bridge Crane Loads on Industrial Buildings. // *XLIV Konferencja Naukowa KILiW PAN i KN PZITB*, Tom 7, Poznan-Krynica, 1998, pp. 171-178.
5. **Pichugin S.** Probabilistic Description of Crane Load on Building Structures. // *XLIII Konferencja Naukowa KILiW PAN i KN PZITB*, Tom III, Poznan-Krynica, 1997, pp. 171-178.
6. **Pichugin S.F., Patenko Iu.E., Maslova S.A.** Comparative Analysis of Loads from the Travelling Cranes of Different Producers. // *International Journal of Engineering and Technology*, 2018, Vol. 7 (3.2), pp. 36-39.
7. **Pichugin S.F., Patenko Iu.E., Maslova S.A.** Probabilistic Numerical Characteristics of Loads of Overhead Cranes on Framewokrs of Industrial Buildings. // *Academic Journal. Series: Industrial Machine Building, Civil Engineering*, 2018, Vol. 1(50), pp. 62-68.
8. **Pichugin S.** Reliability Estimation of Steel Elements under Variable Loads. // *XLI Konferencja Naukowa KILiW PAN i KN PZITB*. "Krynica 1995", Tom 3, Krakow-Krynica, 1995. pp. 151-156.
9. **Pichugin S.F., Patenko Iu.E.** Reliability of Steel Frameworks of Industrial Buildings. // METNET International Seminar, 11-12 October, 2017, Cottbus, Germany, 2018, pp. 83-93.
10. **Pasternak H., Rozmarynowski B., Wen Y.-K.** Crane Load Modelling. // *Structural Safety*, 1996, Vol. 17, pp. 205-224.
11. **Perel'muter A.V.** Statisticheskoye Modelirovaniye Kranovykh Nagruzok i Raschetnyye Sochetaniya Usiliy [Crane Loads Statistical Modelling and Design Combinations of the Internal Forces]. // *International Journal for Computational Civil and Structural Engineering*, 2017. Volume 13, Issue 2, pp. 136-144 (in Russian).
12. DBN V.1.2-2:2006. Navantazhennya i vplyvy: [Chynnyy vid 2007-01-01] / Minbud Ukrayiny. Kiev, Vyd-vo "Stal'", 2006, 60 pages.

СПИСОК ЛИТЕРАТУРЫ

1. **Пичугин С.Ф.** Крановые нагрузки на строительные конструкции. – Полтава: ООО «АСМИ», 2014.
2. **Гордеев В.Н., Лантух-Лященко А.И., Пашинский В.А., Перельмутер А.В., Пичугин С.Ф.** Нагрузки и воздействия на здания и сооружения. – Москва, SCAD Soft, АСВ, ДМК Пресс, 2011. – 514 с.
3. **Pichugin S.F., Demchenko N.A.** Reliability of Crane Loads. Poltava, PNTU, 2005, 91 pages.
4. **Pichugin S.** Analysis of Bridge Crane Loads on Industrial Buildings. // *XLIV*

Konferencja Naukowa KILiW PAN i KN PZITB, Tom 7, Poznan-Krynica, 1998, pp. 171-178.

5. **Pichugin S.** Probabilistic Description of Crane Load on Building Structures. // *XLIII Konferencja Naukowa KILiW PAN i KN PZITB*, Tom III, Poznan-Krynica, 1997, pp. 171-178.
6. **Pichugin S.F., Patenko Iu.E., Maslova S.A.** Comparative Analysis of Loads from the Travelling Cranes of Different Producers. // *International Journal of Engineering and Technology*, 2018, Vol. 7 (3.2), pp. 36-39.
7. **Pichugin S.F., Patenko Iu.E., Maslova S.A.** Probabilistic Numerical Characteristics of Loads of Overhead Cranes on Framewokrs of Industrial Buildings. // *Academic Journal. Series: Industrial Machine Building, Civil Engineering*, 2018, Vol. 1(50), pp. 62-68.
8. **Pichugin S.** Reliability Estimation of Steel Elements under Variable Loads. // *XLI Konferencja Naukowa KILiW PAN i KN PZITB*. "Krynica 1995", Tom 3, Krakow-Krynica, 1995. pp. 151-156.
9. **Pichugin S.F., Patenko Iu.E.** Reliability of Steel Frameworks of Industrial Buildings. // METNET International Seminar, 11-12 October, 2017, Cottbus, Germany, 2018, pp. 83-93.
10. **Pasternak H., Rozmarynowski B., Wen Y.-K.** Crane Load Modelling. // Structural Safety, 1996, Vol. 17, pp. 205-224.
11. **Перельмутер А.В.** Статистическое моделирование крановых нагрузок и расчетные сочетания усилий. // *International Journal for Computational Civil and Structural Engineering / Международный журнал по расчету гражданских и промышленных конструкций*, 2017. Volume 13, Issue 2, pp. 136-144.
12. ДБН В.1.2-2:2006 Навантаження і впливи [Чинний від 2007-01-01]. Мінбуд України. – К. : Вид-во «Сталь», 2006. – 60 с.

Sergii F. Pichugin, Doctor of Sciences, Professor, Head of the Department of Metal, Wooden and Plastic Structures; Poltava National Technical Yuri Kondratyuk University; 36011, Ukraine, m. Poltava, Pershotravnevyj Ave. 24, phone: +380 5325 61604; e-mail: vstup@pntu.edu.ua.

Yulia E. Patenko, Candidate of Technical Sciences, Associated Professor, Department of Descriptive Geometry and Graphics; Poltava National Technical Yuri Kondratyuk University; 36011, Ukraine, m. Poltava, Pershotravnevyj Ave. 24, phone: +380 5325 61604; E-mail: vstup@pntu.edu.ua.

Пичугин Сергей Федорович, доктор технических наук, профессор, заведующий кафедрой конструкций из металла, дерева и пластмасс; Полтавский национальный технический университет имени Юрия Кондратюка; Першотравневий проспект, 24, Полтава, Полтавська область, Украина, 36000; тел. +380 5325 61604; e-mail: vstup@pntu.edu.ua.

Патенко Юлия Эдуардовна, кандидат технических наук, доцент кафедры начертательной геометрии и графики; Полтавский национальный технический университет имени Юрия Кондратюка; Першотравневий проспект, 24, Полтава, Полтавська область, Украина, 36000; тел. +380 5325 61604; E-mail: vstup@pntu.edu.ua.

THE STUDY OF COMPLEX STRESS STATES OF ELEMENTS FILLING THE CELLS BETWEEN THE RIBS OF WOODEN LARGE-SPAN DOMES

Konstantin P. Pyatikrestovsky, Boris S. Sokolov
JSC "Research Centre "Construction", Moscow, RUSSIA

Abstract: The article is devoted to the research of complex stress states of anisotropic materials under long-term loads. The article considers the design of criteria for short-term and long-term strengths proposed by G.A. Geniev in connection with the calculation of large-span structures of domes of laminated and solid wood, where the enclosure elements are included in the joint work with the power set in the form of meridional and circular ribs. In this case, the elements of an enclosure-plate are at a complex stress state and they work under compression with a shift. Joint work of such systems was studied by experiments on large-scale models and experimental construction. Large reserves of strength resistance are revealed. In particular, in 1985, the indoor skating rink at the stadium "Lokomotiv" was built as an experimental facility which implemented these conditions and it has been successfully operated for many years. However, there are some unsolved issues with the refinement of the actual operation of the structures and the development of the calculation algorithm. Some generalizations of the studied approaches are given.

Keywords: long-span structures, glued wood, mechanical models of anisotropic material, strength criteria, long-term strength, shifting forces

ИССЛЕДОВАНИЕ СЛОЖНЫХ НАПРЯЖЕННЫХ СОСТОЯНИЙ ЭЛЕМЕНТОВ ЗАПОЛНЕНИЯ ЯЧЕЕК МЕЖДУ РЕБРАМИ БОЛЬШЕПРОЛЕТНЫХ КУПОЛОВ ИЗ ДРЕВЕСИНЫ

К.П. Пятикрестовский, Б.С. Соколов
Научно-исследовательский центр «Строительство», г. Москва, РОССИЯ

Аннотация: Статья посвящена исследованиям сложных напряженных состояний анизотропных материалов при длительных воздействиях нагрузок. Рассматривается построение критериев кратковременной и длительной прочности, предложенное Г.А. Гениевым, в связи с расчетом большепролетных конструкций куполов из клееной и цельной древесины, в которых элементы ограждения включаются в совместную работу с силовым набором в виде меридиональных и кольцевых ребер. При этом элементы ограждения – плиты – оказываются в сложном напряженном состоянии и работают при сжатии со сдвигом. Совместная работа таких систем изучалась экспериментально на крупномасштабных моделях и опытном строительстве. Выявлены большие резервы силового сопротивления. В частности, в 1985 году построен экспериментальный объект: крытый каток на стадионе «Локомотив», на котором реализованы указанные предпосылки, и он успешно эксплуатируется много лет. Однако остались некоторые нерешенные вопросы с уточнением действительной работы конструкций и построением алгоритма расчета. Исследуются дощато-гвоздевые плиты различной толщины при длительном воздействии сдвигающих усилий. Даются некоторые обобщения исследуемых подходов.

Ключевые слова: большепролетные конструкции, клееная древесина, механические модели анизотропного материала, критерии прочности, длительная прочность, сдвигающие усилия

Current state of timber building is characterized by mass appliance of large span and tall structures. Domes and similar to dome structures of envelopes are widespread among large span structures and multi-storey residential building, for example 30-storey buildings in Canada, are spread among tall structures. In Russia, currently 4 - 9-storey residential buildings are constructed. The feature of such buildings and structures is appliance of glued wood elements of large cross section and especial internal forces distribution between elements. In some case it is required cross section sizes, which exceed technological possibilities of timber structure plants, and it leads to use structures like trusses.

However, there are another possibilities to decrease cross section sizes, which are provided by designing of statically undetermined systems of high order of indetermination that leads to joint work of neighbor elements that is to creation of spatial structures. In this case such system allows plastic deformations and has property to redistribute internal forces that gives economic effect based on the material consumption decreasing.

There is a system of meridional and ring ribs in spatial structures like a dome. The cells between ribs can be filled by envelope structures such a shield, panel or brace. At the same time, the elements, filling these cells, work at complex stress state (compression, tension and shear), if the ribs are subjected stresses action as it is inherent to linear structures.

Calculation of such structures linked with some troubles and requires introduction of strength theories and criteria that can be incomprehensible for specialists of design institutions.

There are a large number theoretical and experimental investigation of wood strength at two-dimensional stress states, for example [1-7] and etc. The majority of authors, which are classic today, recognize that such theories are hard to practical appliance.

G.A. Geniev [2, 8-10] devoted many years to develop practically applicable strength criteria for different materials.

Despite the main provisions for Geniev strength criteria are published [2, 10, 11], let us present in the paper derivation of long term strength criterion for anisotropic material and example of it usage, and apply such criterion to investigate two-dimensional stress state of envelopes of a large span dome.

Mechanical and physical models of long term strength for anisotropic material.

The mechanic model of anisotropic material is presented in Figure 1. This one gives analytical and quantitative performance of long term and dynamic strength on the basis of general physical concept in the wide range of load action time, from a few days or several months to tenth or hundredth part of second.

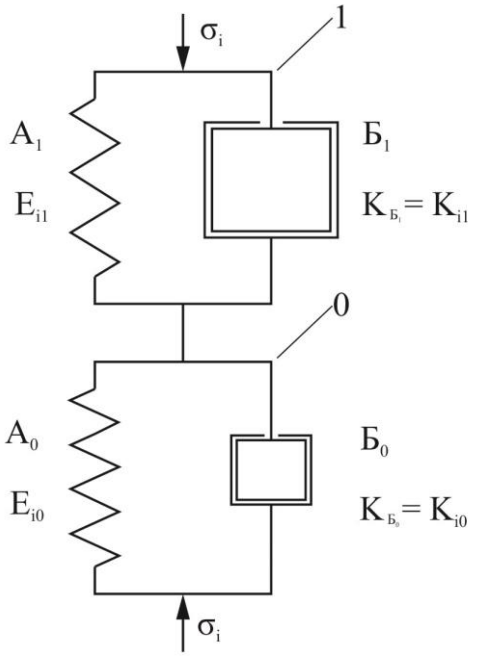


Figure 1. Mechanical model of anisotropic material.

The model consists of two elements connected in series and signed in figure 1 as 0 and 1. Each element represents by Kelvin-Voigt model of parallel connected elements A_0 and B_0, A_1 and B_1, which are characterized by different values of strength and deformation parameters.

The element signed in figure 1 as 0 is intended to represent analytically the process of material quick time deformation; element signed in fig-

ure 1 as 1 is intended to represent long time deformation, linked with creep.

Components A_0 and A_1 correspond to elastic deformation of material. Components B_0 and B_1 correspond to viscous properties only. Rigidity of B_1 element significantly exceed that one of B_0, that is the modulus of viscous resistance K_{B1} exceed modulus K_{B0} by several orders: $K_B >> K_{B0}$. At impact of resultant external force σ_i to mechanical model, including elements 0 and 1, where i = x, y are main axes of anisotropy, the effective time of element B_0 work continues during small part of second. However during this little time range (t_0) the element B_0 promotes to decrease force value, which acts to element A_0 (parts of σ_i), and decrease intensity of deformation developing of A_0, that determines fact of dynamic strength exceeding of strength obtained during standard experiments, when duration is measured by minutes.

Effective time of B_1 element work is commensurate with large time range, corresponding to calculations of long time strength, taking into account accumulation of resultant deformations of 0 and 1 elements during adjusted time t_d.

There are not any mathematical difficulties at analytical representation of mechanical model of material work.

However, from practice position, it is more expedient the divided approach to determine long term and dynamic strength of anisotropic material, since time ranges t_d and t_0 take values of different orders. Really, at determining of long term strength (time scale t_0), the element B_0 work practically do not influence to result, and at determining of dynamic strength (time scale t_d) the element 1 work cannot be occurring during this time range.

In this way, it is expedient to apply the following modification of general mechanical model of material, presented in figure 1. At determination of long term strength, it is necessary to exclude element B_0 from element 0, using A_0 element connected in series with element 1, as it is shown in figure 2. And at determination of dynamic strength it is necessary to exclude element 1 entirely using only element 0, that consists of parallel connected elements A_0 and B_0, as it is shown in figure 3.

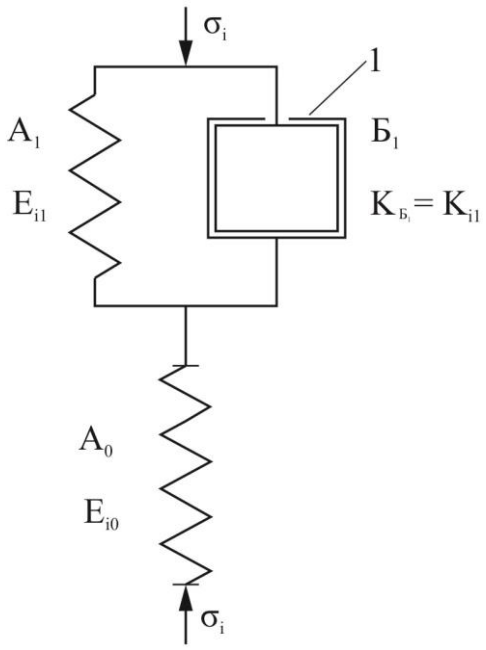


Figure 2. Long term strength mechanical model.

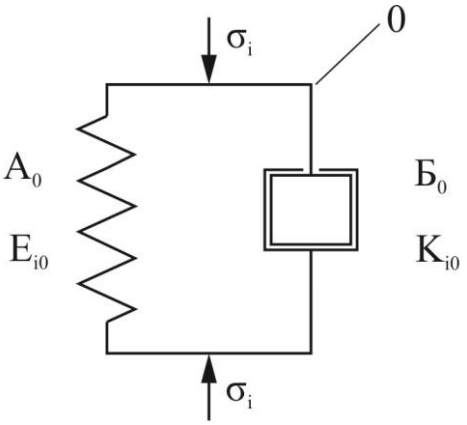


Figure 3. Dynamic strength mechanical model.

The long term and dynamic strength criteria for anisotropic material such as wood, which are obtained in the paper, are formulated for finite elementary material volume, subjected to homogenous complex two-dimensional stress state.

Short term strength criteria of anisotropic material.

In accordance with [2] and [9], three independent mechanisms of anisotropic material destruction are possible. It is tear (tension), crumpling

(compression) and shear, realization of which depends on the type of stress state at reviewing point of solid. These mechanisms may occur at short term action of external loading, that corresponds to time of standard experiments, as well as at long term and dynamic loading action.

One of the main features of the ultimate states of anisotropic materials is difference between dangerous plane orientation for tear, crumpling and shear cases and directions of main normal stresses and greatest tangential stresses in general case.

In accordance with it, the criteria of short term strength for anisotropic material, obtained in the papers [2] and [9], are derived on the basis of the following obvious premises:

- for tear case

$$\frac{d}{d\varphi}\left[\sigma_n(\varphi) - R_p(\varphi)\right] = 0, \qquad (1)$$

- for crumpling case

$$\frac{d}{d\varphi}\left[\sigma_n(\varphi) + R_c(\varphi)\right] = 0, \qquad (2)$$

- for shear case

$$\frac{d}{d\psi}\left[\tau_m(\psi) - R_{c\partial}(\varphi)\right] = 0, \qquad (3)$$

where $\sigma_n(\varphi)$ and $\tau_m(\psi)$ are normal and tangential stresses acting at dangerous planes of tear, crumpling and shear, the direction of which are determined by unknown angles φ and ψ; $R_p(\varphi)$, $R_c(\varphi)$ and $R_{c\partial}(\psi)$ are absolute values of ultimate normal and tangential stresses at tear, crumpling and shear, obtained from experiments at action of one-dimensional tension, compressive and shear stresses as angle functions of φ and ψ.

Wherein

$$\left.\begin{aligned}\sigma_n(\varphi) &= \frac{\sigma_x + \sigma_y}{2} + \frac{\sigma_x - \sigma_y}{2}\cos 2\varphi \\ &+ \tau_{xy}\sin 2\varphi; \\ \tau_m(\psi) &= \frac{\sigma_x - \sigma_y}{2}\sin 2\psi \\ &- \tau_{xy}\cos 2\psi,\end{aligned}\right\} \qquad (4)$$

where σ_x, σ_y, τ_{xy} are normal and tangential stresses, acting along main anisotropy directions (along and across fibers in wood), φ and ψ are angles between axis X and normal to planes, as well as

$$\left.\begin{aligned}R_p(\varphi) &= R_{px}\cos^2\varphi + R_{py}\sin^2\varphi; \\ R_c(\varphi) &= R_{cx}\cos^2\varphi + R_{cy}\sin^2\varphi; \\ R_{c\partial}(\psi) &= C_x\cos^2\psi + C_y\sin^2\psi;\end{aligned}\right\} \qquad (5)$$

where R_{px}, R_{py} are values of short term ultimate strength at tear along axis X and У (along and across fibers);

R_{cx}, R_{cy} are values of short term ultimate strength at crumpling along axes X and У;

C_x and C_y are values of short term ultimate strength at shear along planes, the normal of which coincide with axes X and У.

On the basis of theses presented above and derivations the following analytical relationships for short term strength criteria of anisotropic materials are obtained in the papers [2] and [9]:

- for tear case

$$\left(R_{px} - \sigma_x\right)\left(R_{py} - \sigma_y\right) - \tau_{xy}^2 = 0, \qquad (6)$$

- for crumpling case

$$\left(R_{cx} + \sigma_x\right)\left(R_{cy} + \sigma_y\right) - \tau_{xy}^2 = 0, \qquad (7)$$

- for shear case

$$\left(\sigma_x - \sigma_y\right)^2 - 4\left(C_x + \tau_{xy}\right)\left(C_y - \tau_{xy}\right) = 0. \qquad (8)$$

Long term strength criteria for anisotropic material

As it is outlined above, it is expedient to use mechanical model presented in figure 2 to determine long term strength of anisotropic materials.

At applying of resultant external long term force to connected in series elements 0 (A0) and 1 (A1, B1), the integral resultant deformations take the form

$$\varepsilon_i = \varepsilon_{i0} + \varepsilon_{i1};$$
$$\begin{pmatrix} \varepsilon_x = \varepsilon_{x0} + \varepsilon_{x1}, \\ \varepsilon_y = \varepsilon_{y0} + \varepsilon_{y1}, \\ \varepsilon_{xy} = \varepsilon_{xy0} + \varepsilon_{xy1} \end{pmatrix}. \qquad (9)$$

Separate ultimate strength values (at tear, crumpling and shear) are determined at reaching by resultant deformations values ε_i it corresponding ultimate ones – $Э_{i0} \rightarrow (Э_{x0}, Э_{y0}, Э_{xy0})$, that equals to ultimate deformations of A_0 element at short term external load acting

$$-Э_{i0} = \frac{R_i}{E_{i0}}:$$
$$Э_{x0} = \frac{R_x}{E_{x0}}\ ;\ Э_{y0} = \frac{R_y}{E_{y0}};\ Э_{xy0} = \frac{R_{xy}}{E_{xy0}} \qquad (10)$$

where

$R_x = R_{px}$ or R_{cx}, $R_y = R_{py}$ or R_{cy}, $R_{xy} = C_x$ or C_y;

E_{x0}, E_{y0} and E_{xy0} are linear elastic modulus of A_0 element through the directions X and Y (along and across fibers) and it generalized shear modulus respectively.

Element 1 deformations ε_{i1} are determined on the basis of the following obvious relations

$$\sigma_i = \sigma_{iA1} + \sigma_{iБ1};$$
$$\sigma_{iA1} = E_{i1}\varepsilon_{i1};\ \sigma_{iБ1} = K_{i1}\frac{d\varepsilon_{i1}}{dt}, \qquad (11)$$

where E_{i1} is the generalized elastic modulus of A_1 element, K_{i1} is viscous resistance modulus of B_1 element. On the basis of (11) we obtain

$$\frac{d\varepsilon_{i1}}{dt} + \frac{E_{i1}}{K_{i1}}\varepsilon_{i1} = \frac{\sigma_i}{K_{i1}},$$
$$\text{and at } t = 0,\ \varepsilon_{i1} = 0\ - \qquad (12)$$
$$\varepsilon_{i1} = \frac{\sigma_i}{E_{i1}}(1 - e^{-\omega_{i1}t}),\ \omega_{i1} = \frac{E_{i1}}{K_{i1}}.$$

Thus, in accordance with (9) we obtain:

$$\varepsilon_i = \frac{\sigma_i}{E_{i0}}\left[1 + \delta_i\left(1 - e^{-\omega_{i1}t}\right)\right] = \frac{\sigma_i}{E_{i0}}\Psi_i(t), \qquad (13)$$

where

$$\delta_i = E_{i0} / E_{i1}.$$

In accordance with (10) and (13), the long term strength ultimate values of anisotropic material through main anisotropy direction take the form $\overline{R}_i = \overline{R}_i(\bar{t}_\partial)$:

$$\overline{R}_i = \sigma_i = \frac{E_{i0}\varepsilon_i}{\Psi_i(t_\partial)} = \frac{E_{i0}Э_{i0}}{\Psi_i(t_\partial)} = \frac{R_i}{\Psi_i(t_\partial)};$$
$$\overline{R}_x = \frac{R_x}{\Psi_x(t_\partial)};$$
$$\overline{R}_y = \frac{R_y}{\Psi_y(t_\partial)}; \qquad (14)$$
$$\overline{R}_{xy} = \frac{R_{xy}}{\Psi_{xy}(t_\partial)},$$

where

$$\Psi_x(t_\partial) = 1 + \delta_x\left(1 - e^{-\omega_{x1}t_\partial}\right) > 1;$$
$$\Psi_y(t_\partial) = 1 + \delta_y\left(1 - e^{-\omega_{y1}t_\partial}\right) > 1; \qquad (15)$$
$$\Psi_{xy}(t_\partial) = 1 + \delta_{xy}\left(1 - e^{-\omega_{xy1}t_\partial}\right) > 1,$$

and $t = t_\partial$ is adjusted ultimate time of external long term load action.

Thus, long term strength of anisotropic material determination linked with changing or rather decreasing of short term strength values through main anisotropy directions in accordance with relationships (14) and (15). Introducing (14) into (6), (7), (8), we obtain finally the relationships for long term strength criteria of anisotropic material related with parameter t_∂ :

– for tear case

$$\left[\frac{R_{px}}{\Psi_{px}(t_\partial)}-\sigma_x\right]\left[\frac{R_{py}}{\Psi_{py}(t_\partial)}-\sigma_y\right]-\tau_{xy}^2=0, \quad (16)$$

– for crumpling case

$$\left[\frac{R_{cx}}{\Psi_{cx}(t_\partial)}+\sigma_x\right]\left[\frac{R_{cy}}{\Psi_{cy}(t_\partial)}+\sigma_y\right]-\tau_{xy}^2=0, \quad (17)$$

– for shear case

$$(\sigma_x-\sigma_y)^2- -4\left[\frac{C_x}{\Psi_{xy}(t_\partial)}+\tau_{xy}\right]\left[\frac{C_y}{\Psi_{xy}(t_\partial)}-\tau_{xy}\right]=0 \quad (18)$$

Criteria (16), (17), (18) (besides short term ultimate strength R_{px}, R_{py}, R_{cx}, R_{cy}, C_x, C_y) include three non-dimensional parameters

$$\delta_x=\frac{E_{x0}}{E_{x1}};\ \delta_y=\frac{E_{y0}}{E_{y1}};\ \delta_{xy}=\frac{E_{xy0}}{E_{xy1}},$$

and three dimensional values ω_{i1} (sec^{-1}) —

$$\omega_{x1}=E_{x1}/K_{x1},\ \omega_{y1}=E_{y1}/K_{y1},\ \omega_{xy1}=E_{xy1}/K_{xy1}.$$

Numerical values δ_i and ω_{i1} are determined on the basis of experimental data. The results of δ_i and ω_{i1} determination for wood are presented in the paper below

Presented criteria of long term strength (16), (17), (18) allows to obtain the λ parameter value, corresponding a fracture mechanism of anisotropic material, on the basis of relations between stresses $\sigma_x:\sigma_y:\tau_{xy}$ and accepted time of long term load action t_∂. Inverse problem formulation is determination t_d values on the basis of accepted values of $\lambda\rightarrow(\lambda_0, \lambda_c, \lambda_{c\partial})$.

Determination of characteristics, applying at calculation of long term strength of wood, is carried out in [10] on the basis of G.A. Geniev proposals for anisotropic materials. The results of experimental studies of long term resistance of spruce wood, provided by N.L. Leontiev from 1950 to 1955, are used in the paper [15,16].

Experimental data, characterizing decreasing percent of spruce wood ultimate strength in comparison with corresponding values of ultimate short term strength $\overline{R}_i(t_\partial)$, obtained in accordance with load action time t_∂, measuring in days, are presented in figure 5 (a), (b), (c).

For all three types of spruce wood resistance, the relationships

$$\overline{R}_{px}(t_\partial)/R_{px},\ \overline{R}_{cx}(t_\partial)/R_{cx},\ \overline{R}_{xy}(t_\partial)/R_{xy} \quad (19)$$

at $t_\partial\rightarrow\infty$ (at practically non limited load action time) with enough accuracy order it appears equal to 0.5, that is, maximum decreasing of long term strength is 50 % from short term one. It allows to evaluate values of δ_x and δ_{xy} parameters on the basis of [17] as well as reviewed experimental result ($\Psi_x(\infty)=\Psi_{xy}(\infty)=1/0{,}5=2$), that is

$$\delta_x=\delta_{xy}=1. \quad (20)$$

Below, the value of resistance across to fibers δ_y accepted equal to 1.

Analytical approximation of wood long term resistance graphs allows to determinate the following values of ω_{x1} :

– at tension – $\omega_{x1}=1{,}65\cdot10^{-3}$ сут.$^{-1}$
– at compression – $\omega_{x1}=2{,}50\cdot10\text{-}3$ сут.$^{-1}$ (21)
– at chopping – $\omega_{xy1}=7{,}25\cdot10\text{-}3$ сут.$^{-1}$

Values ω_{y1} at resistance across fibers in accordance with significant creep influence in this

main direction of anisotropy ($K_{y1} < K_{x1}$) are accepted equal to:

– at tension – $\omega_{y1} = 3{,}30 \cdot 10^{-3}$ days^{-1},
– at compression – $\omega_{y1} = 5{,}00 \cdot 10\text{-}3$ days^{-1} (22)
– at shear – $\omega_{xy1} = 7{,}25 \cdot 10\text{-}3$ days^{-1}.

Let us to present numerical example of wood long term strength determination at following values of it strength parameters corresponding to time of short term (standard) tests:

R_{px} = 14.4 MPa, R_{py} = 2.4 MPa,
R_{cx} = 22.8 MPa, R_{cy} = 3.8 MPa, (23)
C_x = 19.2 MPa, C_y = 6.4 MPa.

Let us to carried out calculation of long term strength at the following times

t_∂ = 150 days, t_∂ = 300 days,
t_∂ = 1000 days and $t_\partial \to \infty$.

At the case of simple (proportional) loading, the stress values along main anisotropy directions σ_x, σ_y, τ_{xy} are:

$$\sigma_x = \lambda\xi_x, \quad \sigma_y = \lambda\xi_y, \quad \tau_{xy} = \lambda\eta_{xy}, \qquad (24)$$

where $\xi_x : \xi_y : \eta_{xy}$ are accepted relations between stress values, λ is parameter of long term external load.
Substituting relationships (24) into criteria of long term strength [10, 12] and solving it for λ, we obtain three following quadratic equation for $\lambda = \lambda_0$ values (tear case), $\lambda = \lambda_c$ (crumpling case) and $\lambda = \lambda_{sh}$ (shear case):

$$\left(\xi_x\xi_y - \eta_{xy}^2\right)\lambda_0^2 - \left[\frac{R_{px}}{\Psi_{px}(t_\partial)}\xi_y + \frac{R_{py}}{\Psi_{py}(t_\partial)}\xi_x\right]\lambda_0 + \frac{R_{px}R_{py}}{\Psi_{px}(t_\partial)\Psi_{py}(t_\partial)} = 0; \qquad (25)$$

$$\left(\xi_x\xi_y - \eta_{xy}^2\right)\lambda_c^2 + \left[\frac{R_{cx}}{\Psi_{cx}(t_\partial)}\xi_y + \frac{R_{cy}}{\Psi_{cy}(t_\partial)}\xi_x\right]\lambda_c + \frac{R_{cx}R_{cy}}{\Psi_{cx}(t_\partial)\Psi_{cy}(t_\partial)} = 0; \qquad (26)$$

$$\left[\frac{\left(\xi_x - \xi_y\right)^2}{4} + \eta_{xy}^2\right]\lambda_{c\partial}^2 + \frac{\left(C_x - C_y\right)}{\Psi_{xy}(t_\partial)}\eta_{xy}\cdot\lambda_{c\partial} - \frac{C_xC_y}{\Psi_{xy}^2(t_\partial)} = 0. \qquad (27)$$

Let us to accept relation between stresses equal to:

$$\xi_x : \xi_y : \eta_{xy} = 2 : (-1) : 1, \qquad (28)$$

that is

ξ_x = 2 (tension along fibers)
ξ_y = -1 (compression across fibers)
η_{xy} = 1
(shear in plane formed by main axes x, y).

In accordance with (20), (21), (22) it is obtained:

$\Psi_{px}(150) = 1.2192$; $\Psi_{py}(150) = 1.3904$;
$\Psi_{cx}(150) = 1.3127$; $\Psi_{cy}(150) = 1.5276$;
$\Psi_{xy}(150) = 1.6629$; $\Psi_{px}(300) = 1.3904$;
$\Psi_{py}(300) = 1.6284$; $\Psi_{cx}(300) = 1.5276$;
$\Psi_{cy}(300) = 1.7769$; $\Psi_{xy}(300) = 1.8864$;
$\Psi_{px}(1000) = 1.808$; (29)
$\Psi_{py}(1000) = 1.9631$; $\Psi_{cx}(1000) = 1.9179$;
$\Psi_{cy}(1000) = 1.9933$; $\Psi_{xy}(1000) = 1.9993$;
$\Psi_{px}(0) = \Psi_{py}(0) = \Psi_{cx}(0) =$
$= \Psi_{cy}(0) = \Psi_{xy}(0) = 1$;
$\Psi_{px}(\infty) = \Psi_{py}(\infty) = \Psi_{cx}(\infty) =$
$= \Psi_{cy}(\infty) = \Psi_{xy}(\infty) = 2$.

The values λ_0, λ_c, λ_{sh} presented in Table 1 are obtained from equations (25-27). The reduced values of these ones, presented in Table 1, are obtained from relationships

Table 1. Parameters.

t_∂ *days*	Tear λ_0	Crumpling λ_c	Shear λ_{sh}	Tear Ψ_0	Crumpling Ψ_c	Shear Ψ_{sh}
0	5.3523	3.4079	4.4873	1	1	1
150	4.3489	2.2551	2.6985	0.8125	0.6617	0.6014
300	3.8064	1.9387	2.3788	0.7112	0.5689	0.5301
1000	2.9427	1.7146	2.2444	0.5498	0.5031	0.5002
∞	2.6762	1.7039	2.2437	0.5	0.5	0.5

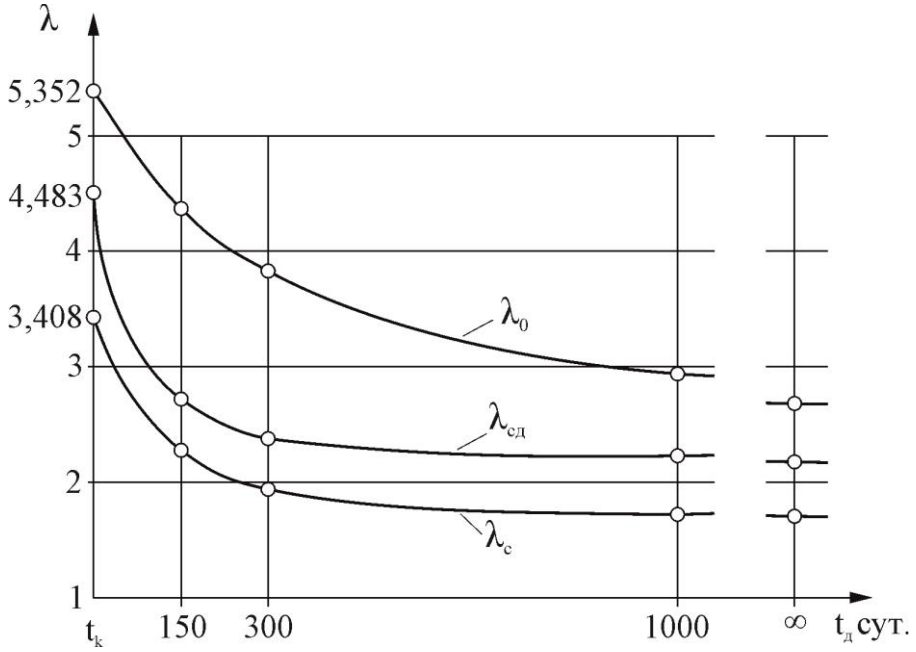


Figure 4. Graphs of external loading parameters $\lambda_0, \lambda_c, \lambda_{sh}$ changing in time, obtained by table 1.

$$\Psi_0 = \frac{\lambda_0(t_\partial)}{\lambda_0(0)}, \quad \Psi_c = \frac{\lambda_c(t_\partial)}{\lambda_c(0)}, \quad \Psi_{c\partial} = \frac{\lambda_{c\partial}(t_\partial)}{\lambda_{c\partial}(0)}, \quad (30)$$

which explicitly characterize material long term strength changing in time.

Thus, at all values of t_d we obtain:

$$\lambda_o > \lambda_{c\partial} > \lambda_c, \quad (31)$$

that is, in the reviewed example external load parameter takes the smallest value, that corresponds to wood destruction caused by crumpling (values λ_c in table 1).

Wherein, the values of ultimate stresses acting along main anisotropy directions are:

$\sigma_x(150)$ = 8.6978 МПа, $\sigma_y(150)$ =
= -2.2551 MPa, τ_{xy} = 2.6985 MPa;
$\sigma_x(300)$ = 7.7548 MPa, $\sigma_y(300)$ =
=-1.9387 MPa, τ_{xy} = 2.9387 MPa; (32)
$\sigma_x(1000)$= 3.4292 MPa, σ_y (1000) =
= -1.7146 MPa, τ_{xy} = 1.7146 MPa.

The graphs of relations between parameters of external loading λ_0 , λ_c , λ_{sh} and time t_d, obtained in accordance with table 1 data are presented in figure 4.

It should be noted that

$$\psi_0 > \psi_c = \psi_{sh},$$

that is, relative (reduced) values of external loading parameter for shear case ψ_{sh} are changed (decrease) in time greater than ψ_c.

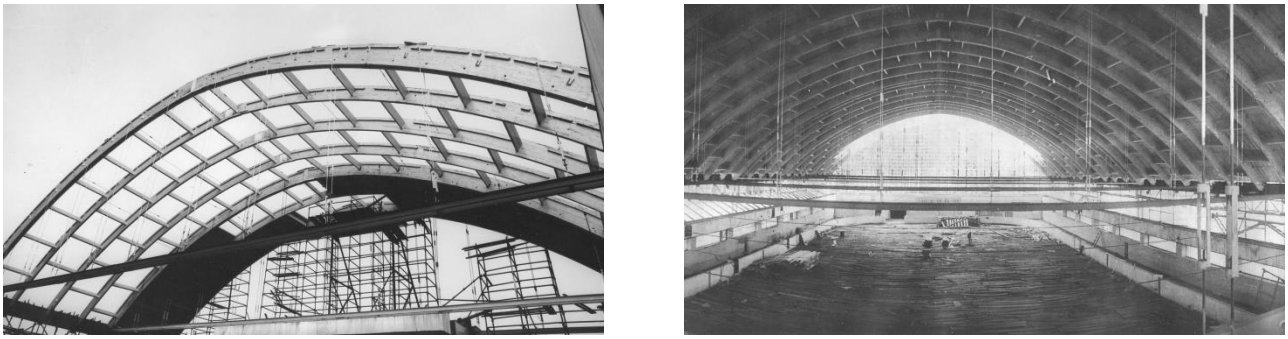


Figure 5. Assembling of short cylindrical shell of 42 m span.

Presented calculation results show calculation principles for anisotropic envelopes subjected plane stress state at long term action of static, though changing in time, loadings. Such computation can be easily programmed and at real designing it can be accepted a row of control points, in which the stress-strain state and coefficients, correcting ultimate stresses of material, are determined. It is supposed that thickness of envelope structure is enough to work without local buckling. Here, the anisotropy of material, subjected complex stress state, and duration of loading action are taken in account.

The entire calculation of shell [11] in accordance with envelope structures shows significant influence of envelopes to resistance against normal and especially shear forces.

It is chosen the simplest construction of cells filling between the ribs in the form of shield, made of cross placed planks jointed by nails, to analyze.

In construction of cylindrical shell which is shown in figure 4, the panels in the form of frame, made of planks of 40 mm thickness and enveloped at lower side by planks of 25 mm thickness, are applied. Due to including such approach to filling cells between ribs, it is reached appliance of ribs with height of section about 1/56 of span [11].

On the basis of general calculation of structure under shear forces, it is obtained main parameters of shields.

The average values of the cell sizes are accepted 2.49 x 2.49 m, the quantity of planks of 13 cm thickness for each layer of shield is 19. The nails quantity at two nails placing in each intersection of planks equals to $19^2 \cdot 2 = 722$. At shield shift, caused by shear, nails cause wood crumpling at contact zone. Bearing capacity of it is determined in accordance with codes $T = 0.8\, a \cdot d \cdot n = 0.8 \cdot 4 \cdot 0.3 \cdot 722 = 693$ kN.

Here d is nail diameter (cm), a is shield thickness, n is nail quantity.

Shear stresses at maximum shift after PC computation are

$$\tau = \frac{\sum T}{b \cdot l} = \frac{693}{0.04 \cdot 2.49} = 6957.8\, kN/\mathrm{m}^2 = 6.96 \text{ MPa}.$$

Obtained value of tangential stress τ is significantly exceed calculation strength even against chopping across fibers 0.8 MPa. In accordance with computation, provided in the paper [11], such shear stress can be reached at 38^{th} stage only at loading 28 kPa and integral exposure during 2580 days (7 years).

Let us present computation results corresponding to 27th stage of loading at 6 kPa and initial exposure during 1980 days (5.42 years) at constant load acting from one side. In this way, the maximum compressive stress is 1.45 MPa. At load value 2 kPa it takes value 0.5 MPa.

It is carried out calculations of reviewed dome at another sizes and thickness of shields to compare. At 2 cm thickness and 2 kPa loading the maximum stresses are equal to 2.43 MPa, and at 8 cm thickness and such loading the stress values decrease to 1.0 MPa.

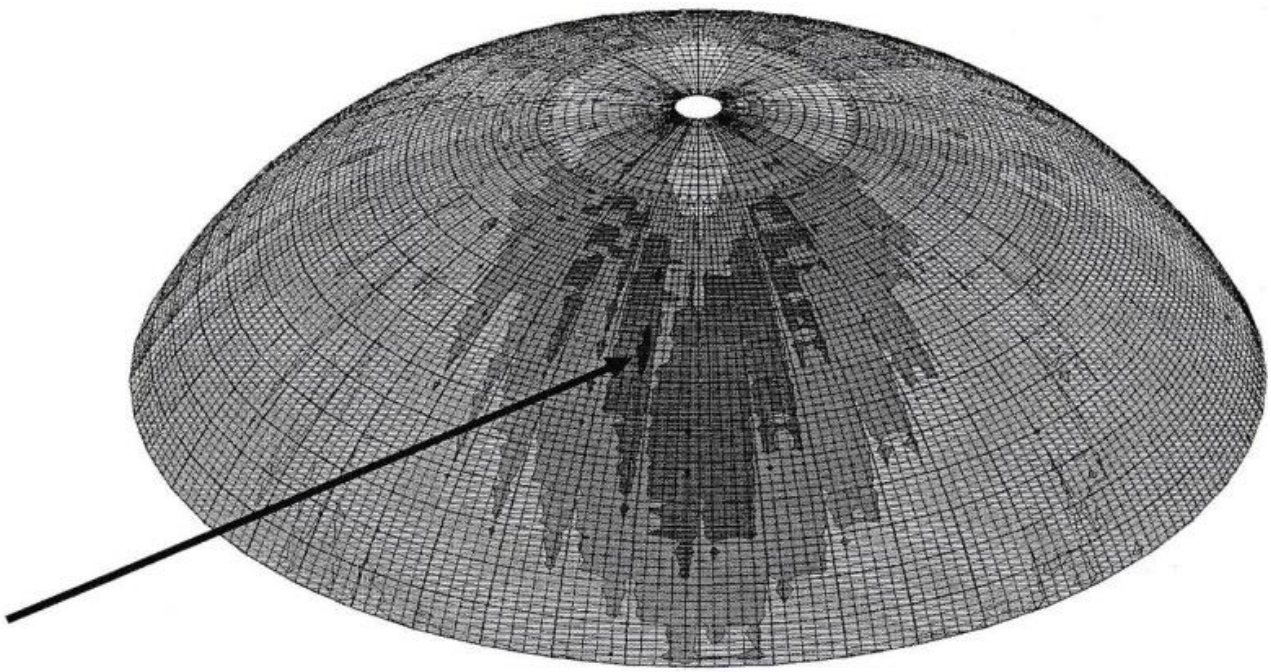


Figure 6. Maximum shear stresses zone.

It is seen, that instead plank shields it can be applied filling by composite material of high strength and small thickness as well as of porous materials of low thermal conductivity.

Construction can resist against load of high intensity during long time at meridional ribs of reduced height of cross section to 1/60 dome diameter. It shows that dome provides high order of structural safety and can be applied to erect structure, operating at hard condition of environmental and technogenic impacts.

CONCLUSIONS

Currently it is required new approaches to develop designing codes, that should take in account complex stress states and contain proposals to effective computation by PC. At the same time, it necessary to simplify techniques of calculation and apply simple strength criteria.

It is expedient to provide row of experimental investigations for two and three-dimensional loading to effective applying of reviewed criteria. It is required to develop new generation designing codes, such as it was carried out 1950th, when ultimate state calculation method was introduced.

Simplifying of PC computation can be reached by automation of the most stressed sections searching, when at each iteration step and deformation modulus correction provides at one section only, and parameters of other section corresponds to linear relationship or parabola in accordance with moment distribution along structure.

Also, there are some problems that requires of experimental investigations at large scale or natural samples. At first, it deals with increasing accuracy of shear stresses distribution between own shear resistance of elements and supporting parts and connections resistance.

REFERENCES

1. **Ashkenazi E.K.** Prochnost' Anizotropnykh Drevesnykh i Sinteticheskikh Materialov [Strength of Anisotropic and Synthetic Materials]. Moscow, Lesnaya promyshlennost', 1966, 166 pages (in Russian).
2. **Geniev G.A.** O Kriterii Prochnosti Drevesiny pri Ploskom Napryazhennom

Sostoyanii [About Wood Strength Criterion at Two-Dimensional Stress State]. // *Stroit. Mekhanika i Raschet Sooruzhenij*, 1981, No. 3, pp. 15-20 (in Russian).

3. **Gol'denblat I.I. Kopnov V.A.** Kriterii Prochnosti i Plastichnosti Konstruktsionnykh Materialov [Strength and Plasticity Criteria of Construction Materials]. Moscow, "Mashinostroenie", 1968, 191 pages (in Russian).
4. **Ezepov G.G.** Prochnost' Drevesiny pri Dvukhosnom Napryazhennom Sostoyanii. Diss. Kand. Tekhn. Nauk [Wood Strength at Two-Dimensional Stress State. Thesis of Cand. Sci. in Tech.]. Moscow, 1986, 142 pages (in Russian).
5. **Orlovich R.B., Ezepov G.G., Najchuk A.YA.** K Otsenke Nekotorykh Kriteriev Prochnosti Anizotropnykh Tel pri Ploskom Napryazhennom Sostoyanii [Evaluation of Strength Criteria for Anisotropic Solids at Plane Stress State]. // Tekhnika, Tekhnologiya, Organizatsiya i Ehkonomika Stroitel'stva: Respublikanskij Mezhvedomstvennyj Sbornik. – Vypusk 10: Stroitel'naya Mekhanika i Stroit. Konstruktsii. Minsk: Vyshejshaya shkola, 1984, pp. 124-127 (in Russian).
6. **Pyatikrestovskij K.P., KHunagov KH.S.** Pereraspredelenie Usilij v Ehlementakh Shatrovoj Obolochki iz Drevesiny i Fanery pri Nesimmetrichnykh Nagruzkakh [Stress Redistribution into Elements of Wood and Plywood Shells in the Form of Tent at Non-Symmetric Loadings]. // V Knige "Issledovaniya i Metody Rascheta Stroitel'nykh Konstruktsij". Moscow, TSNIISK im. V. A. Kucherenko, 1985, pp. 40-49 (in Russian).
7. **Flakserman A.N.** Vliyanie Naklona Volokon na Mekhanicheskie Svojstva Drevesiny Sosny [Fiber Slope Influence to Mechanical Properties of Pine Wood]. // Tr. TSAGI, Vyp. 78, GONTI, Moscow – Leningrad, 1931, pp. 48 (in Russian).
8. **Geniev G.A., Kurbatov A.S.** O Predel'nykh Prochnostnykh Zavisimostyakh dlya anizotropnykh materialov pri sdvige [Ultimate strength relations for anisotropic materials at shear] // Metody rascheta i optimizatsii stroitel'nykh konstruktsij na EHVM. – M.: TSNIISK im. Kucherenko, 1990. – pp. 60-67 (in Russian).
9. **Geniev G.A., Kurbatov A.S., Samedov F.A.** Voprosy Prochnosti i Plastichnosti Anizotropnykh Materialov [Issues on Strength and Plasticity of Anisotropic Materials]. Moscow, Interbuk, 1993, 187 pages (in Russian).
10. **Geniev G.A., Pyatikrestovskij K.P.** Voprosy Dlitel'noj i Dinamicheskoj Prochnosti Anizotropnykh Konstruktsionnykh Materialov [Issues on Long Term and Dynamic Strength of Anisotropic Materials]. Moscow, GUP TSNIISK im. V.A. Kucherenko, 38 pages (in Russian).
11. **Pyatikrestovskij K.P., Sokolov B.S.** Nelinejnyj Raschet Staticheski Neopredelimykh Derevyannykh Konstruktsij i Optimizatsiya Razmerov Sechenij Reber Kupolov [Nonlinear Calculation of Statically Undefined Wood Structures and Cross Section Optimization for Dome Ribs]. // *Sb. tezisov VII Mezhdunarodnogo Simpoziuma "Aktual'nye Problemy Komp'yuternogo Modelirovaniya Konstruktsij i Sooruzhenij"*, Novosibirsk, 2018 (in Russian).
12. **Pyatikrestovskij K.P.** Raschet Rebristykh Prostranstvennykh Konstruktsij iz Drevesiny i Fanery na Dlitel'nye Nagruzki [Calculation of Wood and Plywood Spatial Ribbed Structures at Long Term Loadings]. // *Stroitel'naya Mekhanika i Raschet Sooruzhenij*, 2008, No. 5, pp. 42-48 (in Russian).
13. **Leont'ev N.L.** Uprugie Deformatsii Drevesiny [Elastic Deformations of Wood]. Moscow, Goslesbumizdat, 1952, 120 pages.
14. **Leont'ev N.L.** Dlitel'noe Soprotivlenie Drevesiny [Long Term Resistance of Wood]. Moscow – Leningrad, 1957, 132 pages.
15. **Zajtsev YU.V.** Modelirovanie Deformatsij i Prochnosti Betona Metodami Mekhaniki Razrusheniya [Concrete Deformation and

Strength Modelling by Fracture Mechanics Methods]. Moscow, “Strojizdat”, 1982, 160 pages.

СПИСОК ЛИТЕРАТУРЫ

1. **Ашкенази Е.К.** Прочность анизотропных древесных и синтетических материалов. – М.: Лесная промышленность, 1966. – 166 с.
2. **Гениев Г.А.** О критерии прочности древесины при плоском напряженном состоянии. // *Строительная механика и расчет сооружений*, 1981, №3, с. 15-20.
3. **Гольденблат И.И. Копнов В.А.** Критерии прочности и пластичности конструкционных материалов. – М.: Издательство «Машиностроение», 1968. – 191 с.
4. **Езепов Г.Г.** Прочность древесины при двухосном напряженном состоянии. Диссертация на соискание ученой степени кандидата технических наук по специальности 01.02.04 – «Механика деформируемого твердого тела». – М., 1986. – 142 с.
5. **Орлович Р.Б., Езепов Г.Г., Найчук А.Я.** К оценке некоторых критериев прочности анизотропных тел при плоском напряженном состоянии. // «Техника, технология, организация и экономика строительства». Республиканский межведомственный сборник. – Выпуск 10: «Строительная механика и строительные конструкции. – Минск: Вышейшая школа, 1984, с. 124-127.
6. **Пятикрестовский К.П., Хунагов Х.С.** Перераспределение усилий в элементах шатровой оболочки из древесины и фанеры при несимметричных нагрузках. // В книге Исследования и методы расчета строительных конструкций. – М.: ЦНИИСК им. В.А. Кучеренко, 1985, с. 40-49.
7. **Флаксерман А.Н.** Влияние наклона волокон на механические свойства древесины сосны. Тр. ЦАГИ, вып. 78, ГОНТИ, М.-Л., 1931г. – с. 48.
8. **Гениев Г.А., Курбатов А.С.** О предельных прочностных зависимостях для анизотропных материалов при сдвиге. // Методы расчета и оптимизации строительных конструкций на ЭВМ. – М.: ЦНИИСК им. Кучеренко, 1990, с. 60-67.
9. **Гениев Г.А., Курбатов А.С., Самедов Ф.А.** Вопросы прочности и пластичности анизотропных материалов. – М.: Интербук, 1993. – 187 с.
10. **Гениев Г.А., Пятикрестовский К.П.** Вопросы длительной и динамической прочности анизотропных конструкционных материалов. – М.: ГУП ЦНИИСК им. В.А. Кучеренко, 2000. – 38с.
11. **Пятикрестовский К.П., Соколов Б.С.** Нелинейный расчет статически неопределимых деревянных конструкций и оптимизация размеров сечений ребер куполов. // *Сб. тезисов VII Международного симпозиума «Актуальные проблемы компьютерного моделирования конструкций и сооружений»*, Новосибирск, 2018.
12. **Пятикрестовский К.П.** Расчет ребристых пространственных конструкций из древесины и фанеры на длительные нагрузки. // *Строительная механика и расчет сооружений*, 2008, №5, с. 42-48
13. **Леонтьев Н.Л.** Упругие деформации древесины. – М.: Гослесбумиздат, 1952. – 120 с.
14. **Леонтьев Н.Л.** Длительное сопротивление древесины. – М.-Л.: Гослесбумиздат, 1957. – 132с.
15. **Зайцев Ю.В.** Моделирование деформаций и прочности бетона методами механики разрушения. – М.: Стройиздат, 1982. – 160 с.

Пятикрестовский Константин Пантелеевич, доктор технических наук, старший научный сотрудник, главный научный сотрудник Центрального научно-исследовательского института строительных конструкций им. В.А. Кучеренко Акционерного общества

«Научно-исследовательский центр «Строительство», 109428, г. Москва, 2-я Институтская улица, дом 6, корп.1; тел. +7 (499) 170-10-81; +7(499)170-15-48;
E-mail: stroymex@list.ru.

Соколов Борис Сергеевич, кандидат технических наук, заведующий лабораторией Научно-исследовательского, проектно-конструкторского и технологического института бетона и железобетона (НИИЖБ) им. А.А. Гвоздева Акционерного общества «НИЦ «Строительство», тел. +7 (499) 174-74-80;
E-mail: moo-shell@mail.ru.

Konstantin P. Pyatikrestovsky, Dr.Sc., Senior Researcher, Executive Researcher of the TsNIISK named after V.A. Kucherenko, JSC Research Center of Construction; 109428, Russia, Moscow, 2-nd Institutskaya Street., 6; phone: +7 (499) 170-10-81; +7 (499) 170-15-48;
E-mail: stroymex@list.ru.

Boris S. Sokolov, Ph.D. in Engineering, Head of the Laboratory for thin-walled and spatial structures, Research and Design Institute for Concrete and Reinforced Concrete (NIIZhB) named after A.A. Gvozdev, JSC Research Center of Construction, Moscow.
phone: +7 (499) 174-74-80;
E-mail: moo-shell@mail.ru.

SEARCHING SHEAR FORCES FLOWS FOR AN ARBITRARY CROSS-SECTION OF A THIN-WALLED BAR: DEVELOPMENT OF NUMERICAL ALGORITHM BASED ON THE GRAPH THEORY

Vitalina V. Yurchenko
Kyiv National University of Civil Engineering and Architecture, Kyiv, UKRAINE

Abstract: Searching problem of shear stresses on outside longitudinal edges of an arbitrary cross-section (including open-closed multi-contour cross-sections) of a thin-walled bar subjected to the general load case has been considered in the paper. Detail numerical algorithm intended to solve the formulated problem using mathematical apparatus of the graph theory has been proposed by the paper. The algorithm is oriented on software implementation in systems of computer-aided design of thin-walled bar structures.

Keywords: thin-walled bar, an arbitrary cross-section, shear forces flow, closed contour, graph theory

ПОИСК ПОТОКОВ КАСАТЕЛЬНЫХ УСИЛИЙ ДЛЯ ПРОИЗВОЛЬНОГО СЕЧЕНИЯ ТОНКОСТЕННОГО СТЕРЖНЯ: РАЗРАБОТКА ЧИСЛЕННОГО АЛГОРИТМА НА ОСНОВЕ ТЕОРИИ ГРАФОВ

В.В. Юрченко
Киевский национальный университет строительства и архитектуры, г. Киев, УКРАИНА

Аннотация: Рассмотрена задача поиска значений потоков касательных усилий для произвольного сечения (открыто-замкнутого многоконтурного сечения) тонкостенного стержня для общего случая нагружения. Разработан детальный алгоритм численного решения сформулированной задачи с использованием математического аппарата теории графов, ориентированный на программную реализацию в системах автоматизированного проектирования тонкостенных стержневых систем.

Ключевые слова: тонкостенный стержень, произвольное сечение, потоки касательных усилий, замкнутый контур, теория графов

INTRODUCTION

Let us consider the problem of shear stresses on longitudinal edges of an arbitrary section of a thin-walled bar that can consist of several closed (connected and/or disconnected) contours and/or also open parts. This problem has been studied by V. I. Slivker [1, 2, 8] for the general loading case of the thin-walled bar.

Further investigation in this area requires development of detail algorithm intended to software implementation in a computer-aided design system for thin-walled bar structures. It is reasonable to construct this algorithm using mathematical apparatus of the graph theory [11].

The graph theory has been applied in [7, 10, 12] for calculation the geometrical sectional properties of thin-walled bars with hybrid (open-closed) types of cross-sections. The graph theory has been also used to analysis of thin-walled bars with multi-contour cross-sections by G. Alfano in [6] and A. Prokić, A [10]. Herewith, the problem of the contoured distribution of shear forces flows for hybrid (including multi-contour, open-closed) thin-walled sections was out of consideration.

1. INITIAL DATA AND SYSTEMS OF COORDINATES

Let us introduce on the plane of thin-walled section the Descartes rectangular system of coordinates *yOz* with origin of the system placed in center of mass of the section (Fig. 1.1), direction of the coordinate system axes coincides with direction of principle axes of inertia *uOv*.

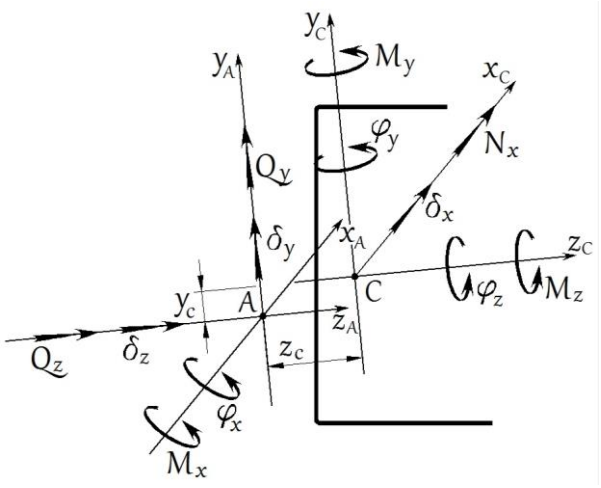


Figure 1.1. Cross-section of a thin-walled bar with indication of positive directions of forces and moments.

Let us introduce in further consideration the system of angular position coordinate with origin of such system in certain (in general case randomly selected) sectional point. Each considered sectional point can be associated with angular position ς. The value ς should be calculated as geometrical length of the curve which is constructed from the origin to the considered sectional point taken along sectional contour. We also assume that increment of the angular position ς corresponds to the positive direction of section path tracing.

We assume that integral geometrical properties of the section are known: A – cross-sectional area, I_y and I_z – second moments of area relating to the main axes of inertia which coincide with axes of global Descartes system of coordinates yOz; I_ω – sectorial moment of inertia; I_t – second moment of area for pure torsion. We also assume that elasticity module E and shear module G are constants for the whole section of the thin-walled bar.

In general case a thin-walled bar is subjected to the action of eight force factors. Axial force N, bending moments M_y and M_z relating to the principle axes of inertia and bi-moment B are applied at the center of mass C (see Fig. 1.1) of the section and caused normal stresses in section $\sigma_i(x,\varsigma)$:

$$\sigma_i(x,\varsigma)=\frac{N(x)}{A}+\frac{M_y(x)}{I_y}z_i(\varsigma)+ \\ +\frac{M_z(x)}{I_z}y_i(\varsigma)+\frac{B(x)}{I_\varpi}\varpi_i(\varsigma) \tag{1.1}$$

where $y_i(\varsigma)$, $z_i(\varsigma)$, $\varpi_i(\varsigma)$ – coordinates and sectorial coordinate of the considered point in cross-section of a thin-walled bar.

Shear forces Q_y and Q_z, free torsion moment M_x and moment of restrained torsion M_ω are applied at the shear center A of the section (Fig. 1.1) and caused shear stresses in cross-section, which can be written in terms of shear forces flows $T_j(x,\varsigma)$ as presented below:

$$\tau_j(x,\varsigma)=\frac{T_j(x,\varsigma)}{\delta_j(\varsigma)} \tag{1.2}$$

where $\delta_j(\varsigma)$ – thickness of considered j^{th} section element.

An arbitrary section of a thin-walled bar can be described by the set of sectional points

$$\mathbf{P}=\left\{\vec{p}_p=\left\{y_p,z_p\right\}\mid p=\overline{1,n_p}\right\}$$

(y_p and z_p – coordinates of p^{th} sectional point in global Descartes coordinate system yOz) and by the set of sectional segments

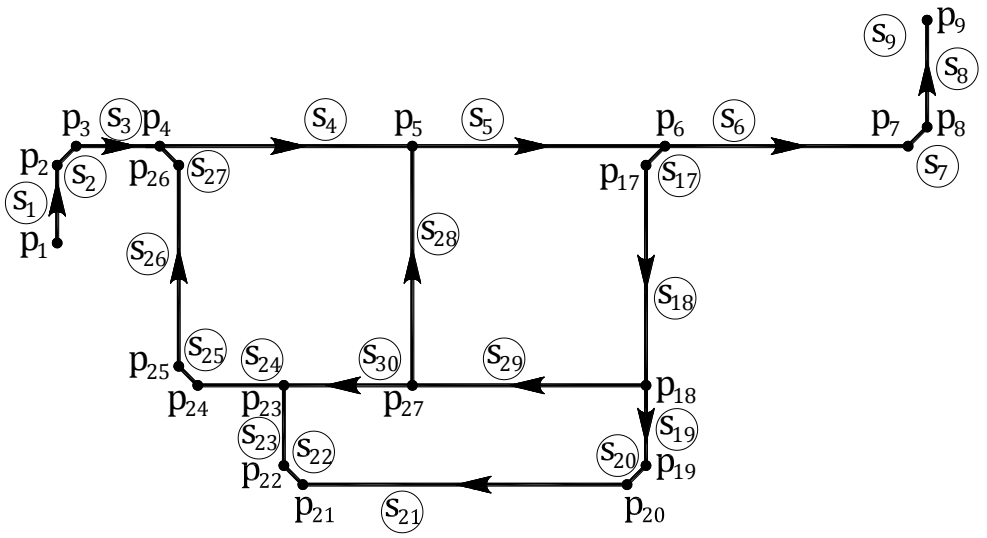


Figure 1.2. Arbitrary cross-section of a thin-walled bar determined on the set of sectional points **P** *and set of sectional segments* **S**.

$$\mathbf{S} = \left\{ \vec{s}_s = \left\{ p_s^{st}, p_s^{end} \right\} \mid s = \overline{1, n_s} \right\},$$

$$\boldsymbol{\varsigma} = \left\{ \vec{\varsigma}_\kappa = \left\{ \varsigma_\kappa^{start}, \varsigma_\kappa^{end} \right\} \mid \kappa = \overline{1, n_\varsigma - 1} \right\}$$

which connect some two sectional points (Fig. 1.2), where n_p and n_s – numbers of sectional points and segments accordingly.
Specified segment thickness

$$\boldsymbol{\delta} = \left\{ \delta_s \mid s = \overline{1, n_s} \right\}$$

corresponds to each sectional segment.
The set of sectorial coordinates

$$\boldsymbol{\omega} = \left\{ \omega_p \mid p = \overline{1, n_p} \right\}$$

and the set of normalized sectorial coordinates

$$\varpi = \left\{ \varpi_p \mid p = \overline{1, n_p} \right\}$$

of the section correspond with the set of sectional points **P**, assuming that the values of the sectorial coordinates and normalized sectorial coordinates in each cross-sectional point are known [4].
The set of angular positions

is actually intended to implement numerical integration taken along thin-walled section contour (for example, when calculating geometrical properties of the cross-section, values of shear forces flows, etc.), where κ – ordinal number of segment, $n_\varsigma - 1$ – number of sectional segments. It should be noted that an angular positions are attributes of the ends of sectional segments.
Initial data about a thin-walled section should be mapped onto the set of angular positions

$$\boldsymbol{\varsigma},\ \kappa = \overline{1, n_\varsigma - 1},$$

by means of formation corresponded sets of sectional segments

$$\mathbf{S}^{\boldsymbol{\varsigma}} = \left\{ \vec{s}_\kappa^{\,\varsigma} = \left\{ \varsigma_\kappa^{start}, \varsigma_\kappa^{end} \right\} : \varsigma_\kappa^{start}, \varsigma_\kappa^{end} \subseteq \boldsymbol{\varsigma} \right\},$$

set of sectorial coordinates

$$\boldsymbol{\omega}^{\boldsymbol{\varsigma}} = \left\{ \vec{\omega}_\kappa^{\,\varsigma} = \left\{ \omega_\kappa^{start}, \omega_\kappa^{end} \right\} : \omega_\kappa^{start}, \omega_\kappa^{end} \subseteq \boldsymbol{\omega} \right\}$$

for ends of sectional segments as well as the set

of thicknesses

$$\boldsymbol{\delta}^{\varsigma} = \left\{ \delta_{\kappa}^{\varsigma} \subseteq \boldsymbol{\delta} \right\}$$

for segments, $\kappa = \overline{1, n_{\varsigma} - 1}$.

2. DISTRIBUTION OF SHEAR FORCES FLOWS TAKEN ALONG CLOSED CONTOURS OF AN ARBITRARY CROSS-SECTION OF THIN-WALLED BAR

2.1. Construction of connected graph $\mathbf{G}^{\varsigma} = \{\mathbf{V}, \mathbf{R}\}$ associated with a section of thin-walled bar.

An arbitrary cross-section of thin-walled bar can be associated with planar connected non-oriented graph $\mathbf{G}^{\varsigma}$ determined on the sets of $\mathbf{G}^{\varsigma} = \{\mathbf{V}, \mathbf{R}\}$, where $\mathbf{V}$ – finite set of graph vertices, $\mathbf{R}$ – the set of graph edges or the set of unordered pairs on $\mathbf{V}$ (see Fig. 2.1) [9]. Herewith, for each graph edge

$$\mathbf{r} = \{u, v\} \in \mathbf{R}$$

we assume that $u \neq v$.

Vertices of the graph $\mathbf{G}^{\varsigma}$ are associated with *characteristic sectional points* only, which are:

1) *branch points* – sectional points connected with more than two sectional segments,

$$\mathbf{v}^{\mathbf{p}} = \left\{ \vec{p}_{v} \mid v = \overline{1, n_{v}} \right\},$$

here n_{v} – number of these points;

2) *end points* – sectional points connected with only one sectional segment

$$\mathbf{v}_{end}^{\mathbf{p}} = \left\{ \vec{p}_{g} \mid g = \overline{1, n_{g}} \right\},$$

here n_{g} – number of these points.

Edges of graph $\mathbf{G}^{\varsigma}$ are associated with sectional parts located between characteristic sectional points (with *unbranched sectional parts*).

An edge of the graph $\mathbf{G}^{\varsigma}$, as a rule, may contain several sectional segments, so full information about edge $\mathbf{R}_{j}^{\varsigma}$ of the graph can be described by the set of sectional segments

$$\vec{s}_{r}^{\varsigma},\ r = \overline{1, n_{\varsigma rj}},$$

from the array

$$\mathbf{S}^{\varsigma} = \left\{ \vec{s}_{\kappa}^{\varsigma} = \left\{ \varsigma_{\kappa}^{start}, \varsigma_{\kappa}^{end} \right\} \mid \kappa = \overline{1, n_{\varsigma} - 1} \right\},\ \vec{s}_{r}^{\varsigma} \in \mathbf{S}^{\varsigma},$$

belonged to considered graph edge, $\vec{s}_{r}^{\varsigma} \in \mathbf{R}_{j}$:

$$\mathbf{R}_{j}^{\varsigma} = \left\{ \vec{s}_{r}^{\varsigma} : \vec{s}_{r}^{\varsigma} \in \mathbf{S}^{\varsigma} \wedge \vec{s}_{r}^{\varsigma} \in \mathbf{R}_{j} \mid r = \overline{1, n_{\varsigma rj}} \right\},$$

here $n_{\varsigma rj}$ – number of segments for j^{th} graph edge. The set of all graph edges defined on the set of segments $\mathbf{S}^{\varsigma}$ can be expressed as

$$\mathbf{R}^{\varsigma} = \left\{ \mathbf{R}_{j}^{\varsigma} \mid j = \overline{1, n_{r}} \right\}.$$

We also assume that an arbitrary section of thin-walled bar may contain some quantity of closed contours. Each closed section contour is associated with cycle of graph $\mathbf{G}^{\varsigma}$ or with vertices cortege v_{0}^{k}, v_{1}^{k}, v_{2}^{k}, ..., v_{n}^{k}, such that

$$v_{i}^{k} \mapsto v_{i+1}^{k} \forall i \Leftrightarrow \exists v_{i+1}^{k},$$

where n_{k} – number of closed contours in section (number of graph $\mathbf{G}^{\varsigma}$ cycles).

Some closed section contour $\boldsymbol{\Gamma}_{k}^{r\varsigma}$ (basic cycle of the graph $\mathbf{G}^{\varsigma}$) can be definitely determined by the set of graph edges $\mathbf{R}_{j}^{\varsigma} \in \mathbf{R}^{\varsigma}$ belonged to the considered contour

$$\boldsymbol{\Gamma}_{k}^{r\varsigma} = \left\{ \mathbf{R}_{j}^{\varsigma} \mid j = \overline{1, n_{r\varsigma\Gamma_{k}}} \right\},$$

where $n_{r\varsigma\Gamma_{k}}$ – number of graph edges belonged to k^{th} closed section contour.

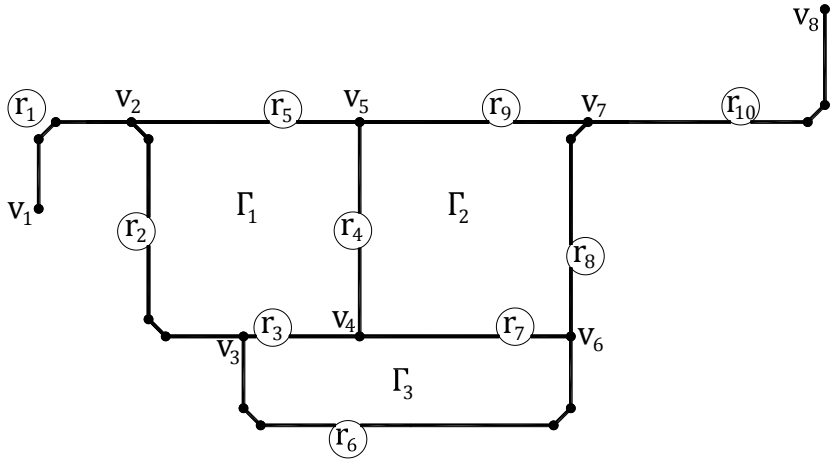


Figure 2.1. Graph $\mathbf{G}^{\varsigma}=\{\mathbf{V},\mathbf{R}\}$ *associated with cross-section of thin-walled bar (graph vertices –* v_1, $v_2 \dots v_{10}$, *graph edges –* r_1, $r_2 \dots r_{13}$*).*

Besides, it's convenient to have the mapping of closed section contour $\mathbf{\Gamma}_k^{r\varsigma}$ onto the set of sectional segments

$$\vec{s}_m^{\,\varsigma},\ \vec{s}_m^{\,\varsigma} \in \mathbf{S}^{\varsigma},$$

belonged to considered closed contour, $\forall m = \overline{1, n_{\varsigma\Gamma_k}}$:

$$\mathbf{\Gamma}_k^{\varsigma} = \left\{ \vec{s}_m^{\,\varsigma} : \begin{bmatrix} \vec{s}_m^{\,\varsigma} \in \mathbf{S}^{\varsigma} \\ \exists \mathbf{R}_\alpha^{\varsigma} \subseteq \mathbf{R}^{\varsigma} : \vec{s}_m^{\,\varsigma} \subseteq \mathbf{R}_\alpha^{\varsigma} \wedge \mathbf{R}_\alpha^{\varsigma} \subseteq \mathbf{\Gamma}_k^{r\varsigma} \end{bmatrix} \right\}$$

here $n_{\varsigma\Gamma_k}$ – number of sectional segments belonged to k^{th} closed section contour.

Closed section contours (basic cycles of the graph $\mathbf{G}^{\varsigma}$) defined on the set of graph edges $\mathbf{R}^{\varsigma}$ and on the set of section segments $\mathbf{S}^{\varsigma}$ can be described as

$$\mathbf{\Phi}^{r\varsigma} = \left\{ \mathbf{\Gamma}_k^{r\varsigma} \mid k = \overline{1, n_k} \right\}$$

and

$$\mathbf{\Phi}^{\varsigma} = \left\{ \mathbf{\Gamma}_k^{\varsigma} \mid k = \overline{1, n_k} \right\}$$

accordingly. It should be noted that identification of closed contours in the section $\mathbf{\Phi}^{r\varsigma}$ and $\mathbf{\Phi}^{\varsigma}$ can be easily implemented using depth-first search algorithms on the graph.

Let us compose incidence matrix $\dot{\mathbf{I}}$ for graph $\mathbf{G}^{\varsigma}$ with dimensions $n_v \times n_r$,

$$\dot{\mathbf{I}} = \left\{ g_{ij} \mid i = \overline{1, n_v},\ j = \overline{1, n_r} \right\}.$$

Components of the matrix take on following values: $g_{ij} = 1$ – if i^{th} graph vertex is start vertex for j^{th} edge; $g_{ij} = -1$ – if i^{th} graph vertex is end vertex for j^{th} edge; $g_{ij} = 0$ – otherwise. Let us also introduce in further consideration matrix

$$\left|\dot{\mathbf{I}}\right| = \left\{ \left| g_{ij} \right| \mid i = \overline{1, n_v},\ j = \overline{1, n_r} \right\}$$

composed using modulus of elements g_{ij} of matrix $\dot{\mathbf{I}}$.

Next, we can compose the matrix of basic graph cycles $\mathbf{J}$ with dimension $n_k \times n_r$,

$$\mathbf{J} = \left\{ f_{kj} \right\},\ k = \overline{1, n_k},\ j = \overline{1, n_r}.$$

Components of the matrix take on following values: $f_{kj} = 1$ – if j^{th} graph edge belongs to k^{th} basic graph cycle $\left(\mathbf{R}_j^{\varsigma} \subseteq \mathbf{\Gamma}_k^{\varsigma}\right)$ and edge direction coincides with the positive direction of path

tracing; $f_{kj}=-1$ – if j^{th} graph edge belongs to k^{th} basic graph cycle $\left(\mathbf{R}_j^{\varsigma}\subseteq\mathbf{\Gamma}_k^{\varsigma}\right)$ and edge direction does not coincide with positive direction of path tracing; $f_{kj}=0$ – if j^{th} graph edge does not belong to k^{th} basic graph cycle $\left(\mathbf{R}_j^{\varsigma}\bigcap\mathbf{\Gamma}_k^{\varsigma}=\varnothing\right)$.

2.2. Distribution of the shear forces flows taken along closed section contours

Each j^{th} edge $\mathbf{R}_j^{\varsigma}$, $j=\overline{1,n_r}$ of graph $\mathbf{G}^{\varsigma}$ corresponds with a constant – *edge weight*, $\forall\kappa:\vec{s}_{\kappa}^{\varsigma}\in\mathbf{R}_j^{\varsigma}\wedge\vec{s}_{\kappa}^{\varsigma}\in\mathbf{S}^{\varsigma}$:

$$p_j=\int\limits_{\ell_{rj}}\frac{d\varsigma}{\delta(\varsigma)}=\sum_{r=1}^{n_{\varsigma rj}}\int\limits_{\ell_{\varsigma}\in\mathbf{R}_j^{\varsigma}}\frac{d\varsigma}{\delta(\varsigma)}=$$
$$=\sum_{r=1}^{n_{\varsigma rj}}\frac{1}{\delta_{\kappa}^{\varsigma}}\int\limits_{\varsigma_{\kappa}}^{\varsigma_{\kappa+1}}d\varsigma=\sum_{r=1}^{n_{\varsigma rj}}\frac{l_{\kappa}^{\varsigma}}{\delta_{\kappa}^{\varsigma}}. \tag{2.1}$$

Let us also compose *weighting matrix* of unbranched sectional parts (edges of graph $\mathbf{G}^{\varsigma}$) – square matrix $\mathbf{W}$ with dimensions $n_r\times n_r$ and diagonal elements p_j, $j=\overline{1,n_r}$:

$$\mathbf{W}=\begin{bmatrix}p_1&0&\dots&0\\0&p_2&\dots&0\\\vdots&\vdots&\ddots&\vdots\\0&0&0&p_{n_r}\end{bmatrix} \tag{2.2}$$

Besides, each j^{th} graph edge $\mathbf{R}_j^{\varsigma}$ corresponds with the increment of sectorial coordinate

$$\mathbf{\Delta\omega}_{\mathbf{r}}^{\varsigma}=\left\{\Delta\omega_{r,j}^{\varsigma}\mid j=\overline{1,n_r}\right\}^T,$$
$$\forall\kappa:\vec{s}_{\kappa}^{\varsigma}\in\mathbf{R}_j^{\varsigma}\wedge\vec{s}_{\kappa}^{\varsigma}\in\mathbf{S}^{\varsigma}:$$
$$\Delta\omega_{r,j}^{\varsigma}=\int\limits_{\ell_{rj}}\rho d\varsigma=\int\limits_{\ell_{rj}}d\omega=\sum_{r=1}^{n_{\varsigma rj}}\int\limits_{\ell_{\varsigma}\in\mathbf{R}_j^{\varsigma}}d\omega=$$
$$=\sum_{r=1}^{n_{\varsigma rj}}\int\limits_{\varsigma_{\kappa}}^{\varsigma_{\kappa+1}}d\omega=\sum_{r=1}^{n_{\varsigma rj}}\Delta\omega_{\kappa}^{\varsigma}. \tag{2.3}$$

Each closed contour of the section $\mathbf{\Gamma}_k^{r\varsigma}$, $k=\overline{1,n_k}$, corresponds to the following constant – *contour weight*, $f_{kj}\in\mathbf{F}$, $\forall j:\mathbf{R}_j^{\varsigma}\subseteq\mathbf{\Gamma}_k^{r\varsigma}$:

$$\tilde{p}_k=\oint\limits_{\mathbf{\Gamma}_k^{r\varsigma}}\frac{d\varsigma}{\delta(\varsigma)}=\int\limits_{\mathbf{R}_j^{\varsigma}\subseteq\mathbf{\Gamma}_k^{r\varsigma}}\frac{d\varsigma}{\delta(\varsigma)}=\sum_{j=1}^{n_{r\varsigma\Gamma k}}\left|f_{kj}\right|p_j. \tag{2.4}$$

Let us consider the problem of free torsion for an arbitrary thin-walled section which consists of certain number of closed (connected and/or disconnected) contours as well as of open parts. In general case the following resolving system of equation for calculation the distribution factors $\tilde{a}_k$, $k=\overline{1,n_k}$, of shear forces flows taken along closed contours of the section has been formulated in [2] and presented below:

$$\begin{bmatrix}\tilde{p}_{11}&-p_{12}&\cdots&-p_{1k}&\cdots&-p_{1n_k}&\Omega_1\\-p_{21}&\tilde{p}_{22}&\cdots&-p_{2k}&\cdots&-p_{2n_k}&\Omega_2\\\vdots&\vdots&\ddots&\vdots&\vdots&\vdots&\vdots\\-p_{k1}&-p_{k2}&\cdots&\tilde{p}_{kk}&\cdots&-p_{kn_k}&\Omega_k\\\vdots&\vdots&\vdots&\vdots&\ddots&\vdots&\vdots\\-p_{n_k1}&-p_{n_k2}&\cdots&-p_{n_kk}&\cdots&\tilde{p}_{n_kn_k}&\Omega_{n_k}\\\Omega_1&\Omega_2&\cdots&\Omega_k&\cdots&\Omega_{n_k}&0\end{bmatrix}\times\begin{bmatrix}\tilde{a}_1\\\tilde{a}_2\\\vdots\\\tilde{a}_k\\\vdots\\\tilde{a}_{n_k}\\\lambda\end{bmatrix}=\begin{bmatrix}0\\0\\\vdots\\0\\\vdots\\0\\\Omega_0\end{bmatrix}; \tag{2.5}$$

here diagonal elements of the matrix are weights of k^{th} closed contour,

$$\tilde{p}_{kk} = \tilde{p}_k,\ k = \overline{1, n_k};$$

Ω_k – double area embraced by k^{th} closed contour $\mathbf{\Gamma}_k^{\varsigma}$,

$$\Omega_0 = \sum_{k=1}^{n_k} \Omega_k .$$

Other elements of matrix $p_{\alpha\beta}$ take on zero value $p_{\alpha\beta} = p_{\beta\alpha} = 0$, when corresponded closed contours have no common edges:

$$\mathbf{\Gamma}_{\alpha}^{\varsigma} \bigcap \mathbf{\Gamma}_{\beta}^{\varsigma} = \varnothing,$$

and the sum value of weights for all common edges [3]:

$$p_{\alpha\beta} = p_{\beta\alpha} = \sum_r p_r, \forall r\ :\ \mathbf{R}_r^{\varsigma} \subseteq \mathbf{\Gamma}_{\alpha}^{\varsigma} \wedge \mathbf{R}_r^{\varsigma} \subseteq \mathbf{\Gamma}_{\beta}^{\varsigma}.$$

Solution of the system of algebraic equations returns the column vector of factors

$$\mathbf{A}_k = \left\{ \tilde{a}_k \mid k = \overline{1, n_k} \right\}$$

for distribution of shear forces flows taken along closed contours of the section. Based on $\mathbf{A}_k$ we can generate the column vector of factors for distribution of shear forces flows taken along graph $\mathbf{G}^{\varsigma}$ edges:

$$\mathbf{A}_r = \left\{ a_j \mid j = \overline{1, n_r} \right\},$$

where each element should be determined as:

$$a_j = \sum_{k=1}^{n_k} f_{kj} \overline{a}_k,\ f_{kj} \in \mathbf{F},\ \forall j = \overline{1, n_r}. \qquad (2.6)$$

Since each graph edge $\mathbf{R}_j^{\varsigma}$, $j = \overline{1, n_r}$, is described by the set of sectional segments $\vec{s}_r^{\varsigma} \in \mathbf{S}^{\varsigma}$ as:

$$\mathbf{R}_j^{\varsigma} = \{ \vec{s}_r^{\varsigma} : \vec{s}_r^{\varsigma} \in \mathbf{S}^{\varsigma} \wedge \vec{s}_r^{\varsigma} \in \mathbf{R}_j \mid r = \overline{1, n_{\varsigma rj}} \},$$

then it is possible to determine for each sectional segment $\vec{s}_{\kappa}^{\varsigma} \in \mathbf{S}^{\varsigma}$ the value of piecewise constant *distribution function for shear flows taken along section* $a^{\varsigma}(\varsigma)$ as the set of

$$\mathbf{a}^{\varsigma} = \left\{ a_{\kappa}^{\varsigma} \mid \kappa = \overline{1, n_{\varsigma} - 1} \right\}$$

as follows:

$$a_{\kappa}^{\varsigma} = a_j,\ \forall \kappa : \vec{s}_{\kappa}^{\varsigma} \bigcap \mathbf{\Phi}^{\varsigma} \neq \varnothing,$$

and

$$a_{\kappa}^{\varsigma} = 0,$$

otherwise.

3. RESOLVING EQUATIONS FOR AN ARBITRARY CROSS-SECTION OF THIN-WALLED BAR

Search problem of shear forces flows for an arbitrary cross-section of thin-walled bar (including open-closed multi-contour cross-sections) can be transformed into minimization problem of Castigliano's functional $\mathbf{C}$ subject to constraints-equalities of shear forces flows equilibrium formulated for cross-section branch points as well as subject to equilibrium equation for the whole cross-section relating to longitudinal axes of the thin-walled bar [2].

Let present the formulated problem as mathematical programming task, namely as searching of unknown values of shear forces flows at start points of unbranched parts of a section:

$$\overset{\mathrm{r}}{T}_S = \left\{T_{S,j}\right\}^T,\ j=\overline{1,n_r}, \tag{3.1}$$

which ensure the least value of optimum criterion – Castigliano's functional $\mathbf{C}$:

$$\mathbf{C}^* = \mathbf{C}(\vec{T}_S^{\,*}) = \min_{\vec{T}_S \in \Im_T} \mathbf{C}\left(\vec{T}_S\right), \tag{3.2}$$

on hyperplane of feasible decisions $\Im_T$ described by the follow system of constraints-equalities:

$$\begin{cases} \mathbf{f}\left(\vec{T}_S\right) = \left\{ f_v\left(\vec{T}_S\right) = 0 \mid v = \overline{1, n_v - 1} \right\}; \\ f_x\left(\vec{T}_S\right) = 0; \end{cases} \tag{3.3}$$

where $\overset{\mathrm{r}}{T}_S$ – vector of design variables (searched shear flows); n_r – number of unknown shear flows; $\vec{T}_S^{\,*}$ – optimum decision of the problem; $\mathbf{C}^*$ – minimum value of Castigliano's functional; f_v – function of the vector argument $\overset{\mathrm{r}}{T}_S$; n_v – general number of constraints-equalities $f_v\left(\vec{T}_S\right)$ and $f_x\left(\vec{T}_S\right)$ which define hyperplane of feasible decisions $\Im_T$ in search space.

For Castigliano's functional $\mathbf{C}$ in further we will consider Euler's equations only which define strain compatibility conditions and are expressed depending on shear forces flows

$$\overset{\mathrm{r}}{T}_S = \left\{T_{S,j}\right\}^T,\ j=\overline{1,n_r}.$$

So it is well known that in case of quadratic functional Euler's equations don't depend on boundary conditions, then kinematic boundary conditions can be accept as homogeneous. As it was shown by V. Slivker in [2, p. 405], Castigliano's functional in this case can be identified with expression for strain energy formulated in terms of stresses as presented below:

$$\mathbf{C} = \sum_{j=1}^{n_r} \left(\int_{l_j} \frac{\left(\sigma(\varsigma)\right)^2}{2Ee(\varsigma)} \delta(\varsigma)\, d\varsigma + \int_{l_j} \frac{\left(\tau(\varsigma)\right)^2}{2Gg(\varsigma)} \delta(\varsigma)\, d\varsigma \right),$$

or for isotropic material:

$$\mathbf{C} = \frac{1}{2}\left(\sum_{j=1}^{n_r} \left(\int_{l_j} \frac{\left(\sigma(\varsigma)\right)^2}{E} \delta(\varsigma)\, d\varsigma + \int_{l_j} \frac{\left(\tau(\varsigma)\right)^2}{G} \delta(\varsigma)\, d\varsigma \right) \right);$$

$$\mathbf{C} = \frac{1}{2G}\left(\sum_{j=1}^{n_r} \left(\int_{l_j} \frac{\left(\sigma(\varsigma)\right)^2}{2(1+\nu)} \delta(\varsigma)\, d\varsigma + \int_{l_j} \left(\tau(\varsigma)\right)^2 \delta(\varsigma)\, d\varsigma \right) \right); \tag{3.4}$$

Let rewrite Castigliano's functional $\mathbf{C}$ (3.4) with replacement normal stresses $\sigma(\varsigma)$ by the expression (1.1), and shear stresses $\tau(\varsigma)$ – by the dependence from shear forces flows (1.2) as presented below:

$$\tau_j(\varsigma) = \frac{T_j(\varsigma)}{\delta_j(\varsigma)} = \frac{1}{\delta_j(\varsigma)}\left(T_{S,j} - \frac{Q_z}{I_y} S_{oy,j}(\varsigma) - \frac{Q_y}{I_z} S_{oz,j}(\varsigma) - \frac{M_\varpi}{I_\varpi} S_{o\varpi,j}(\varsigma) \right); \tag{3.5}$$

$$\mathbf{C}=\frac{1}{2G}\left(\left(\sum_{j=1}^{n_r}\left(\int_{l_j}\frac{1}{2(1+\nu)}\left(\frac{N}{A}+\frac{M_y}{I_y}z_j+\frac{M_z}{I_z}y_j+\frac{B}{I_\varpi}\varpi_j\right)^2\delta_j d\varsigma+\right.\right.\right.$$
$$\left.\left.\left.+\int_{l_j}\left(T_{S,j}^2-2T_{S,j}\frac{Q_z}{I_y}S_{oy,j}-2T_{S,j}\frac{Q_y}{I_z}S_{oz,j}-2T_{S,j}\frac{M_\varpi}{I_\varpi}S_{o\varpi,j}+\left(\frac{Q_z}{I_y}S_{oy,j}+\frac{Q_y}{I_z}S_{oz,j}+\frac{M_\varpi}{I_\varpi}S_{o\varpi,j}\right)^2\right)\frac{d\varsigma}{\delta_j}\right)\right)\right). \quad (3.6)$$

here we omitted functional dependence from angular position ς (to simplify presented formulas):

Let us leave in (3.6) those summands which are dependent from shear forces flows values

$$\overset{\mathrm{r}}{T}_S=\left\{T_{S,j}\right\}^T,\ j=\overline{1,n_r},$$

and also denote by the symbol K all other summands that are don't dependent from the vector $\overset{\mathrm{r}}{T}_S$. In this way we have obtain expression for Castigliano's functional $\mathbf{C}$ in terms of shear forces flows [2]

$$\overset{\mathrm{r}}{T}_S=\left\{T_{S,j}\right\}^T$$

as presented below:

$$\mathbf{C}=\sum_{j=1}^{n_r}\left(\int_{l_j}\left(\frac{T_{S,j}^2}{2G}-T_{S,j}\frac{Q_z}{GI_y}S_{oy,j}-T_{S,j}\frac{Q_y}{GI_z}S_{oz,j}-T_{S,j}\frac{M_\varpi}{GI_\varpi}S_{o\varpi,j}\right)\frac{d\varsigma}{\delta_j}+\mathrm{K}\right); \quad (3.7)$$

$$\mathbf{C}=\sum_{j=1}^{n_r}\left(\frac{T_{S,j}^2}{2G}\int_{l_j}\frac{d\varsigma}{\delta_j}-T_{S,j}\frac{Q_z}{GI_y}\int_{l_j}S_{oy,j}\frac{d\varsigma}{\delta_j}-T_{S,j}\frac{Q_y}{GI_z}\int_{l_j}S_{oz,j}\frac{d\varsigma}{\delta_j}-T_{S,j}\frac{M_\varpi}{GI_\varpi}\int_{l_j}S_{o\varpi,j}\frac{d\varsigma}{\delta_j}+\mathrm{K}\right) \quad (3.8)$$

where integral

$$\int_{l_j}\frac{d\varsigma}{\delta_j}$$

can be calculated according to (4.5), and integrals

$$\int_{l_j}S_{oy,j}\frac{d\varsigma}{\delta_j},\ \int_{l_j}S_{oz,j}\frac{d\varsigma}{\delta_j}\ \text{and}\ \int_{l_j}S_{o\varpi,j}\frac{d\varsigma}{\delta_j}$$

– using following equations (3.9), (3.10) and (3.11) accordingly presented below,

$$\forall\kappa:\vec{s}_\kappa^{\,\varsigma}\in\mathbf{R}_j^{\varsigma}\wedge\vec{s}_\kappa^{\,\varsigma}\in\mathbf{S}^{\varsigma}:$$

$$S_{hz,j}=\int_{\ell_{rj}}\frac{S_{oz,j}^{\varsigma}(\varsigma)d\varsigma}{\delta(\varsigma)}=$$
$$=\sum_{\kappa=1}^{n_{\varsigma rj}}\left(\frac{l_\kappa^{\varsigma}}{6\delta_\kappa^{\varsigma}}\left(S_{oz,\kappa}^{\varsigma,start}+4S_{oz,\kappa}^{\varsigma,mid}+S_{oz,\kappa}^{\varsigma,end}\right)\right); \quad (3.9)$$

$$S_{hy,j}=\int_{\ell_{rj}}\frac{S_{oy,j}^{\varsigma}(\varsigma)d\varsigma}{\delta(\varsigma)}=$$
$$=\sum_{\kappa=1}^{n_{\varsigma rj}}\left(\frac{l_\kappa^{\varsigma}}{6\delta_\kappa^{\varsigma}}\left(S_{oy,\kappa}^{\varsigma,start}+4S_{oy,\kappa}^{\varsigma,mid}+S_{oy,\kappa}^{\varsigma,end}\right)\right); \quad (3.10)$$

$$S_{h\varpi,j}=\int_{\ell_{rj}}\frac{S_{o\varpi,j}^{\varsigma}(\varsigma)d\varsigma}{\delta(\varsigma)}=$$
$$=\sum_{\kappa=1}^{n_{\varsigma rj}}\left(\frac{l_\kappa^{\varsigma}}{6\delta_\kappa^{\varsigma}}\left(S_{o\varpi,\kappa}^{\varsigma,start}+4S_{o\varpi,\kappa}^{\varsigma,mid}+S_{o\varpi,\kappa}^{\varsigma,end}\right)\right). \quad (3.11)$$

Let us define the following column vectors

consisting of n_r elements, $\forall j = \overline{1, n_r}$ (according to the number of edges of graph $\mathbf{G}$):

$$\vec{S}_{hz} = \begin{bmatrix} S_{hz,1} \\ S_{hz,2} \\ \vdots \\ S_{hz,n_r} \end{bmatrix}; \quad \vec{S}_{hy} = \begin{bmatrix} S_{hy,1} \\ S_{hy,2} \\ \vdots \\ S_{hy,n_r} \end{bmatrix}; \quad \vec{S}_{h\omega} = \begin{bmatrix} S_{h\omega,1} \\ S_{h\omega,2} \\ \vdots \\ S_{h\omega,n_r} \end{bmatrix}; \tag{3.12}$$

Using weighting matrix of unbranched sectional parts $\mathbf{W}$ (2.2) introduced above as well as column vectors $\vec{S}_{hz}$, $\vec{S}_{hy}$ and $\vec{S}_{h\varpi}$ presented above (3.12) we can rewrite Castigliano's functional (3.8) as the following vector-matrix equation:

$$1. \quad \mathbf{C} = \frac{1}{2G} \overset{\mathrm{r}}{T}_S^T \mathbf{W} \overset{\mathrm{r}}{T}_S - \overset{\mathrm{r}}{T}_S^T \frac{Q_y}{GI_z} \overset{\mathrm{r}}{S}_{hz} - \overset{\mathrm{r}}{T}_S^T \frac{Q_z}{GI_y} \overset{\mathrm{r}}{S}_{hy} - \overset{\mathrm{r}}{T}_S^T \frac{M_\varpi}{GI_\varpi} \overset{\mathrm{r}}{S}_{h\varpi} + \mathrm{K} \tag{3.13}$$

Next, for each section branch point we can work out equation of shear forces flows equilibrium in terms of projections on the longitudinal axis of the thin-walled bar. In order to obtain general view for these equations (the system of equations by the number of branch points in the section) we can use incidence matrixes $\dot{\mathbf{I}}$ and $|\dot{\mathbf{I}}|$ introduced above which reflect topological structure of considered cross-section of the thin-walled bar:

$$\left(|\dot{\mathbf{I}}| + \dot{\mathbf{I}}\right)\vec{T}_S - \left(|\dot{\mathbf{I}}| - \dot{\mathbf{I}}\right)\vec{T}_E = \mathbf{0}, \tag{3.14}$$

where $\overset{\mathrm{r}}{T}_S = \left\{T_{S,j}\right\}^T$, $j = \overline{1, n_r}$ – vector of shear forces flows at start points of unbranched sectional parts; $\overset{\mathrm{r}}{T}_E = \left\{T_{E,j}\right\}^T$, $j = \overline{1, n_r}$ – vector of shear forces flows at end points of unbranched sectional parts:

$$\overset{\mathrm{r}}{T}_E = \overset{\mathrm{r}}{T}_S - \Delta \overset{\mathrm{r}}{T}; \tag{3.15}$$

here $\Delta \overset{\mathrm{r}}{T} = \left\{\Delta T_j\right\}^T$, $j = \overline{1, n_r}$ – vector of shear forces flows increments for each unbranched sectional part:

$$\Delta \overset{\mathrm{r}}{T}_j = \frac{Q_y}{I_z} \overset{\mathrm{r}}{S}_{z,j} + \frac{Q_z}{I_y} \overset{\mathrm{r}}{S}_{y,j} + \frac{M_\varpi}{I_\varpi} \overset{\mathrm{r}}{S}_{\varpi,j}; \tag{3.16}$$

where vectors $\overset{\mathrm{r}}{S}_{z,j}$, $\overset{\mathrm{r}}{S}_{y,j}$, $\overset{\mathrm{r}}{S}_{\varpi,j}$ are presented below:

$$\vec{S}_z = \begin{bmatrix} S_{z,1} \\ S_{z,2} \\ \vdots \\ S_{z,n_r} \end{bmatrix}; \quad \vec{S}_y = \begin{bmatrix} S_{y,1} \\ S_{y,2} \\ \vdots \\ S_{y,n_r} \end{bmatrix}; \quad \vec{S}_\varpi = \begin{bmatrix} S_{\varpi,1} \\ S_{\varpi,2} \\ \vdots \\ S_{\varpi,n_r} \end{bmatrix}; \tag{3.17}$$

and components of vectors $\overset{\mathrm{r}}{S}_{z,j}$, $\overset{\mathrm{r}}{S}_{y,j}$, $\overset{\mathrm{r}}{S}_{\varpi,j}$ can be calculated as follow, $\forall \kappa : \vec{s}_\kappa^{\,\varsigma} \in \mathbf{R}_j^\varsigma \wedge \vec{s}_\kappa^{\,\varsigma} \in \mathbf{S}^\varsigma$:

$$S_{z,j} = \int_{\ell_{rj}} y^\varsigma(\varsigma)\delta(\varsigma)d\varsigma = \sum_{\kappa=1}^{n_{\varsigma rj}} \left(\delta_\kappa^\varsigma l_\kappa^\varsigma \left(y_\kappa^{\varsigma,start} + \frac{1}{2}\Delta y_\kappa^\varsigma \right) \right); \tag{3.18}$$

$$S_{y,j} = \int_{\ell_{rj}} z^\varsigma(\varsigma)\delta(\varsigma)d\varsigma = \sum_{\kappa=1}^{n_{\varsigma rj}} \left(\delta_\kappa^\varsigma l_\kappa^\varsigma \left(z_\kappa^{\varsigma,start} + \frac{1}{2}\Delta z_\kappa^\varsigma \right) \right); \tag{3.19}$$

$$S_{\varpi,j} = \int\limits_{\ell_{rj}} \varpi^{\varsigma}(\varsigma)\delta(\varsigma)d\varsigma = \\ = \sum_{\kappa=1}^{n_{\varsigma rj}} \left(\delta_{\kappa}^{\varsigma} l_{\kappa}^{\varsigma} \left(\varpi_{\kappa}^{\varsigma,start} + \frac{1}{2}\Delta\varpi_{\kappa}^{\varsigma} \right) \right). \quad (3.20)$$

Let us rewrite the equation (3.14) taken into account the equation (3.15), we obtain the following:

$$\left(\left|\dot{\mathbf{I}}\right| + \dot{\mathbf{I}}\right)\vec{T}_S - \left(\left|\dot{\mathbf{I}}\right| - \dot{\mathbf{I}}\right)\times\left(\vec{T}_S - \Delta\vec{T}\right) = \mathbf{0};$$
$$\left(\left|\dot{\mathbf{I}}\right| + \dot{\mathbf{I}}\right)\vec{T}_S - \left(\left|\dot{\mathbf{I}}\right| - \dot{\mathbf{I}}\right)\vec{T}_S + \left(\left|\dot{\mathbf{I}}\right| - \dot{\mathbf{I}}\right)\Delta\vec{T} = \mathbf{0};$$
$$2\dot{\mathbf{I}}\vec{T}_S + \left(\left|\dot{\mathbf{I}}\right| - \dot{\mathbf{I}}\right)\Delta\vec{T} = \mathbf{0};$$

or taken into account the equation (3.16):

$$2\dot{\mathbf{I}}\vec{T}_S + \left(\left|\dot{\mathbf{I}}\right| - \dot{\mathbf{I}}\right)\times \\ \times\left(\frac{Q_y}{I_z}\vec{S}_{z,j} + \frac{Q_z}{I_y}\vec{S}_{y,j} + \frac{M_{\varpi}}{I_{\varpi}}\vec{S}_{\varpi,j}\right) = \mathbf{0}. \quad (3.21)$$

The system of equation (3.21) has n_v equilibrium equations. The last equation is linear-dependent or a linear combination from the previous equations. Let us rewrite the system of equations (3.21) excluding the last equilibrium equation:

$$2\dot{\mathbf{I}}'\vec{T}_S + \left(\left|\dot{\mathbf{I}}'\right| - \dot{\mathbf{I}}'\right)\times \\ \times\left(\frac{Q_y}{I_z}\vec{S}_{z,j} + \frac{Q_z}{I_y}\vec{S}_{y,j} + \frac{M_{\varpi}}{I_{\varpi}}\vec{S}_{\varpi,j}\right) = \mathbf{0}; \quad (3.22)$$

where $\dot{\mathbf{I}}'$ – incidence matrix of the graph $\mathbf{G}$ truncated by the last row with dimensions

$$(n_v - 1)\times n_r,\ \dot{\mathbf{I}}' = \left\{ g_{ij} \mid i = \overline{1, n_v - 1},\ j = \overline{1, n_r} \right\};$$

$\left|\dot{\mathbf{I}}'\right|$ – matrix composed using modulus of elements g_{ij} of truncated matrix $\dot{\mathbf{I}}'$ as

$$\left|\dot{\mathbf{I}}'\right| = \left\{ \left| g_{ij} \right| \mid i = \overline{1, n_v - 1},\ j = \overline{1, n_r} \right\}.$$

We also can work out the last equilibrium equation relating to the longitudinal axes $x-x$ of a thin-walled bar as condition of static equivalence of torsional moment caused by the shear forces flows to the free torsional moment M_x acting in the cross-section of the thin-walled bar:

$$M_x - \sum_{j=1}^{n_r} \int_{l_j} T_j(\varsigma)\, d\omega = 0; \quad (3.23)$$

where $T_j(\varsigma)$ – shear forces flow at some point of the cross-section which can be expressed depending on shear forces flow $T_{S,j}(\varsigma)$ at start point of the corresponded unbranched part of the section as follow:

$$T_j = T_{S,j} - \frac{Q_y}{I_z}S_{oz,j} - \frac{Q_z}{I_y}S_{oy,j} - \frac{M_{\varpi}}{I_{\varpi}}S_{o\varpi,j}; \quad (3.24)$$

here we omitted functional dependence from angular position ς (to simplify presented formulas).
Then:

$$M_x - \sum_{j=1}^{n_r} \int_{l_j} \left(T_{S,j} - \frac{Q_y}{I_z}S_{oz,j} - \frac{Q_z}{I_y}S_{oy,j} - \frac{M_{\varpi}}{I_{\varpi}}S_{o\varpi,j} \right)\rho d\varsigma = 0;$$
$$M_x - \sum_{j=1}^{n_r} \left(T_{S,j}\int_{l_j}\rho d\varsigma - \frac{Q_y}{I_z}\int_{l_j} S_{oz,j}\rho d\varsigma - \frac{Q_z}{I_y}\int_{l_j} S_{oy,j}\rho d\varsigma - \frac{M_{\varpi}}{I_{\varpi}}\int_{l_j} S_{o\varpi,j}\rho d\varsigma \right) = 0.$$

Finally, we've obtained [2]:

$$M_x - \sum_{j=1}^{n_r}\left(T_{S,j}\int_{l_j}\rho d\varsigma - \frac{Q_y}{I_z}\int_{l_j} S_{oz,j}\rho d\varsigma - \frac{Q_z}{I_y}\int_{l_j} S_{oy,j}\rho d\varsigma - \frac{M_\varpi}{I_\varpi}\int_{l_j} S_{o\varpi,j}\rho d\varsigma \right) = 0;$$

$$\sum_{j=1}^{n_r} T_{S,j}\int_{l_j}\rho d\varsigma - \frac{Q_y}{I_z}\sum_{j=1}^{n_r}\int_{l_j} S_{oz,j}\rho d\varsigma - \frac{Q_z}{I_y}\sum_{j=1}^{n_r}\int_{l_j} S_{oy,j}\rho d\varsigma - \frac{M_\varpi}{I_\varpi}\sum_{j=1}^{n_r}\int_{l_j} S_{o\varpi,j}\rho d\varsigma - M_x = 0 \qquad (3.25)$$

here integrals

$$\sum_{j=1}^{n_r}\int_{l_j} S_{oz,j}\rho d\varsigma\,,\ \sum_{j=1}^{n_r}\int_{l_j} S_{oy,j}\rho d\varsigma\,,\ \sum_{j=1}^{n_r}\int_{l_j} S_{o\varpi,j}\rho d\varsigma$$

can be calculated using equations (3.26), (3.27) and (3.28) accordingly as presented below,

$$\forall \kappa : \vec{s}_\kappa^{\,\varsigma} \in \mathbf{R}_j^{\varsigma} \wedge \vec{s}_\kappa^{\,\varsigma} \in \mathbf{S}^{\varsigma}:$$

$$\begin{aligned} S_{\rho z} &= \sum_{j=1}^{n_r}\int_{\ell_{rj}} S_{oz,j}^{\varsigma}(\omega)\rho d\varsigma = \\ &= \sum_{j=1}^{n_r}\left(\sum_{\kappa=1}^{n_{\varsigma rj}} \frac{\Delta\omega_\kappa^{\varsigma}}{6}\left(S_{oz,\kappa}^{\varsigma,start} + 4S_{oz,\kappa}^{\varsigma,mid} + S_{oz,\kappa}^{\varsigma,end} \right) \right); \end{aligned} \qquad (3.26)$$

$$\begin{aligned} S_{\rho y} &= \sum_{j=1}^{n_r}\int_{\ell_{rj}} S_{oy,j}^{\varsigma}(\omega)\rho d\varsigma = \\ &= \sum_{j=1}^{n_r}\left(\sum_{\kappa=1}^{n_{\varsigma rj}} \frac{\Delta\omega_\kappa^{\varsigma}}{6}\left(S_{oy,\kappa}^{\varsigma,start} + 4S_{oy,\kappa}^{\varsigma,mid} + S_{oy,\kappa}^{\varsigma,end} \right) \right); \end{aligned} \qquad (3.27)$$

$$\begin{aligned} S_{\rho\varpi} &= \sum_{j=1}^{n_r}\int_{\ell_{rj}} S_{o\varpi,j}^{\varsigma}(\omega)\rho d\varsigma = \\ &= \sum_{j=1}^{n_r}\left(\sum_{\kappa=1}^{n_{\varsigma rj}} \frac{\Delta\omega_\kappa^{\varsigma}}{6}\left(S_{o\varpi,\kappa}^{\varsigma,start} + 4S_{o\varpi,\kappa}^{\varsigma,mid} + S_{o\varpi,\kappa}^{\varsigma,end} \right) \right) \end{aligned} \qquad (3.28)$$

Let us rewrite the constraints-equality (3.25) using vector representation taken into account equations (3.26), (3.27) and (3.28) as presented below:

$$\begin{aligned} &\overset{\mathrm{r}}{\omega}^T \overset{\mathrm{r}}{T}_S - \frac{Q_y}{I_z} S_{\rho z} - \frac{Q_z}{I_y} S_{\rho y} - \\ &- \frac{M_\varpi}{I_\varpi} S_{\rho\varpi} - M_x = 0. \end{aligned} \qquad (3.29)$$

Thus, the formulated problem is presented as mathematical programming task, namely as searching of unknown values of shear forces flows at start points of unbranched parts of a section:

$$\overset{\mathrm{r}}{T}_S = \left\{ T_{S,j} \right\}^T,\ j = \overline{1, n_r} \qquad (3.30)$$

which ensure the least value of the following Castigliano's functional $\mathbf{C}$ (3.13):

$$\begin{aligned} \mathbf{C} = &\frac{1}{2G}\overset{\mathrm{r}}{T}_S^T \mathbf{W} \overset{\mathrm{r}}{T}_S - \overset{\mathrm{r}}{T}_S^T \frac{Q_y}{GI_z}\overset{\mathrm{r}}{S}_{hz} - \\ &- \overset{\mathrm{r}}{T}_S^T \frac{Q_z}{GI_y}\overset{\mathrm{r}}{S}_{hy} - \overset{\mathrm{r}}{T}_S^T \frac{M_\varpi}{GI_\varpi}\overset{\mathrm{r}}{S}_{h\varpi} + \mathrm{K} \to min \end{aligned} \qquad (3.31)$$

subject to the following equilibrium conditions (3.22) and (3.29):

$$\begin{cases} 2\dot{\mathbf{I}}'\vec{T}_S + \left(\left|\dot{\mathbf{I}}'\right| - \dot{\mathbf{I}}' \right)\left(\dfrac{Q_y}{I_z}\vec{S}_{z,j} + \dfrac{Q_z}{I_y}\vec{S}_{y,j} + \dfrac{M_\varpi}{I_\varpi}\vec{S}_{\varpi,j} \right) = \mathbf{0}; \\ \vec{\omega}^T\vec{T}_S - \dfrac{Q_y}{I_z}S_{\rho z} - \dfrac{Q_z}{I_y}S_{\rho y} - \dfrac{M_\varpi}{I_\varpi}S_{\rho\varpi} - M_x = 0. \end{cases} \qquad (3.32)$$

Method of Lagrange multipliers can be used to reduce the mathematical programming task (3.30) – (3.32) to the searching of stationary point of the following modified functional $\mathbf{\Lambda}\left(\overset{\mathrm{r}}{T}_S,\overset{\mathrm{r}}{\lambda}^T,\lambda_{n_v}\right)$:

$$\begin{aligned}\mathbf{\Lambda}\left(\overset{\mathrm{r}}{T}_S,\overset{\mathrm{r}}{\lambda}^T,\lambda_{n_v}\right)=&\frac{1}{2G}\overset{\mathrm{r}}{T}_S^T\mathbf{W}\overset{\mathrm{r}}{T}_S-\overset{\mathrm{r}}{T}_S^T\frac{Q_y}{GI_z}\overset{\mathrm{r}}{S}_{hz}-\overset{\mathrm{r}}{T}_S^T\frac{Q_z}{GI_y}\overset{\mathrm{r}}{S}_{hy}-\overset{\mathrm{r}}{T}_S^T\frac{M_\varpi}{GI_\varpi}\overset{\mathrm{r}}{S}_{h\varpi}+\\&+\overset{\mathrm{r}}{\lambda}^T\left[2\dot{\mathbf{I}}'\overset{\mathrm{r}}{T}_S+\left(\left|\dot{\mathbf{I}}'\right|-\dot{\mathbf{I}}'\right)\left(\frac{Q_y}{I_z}\overset{\mathrm{r}}{S}_{z,j}+\frac{Q_z}{I_y}\overset{\mathrm{r}}{S}_{y,j}+\frac{M_\varpi}{I_\varpi}\overset{\mathrm{r}}{S}_{\varpi,j}\right)\right]+\\&+\lambda_{n_v}\left[\overset{\mathrm{r}}{\omega}^T\overset{\mathrm{r}}{T}_S-\frac{Q_y}{I_z}S_{\rho z}-\frac{Q_z}{I_y}S_{\rho y}-\frac{M_\varpi}{I_\varpi}S_{\rho\varpi}-M_x\right]\to min.\end{aligned}\tag{3.33}$$

here

$$\overset{\mathrm{r}}{\lambda}=\left\{\lambda_f\right\},\ f=\overline{1,n_v-1}$$

– vector of Lagrange multipliers consisting of n_v-1 elements; λ_{n_v} – additional Lagrange multiplier.

Stationary conditions of the modified functional $\mathbf{\Lambda}\left(\overset{\mathrm{r}}{T}_S,\overset{\mathrm{r}}{\lambda}^T,\lambda_{n_v}\right)$ (3.33) can be transformed into the system of n_r+n_v linear algebraic equations and presented using vector-matrix form as follow [2]:

$$\begin{aligned}&\left\|\begin{matrix}\frac{1}{G}\mathbf{W}&2\dot{\mathbf{I}}'^T&\Delta\boldsymbol{\omega}_{\mathbf{r}}^{\varsigma}\\2\dot{\mathbf{I}}'&\mathbf{\Theta}_{n_v-1,n_v-1}&\mathbf{0}_{n_v-1}\\\left(\Delta\boldsymbol{\omega}_{\mathbf{r}}^{\varsigma}\right)^T&\mathbf{0}_{n_v-1}^T&0\end{matrix}\right\|\times\left\|\begin{matrix}\vec{T}_S\\\vec{\lambda}\\\lambda_{n_v}\end{matrix}\right\|=M_x\times\left\|\begin{matrix}\mathbf{0}_{n_r}\\\mathbf{0}_{n_v-1}\\1\end{matrix}\right\|+\frac{Q_y}{I_z}\times\left\|\begin{matrix}\frac{\vec{S}_{hz}}{G}\\\left(\dot{\mathbf{I}}'-\left|\dot{\mathbf{I}}'\right|\right)\vec{S}_z\\S_{\rho z}\end{matrix}\right\|+\\&+\frac{Q_z}{I_y}\times\left\|\begin{matrix}\frac{\vec{S}_{hy}}{G}\\\left(\dot{\mathbf{I}}'-\left|\dot{\mathbf{I}}'\right|\right)\vec{S}_y\\S_{\rho y}\end{matrix}\right\|+\frac{M_\varpi}{I_\varpi}\times\left\|\begin{matrix}\frac{\vec{S}_{h\varpi}}{G}\\\left(\dot{\mathbf{I}}'-\left|\dot{\mathbf{I}}'\right|\right)\vec{S}_\varpi\\S_{\rho\varpi}\end{matrix}\right\|.\end{aligned}\tag{3.34}$$

where:

$$\mathbf{M}=\left\|\begin{matrix}\frac{1}{G}\mathbf{W}&2\dot{\mathbf{I}}'^T&\Delta\boldsymbol{\omega}_{\mathbf{r}}^{\varsigma}\\2\dot{\mathbf{I}}'&\mathbf{\Theta}_{n_v-1,n_v-1}&\mathbf{0}_{n_v-1}\\\left(\Delta\boldsymbol{\omega}_{\mathbf{r}}^{\varsigma}\right)^T&\mathbf{0}_{n_v-1}^T&0\end{matrix}\right\|;$$

$\mathbf{M}$ – square matrix with dimensions $(n_r + n_v)\times(n_r + n_v)$, here n_r and n_v – number of edges and vertices of the graph $\mathbf{G}$ accordingly; $\mathbf{\Delta\omega}^{\varsigma}_{\mathbf{r}}$ – column vector of sectorial coordinates increments

$$\mathbf{\Delta\omega}^{\varsigma}_{\mathbf{r}} = \left\{\Delta\omega^{\varsigma}_{r,j} \mid j = \overline{1, n_r}\right\}^T$$

consisting of n_r components calculated according to (2.3); $\vec{S}_y$, $\vec{S}_z$, $\vec{S}_{\varpi}$ – column vectors (3.17) with n_r components calculated according to (3.18), (3.19) and (3.20) respectively; $\vec{S}_{hy}$, $\vec{S}_{hz}$, $\vec{S}_{h\varpi}$ – column vectors (3.12) with n_r components calculated according to (3.9), (3.10) and (3.11) respectively; $S_{\rho y}$, $S_{\rho z}$, $S_{\rho\varpi}$ – integral section properties calculated according to (3.26), (3.27) and (3.28) respectively.

Solution of the system of equations (3.34) determines column vector of shear forces flows

$$\overset{\mathrm{r}}{T}_S = \left\{T_{S,j}\right\}^T,\ j = \overline{1, n_r},$$

at the start points of unbranched cross-section parts. The vector $\overset{\mathrm{r}}{T}_S$ can be also presented as follow:

$$\overset{\mathrm{r}}{T}_S = M_x \overset{\mathrm{r}}{b}_x + \frac{Q_y}{I_z}\overset{\mathrm{r}}{b}_z + \frac{Q_z}{I_y}\overset{\mathrm{r}}{b}_y + \frac{M_{\varpi}}{I_{\varpi}}\overset{\mathrm{r}}{b}_{\varpi}. \qquad (3.35)$$

In this case the system of algebraic equations (3.34) disintegrates and transforms into the four systems of $n_r + n_v$ algebraic equations relating to the column vectors $\overset{\mathrm{r}}{b}_x$, $\overset{\mathrm{r}}{b}_y$, $\overset{\mathrm{r}}{b}_z$ and $\overset{\mathrm{r}}{b}_{\varpi}$ consisting of n_r elements [2] as presented below:

$$\mathbf{M}\times\begin{Vmatrix}\vec{b}_x\\ \vec{\lambda}_x\\ \lambda_{n_v x}\end{Vmatrix} = \begin{Vmatrix}\mathbf{0}_{n_r}\\ \mathbf{0}_{n_v-1}\\ 1\end{Vmatrix};$$

$$\mathbf{M}\times\begin{Vmatrix}\vec{b}_y\\ \vec{\lambda}_y\\ \lambda_{n_v y}\end{Vmatrix} = \begin{Vmatrix}\dfrac{\vec{S}_{hy}}{G}\\ \left(\mathbf{\dot{I}}' - \left|\mathbf{\dot{I}}'\right|\right)\times\vec{S}_y\\ S_{\rho y}\end{Vmatrix};$$

$$\mathbf{M}\times\begin{Vmatrix}\vec{b}_z\\ \vec{\lambda}_z\\ \lambda_{n_v z}\end{Vmatrix} = \begin{Vmatrix}\dfrac{\vec{S}_{hz}}{G}\\ \left(\mathbf{\dot{I}}' - \left|\mathbf{\dot{I}}'\right|\right)\times\vec{S}_z\\ S_{\rho z}\end{Vmatrix}; \qquad (3.36)$$

$$\mathbf{M}\times\begin{Vmatrix}\vec{b}_{\varpi}\\ \vec{\lambda}_{\varpi}\\ \lambda_{n_v \varpi}\end{Vmatrix} = \begin{Vmatrix}\dfrac{\vec{S}_{h\varpi}}{G}\\ \left(\mathbf{\dot{I}}' - \left|\mathbf{\dot{I}}'\right|\right)\times\vec{S}_{\varpi}\\ S_{\rho\varpi}\end{Vmatrix};$$

where

$$\vec{\lambda}_x = \left\{\lambda_{x,f}\right\}^T,\ \vec{\lambda}_y = \left\{\lambda_{y,f}\right\}^T,\ \vec{\lambda}_z = \left\{\lambda_{z,f}\right\}^T,$$
$$\vec{\lambda}_{\varpi} = \left\{\lambda_{\varpi,f}\right\}^T,\ f = \overline{1, n_v - 1}$$

– unknown column vectors of Lagrange multipliers consisting of $n_v - 1$ elements;

$$\lambda_{n_v x},\ \lambda_{n_v y},\ \lambda_{n_v z},\ \lambda_{n_v \varpi}$$

– additional Lagrange multipliers.

Projection of the vector

$$\vec{b}_x = \left\{b_{x,j} \mid j = \overline{1, n_r}\right\}$$

defined of the set of n_r unbranched sectional parts into the set of sectional segments

$$\vec{b}_x^{\,\varsigma} = \left\{ b_{x,\kappa}^{\varsigma} \mid \kappa = \overline{1, n_\varsigma - 1} \right\}$$

can be written as:

$$b_{x,\kappa}^{\varsigma} = b_{x,j} \quad \forall \kappa : \vec{s}_\kappa^{\,\varsigma} \subseteq \mathbf{R}_j^{\varsigma};$$

and

$$b_{x,\kappa}^{\varsigma} = 0 \quad \forall \kappa : \vec{s}_\kappa^{\,\varsigma} \bigcap \mathbf{R}_j^{\varsigma} = \varnothing .$$

By analogy column vectors

$$\vec{b}_y = \left\{ b_{y,j} \mid j = \overline{1, n_r} \right\},\ \vec{b}_z = \left\{ b_{z,j} \mid j = \overline{1, n_r} \right\}$$

and $\vec{b}_\varpi = \left\{ b_{\varpi,j} \mid j = \overline{1, n_r} \right\}$ can be also projected into the set of sectional segments obtaining corresponded column vectors

$$\vec{b}_y^{\,\varsigma} = \left\{ b_{y,\kappa}^{\varsigma} \mid \kappa = \overline{1, n_\varsigma - 1} \right\},$$
$$\vec{b}_z^{\,\varsigma} = \left\{ b_{z,\kappa}^{\varsigma} \mid \kappa = \overline{1, n_\varsigma - 1} \right\},$$
$$\vec{b}_\varpi^{\,\varsigma} = \left\{ b_{\varpi,\kappa}^{\varsigma} \mid \kappa = \overline{1, n_\varsigma - 1} \right\}.$$

The following transformations for the first moments of inertia and for the sectorial moment of inertia should be performed, $\forall \kappa = \overline{1, n_\varsigma - 1}$:

$$\begin{aligned} \bar{S}_{oz,\kappa}^{\varsigma} &\leftarrow \left\{ S_{oz,\kappa}^{\varsigma} - b_{z,\kappa}^{\varsigma} \right\}; \\ \bar{S}_{oy,\kappa}^{\varsigma} &\leftarrow \left\{ S_{oy,\kappa}^{\varsigma} - b_{y,\kappa}^{\varsigma} \right\}; \\ \bar{S}_{o\varpi,\kappa}^{\varsigma} &\leftarrow \left\{ S_{o\varpi,\kappa}^{\varsigma} - b_{\varpi,\kappa}^{\varsigma} \right\}; \end{aligned} \tag{3.37}$$

$$\tilde{S}_{o\varpi,\kappa}^{\varsigma} \leftarrow \left\{ \bar{S}_{o\varpi,\kappa}^{\varsigma} - a_\kappa^{\varsigma} \frac{I_\varpi}{\Omega_0} \right\}. \tag{3.38}$$

4. SHEAR FORCES FLOWS AND SHEAR STRESSES

Let us define the sets of shear forces flows values for the start, middle and end points at the middle line of the sectional segments

$$\mathbf{T}^{\varsigma,\mathrm{st}} = \left\{ T_\kappa^{\varsigma,\mathrm{st}} \right\},\ \mathbf{T}^{\varsigma,\mathrm{mid}} = \left\{ T_\kappa^{\varsigma,\mathrm{mid}} \right\},$$
$$\mathbf{T}^{\varsigma,\mathrm{end}} = \left\{ T_\kappa^{\varsigma,\mathrm{end}} \right\},\ \kappa = \overline{1, n_\varsigma - 1},$$

consisting of $n_\varsigma - 1$ elements (by the number of sectional segments) as presented below [5]:

$$\begin{aligned} T_\kappa^{\varsigma,\mathrm{start}} &= \frac{\wp H}{\Omega_0} a_\kappa^{\varsigma} - \frac{Q_y}{I_z} \bar{S}_{oz,\kappa}^{\varsigma,\mathrm{start}} - \\ &- \frac{Q_z}{I_y} \bar{S}_{oy,\kappa}^{\varsigma,\mathrm{start}} - \frac{M_\varpi}{I_\varpi} \tilde{S}_{o\varpi,\kappa}^{\varsigma,\mathrm{start}}; \end{aligned} \tag{4.1}$$

$$\begin{aligned} T_\kappa^{\varsigma,mid} &= \frac{\wp H}{\Omega_0} a_\kappa^{\varsigma} - \frac{Q_y}{I_z} \bar{S}_{oz,\kappa}^{\varsigma,mid} - \\ &- \frac{Q_z}{I_y} \bar{S}_{oy,\kappa}^{\varsigma,mid} - \frac{M_\varpi}{I_\varpi} \tilde{S}_{o\varpi,\kappa}^{\varsigma,mid}; \end{aligned} \tag{4.2}$$

$$\begin{aligned} T_\kappa^{\varsigma,end} &= \frac{\wp H}{\Omega_0} a_\kappa^{\varsigma} - \frac{Q_y}{I_z} \bar{S}_{oz,\kappa}^{\varsigma,end} - \\ &- \frac{Q_z}{I_y} \bar{S}_{oy,\kappa}^{\varsigma,end} - \frac{M_\varpi}{I_\varpi} \tilde{S}_{o\varpi,\kappa}^{\varsigma,end}; \end{aligned} \tag{4.3}$$

here the first moments of inertia $\bar{S}_{oz,\kappa}^{\varsigma}$, $\bar{S}_{oy,\kappa}^{\varsigma}$ and sectorial moment of inertia $\tilde{S}_{o\varpi,\kappa}^{\varsigma}$ should be calculated using transformations (3.37) and (3.38) accordingly.

Shear stresses for each $\kappa^{\,\mathrm{th}}$ sectional segment

$$\boldsymbol{\tau}^{\varsigma} = \left\{ \vec{\tau}_\kappa^{\,\varsigma} = \left\{ \tau_\kappa^{\varsigma,\mathrm{start}}, \tau_\kappa^{\varsigma,\mathrm{mid}}, \tau_\kappa^{\varsigma,\mathrm{end}} \right\} \right\},\ \kappa = \overline{1, n_\varsigma - 1},$$

can be calculated as presented below:

$$\boldsymbol{\tau}_\kappa^{\varsigma} = \left\{ \begin{aligned} \tau_\kappa^{\varsigma,\mathrm{start}} &= \left| \frac{T_\kappa^{\varsigma,\mathrm{start}}}{\delta_\kappa^{\varsigma}} \right| \pm \frac{(1-\wp) H \delta_\kappa^{\varsigma}}{I_k} \\ \tau_\kappa^{\varsigma,\mathrm{mid}} &= \left| \frac{T_\kappa^{\varsigma,\mathrm{mid}}}{\delta_\kappa^{\varsigma}} \right| \pm \frac{(1-\wp) H \delta_\kappa^{\varsigma}}{I_k} \\ \tau_\kappa^{\varsigma,\mathrm{end}} &= \left| \frac{T_\kappa^{\varsigma,\mathrm{end}}}{\delta_\kappa^{\varsigma}} \right| \pm \frac{(1-\wp) H \delta_\kappa^{\varsigma}}{I_k} \end{aligned} \right\}, \tag{4.4}$$

here torsion moment of inertia I_x and parameter

$\wp$ should be calculated as:

$$I_x = I_k + I_\Gamma = \frac{1}{3}\sum_{\kappa=1}^{n_\varsigma - 1} l_\kappa^\varsigma \left(\delta_\kappa^\varsigma\right)^3 + I_\Gamma; \qquad (4.5)$$

$$\wp = 1 - \frac{I_k}{I_x}; \qquad (4.6)$$

and components

$$\left|\frac{T_\kappa^{\varsigma,\text{start}}}{\delta_\kappa^\varsigma}\right|, \left|\frac{T_\kappa^{\varsigma,\text{mid}}}{\delta_\kappa^\varsigma}\right| \text{ and } \left|\frac{T_\kappa^{\varsigma,\text{end}}}{\delta_\kappa^\varsigma}\right|$$

in equations (4.4) define shear stresses values for start, middle and end points at the middle line of κ^{th} sectional segment accordingly. Besides, transition from the shear stresses related to the middle line of κ^{th} segment to the shear stresses at the outside longitudinal edges of this segment can be performed by addition or subtraction of the member

$$\frac{(1-\wp)}{I_k} H \delta_\kappa^\varsigma .$$

CONSLUSIONS

Searching problem of shear stresses on outside longitudinal edges of an arbitrary cross-section (including open-closed multi-contour cross-sections) of a thin-walled bar subjected to the general load case has been considered in the paper. Formulated problem has been transformed into minimization problem of Castigliano's functional subject to constraints-equalities of shear forces flows equilibrium formulated for cross-section branch points as well as subject to equilibrium equation for the whole cross-section relating to longitudinal axes of the thin-walled bar.

Detail numerical algorithm intended to solve the formulated problem using mathematical apparatus of the graph theory has been proposed by the paper. The algorithm is oriented on software implementation in systems of computer-aided design of thin-walled bar structures.

REFERENCES

1. **Perelmuter A.V., Slivker V.I.** Raschetnie Modeli Soorujenii i Vozmojnost ih Analiza [Design Models of Structures and Analysis Possibilities]. Moscow, Publishers DMK, 2007, 595 pages (in Russian).
2. **Slivker V.I.** Stroitelnaya Mehanika. Variacionnie Osnovi [Structural mechanic. Variation Principles]. Moscow, Publishers ASV, 2005, 736 pages (in Russian).
3. **Yurchenko V.V**. Rozpodil Potokiv Dotichnih Zusil Vzdovj Zamknenih Konturiv Pererizu Tonkostinnogo Sterjnya: Rozrobka Chislovogo Algoritmu z Vikoristannyam Teoriï Grafiv [Distribution of the Shear Forces Flows Along the Closed Contours of a Section of a Thin-Walled Bar: Development of Numerical Algorithm Based on the Graph Theory]. // Resursoekonomni Materiali, Konstrukciï, Budivli ta Sporudi [Resource-Economical Materials, Structures and Buildings]. Collection of Scientific Papers, Issue 30, Rivne, 2015. pp. 306-316.
4. **Yurchenko V.V.** Uzagalneni Sektorialni Koordinati Dlya Dovilnogo Pererizu Tonkostinnogo Sterjnya_ Rozrobka Chislovogo Algoritmu z Vikoristannyam Teoriï Grafiv [Normalized Sectorial Coordinates for an Arbitrary Section of a Thin-Walled Bar: Development of Numerica Algorithm based on the Graph Theory]. // Resursoekonomni Materiali, Konstrukciï, Budivli ta Sporudi [Resource-Economical Materials, Structures and Buildings]. // Collection of Scientific papers, Issue 31, Rivne, 2015, pp. 538-549.
5. **Yurchenko V.V.** Chislennoe Reshenie Zadachi o Raspredelenii Kasatelnih Napryajenii v Sechenii Tonkostennogo Sterjnya Proizvolnoi Konfiguracii [Numerical Solution for the Problem About Distribution of Shear Forces Flows for an

Arbitrary Section of a Thin-Walled Bar]. // Stroitelnaya Mehanika i Stroitelnie Konstrukcii [Structural Mechanic and Building Structures]: Collection of Papers. Moscow, Publishers SCAD SOFT, 2013, pp. 487-505 (in Russian).

6. **Alfano G., Marotti de Sciarra F., Rosati L.** Automatic Analysis of Multicell Thin-Walled Sections. // *Computer and Structures*, 1996, No. 59, pp. 641-655.
7. **Paz M., Strehl C.P., Schrader P.** Computer Determination of the Shear Center of Open and Closed Sections. // *Computer and Structures*, 1976, No. 6, pp. 117-125.
8. **Perelmuter A.V., Slivker V. I.** Numerical structural analysis: models, methods and pitfalls. – Berlin-Heidelberg-New York-Hong Kong-London-Milan-Paris-Tokyo: Springer Verlag, 2003, 600 pages.
9. **Perelmuter A., Yurchenko V.** Shear Stresses in Hybrid Thin-Walled Section: Development of Detail Numerical Algorithm Based on the Graph Theory. // *Proceedings of 3rd Polish Congress of Mechanics and 21st International Conference on Computer Methods in Mechanics*. Short Papers, Vol. 2, Gdańsk, 2015, pp. 943-944.
10. **Prokić A.** Computer Program for Determination of Geometrical Properties of Thin-Walled Beams with Open-Closed Section. // *Computers and Structures*, 2000, No. 74, pp. 705-715.
11. **Tarjan R.** Depth-First Search and Linear Graph Algorithms. // *SIAM Journal Computing*, 1972, No. 1, pp. 146-160.
12. **Waldron P.** Sectorial Properties of Straight Thin-Walled Beams. // *Computers & Structures*, 1986, Vol. 24, Issue 1, pp. 147-156.

СПИСОК ЛИТЕРАТУРЫ

1. **Перельмутер А.В., Сливкер В.И.** Расчетные модели сооружений и возможность их анализа. – М.: ДМК Пресс, 2007. – 595 с.
2. **Сливкер В.И.** Строительная механика. Вариационные основы. – М.: АСВ, 2005. – 736 с.
3. **Юрченко В.В.** Розподіл потоків дотичних зусиль вздовж замкнених контурів перерізу тонкостінного стержня: розробка числового алгоритму з використанням теорії графів [Распределение потоков касательных усилий вдоль замкнутых контуров сечения тонкостенного стержня: разработка численного алгоритма с использованием теории графов]. // Ресурсоекономні матеріали, конструкції, будівлі та споруди [Ресурсоэкономные материалы, конструкции, здания и сооружения]. Сборник научных трудов. Выпуск 30, Ровно, 2015, с. 306-316.
4. **Юрченко В.В.** Узагальнені секторіальні координати для довільного перерізу тонкостінного стержня: розробка числового алгоритму з використанням теорії графів [Обобщенные секториальные координаты для произвольного сечения тонкостенного стержня: разработка численного алгоритма с использованием теории графов]. // Ресурсоекономні матеріали, конструкції, будівлі та споруди [Ресурсоэкономные материалы, конструкции, здания и сооружения]. Сборник научных трудов. Выпуск 31, Ровно, 2015, с. 538-549.
5. **Юрченко В.В.** Численное решение задачи о распределении касательных напряжений в сечении тонкостенного стержня произвольной конфигурации // Строительная механика и строительные конструкции: Сборник статей. – М.: SCAD Soft, 2013, с. 487-505.
6. **Alfano G., Marotti de Sciarra F., Rosati L.** Automatic Analysis of Multicell Thin-Walled Sections. // *Computer and Structures*, 1996, No. 59, pp. 641-655.
7. **Paz M., Strehl C.P., Schrader P.** Computer Determination of the Shear Center of Open and Closed Sections. //

Computer and Structures, 1976, No. 6, pp. 117-125.
8. **Perelmuter A.V., Slivker V. I.** Numerical structural analysis: models, methods and pitfalls. – Berlin-Heidelberg-New York-Hong Kong-London-Milan-Paris-Tokyo: Springer Verlag, 2003. 600 p.
9. **Perelmuter A., Yurchenko V.** Shear Stresses in Hybrid Thin-Walled Section: Development of Detail Numerical Algorithm Based on the Graph Theory. // *Proceedings of 3rd Polish Congress of Mechanics and 21st International Conference on Computer Methods in Mechanics*. Short Papers, Vol. 2, Gdańsk, 2015, pp. 943-944.
10. **Prokić A.** Computer Program for Determination of Geometrical Properties of Thin-Walled Beams with Open-Closed Section. // *Computers and Structures*, 2000, No. 74, pp. 705-715.
11. **Tarjan R.** Depth-First Search and Linear Graph Algorithms. // *SIAM Journal Computing*, 1972, No. 1, pp. 146-160.
12. **Waldron P.** Sectorial Properties of Straight Thin-Walled Beams. // *Computers & Structures*, 1986, Vol. 24, Issue 1, pp. 147-156.

Vitalina V. Yurchenko, Candidate of Technical Science, Associate Professor, Kyiv National University of Civil Engineering and Architecture, 03680, Povitroflotskyj avenue, 31, Kyiv, Ukraine;
E-mail: vitalina@scadsoft.com.

Юрченко Виталина Витальевна, кандидат технических наук, доцент, Киевский национальный университет строительства и архитектуры; 03680, Воздухофлотский проспект, 31, Киев, Украина;
E-mail: vitalina@scadsoft.com.

CONTROL AND QUALITY OF PILES BY NON-DESTRUCTIVE EXPRESS METHODS: LOW STRAIN METHOD AND CROSS-HOLE SONIC LOGGING

Askar Zhussupbekov [1], Yoshinori Iwasaki [2], Eun Chul Shin [3], Nurgul Shakirova [1]
[1] L.N. Gumilyov Eurasian National University, Astana, KAZAKHSTAN
[2] Geo-Research Institute, Osaka, JAPAN
[3] Incheon National University, Songdo, SOUTH KOREA

Abstract: This paper described using Low Strain Method and Cross-Hole Sonic logging (CSL) for identify of integrity of bridge foundations of LRT in Astana, Kazakhstan. The CSL is a method prescribed by ASTM D6760 – 08, Standard Test Method for Integrity Testing of Concrete Deep Foundations. This method is considered to be more accurate than sonic echo testing in the determination of soundness of concrete. The sonic access tubes do not contribute to the structural capacity of the pile. The bored piles of LRT are 1.0÷1.5 m of diameters and 10÷55 m of lengths. Design bearing capacity of piles is more than 4500 kN. At the testing period were founded defects in foundation bodies. To check of integrity were conducted by static load tests. The CSL test is based on the length of time for an ultrasonic wave to be propagated between any two of the selected tubes. The velocity of the propagated wave depends on the material through which the wave is transmitted. The aim of this paper is to discuss the advantages and disadvantages of Low Strain Method and CSL methods by analysis of field testing. For checking integrity applying two methods - Low Strain Method and Cross-Hole Sonic Logging. The aim of this paper is to discuss the advantages and disadvantages of each method using the examples of a real application.

Keywords: Cros-hole section, PIT, integrity, concrete

КОНТРОЛЬ КАЧЕСТВА СВАЙ НЕРАЗРУШАЮЩИМИ ЭКСПРЕСС-МЕТОДАМИ: МЕТОДЫ ОТРАЖЕННОЙ ВОЛНЫ ПРИ НИЗКОЙ НАГРУЗКЕ И МЕЖСКВАЖИННОЙ ДЕФЕКТОСКОПИИ

А. Жусупбеков [1], Й. Ивасаки [2], Юн Чул Шин [3], Н. Шакирова [1]
[1] Евразийский университет имени Л.Н. Гумилева, г. Астана, КАЗАХСТАН
[2] Geo-Research Institute, г. Осака, ЯПОНИЯ
[3] Incheon National University, г. Сонгдо, ЮЖНАЯ КОРЕЯ

Аннотация: В данной статье представлены методы отраженной волны при низкой нагрузке и межскважинной дефектоскопии (CSL) для определения целостности мостовых фундаментов на строительной площадке LRT в Астане, Казахстан. CSL – это метод, предписанный ASTM D6760-08, Стандартный метод испытаний для проверки целостности бетонных глубоких фундаментов. Этот метод считается более точным, чем тестирование акустического эха при определении прочности бетона. Звуковые трубки доступа не влияют на структурную емкость сваи. Буронабивные сваи LRT имеют диаметр 1,0 ÷ 1,5 м и длину 10 ÷ 55 м. Расчетная несущая способность свай составляет более 4500 кN. На период испытаний были выявлены дефекты в фундаментах. Для проверки целостности были проведены статические нагрузочные испытания. Тест CSL основан на продолжительности распространения ультразвуковой волны между любыми двумя выбранными трубками. Скорость распространяющейся волны зависит от материала, через который она проходит. Для проверки целостности применяют два метода - метод отраженной волны при низкой нагрузке и межскважинной дефектоскопии. Целью данной статьи является обсуждение преимуществ и недостатков каждого метода с использованием примеров реального применения.

Ключевые слова: поперечное сечение, PIT, сплошность, бетон

INTRODUCTION

At the present time, in Astana city is going on works by construction public transport system LRT (Light Railway Transport). The first stage of construction is including construction of overhead road (bridge) with 22,4 km length and 18 stations. Height of the bridge is 7÷14 m above the ground. Overhead road based on columns every 30 meters. The foundation of each column is include 4 or 6 bored piles with cross-section 1.0÷1.5 m and length 8÷55 m. Design bearing capacity of each bored piles is from 4500 to 12000 kN.



Figure 1. Perspective view of LRT, Astana, Kazakhstan.

In order to reduce the time for construction and cost of piling works Chinese companies are use Chinese drilling rigs Zoomlion without casing. To maintain the walls of boreholes in sand and gravel soils using polymer slurry. Application of polymer slurry allow reducing time for drilling, allow to use less powerful drilling rigs and equipment, but at the same time increase the risk of collapsing soil during drilling or concreting piles. In these conditions, very important to control integrity of concrete body of each bored piles. For checking integrity of bored piles applying two methods - Low Strain Method and Cross-Hole Sonic Logging.

INTEGRITY TESTING

Everybody with experience in reinforced concrete construction has encountered columns that, upon dismantling of the forms, exhibit air voids and honeycombing. Although these columns may have been cast with good-quality concrete, in properly assembled forms and with careful vibration, they still exhibit defects. Cast-in-situ piles are also columns, but instead of forms made of wood or metal we have a hole in the ground. This hole may pass through layers of dumped fill, loose sand, organic matter, and ground water, which may be fast flowing or corrosive. Obviously, such conditions are not conducive to a high-quality end product. The fact that on most sites we still manage to get excellent piles is only a tribute to a dedicated team that makes this feat possible: geotechnical engineer, structural engineer, quantity surveyor, contractor, site supervisor and quality control laboratory. This is obviously a chain, the strength of which is determined by the weakest link [7].

A flaw is any deviation from the planned shape and/or material of the pile. A comprehensive list of events, each of which can lead to the formation a flaw in a pile: use of concrete that is too dry, water penetration into the borehole, collapse in soft strata, falling of boring spoils from the surface, tightly-spaced rebars etc.

Therefore, we have to face the fact that on any given site some piles may exhibit flaws. Of course, not all flaws are detrimental to the performance of the pile. Only a flaw that, because of either size or location, may detract from the pile's load carrying capacity or durability is defined as a defect. The geotechnical engineer and the structural engineer are jointly responsible to decide which flaw comprises a defect.

The two techniques currently dominating pile integrity testing, namely the Low Strain Method and Cross-Hole Sonic Logging, both utilize sound waves (Amir et al 2009).

Low Strain Method.

The low strain (sonic) method for the integrity testing of piles is aimed at routinely testing complete piling sites. To perform this test, a sensor (usually accelerometer) is pressed against

the top of the pile while the pile is hit with a small hand-held hammer. Output from the sensor is analyzed and displayed by a suitable computerized instrument, the results providing meaningful information regarding both length and integrity of the pile.

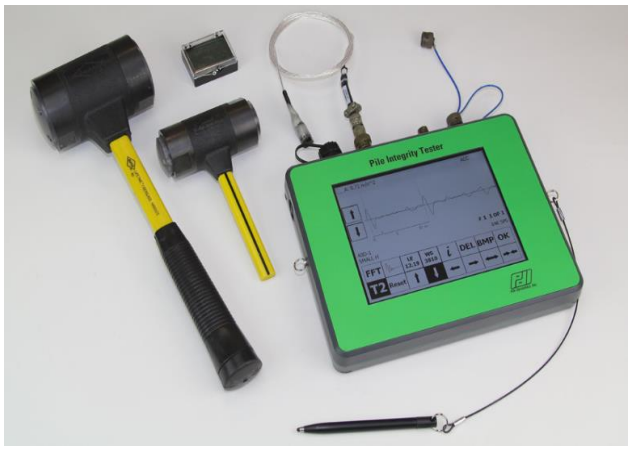


Figure 2. Pile Integrity Tester - PIT-QV.

The sonic test is fast and inexpensive, with less than a minute needed to test a given pile.

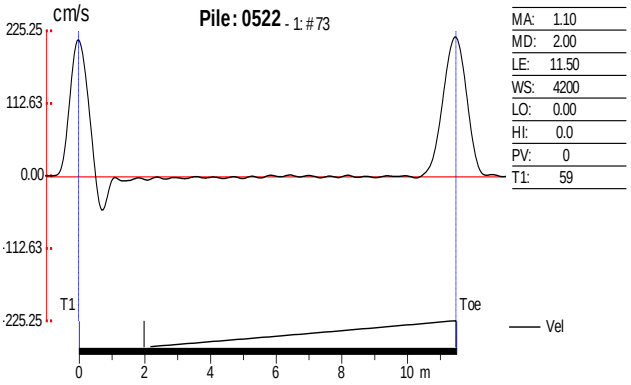


Figure 3. Example of normally result graph ("good" pile).

The surface vibrations are measured by means of an accelerometer attached to the top of the pile. Although the acceleration curve could be interpreted directly, integration to velocity generally enhances the record by bringing out details otherwise overlooked. The pile top acceleration signal, is therefore digitized and stored in the PIT device memory, and it is numerically integrated to produce a velocity signal. It should be noted that v is a particle velocity, i.e., the actual velocity of movement of the pile top surface.

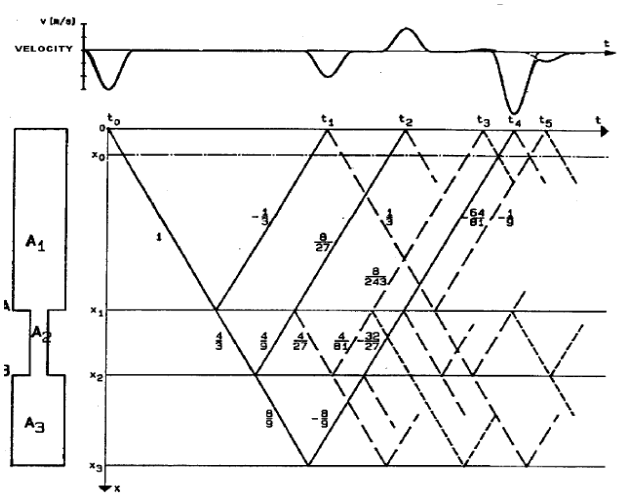


Figure 4. Characteristics for a rod with a reduced cross-section (A2=A1/2, A3=A1).

Wave Speed in Concrete.

The Impact wave speed in concrete depends on the quality of the concrete and for in-situ casted piles the curing time of the concrete. The wave speed is used to determine the length of the pile based on the return signal. An example of the wave speed in concrete is shown below.

Table 1. Soil Properties Used in Analysis.

Concrete quality	Impact wave speed (m/s)
Bad	<2.700
Acceptable	2.700-3.300
Good	3.300-3.800
Very good	3.800-4.000
Excellent	4.000-4.500
Unlikely Normal Conditions	>4.500

Interpretation results obtained by Low Strain Method.

An assessment by this method can give a rapid and accurate appraisal of pile integrity. An integrity test will indicate when a pile should be investigated further but it cannot give information about any load carrying capacity of the pile.

Interpretation of the results obtained must take into account the specific pile circumstances, i.e. construction technique and localized soil conditions. An anomaly does not necessarily indicate a deficiency in the pile, but would certainly merit further investigation to establish the cause of the anomaly. Full interpretation of the signal responses must only be undertaken by fully trained personnel.
For interpretation ten classes are distinguished:

Low Strain Testing Constraints.
The following items may often be detected:
- Pile length.
- Inclusions of foreign material with different acoustic properties.
- Cracking perpendicular to the axis.
- Joints and staged concreting.
- Abrupt changes in cross section.
- Distinct changes in soil layers.

All physical measurements have limitations, and low strain (sonic) test probably has more limitations than any other test. For instance, the sonic test will normally not detect the following items:
- The toe reflection when the L/D ratio roughly exceeds 20 (In hard soils) to 60 (In very soft soils).
- Gradual changes in cross-section.
- Minor inclusions and changes in cross-section.
- Impedance changes of small axial dimension.
- Small variations in length.
- Features located below either a fully-cracked cross section or a major (1:2) change in impedance.
- Debris at the toe.
- Deviations from the straight line and from the vertical.
- Load-carrying capacity.
- The consistency of concrete cover.
- The length of reinforcement.

Cross-Hole Sonic Logging.
"Crosshole Sonic Logging" (CSL) is a testing method for the determination of pile integrity in accordance with relative change of such acoustic parameters as sonic time, frequency and amplitude attenuation when actual measured sound wave transmitted in the concrete media, shooting and receiving sound waves among pre-buried sonic-testing tubes of the pile (ASTM D6760 – 08 (2008)).



Figure 5. Transmitter and Receiver Probes.

The Low Strain method belongs to the external test-methods, as it accesses only the top of the pile. Ultrasonic logging, on the other hand, is intrusive and necessitates the prior installation of access tubes (usually two or more) in the pile.

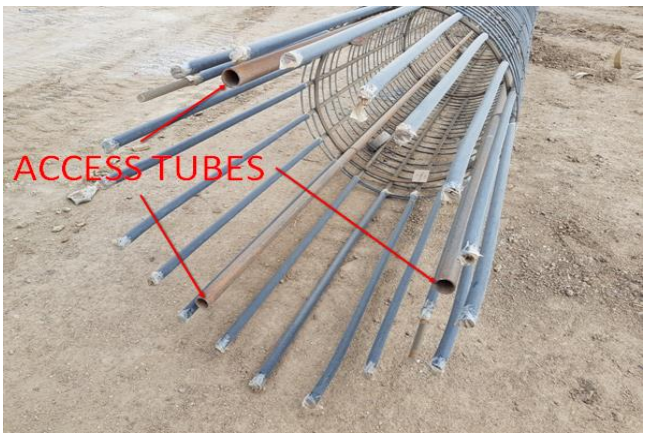


Figure 6. Installation of Access Tubes.

Before the test they have to be filled with water (to obtain good coupling) and two probes are lowered inside two of the tubes. One of these probes is an emitter and the other a receiver of ultrasonic pulses. Having been lowered to the

bottom, the probes are then pulled simultaneously upwards to produce an ultrasonic logging profile. The transmitter produces a series of acoustic waves in all directions. Some of these waves do eventually reach the receiver.

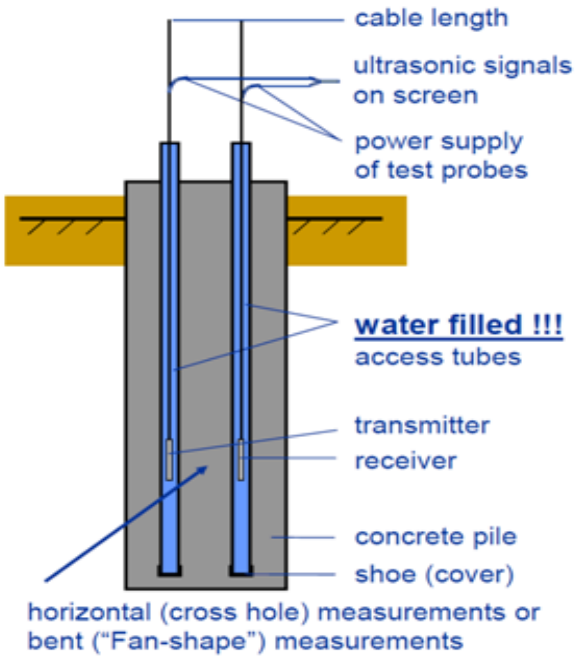


Figure 7. Cross-Hole Sonig Logging – Principle.

The testing instrument then plots the travel time between the tubes versus the depth. As long as this time is fairly constant, it shows that there is no change in concrete quality. A sudden increase of the travel time at any depth may indicate a flaw at this depth.

The number of access tubes cast in the pile concrete is a function of the pile diameter, the importance of the pile and, of course, economic consideration. A good rule of thumb is to specify one tube per each 30 cm of pile diameter. Thus for a pile with a diameter of 1.2 m, four tubes will normally do. For best effect, the tubes should be equally spaced inside the spiral reinforcement and rigidly attached to it by wire or spot welding. Where tubes are extended below the reinforcement cage, they have to be stabilized by suitable steel hoops.

Cross-Hole Sonic Logging Results.

Usually the report includes presentation of Cross-Hole Sonic logs for all tested tube pairs including:

- Presentation of the traditional signal peak diagram as a function of time plotted versus depth.
- Computed initial pulse arrival time or pulse wave speed versus depth.
- Computed relative pulse energy or amplitude versus depth.

A Cross-Hole Sonic log will be presented for each tube pair. Defect zones, if any, will be indicated on the logs and their extent and location discussed in the report text. Defect zones are defined by an increase in arrival time of more than 20 percent relative to the arrival time in a nearby zone of good concrete, indicating a slower pulse velocity.

Tomography by the data of Cross-Hole Sonic Logging.

The same procedure, which is carried out in two dimensions on a single profile, can be used in three dimensions for the whole pile. In this case, the pile is divided into elementary voxels, or volume pixels, this process is usually called a tomography.

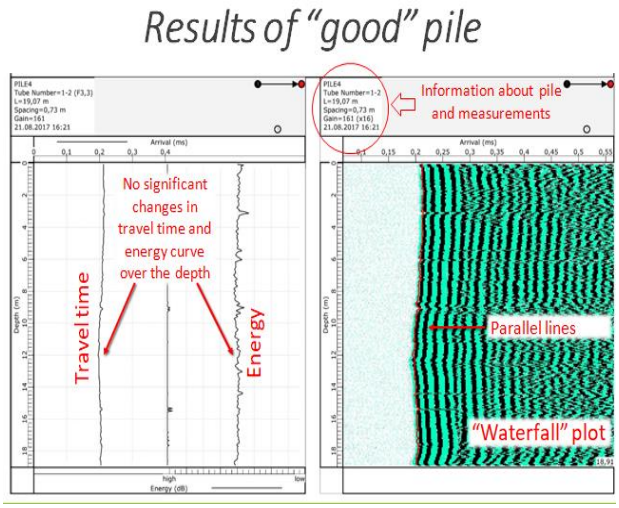


Figure 8. Typical Ultrasonic Profile.

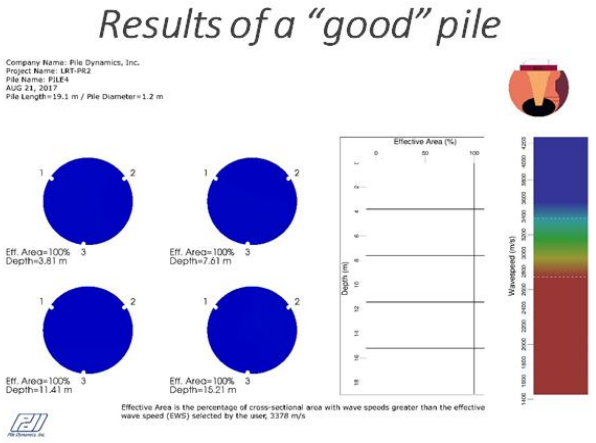


Figure 9. Horizontal cross-sections of pile in PDI-TOMO software.

Tomography is a mathematical procedure that is applied to Crosshole Sonic Logging (CSL) data, providing the user with a visual image of a shaft's internal defects. The procedure involves solving a system of equations based on First Arrival Times (FAT) in order to calculate wave speeds at various points within the shaft. Tomography wave speeds distributed throughout the shaft are directly proportional to density, indicating concrete quality. PDI-TOMO is an extension of the CHA-W software designed for superior tomographic analysis results from CHAMP data with increased efficiency for the user.

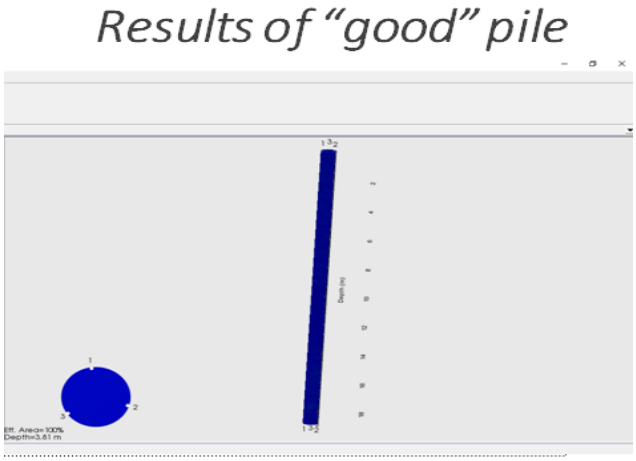


Figure 10. Three-dimensional visualization in PDI-TOMO software.

PDI-TOMO software features:

- Provides a more precise location, shape and size of defective areas within a shaft.
- Offers an intuitive visual identification of the damaged areas and generates easily comprehensible and professional outputs for the consumer of the CSL reports.
- Provides a valuable add-on service for the testing engineer.

Cross-Hole Sonic Testing Constraints

The Cross-Hole Sonic Test will normally detect the following items:

- Finds multiple defects, depth and quadrant.
- Finds "soft bottoms" if tubes go to bottom.
- Finds voids better than soil inclusions.
- Finds larger defects easier than small defects.
- Waterfall, FAT (First arrival time), & energy all help find defect.
- Not sensitive to surrounding soils or pile length.

The Cross-Hole Sonic Test will normally not detect the following items:

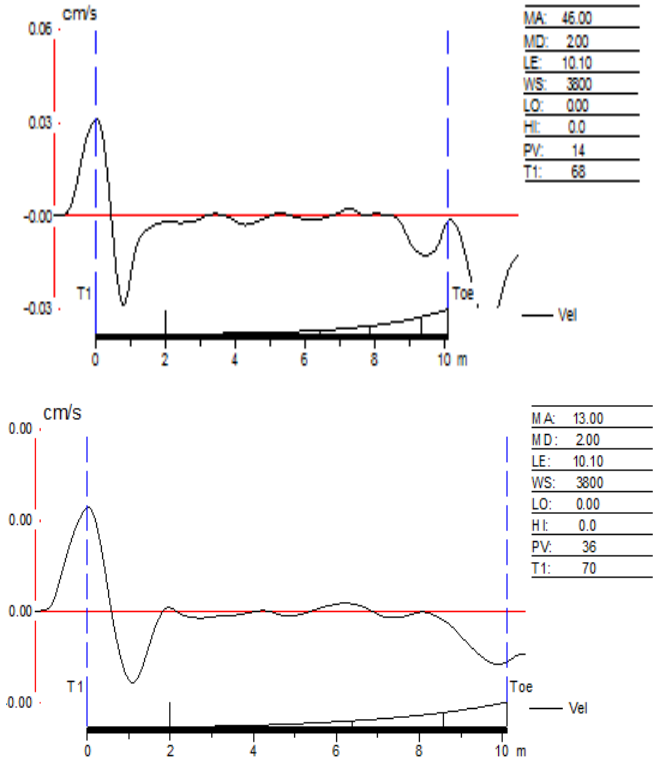
- Cannot find diameter changes or bulges.
- If too few tubes, can miss a defect.
- Can find defect on direct path.
- Cannot find defect outside cage.
- Major diagonal defects more difficult to find.
- Need more than 4 tubes for 1500 mm pile (recommend 6 tubes for shaft this size).

Comparison test results obtained by two methods.

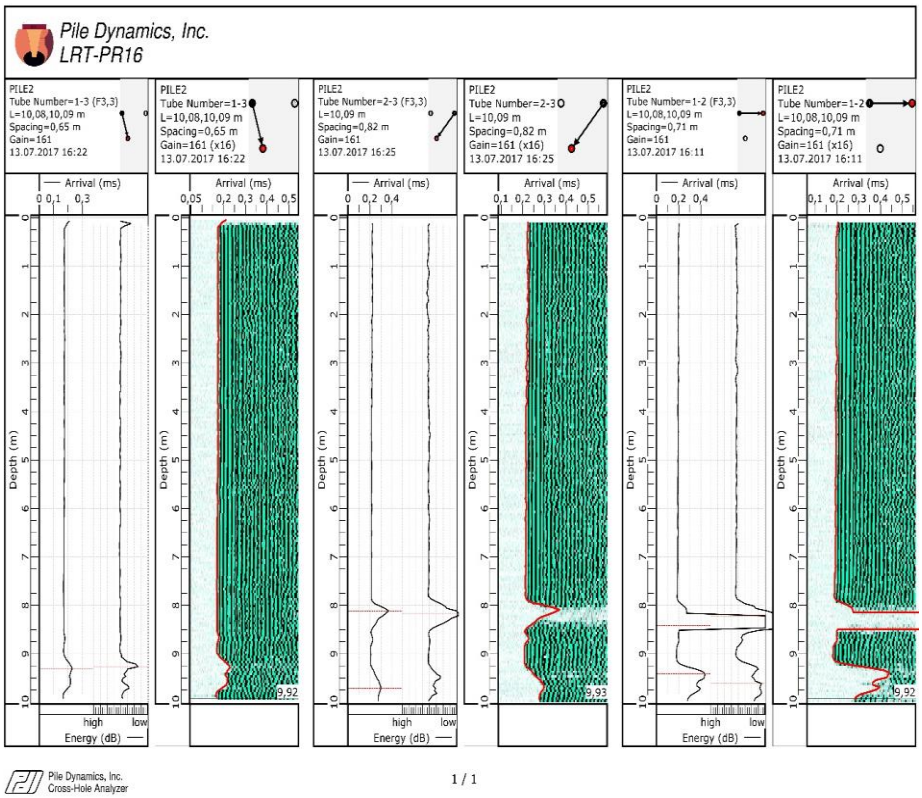
In 2017-2018 at the construction site of LRT in Astana city, more than 1500 bored piles were integrity tested by using two methods: 45 % by Cross-Hole Sonic Logging and other 55 % by Low Strait Test. Client gives a technical assignment for integrity testing piles:

- if one foundation of the bridge consists of four bored piles, then one pile is tested by Cross-Hole Sonic Logging and other three piles tested by Low Strait Test.
- if one foundation of the bridge consists of six bored piles, then two pile is tested by Cross-Hole Sonic Logging and other four piles tested by Low Strait Test.

One of the tested pile PR16-2 contained a serious defect of integrity.



<u>Figure 11.</u> Two reflectograms of one bored ''bad'' pile PR16-2 obtained by Pile Integrity Tester - PIT-QV.



<u>Figure 12.</u> Three Ultrasonic Profile of one pile PR16-2 (''bad'' pile).

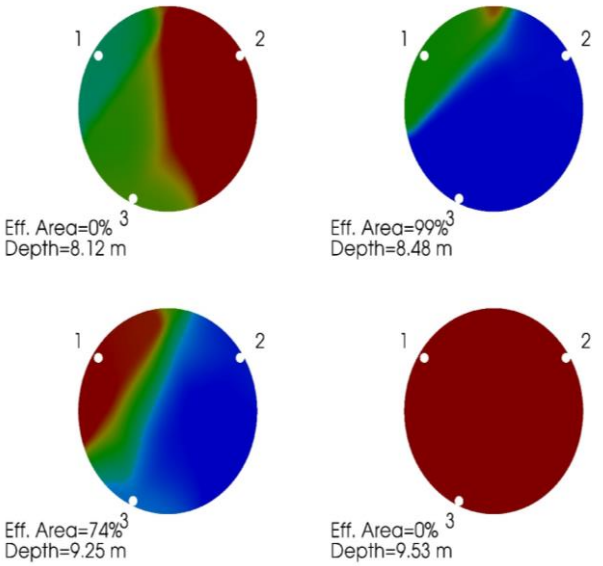


Figure 13. Horizontal cross-sections of pile PR16-2 in PDI-TOMO software.

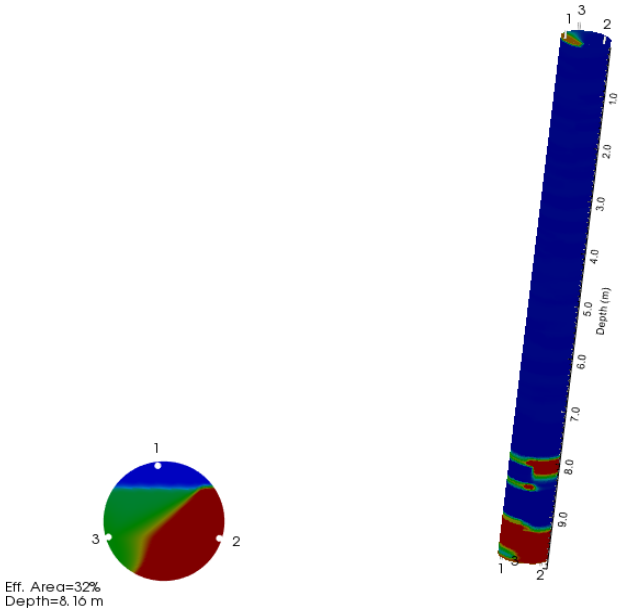


Figure 14. Three-dimensional visualization in PDI-TOMO software for bored pile PR16-2.

Analyzing the data obtained by Low Strain Test (Fig. 11) we can say only that at the depth 8.5 m this pile has crack and its cross-section is decreasing.

Analyze the data of Cross-Hole Sonic Test can show 3D location of cracks, approximately size of cracks, effective cross-section of pile at any depth. Cross-Hole Sonic Test provide more useful information about integrity and allows the engineer to evaluate the seriousness of the problem and the possibility of using this pile in foundation.

CONCLUSIONS

At the final consideration on results of CSL testing presented following concluding remarks: the defects are had different issues as well as low quality of concrete (strength is not reach to the project), non-observance of the work of production technology or soil ingress into the concrete pouring into the drilling shaft. Also big influence was affected the soil condition of construction site. The Cross-hole logging testing is most accurately and quality for field observation of deep pile foundations. Since resolution is strongly dependent on the wave length, the cross-hole method enables us to detect much smaller flaws with high accuracy.

The Pile Integrity Tester (PIT) is an instrument for integrity testing of foundations by low-strain surface-impact methods. The Low Strain test is a powerful quality-control tool, not so expensive and need about one minute for application but we must never forget that it is not omnipotent. Since the sonic method is based on the use of stress-waves, it can identify only those pile attributes that influence wave propagation and have a fairly large size. Data collected by the PIT can and should be further analyzed using the PIT-W software for a more thorough data interpretation and report quality output.

REFERENCES

1. **Joram M.A.** Pile Integrity Testing, Israel, 2009.
2. ASTM Standard D. Standard Test Method for Low Strain Impact Integrity Testing of Deep Foundations. ASTM International, West Conshohocken, PA, 2000.
3. ASTM Standard D 6760. Standard Test Method for Integrity Testing of Concrete Deep Foundations by Ultrasonic Crosshole

Testing. ASTM International, West Conshohocken, PA, 2002.
4. **White B., Nagy M., Allin R.** Comparing Cross-Hole Sonic logging and Low-Strain Integrity Testing Results. // *Proceedings of the 8th International Conference of Application of Stress Wave Theory to Piles*, Lisbon, 2008, pp. 471-476.
5. **Bungenstab F.C., Beim J.W.** Continuous Flight Auger (CFA) Piles – A Review of the Execution Process and Integrity Evaluation by Low Strain Test. Buenos Aires, Argentina, IOS Press, 2015, pp. 414-421.
6. **Massoudi N., Teferra W.** Non-Destructive Testing of Piles Using the Low Strain Integrity Method. // *Proceedings of the Fifth International Conference on Case Histories in Geotechnical Engineering*, New-York, NY, 2004, pp. 1-6.
7. **Zhussupbekov A., Iwasaki Y., Omarov A.R.** The Experience Different of Piling Testing on Problematical Soil Ground of Astana, Kazakhstan. // *International Journal for Computational Civil and Structural Engineering*, 2018, Volume 14, Issue 4, pp. 158-171.

СПИСОК ЛИТЕРАТУРЫ

1. **Joram M.A.** Pile Integrity Testing, Israel, 2009.
2. ASTM Standard D. Standard Test Method for Low Strain Impact Integrity Testing of Deep Foundations. ASTM International, West Conshohocken, PA, 2000.
3. ASTM Standard D 6760. Standard Test Method for Integrity Testing of Concrete Deep Foundations by Ultrasonic Crosshole Testing. ASTM International, West Conshohocken, PA, 2002.
4. **White B., Nagy M., Allin R.** Comparing Cross-Hole Sonic Logging and Low-Strain Integrity Testing Results. // *Proceedings of the 8th International Conference of Application of Stress Wave Theory to Piles*, Lisbon, 2008, pp. 471-476.
5. **Bungenstab F.C., Beim J.W.** Continuous Flight Auger (CFA) Piles – A Review of the Execution Process and Integrity Evaluation by Low Strain Test. Buenos Aires, Argentina, IOS Press, 2015, pp. 414-421.
6. **Massoudi N., Teferra W.** Non-Destructive Testing of Piles Using the Low Strain Integrity Method. // *Proceedings of the Fifth International Conference on Case Histories in Geotechnical Engineering*, New-York, NY, 2004, pp. 1-6.
7. **Zhussupbekov A., Iwasaki Y., Omarov A.R.** The Experience Different of Piling Testing on Problematical Soil Ground of Astana, Kazakhstan. // *International Journal for Computational Civil and Structural Engineering / Международный журнал по расчету гражданских и промышленных конструкций*, 2018, Volume 14, Issue 4, pp. 158-171.

Askar Zhussupbekov, Professor, Dr.Sc., Head of Department of Civil Engineering, L.N. Gumilyov Eurasian National University; 13a, Kazhimukan st., Astana, Republic of Kazakhstan, 010010;
phones +7(7172) 344796 (office),
+7(7015) 118382 (mobile); fax +7 (7172) 709457;
E-mail: enu@enu.kz.

Yoshinori Iwasaki, Professor, Ph.D., Executive Director, Geo-Research Institute; Invited Professor, L.N. Gumilyov Eurasian National University; Honorary Professor, SaintPetersburg State University of Architecture and Civil Engineering; 4-3-2 Itachi-bori, Nishi-ku, Osaka 550-0012, Japan; phones +81-6-6941-8800 (office), +81-90-8938-1191 (mobile); fax +81-6-6941-8882;
E-mail: yoshi-iw@geor.or.jp.

Eun Chul Shin, Department of Civil and Environmental Engineering, Incheon National University; 119 Academy-ro, Songdo 1(il)-dong, Yeonsu-gu, Incheon, South Korea.

Nurgul Shakirov, Department of Civil Engineering, L.N. Gumilyov Eurasian National University; 13a, Kazhimukan st., Astana, Republic of Kazakhstan, 010010; phones +7(7172) 344796 (office);
fax +7 (7172) 709457; E-mail: enu@enu.kz.

Жусупбеков Аскар Жагпарович, профессор, доктор технических наук, заведующий кафедрой Проектирование зданий и сооружений», Евразийский национальный университет им. Л.Н. Гумилева; председатель ТС 305 (ISSMGE); президент Казахской геотехнической ассоциации; 010010, Казахстан, г. Астана, ул. Кажымукана 13а; тел.: +7(7172) 344796 (рабочий), +7(7015) 118382 (мобильный);
факс +7 (7172) 709457; E-mail: enu@enu.kz.

Ивасаки Йошинори, профессор, доктор философии (Ph.D.); исполнительный директор, Геоисследовательский институт; председатель АТС 19 Геопамятники культурного наследия (ISSMGE); приглашенный профессор, Евразийский национальный университет им. Л.Н. Гумилева; Почетный профессор Санкт-Петербургского государственного архитектурно-строительного университета; 2-1-2, Отамае, Чуо-ку, Осака 540-008, Япония; тел.: +81-6-6941-8800 (рабочий),
+81-90-8938-1191 (мобильный);
факс +81-6-6941-8882; e-mail: yoshi-iw@geor.or.jp.

Юн Чул Шин, факультет гражданского и экологического строительства, Национальный университет Инчхон, Сонгдо, Южная Корея; 119 Academy-ro, Songdo 1(il)-dong, Yeonsu-gu, Incheon.

Нургул Шакиров, кафедра Проектирование зданий и сооружений», Евразийский национальный университет им. Л.Н. Гумилева; 010010, Казахстан, г. Астана, ул. Кажымукана 13а; тел.: +7(7172) 344796 (рабочий); факс +7 (7172) 709457; E-mail: enu@enu.kz.